Antigenic variation and stumpy development in *Trypanosoma brucei*

Dissertation zur Erlangung des

naturwissenschaftlichen Doktorgrades

der Julius-Maximilians-Universität Würzburg

vorgelegt von

Henriette Zimmermann

geboren in Bergisch Gladbach

Würzburg, 2017

Eingereicht am: 05.04.2017

Mitglieder der Promotionskommission:

Vorsitzender:

Gutachter: Prof. Dr. Markus Engstler

Gutachter: Prof. Dr. Klaus Brehm

Tag des Promotionskolloquiums:

Doktorurkunde ausgehändigt am:

List of contents

1 Summary

Summary

The eukaryotic parasite *Trypanosoma brucei* has evolved sophisticated strategies to persist within its mammalian host. Trypanosomes evade the hosts' immune system by antigenic variation of their surface coat, consisting of variant surface glycoproteins (VSGs). Out of a repertoire of thousands of *VSG* genes, only one is expressed at any given time from one of the 15 telomeric expression sites (ES). The VSG is stochastically exchanged either by a transcriptional switch of the active ES (*in situ* switch) or by a recombinational exchange of the *VSG* within the active ES. However, for infections to persist, the parasite burden has to be limited. The slender (sl) bloodstream form secretes the stumpy induction factor (SIF), which accumulates with rising parasitemia. SIF induces the irreversible developmental transition from the proliferative sl to the cell cycle-arrested but fly-infective stumpy (st) stage once a concentration threshold is reached. Thus, antigenic variation and st development ensure persistent infections and transmissibility.

A previous study in monomorphic cells indicated that the attenuation of the active ES could be relevant for the development of trypanosomes. The present thesis investigated this hypothesis using the inducible overexpression of an ectopic VSG in pleomorphic trypanosomes, which possess full developmental competence. These studies revealed a surprising phenotypic plasticity: while the endogenous *VSG* was always down-regulated upon induction, the ES-activity determined whether the VSG overexpressors arrested in growth or kept proliferating. Full ES-attenuation induced the differentiation of *bona fide* st parasites independent of the cell density and thus represents the sole natural SIF-independent differentiation trigger to date. A milder decrease of the ES-activity did not induce phenotypic changes, but appeared to prime the parasites for SIF-induced differentiation. These results demonstrate that antigenic variation and development are linked and indicated that the ES and the *VSG* are independently regulated. Therefore, I investigated in the second part of my thesis how ES-attenuation and *VSG*-silencing can be mediated. Integration of reporters with a functional or defective *VSG* 3'UTR into different genomic loci showed that the maintenance of the active state of the ES depends on a conserved motif within the *VSG* 3'UTR. *In situ* switching was only triggered when the telomere-proximal motif was partially deleted, suggesting that it serves as a DNA-binding motif for a telomere-associated protein. The VSG levels seem to be additionally regulated *in trans* based on the *VSG* 3'UTR independent of the genomic context, which was reinforced by the regulation of a constitutively expressed reporter with *VSG* 3' UTR upon ectopic VSG overexpression.

Zusammenfassung

Der eukaryotische Parasit *Trypanosoma brucei* hat komplexe Strategien entwickelt, um in seinem Säugetierwirt zu überleben. Die Grundlage der Immunevasion ist die antigene Variation des Oberflächenmantels, der aus dem variablen Oberflächenglykoprotein (VSG) besteht. Von mehreren tausend *VSG*-Genen wird zu jedem Zeitpunkt nur ein einziges aus einer der 15 telomerischen Expressionsstellen (ES) exprimiert. Das VSG kann entweder durch einen transkriptionellen Wechsel der aktiven ES (*in situ* Wechsel) oder durch einen rekombinatorischen Wechsel des *VSG*-Gens innerhalb der aktiven ES stochastisch ausgetauscht werden. Damit jedoch eine langanhaltende Infektion des Wirts möglich wird, muss gleichzeitig der Parasitenbefall begrenzt werden. Mit ansteigender Parasitämie akkumuliert der '*stumpy induction factor*' (SIF), welcher von der '*slender*' (sl) Blutstromform sekretiert wird. Sobald ein Schwellenwert in der SIF-Konzentration erreicht ist, wird die irreversible Differenzierung der proliferativen sl in die zellzyklusarretierte '*stumpy*'(st) Form eingeleitet, welche infektiös für den Fliegenvektor ist. Somit stellen antigene Variation und st-Differenzierung das Persistieren der Infektion und die Übertragung des Parasiten sicher.

Eine frühere Arbeit mit monomorphen Zellen deutete darauf hin, dass die Attenuierung der aktiven ES eine Rolle für die Differenzierung der Trypanosomen spielen könnte. Diese Hypothese wurde in der vorliegenden Dissertation untersucht, indem in pleomorphen Zellen mit vollständiger Entwicklungskompetenz ein ektopisches VSG induzierbar überexprimiert wurde. Diese Studien offenbarten eine erstaunliche phänotypische Plastizität: während das endogene *VSG* nach Induktion runter reguliert wurde, arretierten die VSG-Überexpressoren in Abhängigkeit von der ES-Aktivität entweder im Wachstum oder teilten sich weiter. Die vollständige ES-Attenuierung löste die Differenzierung zu echten st Zellen unabhängig von der Zelldichte aus und ist somit der bisher einzige natürliche SIF-unabhängige Differenzierungsauslöser. Eine mildere Abnahme der ES-Aktivität verursachte keinen Phänotyp, scheint aber die Zellen auf die SIF-induzierte Differenzierung vorzubereiten. Diese Ergebnisse zeigen, dass antigene Variation und Differenzierung verbunden sind und deuteten an, dass die ES und das *VSG* unabhängig voneinander reguliert werden. Daher habe ich im zweiten Teil meiner Dissertation untersucht, wie ES-Attenuierung und *VSG*-Stilllegung vermittelt werden können. Die Integration eines Reporters mit funktioneller oder defekter *VSG* 3'UTR an verschiedenen Orten im Genom zeigte, dass die Aufrechterhaltung der ES-Aktivität von einem konservierten Motiv in der *VSG* 3'UTR abhängig ist. Ein *in situ* Wechsel wurde nur ausgelöst, wenn Teile des Telomer-proximalen Motiv deletiert wurden, was nahelegt, dass das Motiv auf DNA-Ebene von einem Telomerbindeprotein erkannt wird. Die VSG-Level scheinen unabhängig vom genomischen Kontext zusätzlich *in trans* basierend auf der *VSG* 3'UTR reguliert zu werden, was durch die Regulation eines konstitutiv exprimierten Reporters mit *VSG* 3'UTR nach VSG-Überexpression bekräftigt wurde.

2 Introduction

2.1 Trypanosomes and disease

African trypanosomes are eukaryotic unicellular parasites that infect a wide range of vertebrate hosts, where they live mostly extracellularly in the blood. The parasites are transmitted via the bite of the tsetse fly vector (*Glossina* spp.) and thus the prevalence of the parasite is restricted to the range of its insect vector, the sub-saharan regions of Africa.

It was first suspected by Livingstone in 1857 that the bite of the tsetse fly causes the animal disease nagana in cattle (Livingstone, 1857), however, 40 years later David Bruce could show that in fact trypanosomes are the causative agent (Bruce, 1895). Only a few years later trypanosomes were also linked to sleeping sickness in humans and it was shown that indeed the fly transmits the parasite (Dutton, 1902; Kleine, 1909). Nowadays, different trypanosome species are known as pathogens of nagana, which not only occurs in wild or domesticated animals but also in livestock. As this disease is fatal for numerous infected animals and can ultimately lead to their death, it has a dramatic impact on African agriculture and causes economical losses (Angara et al., 2014; reviewed in Chanie et al., 2013). The species with the most prevalent epidemiologic effect are *Trypanosoma vivax, Trypanosoma congolense* and *Trypanosoma brucei.* Two subspecies of the latter also influence public health as they are the pathogens of human African trypanosomiasis (HAT), commonly known as sleeping sickness (reviewed in Brun et al., 2010).

Humans, like other primates, are immune against most trypanosome species, because they possess a trypanolytic factor (TLF), consisting of a haptoglobin-related protein and apolipoprotein L1 (APOL1) (reviewed in Wheeler, 2010). When TLF is endocytosed by trypanosomes, APOL1 is incorporated into endosomal/lysosomal membranes. This facilitates the flux of ions, leading to the destruction of the parasites by osmolytic swelling (Pérez-Morga et al., 2005). In contrast to *T. brucei brucei*, the two other subspecies -*T. brucei rhodesiense* and *T. brucei gambiense* - have evolved strategies to survive in the human blood. Resistance of the first one is based on the serum resistance-associated protein (SRA), which binds to the TLF once the parasites have endocytosed it. Thereby, TLF is inactivated and the destruction of the parasite is prevented (Vanhamme et al., 2003; Xong et al., 1998). In contrast, the latter species uses other distinct mechanisms to escape the TLF mediated destruction. For example, the hydrophobic β-sheet of the *T. brucei gambiense* specific glycoprotein (TgsGP) prevents APOL1 toxicity by stiffening membranes (Uzureau et al., 2013).

In general, the course of the infection with trypanosomes is subdivided in two phases: the first haemolymphatic and the second meningo-encephalitic stage. Upon infection, the parasites live in the bloodstream, the lymphatic system and some tissues of its mammalian host. This leads to non-specific symptoms like fever, headache, pain in the limbs, pruritus and shivering attacks.

In the second phase, the trypanosomes have crossed the blood-brain barrier and infected the brain as well as the central nervous system (CNS). This initially provokes sleep and motor system disturbances as well as neuro- psychiatric disorders but, ultimately, leads to coma and death (reviewed in Kennedy, 2013). In HAT these main stages occur during infection with both pathogen species but the time course differs dramatically. While *T. brucei rhodesiense* infects the CNS within weeks and leads to death after a couple of month, *T. brucei gambiense* causes a chronic infection that can last for years. In 2014 the vast majority of the 3796 newly reported cases were *T. brucei gambiense* infections, but the estimated number of unknown cases is considered to be higher (World Health Organization, 2016).

2.2 The model organism *Trypanosoma brucei*

T. brucei is assigned to the order of Kinetoplastida that is defined by the presence of the condensed circular DNA of the single mitochondrion, a structure termed kinetoplast (Vickerman and Preston, 1976). Besides other African trypanosome species, members of this family are the pathogen of the Chagas` disease, *Trypanosoma cruzi*, or various species of *Leishmania,* which provoke visceral or cutaneous leishmaniasis. However, *T. brucei brucei* is the most widely studied kinetoplastid species due to its high degree in similarity to human infective trypanosomes and because laboratory strains are available, that can be easily cultivated and manipulated via forward or reverse genetics. Therefore, the parasite *T. brucei brucei* has evolved as a model organism for different aspects of cell biology.

2.2.1 The cell architecture

The shape of this eukaryotic flagellate is determined by its cytoskeleton consisting of a sub-pellicular corset of microtubules that are regularly spaced, connected to each other and to the plasma membrane they are underlying (Hemphill et al., 1991). The plus ends of the microtubules are localized at the posterior end of the cell and thus define the polarity of the parasite (Robinson et al., 1995). At the posterior pole, the single flagellum emerges the cell body at the flagellar pocket (Figure 1).

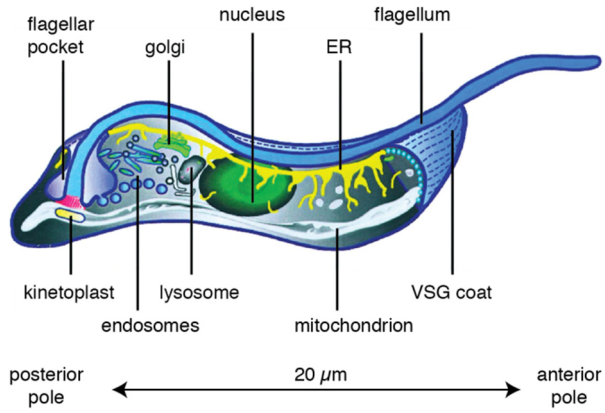

Figure 1: The cell architecture of *Trypanosoma brucei.* Schematic overview of the cell architecture with all major organelles and their location (adapted from Grünfelder et al., 2003). The microtubule corset underlying the plasma membrane, the VSG surface coat and the flagellum are shown. The anterior and posterior pole are indicated as well as the length of the cell.

The flagellum is attached to the cell body via the flagellum attachment zone (FAZ) as it extends towards the anterior end of the parasite, where the distal tip is free (Taylor and Godfrey, 1968). The flagellar pocket is an invagination of the plasma membrane and represents a specialized membrane region as it is the only place where endo- and exocytosis take place (Overath and

Engstler, 2004). Most organelles of trypanosomes, like the flagellum and flagellar pocket, are present as single copy and have a precise location within the cell (Figure 1). The Golgi as well as the endosomal apparatus are positioned between the flagellar pocket and the centrally located nucleus. The endoplasmic reticulum (ER) runs along the longitudinal axis of the cell always adjacent to the flagellum. The single mitochondrion spans the whole cell while the kinetoplast is localized at the posterior pole as it is connected to the origin of the flagellum, the basal body. Hence, trypanosomes are perfectly suited to investigate fundamental cell biological questions because they possess a polarized cell architecture and most of the single copy organelles are precisely localized.

2.2.2 The cell cycle

Trypanosomes duplicate via binary fission approximately every six hours. Thus, the reproduction and segregation of all single copy organelles needs to be exactly timed during proliferation. Single cells within the asynchronous population can be assigned to distinct cell cycle stages as the division of the mitochondrial DNA, the kinetoplast, precedes the division of the nucleus (Woodward and Gull, 1990) (Figure 2).

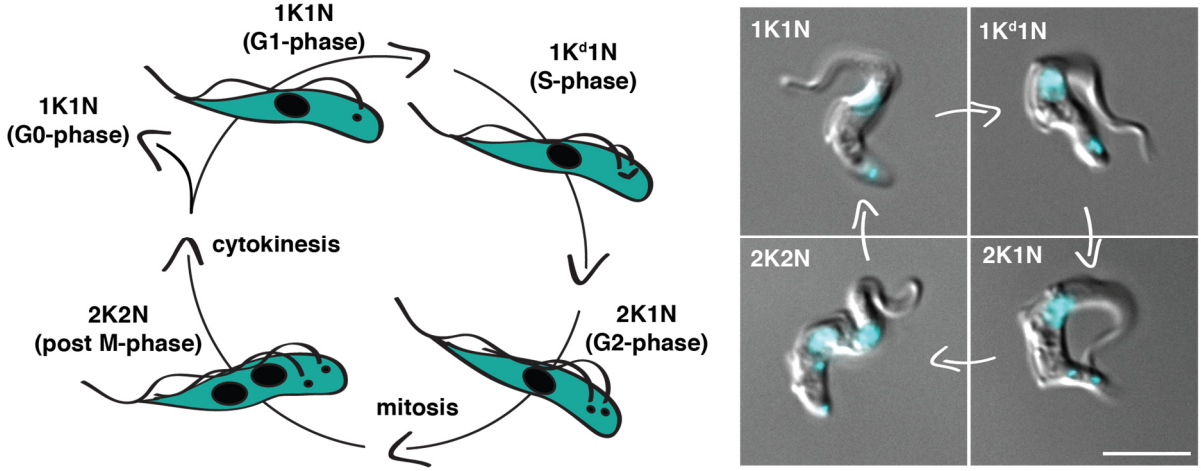

Figure 2: The cell cycle of *Trypanosoma brucei*. On the left a schematic model illustrates the different cell cycle stages of the parasite. The different phases of the cell cycle (G0, G1, S, G2, post M) can be distinguished by the configuration of the kinetoplast (K) and the nucleus (N). On the right a DIC image and DAPI staining (cyan) visualizes the cell cycle in chemically fixed parasites. Scale bar: 5 µm.

The first step in the cell cycle is the duplication of the basal body, which connects the flagellum with the kinetoplast and links the duplication of these organelles (Sherwin and Gull, 1989). The novel basal body serves as nucleation site for the newly synthesized flagellum, that exits the

cell body from the same flagellar pocket as the old one (Lacomble et al., 2010). Meanwhile, the cell entered the S-phase as its mitochondrial DNA was replicated. The separation of the basal bodies causes the segregation of the mitochondrial DNA and the flagellar pocket (Lacomble et al., 2010). This stage with a dividing kinetoplast, termed $1K^d1N$, can be easily discriminated from the 1K1N stage due to the elongated shape of the mitochondrial DNA. During this time, the nuclear DNA is replicated and the cell enters the G2-phase of the cell cycle once the segregation of the kinetoplast is complete. The parasite now has two kinetoplasts and one nucleus (2K1N). The nuclear DNA is separated without a breakdown of the nuclear envelope (closed mitosis) and the cell enters the post M-phase, in which two kinetoplasts and two nuclei are present (2K2N) (Ogbadoyi et al., 2000). Also, the microtubule skeleton elongates and the volume of the cell increases (Rotureau et al., 2011).

Cytokinesis initiates at the anterior end of the cell when all organelles are replicated. Physical forces generated by the motility of the cell support the segregation, while the cleavage furrow proceeds towards the posterior end of the cell along the longitudinal axis between the two flagella (Broadhead et al., 2006; Ralston et al., 2006). Hereby, the organelles are equally distributed and two daughter cells originate, which reenter the cell cycle. Thus, another advantage of trypanosomes as model system is their comparably simple and accurately timed cell cycle.

2.3 The parasite cycle of *Trypanosoma brucei*

Trypanosomes possess a complex parasite cycle as they alternate between the mammalian host and the insect vector (Figure 3). During this transition and the journey in the fly the parasites are exposed to dramatic changes in their environment like temperature, pH or availability of nutrients. To cope with these problems, the parasites have evolved sophisticated adaption strategies including alterations in metabolism, surface proteins and morphology. So far, seven different stages have been described in the fly and two in the mammalian host (Figure 3). Commonly, the bloodstream form (BSF), which naturally occurs in the mammal, or the procyclic form (PCF), which colonizes the midgut of the insect, can be cultivated *in vitro* and are therefore used for experiments. However, the parasites also adapted to laboratory conditions due to prolonged syringe passaging. The changes are particular striking in the BSF because the typically used laboratory strains lost the ability to differentiate and thus are described as monomorphic (reviewed in McCulloch et al., 2004).

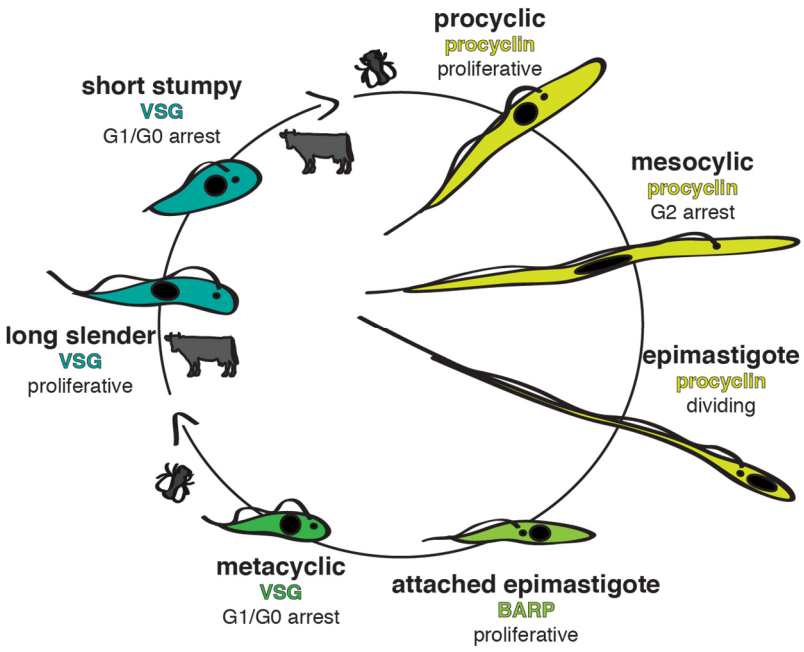

Figure 3: The parasite cycle of *Trypanosoma brucei*. The major mammalian bloodstream (blue) and insect vector (yellow and green) stages of the parasite are schematically illustrated (adapted from Sharma et al., 2009). Changes in cell morphology, the kinetoplast-nucleus configuration, flagellar length and positioning occur during developmental progression. These characteristic features of the different developmental stages are represented. The main surface proteins of the different stages are color-coded and the status of the stages within the cycle is given (dividing, proliferative, G1 or G2 arrest).

2.3.1 The development within the insect vector

The tsetse fly takes up the parasites with the blood meal when it feeds on a mammal infected with trypanosomes. Subsequently, the meal, which can contain thousands of trypanosomes, is transported into the crop and then into the anterior midgut of the fly. During this first part of the parasites journey within the fly, differentiation from the BSF to the PCF takes place. The cells not only change their morphology, but also adapt their gene expression and metabolism. For example, the distance between kinetoplast and posterior pole of the cells is increased due to the elongation of microtubules at the posterior end and the migration of the kinetoplast in the vicinity of the nucleus (Matthews et al., 1995). Also, the variant surface glycoprotein (VSG), which dominates the surface of the BSF, is replaced by procyclins like GPEETs and EPs (Overath et al., 1983; Roditi et al., 1989). The procyclins are suggested to protect the parasites from digestive enzymes of the alimentary system of the fly and are essential for the establishment of the infection (Acosta-Serrano et al., 2001; Ruepp et al., 1997). Beyond that, the parasites are exposed to a drastic change in the availability of nutrients. The BSF relies exclusively on glycolysis to produce energy, but glucose is barely accessible in the fly. Thus, the cells have to elaborate and activate their mitochondrion to produce energy via the respiratory system using amino acids or peptides as nutrients (reviewed in Van Hellemond et al., 2005). Next, the PCF parasites start to proliferate and invasion of the midgut is initiated. The immune system of the fly is activated due to its infection with trypanosomes, which results in either a reduction of parasite burden or their complete removal.

However, if an infection of the midgut is successfully established, the parasites can cross the peritrophic matrix, which separates the lumen of the midgut from the epithelium. Thus, the PCF parasites can colonize the area between the peritrophic matrix and the epithelium, the epitrophic space. Once they start to migrate towards the next fly compartment, the proventriculus, differentiation to the mesocyclic stage proceeds. While the cells elongate and their diameter reduces, the distance between the kinetoplast and the also lengthened nucleus increases (Rotureau et al., 2011). Further, the cells arrest in the G2-phase and posses now a replicated nuclear and mitochondrial genome, which has not yet started to segregate (Sharma et al., 2008). The transition to the next stage, the epimastigote form, is initiated once the nucleus starts to migrate towards the posterior end of the cell. Thus, the nucleus is localized more posterior to the kinetoplast, in contrast to trypomastigote stages like BSF or PCF. The parasites now reenter the cell cycle and due to asymmetric division a long and a short epimastigote daughter cell emerge after cytokinesis (Sharma et al., 2008). Experimental evidence for the function of the long epimastigotes is missing. However, it is suggested that this form is responsible for the transport of the short epimastigotes to the salivary glands (Rotureau et al., 2011), which in turn appears to be the critical step for the completion of the parasite cycle within the fly (Oberle et al., 2010). The short form attaches to the epithelium of

the salivary glands and elongates (Van Den Abbeele et al., 1999). These attached epimastigotes proliferate and ensure the colonization of the salivary glands. They divide either in a symmetric fashion and produce two epimastigote daughter cells or asymmetrically, whereby one cell with an epimastigote and one with a trypomastigote kinetoplast/nucleus configuration emerges (Rotureau et al., 2012). The latter one is suggested to be a pre-metacyclic cell, that can further differentiate to the metacyclic stage (Rotureau et al., 2012). During this process, the kinetoplast migrates to the posterior pole of the cell and the parasite arrests in the G1-phase (Rotureau et al., 2012). Other processes like the exchange of the surface coat, now representing a metacyclic VSG (mVSG) on the plasma membrane, or the regression of the mitochondrion ensure the pre-adaption of the parasite for the survival in the mammalian host. The trypanosomes are now finally prepared for the re-transmission to the mammalian host after a 20-30 days long journey through the alimentary system of the tsetse fly (reviewed in Sharma et al., 2009).

2.3.2 The development within the mammalian host

If a fly with a salivary gland infection bites a mammal, the metacyclic parasites get injected into the skin, where they reenter the cell cycle. During the first days of infection the metacyclic form resides in the dermis in the region of the insect bite and differentiation to the long slender (sl) BSF stage is initiated (Akol and Murray, 1982; Dwinger et al., 1988). After a few days, the sl parasites, which express a non-metacylic VSG, invade the bloodstream of the host via its lymphatic system. The cells are now directly exposed to the immune system of the host and their struggle for survival starts.

BSF trypanosomes have developed sophisticated strategies based on their main surface coat protein, the VSG, to evade the immune system of the host (discussed in detail in chapter 2.4). The VSGs serve as physical barrier at low antibody titers and once an antibody binds to it the complex can be internalized via endocytosis resulting in the degradation of the antibody while the VSG is recycled (Engstler et al., 2007). In the presence of high antibody concentrations, however, this system is not sufficient anymore to conceal the parasites. Only cells that express another VSG variant, that is novel for the immune system, survive and establish a new population. Due to this process termed antigenic variation a population of trypanosomes can consist of multiple subpopulations expressing immunologically distinct VSG variants (Mugnier et al., 2015).

However, proliferation of the cells has to be limited to maintain an infection, as constantly high parasitemia damages the host and accelerates its death (Seed and Wenck, 2003). This is ensured by the transition to another BSF stage, the short stumpy (st) form. These cells are irreversible arrested in the G1/G0-phase of the cell cycle and have a limited life span of two to

three days, in contrast to the proliferating sl parasites (MacGregor et al., 2011; Shapiro et al., 1984). The differentiation is initiated once a threshold in the concentration of the up till now elusive stumpy induction factor (SIF) is reached (Vassella et al., 1997). SIF is secreted by the proliferating sl cells and accumulates with increasing parasite number (Reuner et al., 1997; Vassella et al., 1997). Consequently, st development occurs at high levels of parasitemia, which limits the parasite burden in the host and guarantees the maintenance of trypanosome infection, as some parasites remain in the sl stage. The developmental transition ensures also transmissibility and the completion of the parasite cycle, because only st cells are thought to be infective for the tsetse fly.

The differentiation from the sl to the st stage is accompanied by changes in morphology and gene expression (Figure 4). Compared to the sl form, the cells have a shorter stout shape, the flagellar length is reduced and the now round nucleus is localized more posterior (Tyler et al., 1997, 2001). A hallmark for the sl to st transition is the elaboration of the mitochondrion. This organelle is a simple single strand in sl cells but grows and branches during st development (Vickerman, 1965). The mitochondrion is literally inactive in sl cells but mitochondrial protein expression, like the lipoamide dehydrogenase (LipDH), is initiated during the expansion of the organelle (Tyler et al., 1997). These changes most likely occur as a pre-adaption to metabolic changes when the parasite is ingested by its vector (Brown et al., 1973). Another preparation for the infection of the fly is the cell cycle arrest of the st cells. Once sl and st parasites enter the tsetse fly with the blood meal, st cells reenter the cell cycle and thus are able to synchronously differentiate to the PCF, while the sl parasites die (reviewed in MacGregor et al., 2012). Also the presence of doomed sl cells might be an advantage during fly infection as a recent study suggested that free VSG molecules could promote the parasite colonization (Aksoy et al., 2016).

The parasites have to be capable to sense the entry in the fly to guarantee a synchronous differentiation. The 'proteins associated with differentiation' (PAD) 1 and 2, which are surface localized carboxylate-transporters, play an important role in the perception of the environmental changes (Dean et al., 2009). Early during the sl/st transition when the cells exit the cell cycle, the expression of *PAD1* mRNA is initiated and the transcripts accumulate subsequently (MacGregor and Matthews, 2012). This is considered as a characteristic of an intermediate stage during st development as the transcript is absent in sl cells and has a maximal expression once the cells have reached a st appearance (reviewed in MacGregor et al., 2012). However, the PAD1 protein is only expressed after the morphological transformation has already started and is then distributed all over the plasma membrane of the st cells (Dean et al., 2009). In contrast, PAD2 is restricted to the flagellar pocket of st parasites (Dean et al., 2009). Once a drop in temperature occurs, like when the parasites enter the alimentary system of the fly, PAD2 expression is increased and the protein is relocated to the surface of the

parasite. Thus, its higher expression in PCF rather reflects the thermo-regulated expression of the protein than stage specificity. The combination of a st specific carboxylate-transporter (PAD1) and a thermo-regulated one (PAD2), allows st parasites to perceive citrate/*cis*-aconitate in the fly gut in a temperature-dependent manner. The transduction of the citrate/*cis*-aconitate signal via the PAD receptors leads then to the development of PCF cells in the alimentary system of the fly.

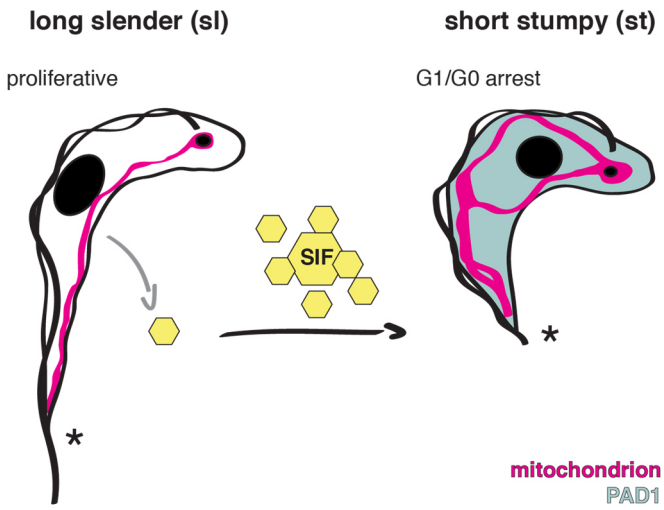

Figure 4: The differentiation from the long slender to the short stumpy stage. Schematic representation of a long slender (sl, left) and a short stumpy (st, right) parasite. The proliferating sl form secretes the stumpy induction factor (SIF). The accumulation of SIF with rising parasitemia induces the differentiation from the sl to the st stage. The characteristic changes in cell dimension and flagellar length (indicated by asterisk) upon developmental transition are illustrated. Also, the reorganization of the mitochondrion (magenta), from a slim and elongated shape in the sl stage to an elaborated branched form in st parasites, is shown. The expression of the st specific 'protein associated with differentiation 1' (PAD1) is indicated as well (grey).

Though RNA-synthesis is generally reduced in the st stage (Amiguet-Vercher et al., 2004), other examples for the differential gene expression during st development are the up-regulation of *ESAG9* transcripts or the down-regulation of the sl-specific haptoglobin–haemoglobin receptor (Barnwell et al., 2010; Vanhollebeke et al., 2008). Another characteristic of the st stage is the silencing of the active *VSG* expression site (ES), the region of the genome encoding the actively transcribed *VSG* (Amiguet-Vercher et al., 2004). Thus, st cells cannot escape the immune response of the host anymore via antigenic variation and have to maintain their surface coat without *de-novo* synthesized VSGs. In part this is compensated by the higher endocytosis rate of st parasites, ensuring a higher rate of VSG recovery and destruction of VSG-bound antibodies via internalization (Engstler et al., 2007). This could also explain the increased resistance to antibody-mediated killing of st parasites compared to the sl cells

(McLintock et al., 1993). An additional explanation is the down-regulation of the haptoglobin–haemoglobin receptor as it is responsible for the uptake of TLF and thus TLF-mediated killing of trypanosomes is prevented in st parasites (Vanhollebeke et al., 2010). Therefore, st parasites can outlive sl cells at peak parasitemia and the transmissibility of the parasites is increased. It remains elusive how st parasites can dominate the trypanosome population over longer periods like in chronic infection if the differentiation is solely density-dependent and the irreversibly arrested cells have a limited life span (MacGregor et al., 2011).

2.3.3 The molecular mechanisms of stumpy differentiation

First evidence for the existence of a factor inducing st development was obtained by the observation that trypanosomes stall proliferation when treated with plasma of infected animals with high parasitemia (Seed and Sechelski, 1989). Next, it was shown that the factor is secreted by the parasite itself as st development could be induced *in vitro* in a density-dependent manner (Reuner et al., 1997). This further implicated that the factor accumulates over time and thus induces developmental transitions once a critical threshold in the concentration is reached.

Such a scenario is reminiscent to a quorum sensing mechanism of several prokaryotes. This mechanism involves (i) a signaling molecule, (ii) a receptor that perceives this signal and (iii) its transduction via signaling cascades, which ultimately leads to developmental changes. Vassella and colleagues termed the signaling molecule for st differentiation SIF (stumpy induction factor) and revealed that it is a soluble compound with low molecular weight (Vassella et al., 1997). They provided evidence that monomorphic cells, even though they have lost the capability to differentiate to the st stage, still produce SIF. Therefore, and due to the differentiation to a "st-like" stage, when treated with an analogue of cyclic adenosine monophosphate (cAMP), monomorphic trypanosomes are suggested to be "signal-blind" (Breidbach et al., 2002; Reuner et al., 1997). However, SIF evaded several attempts to identify its exact biochemical nature and remains elusive to date. Besides, it is unknown if SIF is perceived by a cell surface receptor or is able to pass the membrane via a selective channel or through diffusion. It is also unknown if the signaling cascade is initiated from the extracellular or intracellular milieu.

The intracellular signaling during st development is also still mysterious. Early experiments suggested a role of cAMP during sl/st transition. A two- to threefold increase in cAMP concentration was measured at peak parasitemia followed by a concomitant decline when st forms appeared (Mancini and Patton, 1981). This was further supported by the finding that treatment of pleomorphic cells with SIF enriched medium caused an increase in cAMP levels (Vassella et al., 1997). A membrane permeable cAMP analogue, 8-pCPT-2´-O-Me-cAMP

(pCPT-cAMP), inhibited growth of trypanosomes due to an arrest in G1/G0-phase and induced differentiation to the st stage (Vassella et al., 1997). Therefore, it was generally accepted that cAMP is the second messenger that mediates the SIF signal until evidence arose that not cAMP *per se* but rather its hydrolysis products cause the differential transition (Laxman et al., 2006). When monomorphic trypanosomes were treated with a hydrolysis resistant and membrane permeable cAMP analogue, no anti-proliferative effect was observed. When the cAMP hydrolysis products AMP or adenosine were added, a comparable effect to the treatment with pCPT-cAMP was observed, meaning proliferation was inhibited and the cells arrested in the G1/G0-phase of the cell cycle (Breidbach et al., 2002; Laxman et al., 2006). Further, the depletion of cyclic nucleotide specific phosphodiesterases (PDEs) of *T. brucei* caused a dramatic increase in intracellular cAMP levels. This disrupted cytokines and caused cell death but did not promote st development in the BSF form (Oberholzer et al., 2007). Additional evidence for the role of the cAMP hydrolysis products in st differentiation is provided by a study of the protein kinase target of rapamycin (TOR) 4. Knock-down of *TOR 4* inhibited growth of monomorphic parasites as they developed to a st-like stage and addition of hydrolysable cAMP or AMP resulted in a decrease in TOR4 expression, whereas the hydrolysis resistant cAMP analogue was not sufficient to cause a reduction (Barquilla et al., 2012). Thus, the expression of a negative regulator of st differentiation is controlled by a hydrolysis product of cAMP and not the compound itself.

The molecular components involved in the SIF pathway are largely unidentified and the integration of the known ones in a network or signaling cascade is puzzling. Besides the TOR4 kinase, a zinc finger kinase (ZFK) was shown to play a role during st differentiation. The knock-out of ZFK in pleomorphic cells affected growth and caused an increase in the rate of sl to st transition (Vassella et al., 2001). A comparable phenotype was observed when a null mutant of the mitogen-activated protein kinase (MAPK) 5 in a pleomorphic strain was analyzed. These cells differentiated earlier to the st stage and infection of mice resulted, consequently, in a reduced parasitemia (Pfister et al., 2006). Recapitulatory, TOR4, MAPK5 and ZFK can be considered as negative regulators of st differentiation and as sl retainers (reviewed in Mony and Matthews, 2015).

A recent study identified a couple of additional factors involved in st development using a genome wide RNAi library screen in combination with 8-pCPT-cAMP/AMP treatment. If cells were able to escape 8-pCPT-cAMP/AMP mediated growth retardation once RNAi was induced, it was assumed that the genes affected by RNAi are involved in the perception or transduction of the st differentiation signal. Several potential components of the SIF pathway were thereby identified, further validated by individual knock-down and screening for SIF resistance (Mony et al., 2013). It was shown that members of a *Ser/Thr protein phosphatases of type 1 (PP1)* gene array are essential for st differentiation, as their simultaneous knock-

down prevented developmental transition. A dual specificity phosphatase (DsPhos) seems to be involved in the transduction of differential cues as well. Depletion of a potential YAK kinase resulted in an elevated resistance to SIF pathway signals and thus prolonged presence of sl cells. Similarly, RNAi mediated knock-down of members of a *NEK kinase* array caused a delay in st differentiation. The contribution of a mitogen-activated protein kinase (MAPK) cascade was indicated as sl cells did not react anymore to SIF after knock-down of a protein with a MEKK domain. Further, hypothetical proteins with so far unknown function were found to play a role during sl/st transition. Some of them possess domains indicating a potential mitochondrial function, which could imply that also mitochondrial proteins have an essential role in the initial differentiation process.

Thus, Mony and colleagues could identify a couple of components of the SIF pathway including phosphatases and kinases, but their exact function, targets or order in the signaling cascade remains mostly unknown (reviewed in Mony and Matthews, 2015; Mony et al., 2013). At the moment they propose a simplistic model in which st development is controlled by the balance of sl retainers and st inducers. They assume that sl retainers preserve the sl state of a cell as they are constitutively expressed at this stage. Once SIF accumulation reaches a threshold, sl retainers are repressed while st inducers are activated. The balance is shifted towards st inducers causing an irreversible commitment of the cell, which ultimately leads to the morphological transition of the parasite (reviewed in Mony and Matthews, 2015).

2.4 The variant surface glycoprotein

The survival of trypanosomes within their mammalian host mainly depends on their protein surface coat, which consists of a monolayer of approximately 10^7 identical copies of the variant surface glycoprotein (VSG) (Jackson et al., 1985). The importance of this protein is already implied by its abundance, as VSG makes up 10% of the total protein amount of the BSF. VSGs are homodimers composed of two monomers with an approximate molecular weight of 55 kDa. The N-terminal domain is oriented towards the extracellular space, while the glycosylphosphatidylinositol (GPI)-anchor of the short C-terminal domain tethers the protein to the plasma membrane of the parasite (Blum et al., 1993; Ferguson et al., 1988). The densely packed VSG coat shields the parasite from the extracellular environment as antibodies cannot penetrate this physical barrier of the cell (Schwede et al., 2011). However, the VSG is highly immunogenic and provokes a fast reaction of the host' immune system. At low antibody titers, the parasite internalizes antibodies that bind to the VSGs by a high rate of endocytosis. One equivalent of the complete surface coat is exchanged every 12 minutes via endo- and exocytosis at the posterior end of the cell, the flagellar pocket (Engstler et al., 2004). This process is supported by the free diffusion of the VSG molecules on the plasma membrane and a hydrodynamic force that is generated by the anterior directed movement of the cells (Engstler et al., 2007; Hartel et al., 2015). Within the cell, the VSG is recycled to the cell surface while the antibodies are degraded in the lysosome (Engstler et al., 2007). However, this system for immune evasion is only sufficient at low antibody titers as high antibody titers result in a drastic reduction of parasitemia.

2.4.1 Antigenic variation

All parasites that express a distinct VSG variant will be cleared once the immune system of the host mounts a VSG variant-specific antibody response and the antigen levels are high. Some parasites express another *VSG* gene of the great repertoire of *VSGs* due to a stochastic switch in expression. If this variant is immunologically novel for the immune system, the parasites survive and replicate until also this variant is recognized by the host. Thus, typical waves of parasitemia arise during the infection with trypanosomes. Such strategies for altering the surface proteins in order to evade the host immune response are referred to as antigenic variation and are a common phenomenon in bacterial, fungal as well as protozoan pathogens (reviewed in Deitsch et al., 2009).

Antigenic variation in trypanosomes is based on the expression of a single *VSG* gene out of a great repertoire. More than 2,000 *VSG* genes and pseudo-genes are encoded in the genome

of the parasite, which consists of 11 megabase chromosomes and approximately 100 minichromosomes (Cross et al., 2014; Wickstead, 2004). The vast majority of the *VSG* genes (≈80%) is localized in silent *VSG* arrays in the subtelomeric region of the megabase chromosomes while the remaining genes are encoded on minichromosomes (Berriman et al., 2005). *VSG* genes are exclusively transcribed from specialized regions of the genome, the VSG expression sites (ESs), which are located at the telomeric ends of the megabase chromosomes (Figure 5). Approximately 15 ESs are present in the genome but only one is transcriptionally active at any given time (Hertz-Fowler et al., 2008).

Each ES represents a transcriptional unit controlled by one promotor that is localized approximately 50 kbp upstream of the end of the ES and is recognized by RNA polymerase I (PolI). Other components of the ES are the *expression site associated* genes (*ESAGs*) and a large region of repetitive DNA sequences (70 bp repeats) that are located upstream of the telomere-proximal *VSG*. The complete ES is transcribed into a polycistronic pre-mRNA, which is then further processed via *trans*-splicing and polyadenylation to the mature mRNAs of the individual genes (reviewed in Liang et al., 2003). Although the general architecture of the ESs is similar, they differ in the composition as well as in the number of *ESAGs*. The coding sequences of the different *ESAGs* can also vary between ESs. It is suggested that the expression of different ESs could provide advantages for the survival of the parasite in diverse host environments (reviewed in Pays, 2006; reviewed in Pays et al., 2001).

Figure 5: Schematic model of a consensus ES of *Trypanosoma brucei*. As the order of the *ESAGs* (*1-8)* varies between the different ESs, the consensus succession is represented (Hertz-Fowler et al., 2008). All of the ESs described so far consist of a PolI promotor (arrow) and a telomere-proximal *VSG* (black box), with the 70 bp repeats (grey box) located upstream. A circle indicates the telomere and the blues boxes the different *ESAGs (1-8)*.

2.4.2 The mechanisms of antigenic variation

Switching the expression from one *VSG* to another can occur by two main mechanisms. One mechanism is a so-called *in situ* switch, which represents a transcriptional change as the previously active ES is silenced while another ES is activated. In contrast, the other mechanism is based on the recombinational exchange of the *VSG* gene within the active ES.

Such a genomic rearrangement can be achieved by different mechanisms. The telomeric *VSG* exchange (Figure 6, left) is caused by a cross-over of the chromosome ends (Pays et al.,

1985). Consequently, parts of the active and the silent ES, including the *VSGs*, are exchanged and both *VSG* genes are maintained within the genome. Most frequently, a silent but functional *VSG* gene is duplicated into the active ES (Figure 6, middle). It replaces the previously active *VSG* gene, which results in the deletion of the previously ES-resident *VSG* gene. During this process termed gene conversion, either a *VSG* gene from the silent *VSG* arrays or from an inactive ES can serve as donor for gene duplication. Often not only the *VSG* open reading frame (ORF) is duplicated but also upstream and downstream regions, which are thought to serve as recombination sites. The 70 bp repeats upstream of the *VSG* gene are often used for recombination and then represent the 5' border for translocation (Hovel-Miner et al., 2016; Liu et al., 1983). However, if a silent ES is the donor for gene conversion, duplication can extend further upstream (Pays et al., 1983). In this case, the copy can expand even to the promotor region located 50 kbp upstream, resulting in the duplication of a complete ES (Hertz-Fowler et al., 2008). Downstream, conserved regions in the 3' end of the *VSG* ORF or its untranslated region (UTR) can provide homology for recombination (Bernards et al., 1981). Nevertheless, gene conversion can extend down to the chromosome ends (de Lange et al., 1983). If the cross over takes place within the *VSG* ORF, e.g. in the homologues regions of the 3' end, a new mosaic *VSG* gene is generated consisting of parts of the resident and parts of the duplicated *VSG* (Pays et al., 1983). Mosaic *VSG* genes can also be produced by combining parts of different pseudogenes using this segmental gene conversion, but it is unclear how they are assembled and where in the genome (reviewed in Marcello and Barry, 2007; Thon et al., 1989).

The described recombinational changes are exclusively based on DNA rearrangement as the *VSG* within the active ES is replaced and no changes in the transcriptional status of the active ES occur. However, 15 ESs are present in the genome of *T. brucei* and only one is transcribed at any given time while the others remain silent. The expressed VSG can also be switched due to a change in the activity of the ESs (Figure 6, right). During an *in situ* switch, the transcriptional status of the ESs changes when a previously silent ES is activated while the actively transcribed ES is silenced (Bernards et al., 1984; Michels et al., 1984). It is suggested that remodeling of the chromatin structure is essential for this process as the active ES is depleted of nucleosomes while silent ESs are tightly packed in heterochromatin (Figueiredo and Cross, 2010; Stanne and Rudenko, 2010). Several proteins, especially chromatin modifiers, are involved in the maintenance of the inactive status of the silent ES. However, it remains elusive how a transcriptional switch takes place. The molecular players are widely unknown and even the order of events - first ES-attenuation or first ES-activation - is controversial (Batram et al., 2014; reviewed in Borst and Ulbert, 2001).

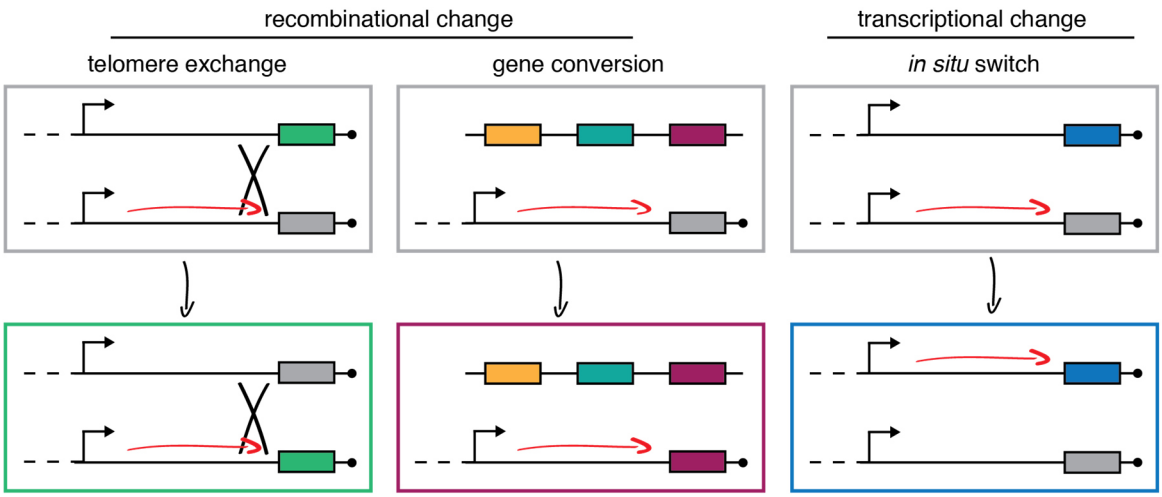

Figure 6: The main mechanisms of antigenic variation in *Trypanosoma brucei*. The colored borders represent one parasite expressing a single *VSG* from the active telomeric ES (box with the same color). The transcribed ES is indicated by a red arrow and the ES promotor by a black arrow. In the upper panel, the "grey" *VSG* (grey box) is expressed and silent *VSGs* (colored boxes) are located in subtelomeric regions (upper middle) or in inactive ESs (upper left and right). The expressed *VSG* gene can be switched by different mechanisms. Recombinational mechanisms involve either the exchange of chromosome ends of inactive and active ESs (telomere exchange, left) or the duplication of a silent *VSG* into the active ES (gene conversion, middle). During an *in situ* switch (right), a new ES is transcriptionally activated and the active ES is silenced. In all cases, a successful switch results in the expression of a new VSG variant as indicated by the colored borders in the lower panel. (adapted from Taylor and Rudenko, 2006)

2.4.3 The advantages of the different mechanisms of antigenic variation.

When comparing transcriptional and recombinational changes, the question arises what the advantage of the different methods could be. Via gene conversion and telomere exchange, the parasites could exploit the enormous *VSG* repertoire and persistent parasitemia might be ensured. Segmental gene conversion creates mosaic *VSGs* that are novel to the immune system of the host and could prevent an exhaustion of the *VSG* repertoire (Futse et al., 2008). This would also prevent immunity of a large proportion of the host population to trypanosomes, a phenomenon termed herd immunity (Futse et al., 2008). These hypotheses are supported by the observation that a hierarchal order of the recombinational exchange of *VSG* genes exists, which is most likely based on the genomic location (Morrison et al., 2005). Telomere-proximal *VSG* genes are used for recombinational switches in the early stage of infections, next, *VSG* genes from silent subtelomeric *VSG* arrays are expressed and mosaic *VSGs* at later stages (reviewed in Marcello and Barry, 2007; Morrison et al., 2005; Thon et al., 1990).

The benefit of *in situ* VSG switching is controversial as only variants within the ESs can be activated, limiting the *VSG* repertoire to the 15 telomeric ES. One possibility is that silent ESs are used to assemble mosaic *VSGs* genes, which are transcribed once the ES is activated.

However, the most prominent theory is the host range hypothesis, which argues that the benefit of possessing and activating different ESs is due to the *ESAGs* and not the ES-resident *VSGs* (reviewed in Pays, 2006; reviewed in Pays et al., 2001). For example ESAG6 and 7 form a heterodimeric receptor for the uptake of transferrin, and their sequence differs between the ESs. Bitter and colleagues showed that the small ES-associated variations of transferrin receptors affect the binding affinity for transferrins from different hosts and thus influence the growth of the parasites (Bitter et al., 1998). Furthermore, when trypanosomes are exposed to sera from different hosts, they tend to switch the actively transcribed ES to one that allows better iron uptake due to the expression of a slightly altered transferrin receptor (Bitter et al., 1998; Gerrits et al., 2002). An adenylate cyclase encoded by *ESAG4* is also involved in the interaction of the host and the parasite as the early innate immune response of the host is affected by the expression of this ESAG (Salmon et al., 2012). Another example underlying the relevance of ESAGs in the interplay of host and trypanosomes is the resistance of *T. brucei rhodesiense* to the human TLF as it depends on the expression of a distinct ES containing the gene encoding for SRA (Xong et al., 1998). Taken together, these results suggest a role of ESAGs at the interface of host - parasite interaction. Thus, the survival in various hosts could be maximized due to differential ESs expression, which in turn is achieved via *in situ* switching.

Although the different switching mechanisms may provide different advantages for the parasite, no conclusions about their relative importance can be drawn. The contribution of each mechanism to the survival of the parasite and thus their relevance could be deduced from the frequency at which the different events occur. However, switching rates already greatly differ between monomorphic (10^{-4}-10^{-6} switches per cell per generation) and pleomorphic (10^{-2}-10^{-3} switches per cell per generation) strains (Aitcheson et al., 2005; Turner and Barry, 1989). An enormous discrepancy in the frequency of the different switching events exists between various experiments using monomorphic cells. For example in studies of Kim and Cross *in situ* switchers were almost absent (less than 2%) and gene conversion was dominant (Kim and Cross, 2010, 2011). In contrast, Devlin et al reported that around 30% of the observed switching events was caused by *in situ* switches and only 10% by gene conversion (Devlin et al., 2016). In the experiments of Aitcheson and colleagues *in situ* switching was the most frequent event with 77% of all switchers (Aitcheson et al., 2005). In pleomorphic cells, only one study discriminated between the different switching mechanisms and showed that gene conversion is dominant (Robinson et al., 1999). Consequently, it remains unclear to what extent each switching strategy contributes to the survival of the parasites, especially considering that only successful switching events are measured and that switching is often only discriminated at the level of VSG expression.

2.5 Maintenance of monoallelic expression of the ES

Monoallelic expression of genes is not a unique feature of trypanosomes. It is a widespread phenomenon and the molecular mechanisms are puzzling. One of the best-known and first discovered examples for monoallelic expression is the X-chromosome inactivation in female mammalian cells. In this case, the dosage of X-linked genes has to be compensated, as two copies are present in female cells. This is achieved by a random silencing of one of the two X-chromosomes (reviewed in Schulz and Heard, 2013). In the 1960s, Pernis and colleagues showed that monoallelic expression occurs as well for autosomal genes, as B-cells express only one of two immunoglobulin alleles (Pernis et al., 1965). In the 1990s it was demonstrated that in the mammalian central nervous system each olfactory sensory neuron expresses only a single olfactory receptor out of a repertoire of more than 1,000 genes, which are epigenetically silenced (reviewed in Monahan and Lomvardas, 2015). At the same time, it became clear that the malaria parasite *Plasmodium falciparum* expresses only one of 60 *var* genes which encode the surface molecule '*P. falciparum* Erythrocyte Membrane Protein 1' (PfEMP1) (Smith et al., 1995; Su et al., 1995). In this case, monoallelic expression is based on a complex interplay between the var promotor and introns as well as epigenetic mechanisms (reviewed in Guizetti and Scherf, 2013). However, monoallelic expression of *VSGs* was discovered already more than 10 years earlier in trypanosomes (Hoeijmakers et al., 1980). Up till now evidence has accumulated that among others epigenetic modifications are involved in allelic exclusion in trypanosomes but a comprehensive model is still missing.

2.5.1 The transcriptional status of the active ES and its nuclear context

The active ES differs from the silent ones in its transcriptional activity. The *VSG* mRNA of inactive ESs is 10^4-10^5-fold less abundant compared to the active one (Figueiredo et al., 2008; Yang et al., 2009). However, this great discrepancy in the transcriptional levels between active and inactive ESs is only observed at the telomere-proximal *VSGs*. Interestingly, 80% of the mRNAs of the promotor-proximal *ESAG6* originate from the active ES, while the other 20% stem from silent ESs (Ansorge et al., 1999). Integration of resistance cassettes in the promotor-proximal regions of inactive ESs resulted in drug resistance (Navarro and Cross, 1996). Although the drug resistance was 100-fold lower compared to the integration into the promotor of the active ES, this suggested that inactive ESs are not completely silenced. This was further confirmed by Yang and colleagues, who showed that promotor-proximal genes were transcribed at approximately 0.3% of the full activity levels, whereas telomere-proximal genes were transcribed only at 0.01% (Yang et al., 2009). Taken together, these studies

demonstrated that low-level transcription occurs at silent ESs, suggesting a regulation of ES transcription at the level of elongation or initiation.

Evidence for the first hypothesis comes from reverse transcription-PCR analyses of different ES components. These indicated that RNA elongation and processing are not functional at silent ESs, although transcription is initiated (Vanhamme et al., 2000). Further support was provided by a study analyzing the ES transcription levels of single cells, which showed that transcription initiates simultaneously at the different ESs (Kassem et al., 2014). However, these studies could not exclude differences in the rate of transcription initiation. Nevertheless, the authors argued that the transcription machinery is recruited to the promotor of silent and active ESs and thus transcription is initiated, whereas it is controlled later on.

On the other hand, the theory that the activity of the ES is regulated via the initiation of transcription, is supported by studies of the class I transcription factor A (CITFA). This factor recognizes PolI promotor sequence, which are present at the beginning of the transcriptional units of *rRNA*, *procycline* or *VSG* genes, and is essential for their PolI-dependent transcription (Brandenburg et al., 2007). Nguyen and colleagues could show that the CITFA-2 and CITFA-7 subunits predominantly occupy the promotor region of the active ES compared to silent ones (Nguyen et al., 2013). The presence of high CITFA levels at the promotor region of the active ES correlated with the occupancy of PolI as well as elevated levels of promotor-proximal unspliced RNA. Depletion of CITFA-7 led to a decrease in the PolI occupancy and RNA abundance. For these reasons, the authors argued that ES transcription is regulated at the level of transcription initiation. Furthermore, they suggested that the initiation of ES transcription by PolI is restricted to the expression site body (ESB) due to the accumulation of CITFA to the promotor.

The ESB is a extranucleolar compartment that consists of an accumulation of PolI and harbors the active ES (Navarro and Gull, 2001). It was shown that after replication of the active ES, both ES copies remain in the single ESB. The sister chromatids are connected via a cohesin complex and are separated considerably later after replication than other gene loci. Thus, it is ensured that one active ES is inherited to one daughter cell (Landeira et al., 2009). The depletion of subunits of the cohesin complex led to a premature separation of the sister chromatids and to an increase in the frequency of *in situ* switching events. Therefore, it was argued that the cohesin complex is essential for the maintenance of the active ES. It has been also suggested that the exclusion of silent ESs from the ESB is responsible for monoallelic expression in trypanosomes (Landeira and Navarro, 2007; Navarro and Gull, 2001). It remains elusive if the ESB indeed excludes other ESs or rather assembles around the active one and no factor specific for the ESB is known up to date.

Interestingly, a recent study identified a protein termed VSG exclusion1 (VEX1) that localizes in a distinct subnuclear spot in the vicinity of the ESB (Glover et al., 2016). This protein is sequestered at the telomere of the active ES in a transcription-dependent manner. A role of VEX1 in ES exclusion has been demonstrated as both its knock-down and overexpression resulted in the derepression of inactive ESs, especially the silent *VSGs*. It seems likely that ESB and VEX1 foci have distinct roles for the regulation of ES transcription, but the exact nature of these foci as well as their contribution to monoallelic expression is not understood.

Nevertheless, the identification of these two foci suggests that the nuclear architecture also plays an important role for the monoallelic expression of the *VSG*. This hypothesis is further supported by the location of the silent ESs in the periphery of the nucleus, where the heterochromatin is positioned (reviewed in Glover et al., 2013). Interestingly, it was shown that the nuclear periphery protein-1 (NUP-1) co-localizes with the telomeres in the periphery of the nucleus (DuBois et al., 2012). NUP-1 is most likely a component of the nuclear envelope, which is essential for the maintenance of the nuclear pore complex and the positioning of the telomeres. Strikingly, the rearrangement of the telomeres upon depletion of NUP-1 was accompanied by a derepression of silent ESs, suggesting that the nuclear position of the telomeres is an important factor for the silencing of the ESs due to the formation of heterochromatin (DuBois et al., 2012).

2.5.2 Epigenetic silencing of the ES

Several recent studies support the idea that epigenetic silencing and chromatin structure play an important role for monoallelic expression in trypanosomes. The differences in the transcriptional activity between silent and active ESs are accompanied by differences in the chromatin architecture of the ESs. While the active ES is depleted of nucleosomes, the silent ESs are tightly packed in heterochromatin (Figueiredo and Cross, 2010; Stanne and Rudenko, 2010).

It has been shown that nucleosomes are indeed essential for the silencing of inactive ESs. First, the depletion of the core histone H3 led to a 11-fold derepression of the promotor region of silent ESs, but not of the downstream-localized *VSG* (Alsford and Horn, 2012). Second, knock-down of the linker histone H1 resulted in an increase of PolI-mediated transcription with the most prominent effect at the promotor region of silent ESs, where a sixfold increase was observed (Pena et al., 2014; Povelones et al., 2012).

Several chromatin remodelers and modifiers have been shown to play a role in determining and maintaining the transcriptional status of ESs. The SWI2/SNF2-like ATPase TbISWI was the first chromatin remodeler discovered to have a function in ES regulation (Hughes et al.,

2007). TbISWI was shown to bind to silent and active ESs, whereas its lowest concentration was observed at the promotor region. Down-regulation of TbISWI led to a 60-fold derepression of a promotor-proximal *GFP* reporter within a silent ES and at least fivefold increase in the transcript levels of previously silent ES-resident *VSGs* (Stanne et al., 2011). The nucleoplasmin-like protein (NLP), the regulator of chromosome condensation 1-like protein (RCCP) and the phenylalanine/ tyrosine rich protein (FYRP) were identified as interaction partners of TbISWI using tandem affinity purification (Stanne et al., 2015). All three identified proteins display a similar distribution to TbISWI at PolI-transcribed loci and possess domains typical for chromatin proteins (Narayanan et al., 2011; Stanne et al., 2015). NLP was previously shown to particularly affect ES regulation as an at least 45-fold derepression of silent ES promotor regions occurred upon its depletion, while no changes in silent *VSG* transcription were observed (Narayanan et al., 2011). A similar increase in ES promotor-proximal transcription occurred, when the other two TbISWI interaction partners were knocked down (Stanne et al., 2015).

In addition, the histone deacetylase DAC3 seems to play a role in the silencing of ES promotors, even though no direct association of the protein with ESs was demonstrated (Wang et al., 2010). The SPT16 subunit of the trypanosome facilitates chromatin transcription (FACT) complex is highly enriched at the promotor regions of silent ESs. Its depletion results in the derepression of the promotor, but not the telomere regions of silent ESs (Denninger and Rudenko, 2014; Denninger et al., 2010). Knock-down of histone chaperones, either the chromatin assembly factor 1b (CAF-1b) or the anti-silencing factor 1A (ASF1A), led to an increase in the transcript levels of a *GFP* reporter integrated in the promotor region of an inactive ES (Alsford and Horn, 2012). In both cases, the increased transcription did not extend up to the telomere-proximal *VSG*, similar to the phenotype observed upon depletion of H3.

In summary, the depletion of numerous proteins associated with chromatin remodeling or modification caused derepression of silent ESs. In all cases, a pronounced effect was only observed at the promotor-proximal regions, whereas the telomeric *VSGs* were only mildly affected or not all. Hence, the chromatin structure has a severe impact on the transcription of the promotor-proximal region. This indicated that in particular epigenetic modifications are involved in the silencing of the promotor-proximal regions of inactive ESs.

However, the exclusive expression of the *VSG* gene from a subtelomeric position led to the hypothesis that also the telomere structure is involved in the regulation of *VSG* expression. The repression of genes adjacent to telomere, termed telomere positioning effect (TPE), was first described in the fruit fly *Drosophila melanogaster* and the budding yeast *Saccharomyces cerevisiae* (Gottschling et al., 1990; Levis et al., 1985). TPE has now been identified in a wide range of organisms and it is evident that this process involves the formation of heterochromatin via hypoacetylation of histones (reviewed in Blasco, 2007). TPE as an epigenetic regulation

mechanism in trypanosomes was first suggested by Glover and Horn, who generated *de novo* assembled telomeres at different positions within the genome (Glover and Horn, 2006). Thereby, they provided evidence that the telomeres repress PolI-mediated transcription locally, with the strongest effect being observed within the ES. Direct evidence for a role of the telomere in ES-silencing comes from the analysis of the telomere-binding protein RAP1 (repressor/activator protein 1). Knock-down of this protein caused the derepression of silent ESs (Yang et al., 2009). The most prominent effect was observed at the telomere-proximal regions and the expression of all *VSGs* from silent ESs was monitored. This VSG co-expression was accompanied by the formation of multiple PolI foci within the nucleus. A component of the inositol phosphate pathway, the phosphatidylinositol 5-phosphatase (TbPIP5-Pase), was recently identified as an interaction partner of RAP1 (Cestari and Stuart, 2015). Similar to RAP1, knock-down of the telomeric TbPIP5-Pase resulted in a pronounced increase in the transcription of inactive ESs, whereby the silent *VSGs* were affected the most. Interestingly, depletion of another component of the pathway, the inner membrane located phosphatidylinositol 5-kinase (TbPIP5K), caused the same derepression phenotype. Knock-down of either protein was also accompanied by the formation of numerous PolI foci and a redistribution of RAP1. Thus, metabolites of the inositol phosphate pathway, which are known to have an impact on chromatin remodeling in other eukaryotes, seem to play a role in the regulation of ES transcription in trypanosomes as well (Steger et al., 2003; Yildirim et al., 2013). Moreover, knock-down of TbPIP5K or TbPIP5Pase implied a repositioning of the telomeres in the nucleus, which strengthens the suggested impact of the nuclear context for monoallelic *VSG* expression.

In summary, the depletion of telomere-binding proteins resulted in a contrasting phenotype to the phenotype observed upon depletion of chromatin proteins (described above). While in the latter case derepression was more pronounced in the promotor-proximal regions, RAP1- or inositol pathway-dependent silencing was stronger at telomere-proximal regions. These results argue together for a regulation of the ES from both ends, promotor and telomere (reviewed in Günzl et al., 2015).

The importance of chromatin for complete ES-silencing irrespective of promotor or telomere positioning becomes apparent by studies of the disruptor-of-telomeric silencing (DOT) 1B protein. This methyltransferase is responsible for the trimethylation of histone H3 at the lysine 76 (H3K76) and is not essential for trypanosomes (Janzen et al., 2006). The knock-out of *DOT1B* caused a 10-fold derepression of a resistance cassette, which was integrated in the promotor region of a silent ES. Simultaneously, a 10-fold increase of the *VSG* transcripts from the same ES was observed. Thus, the trimethylation of H3K76 is essential for complete ES-silencing as depletion of DOT1B led to a similar derepression of promotor and telomere regions of a silent ES (Figueiredo et al., 2008). The same study demonstrated also a role of the

trimethylation during *in situ* switching as the completion of the switching process in DOT1B knock-out cells took up to five times longer than in the parental cell line. It was indicated more recently that DOT1B is as well essential for the reconstruction of the chromatin during the developmental differentiation from the BSF to the PCF (Dejung et al., 2016). Thus, DOT1B is essential for processes involving the reorganization of the chromatin structure such as monoallelic expression, *in situ* switching and developmental transition.

All of the so far discussed epigenetic modifiers and regulators are involved in maintaining ES-silencing. It has been unequivocally demonstrated that the chromatin structure is crucial for silencing ESs and, consequently, regulation of ES transcription. In addition, an epigenetic factor, the high mobility group box protein TDP1, was shown to be essential for the efficient transcription of the active ES (Narayanan and Rudenko, 2013). This architectural protein seems to be present at the completely active ES, whereby it is fivefold enriched at the promotor region of the active ES compared to silent ones. TDP1 distribution at PolI transcription units is inversely related to the occupancy pattern of histone H3, and TDP1 depletion led to an increase of the histones H3, H2A and H1 at these loci. Simultaneously, a reduction of the *VSG* transcript levels by 40-90% was observed upon induction of TDP1 RNAi. The authors suggested that TDP1 replaces histones at PolI-transcribed loci and thus facilitates transcription by maintaining the open chromatin structure of the active ES. In contrast, a recent study indicated that transcription is stalled before the status of the chromatin changes (Aresta-Branco et al., 2015). Aresta-Branco and colleagues could show that the transcription of the active ES was reduced prior to the formation of heterochromatin during the differentiation from the BSF to the PCF. They also demonstrated that the open chromatin state of the active ES was maintained when its transcription was stalled using a system to inducibly block transcription. Furthermore, they found evidence that TDP1 is essential for this transcription-independent regulation of the chromatin.

In conclusion, many epigenetic factors involved in the regulatory network of the ESs have been identified. Most of them play a role in the silencing of the ESs either in the region of the promotor or telomere, but in general the structure of the chromatin seems to influence the transcription. However, even basic questions such as the connection between transcription and chromatin structure are discussed controversially and the complex interplay between all the identified factors remains poorly understood.

2.5.3 The regulation of the ES and replication

In recent years, evidence of a connection between ES regulation and progression in the cell cycle has been accumulating. For example, the ES promotor-proximal derepression upon knock-down of histone H3 or the chaperones CAF-1b and ASF1A was accompanied by an

accumulation of cells in the 2K1N cell cycle stage (Alsford and Horn, 2012). When H3 or CAF-1b were depleted, an increase in transcription of silent ESs was observed predominantly once the cells completed the S-phase. In contrast, transcription initiated at silent ESs in all cell cycle stages, when ASF1A was down-regulated. The authors suggested that the chaperons play a replication-dependent role in the recycling or assembly of chromatin. Likewise, the knock-down of SPT16 caused an accumulation of cells in the 2K1N stage and the increase in silent ESs transcription occurred specifically in the G2/M cell cycle phase (Denninger et al., 2010). These results not only highlighted the crucial role of chromatin in ES-silencing, but indicated that the maintenance of the chromatin structure is connected with the cell cycle, especially at the level of DNA replication. Further evidence for this hypothesis is provided by a study of the origin recognition complex (TbOrc1), which is essential for replication. Depletion of TbOrc1 resulted in the derepression of silent ES-resident *VSGs* and an increase in the switching frequency, notably *in situ* switching (Benmerzouga et al., 2014). In combination, these results pointed towards a function of TbOrc1 in the control of monoallelic *VSG* expression. A recent study found indications for a precise association of the timing of ES replication, which occurs early during DNA replication, and the transcription of the active ES (Devlin et al., 2016). Nevertheless, a connection between replication and monoallelic expression has not been directly shown so far. Another recent study sorted cells via FACS in G1-, S- and G2-phase and combined FAIRE (Formaldehyde-assisted isolation of regulatory elements) with qPCR quantification to determine changes in the chromatin structure of the ESs during cell cycle progression (Aresta-Branco et al., 2015). Changes in the nucleosome abundance between the different cell cycle stages could not be detected. The authors concluded that trypanosomes possess a cell cycle-independent mechanism to maintain an open chromatin structure. However, using this technique a 10-100 fold difference between active and inactive ESs could be measured, whereas an active ES possesses a 10^4-10^5 higher transcriptional activity compared to a silent one (Figueiredo and Cross, 2010; Figueiredo et al., 2008). It seems likely that FAIRE is only suitable for detecting drastic changes in the nucleosome architecture and hence a connection between cell cycle and chromatin formation cannot be excluded.

Consequently, the monoallelic expression of the ESs seems to be controlled at diverse levels: chromatin structure, epigenetic modifications, replication, transcription initiation as well as elongation. Though numerous factors involved in these processes have been identified so far, a comprehensive model of the regulation of the ES is still missing.

2.6 Aim of the thesis

A major step forward in the understanding of ES regulation was recently provided by a study of Batram and colleagues (Batram et al., 2014). They mimicked an *in situ switch* by simulating the activation of a new ES using the inducible overexpression of a second VSG. Overexpression resulted in the replacement of the endogenous VSG (VSG 221) by the ectopic variant (VSG 121) and thus the surface coat was exchanged. However, not only the endogenous *VSG* was silenced but also the complete native ES was gradually attenuated starting at the telomere. They also demonstrated that the ES-attenuation is dependent on epigenetic modifications, as in a DOT1B knock-out background VSG overexpression did not trigger this process. Once the active ES was attenuated, the parasites displayed a prolongated G1-phase of the cell cycle. These dormant cells expressed the st marker PAD1 and showed an enhanced competence for differentiation to the procyclic stage. The gain in developmental competence was only transient and the cells reentered the cell cycle after five days of induction. Thus, it was suggested that ES-attenuation causes the transition of the parasites to a reversible st-like stage and hence ES-attenuation links antigenic variation to development.

The aim of this study was to investigate the indicated connection between ES-attenuation and st development. This question could not be properly addressed in the previous experiments as the used monomorphic cells have lost the capability to differentiate to the st stage. Therefore, in thesis pleomorphic parasites with full developmental competence were used to determine the impact of ectopic overexpression of VSG 121 and VSG 118. An ES-promotor reporter cell line was generated to assess the ES-activity and a stumpy reporter trypanosomes line was used to monitor developmental transition. In addition, stumpy characteristics such as the cell cycle arrest in the G1-phase, the elaboration of the mitochondrion and the competence to complete the parasite cycle were analyzed. As the results showed that ES-attenuation is a density-independent trigger for st development, the combined effect of the triggers was investigated. Also, preliminary RNAseq analyses using monomorphic and pleomorphic VSG overexpressors were conducted to identify potential regulators of the ES.

The VSG overexpression in pleomorphic cells supported previous assumptions that distinct mechanisms are present in trypanosomes to induce *VSG*- and ES-silencing. As the *VSG* with its wild type UTRs was sufficient to induce ES-attenuation and/or *VSG*-silencing, it seemed likely to us that a consensus sequence within the *VSG* or its UTRs is involved in the processes. It is improbable that the 'motif' for silencing is concealed within the ORF as the *VSGs* differ greatly in their sequence. However, the 3’ UTR of all *VSGs* share two conserved motifs: the 16mer and the 8mer (Berberof et al., 1995; Engstler, unpublished data). The first one was shown to be essential for mRNA stability, whereas the function of the 8mer remains elusive

(diploma thesis Batram, 2009; Berberof et al., 1995). Therefore, the other aim of my thesis was to investigate if the 16mer motif could play a role for ES-attenuation and/or *VSG*-silencing. For this purpose, a *GFP* reporter coupled to a *VSG* 3'UTR containing either a functional or defective 16mer was targeted to different genomic loci. Another *VSG* coupled to a functional or defective 3'UTR was integrated downstream of the endogenous *VSG* as a 'native-reporter'. Growth analyses as well as quantifications of the VSG and/or GFP expression were conducted to determine the impact of the presence of a defective 16mer within the DNA. To investigate how *VSG*-silencing can be achieved independently of ES-attenuation, the previous hypothesis that VSG levels are regulated *in trans* based on the *VSG* 3'UTR was further pursued. It was investigated if the VSG controls its own expression, using the ectopic VSG overexpression system in a monomorphic reporter cell line constitutively expressing a *GFP* with *VSG* 3' UTR.

3 Results

3.1 VSG overexpression in pleomorphic cells

In a previous study, the activation of a new expression site (ES) during an *in situ* switch was simulated using the inducible overexpression of an ectopic VSG (Batram et al., 2014). This showed that the endogenous *VSG 221* was silenced and the active ES gradually attenuated upon induction of VSG 121 overexpression. The attenuation of the active ES was accompanied by a retardation in growth due to a prolongation of the G1-phase of the cell cycle. These cells displayed an enhanced sensitivity towards triggers for procyclic development and hence showed characteristics of stumpy (st) parasites. However, the VSG overexpressors neither exit the cell cycle nor had a limited life span like it is the case for st parasites. The VSG overexpressors escaped growth retardation as they reentered the cell cycle after five days of VSG overexpression. Therefore, it was suggested that ES-attenuation-induced growth retardation could provide a window of enhanced developmental competence. The growth-retarded cells could represent an intermediate developmental stage, which is not yet committed to develop to the st stage. These intermediate forms could either reenter the cell cycle as slender (sl) parasite or differentiate further to the procyclic stage (PCF) in the presence of appropriate triggers. However, the experiments were conducted with monomorphic cells, which have lost the capability to differentiate to the st stage. Therefore, it remained unexplored if ES-attenuation indeed links antigenic variation and developmental competence.

To further address this hypothesis, the VSG overexpression system was employed in this thesis in the pleomorphic trypanosome strain EATRO 1125 (serodeme AnTat1.1). These parasites posses full developmental competence and are able to complete the parasite cycle in contrast to the routinely used monomorphic cells (Delauw et al., 1985; Engstler and Boshart, 2004). Even though pleomorphic parasites are closer to the natural situation they are rarely used for investigations for several reasons. First, unlike monomorphic cells, pleomorphic blood stream form (BSF) parasites cannot be cultivated in HMI-9 medium. They have to be either cultured on agarose plates or in viscous medium supplemented with methylcellulose (Vassella and Boshart, 1996; Vassella et al., 2001). Second, the cell densities in the experiments with pleomorphic parasites need to be strictly controlled due to their ability to differentiate to the cell cycle-arrested short st stage. The pleomorphic trypanosomes react to the parasite secreted stumpy induction factor (SIF) and thus developmental transition to the cell cycle-arrested st stage is induced at high densities (density-induced st parasites) (Reuner et al., 1997; Vassella et al., 1997). For this reason, HMI-9 medium supplemented with 1.1% (w/v) methylcellulose was used to cultivate the parasites in the experiments throughout this thesis. This allowed a better control of parasite densities compared to the cultivation on plates and thus maintenance of the sl stage could be ensured. However, this method is time consuming and results in reduced cell yield, as the methylcellulose has to be removed from the cultures via dilution and

filtration to harvest the cells. Besides the reactivity on SIF, pleomorphic cells display an increased sensitivity to occurring changes in temperature or environment. Therefore, pleomorphic sl parasites have to be carefully handled at densities below 6x 10^5 cells/ml avoiding environmental stress (drop in temperature, frequent medium exchange or pH variations) (reviewed in McCulloch et al., 2004). Lastly, the available genomes of two *T. brucei brucei* strains revealed discrepancies and the pleomorphic strain EATRO 1125 (AnTat1.1) has not been sequenced up till now (Becker et al., 2004; Berriman et al., 2005; Brems et al., 2005). Thus, genetic manipulations in the pleomorphic strain are difficult and prone to failure. Nevertheless, in this study we have succeeded in employing the VSG overexpression constructs in different generated pleomorphic reporter cell lines.

3.1.1 Suitable reporter cell lines

Based on previous studies, I decided to generate two reporter cell lines to analyze the impact of ectopic VSG overexpression on pleomorphic parasites. First, a st reporter cell line was generated by transfecting pleomorphic AnTat1.1 13-90 parasites, natively expressing VSG A1.1 ($A1.1^{ES}$), with the GFP:$PAD1_{UTR}$ construct (plasmid p4231, courtesy of Mark Carrington) (Figure 7 A, B). This plasmid integrates into the tubulin intergenic region and consists of a *GFP* open reading frame (ORF) with a nuclear retention signal, which is coupled to the 3´UTR of the `*protein associated with differentiation 1´* (*PAD1*) (Figure 7 A). A sequence motif within the UTR mediates the exclusive increase of *PAD1* transcription upon developmental transition from the sl to the st stage (Dean et al., 2009; MacGregor and Matthews, 2012). Immunostaining of density-induced st parasites with a PAD1 antibody illustrates that a green fluorescent nucleus reflects the expression of the st specific surface protein in the generated GFP:$PAD1_{UTR}A1.1^{ES}$ cell line (Figure 7 B). Thus, the appearance of a green fluorescent nucleus marks the differentiation to the st stage in this trypanosomes line. Second, a reporter cell line was generated to monitor the expression of the active ES (GFP^{ESpro}) (Figure 7 C, D). For this purpose, a *GFP* ORF with *aldolase* UTRs was inserted in the pLF12 plasmid, which targets conserved regions in the promotor region of the ESs (Figure 7 C) (Figueiredo et al., 2008). First, the GFP insert was amplified from the pLew82∆op PDEB1 eGFP plasmid (J. Jung) using the primers JJ44 and HZ16. Ligation of the HindIII digested insert and pLF12 plasmid generated the construct pLF12 GFP. Transfection of the pleomorphic $A1.1^{ES}$ cell line with the SacI/KpnI linearized plasmid yielded the $GFP^{ESpro}A1.1^{ES}$ cell line, which displayed a strong cytoplasmic GFP signal (Figure 7 D).

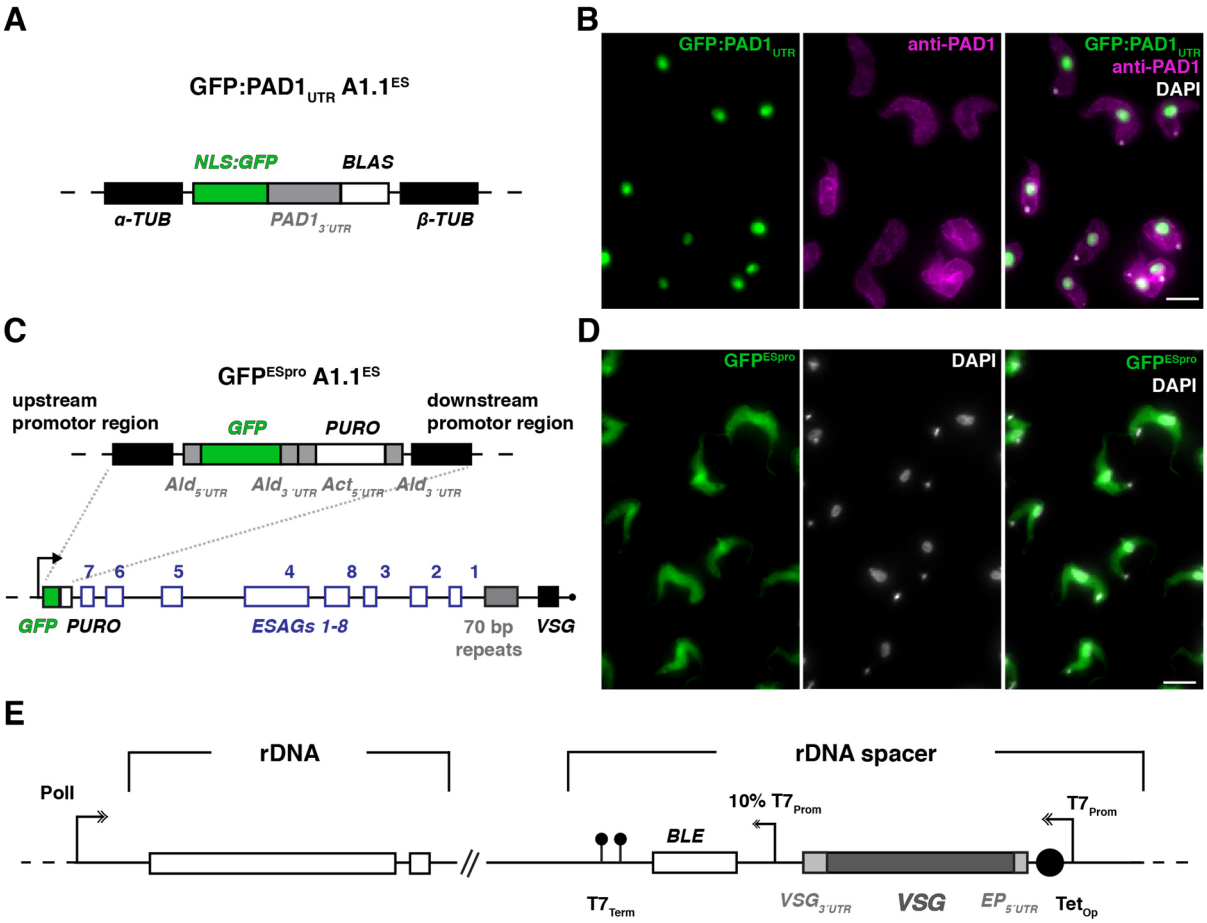

Figure 7: Pleomorphic reporter cell lines for VSG overexpression. **(A)** Schematic representation of the GFP:PAD1$_{UTR}$ construct, which consists of a *GFP* ORF with a nuclear localization signal (*NLS:GFP*, green box), the *PAD1* 3'UTR (grey box) and a *blasticidin* resistance cassette (*BLAS*, white box). Integration of the plasmid into the tubulin intergenic region (black boxes) of pleomorphic AnTat1.1 13-90 parasites generated the GFP:PAD1$_{UTR}$A1.1^{ES} cell line. The 3'UTR of the st marker protein PAD1 is sufficient to mediate the st-specific expression. Thus, the presence of a green fluorescent nucleus marks st parasites in the GFP:PAD1$_{UTR}$A1.1^{ES} cell line. **(B)** Immunofluorescence analysis of density-induced st parasites of the GFP:PAD1$_{UTR}$A1.1^{ES} cell line using a PAD1 antibody. The expression of the nuclear GFP:PAD1$_{UTR}$ st reporter (green, left) and the PAD1 surface protein (magenta, middle) is shown. The DAPI stain (grey) is presented in the merged image only (right). Scale bar: 5 µm. **(C)** Schematic representation of the GFP^{ESpro} construct and its integration into a consensus ES (described in chapter 2.4.1). The plasmid consists of a *GFP* ORF (green box) with *aldolase* UTRs (grey boxes) and a puromycin resistance cassette (*PURO*, white box). The construct targets conserved regions in the promotor region of the ESs (black box). Integration of the GFP^{ESpro} construct into the active ES of pleomorphic AnTat1.1 13-90 parasites natively expressing VSG A1.1 generated the GFP^{ESpro} A1.1^{ES} cell line. **(D)** SI parasites displayed a homogenous cytoplasmic GFP-signal (green, left). The DNA was counterstained with DAPI (grey, middle). Scale bar: 5 µm. **(E)** Schematic representation of pRS.121 plasmid, which was used for ectopic VSG 121 overexpression. The ectopic *VSG* (dark grey box) with its native 3'UTR and an *EP1* 5'UTR (light grey box) integrates into the ribosomal spacer. The VSG expression is regulated by a T7-promotor (T7$_{prom}$) under the control of a tetracycline operator (Tet$_{op}$). The expression of the *phleomycin* resistance cassette (*BLE*, white box), localized downstream of the ectopic *VSG*, is controlled by an additional T7-promotor with reduced activity (10% T7$_{Prom}$). T7 terminators (T7$_{Term}$) terminate the transcription of both.

The pRS.121 plasmid was used for inducible VSG 121 overexpression (Figure 7 E) (Batram et al., 2014). This construct is based on the pLew82v4 vector, which targets the ribosomal spacer (24,009; Addgene plasmid). The T7-polymerase transcribes the *VSG 121* ORF with the corresponding wild type 3'UTR and an *EP1* 5'UTR as well as the *phleomycin* (*BLE*) resistance cassette. The latter one is constitutively expressed, but the T7-promotor upstream of the *VSG* ORF is under the control of a tetracycline repressor. Thus, the inducible expression of high VSG levels upon the addition of tetracycline is ensured as previously shown by Batram et al.. Transfection of both reporter lines with the VSG 121 overexpression construct yielded the trypanosome lines GFP:PAD1$_{UTR}$A1.1^{ES}121^{tet} and GFP^{ESpro}A1.1^{ES}121^{tet}.

3.1.2 Ectopic VSG 121 overexpression causes distinct growth phenotypes

The GFP:PAD1$_{UTR}$A1.1^{ES}121^{tet} cell line showed a surprising phenotypic plasticity upon induction of VSG 121 overexpression (Figure 8). In a subset of clones, growth stopped immediately after induction of VSG 121 overexpression as the cells divided only once within 24 hours (Figure 8 A). Afterwards, the parasites stalled growth for at least four days with an average population doubling time (pdt) of more than 40 hours. Then, the cells slowly resumed growth and regained their original pdt within five to nine days post induction. The non-induced cells grew slightly slower (pdt 7 hours) than the parental cell line (pdt 6 hours). In other clones, VSG 121 overexpression had only minor effects on the growth of the parasites (Figure 8 B). The pdt of the cells decreased from six to seven hours upon induction of VSG 121 overexpression. The same phenotypic plasticity became apparent when the GFP^{ESpro}A1.1^{ES}121^{tet} cell line was analyzed (Figure 8 C, D). This demonstrated that the different growth responses occurred reproducibly upon VSG 121 overexpression and independently of the used pleomorphic parental cell line. The clones were termed according to their growth phenotype 'growth-arrested' if they stopped growth immediately upon induction (four of 14 clones) or 'proliferating' if they kept proliferating (five of 14 clones). However, in both cell lines intermediate growth phenotypes were observed: some clones responded to VSG 121 overexpression with a slowed growth, but did not arrest (five of 14 clones, data not shown). I decided to focus all further analysis on clones displaying the distinct growth responses, proliferating or growth-arrested, as it could not be excluded that the intermediate clones were mixed populations.

For proliferating and growth-arrested clones, Western blot analyses were used to examine whether the clones overexpressed VSG 121 upon the addition of tetracycline (Figure 8 E, F). This showed that the ectopic VSG 121 was overexpressed within 24 hours independently of the growth response of the clones. Thus, the different growth phenotypes were not caused by a deficient overexpression system.

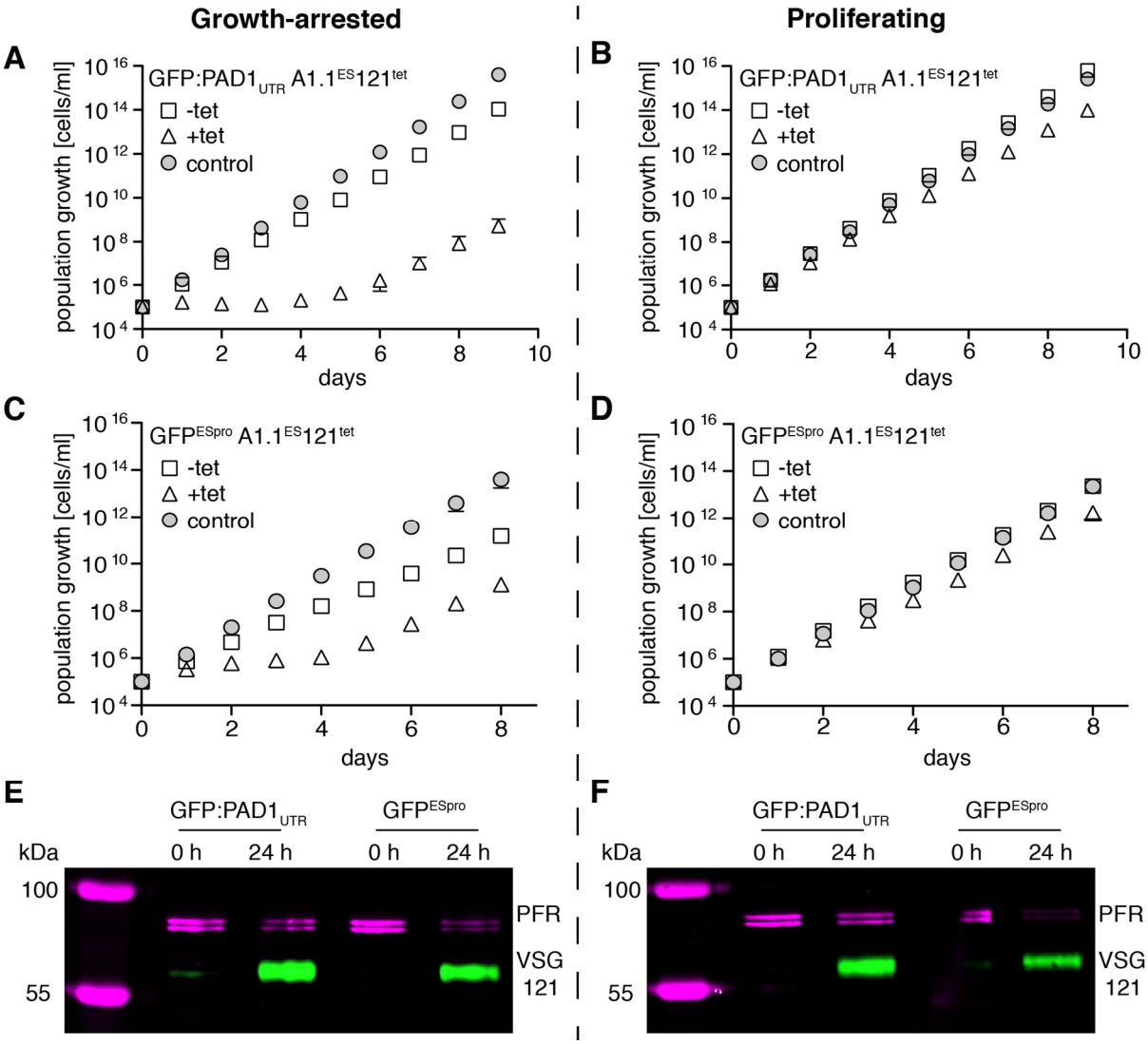

Figure 8: Ectopic overexpression of VSG 121 causes distinct growth phenotypes in pleomorphic trypanosomes. **(A-D)** Representative growth curves of a growth-arrested (left) and a proliferating (right) clone of the **(A, B)** GFP:PAD1$_{UTR}$A1.1^{ES}121^{tet} and the **(C, D)** GFP^{ESpro}A1.1^{ES}121^{tet} cell line. Tetracycline-induced (triangles) and non-induced (squares) parasites were analyzed. The parental AnTat1.1 13-90 cell line (circles) served as a control. Means (± SD) of three experiments of one clone are shown in each graph. Due to the small standard deviation the error bars are not visible. **(E, F)** Western blot analysis of **(E)** a growth-arrested clone and **(F)** a proliferating clone of the GFP:PAD1$_{UTR}$A1.1^{ES}121^{tet} (GFP:PAD1$_{UTR}$) and the GFP^{ESpro}A1.1^{ES}121^{tet} (GFP^{ESpro}) cell line, respectively. Protein samples of non-induced parasites (0 h) and cells induced with tetracycline for 24 hours were analyzed. Western blots were stained with a VSG 121 antibody (green) and a paraflagellar rod (PFR) antibody (magenta) as loading control.

3.1.3 Ectopic VSG 121 overexpression causes a stable exchange of the surface coat

Western blot analyses demonstrated that proliferating and growth-arrested clones expressed the ectopic VSG upon induction. However, Western blots analyze the expression of a protein on the population level and a subpopulation of cells may not express the ectopic VSG. The

homogeneity of the VSG expression was therefore analyzed by immunofluorescence on the single cell level (Figure 9).

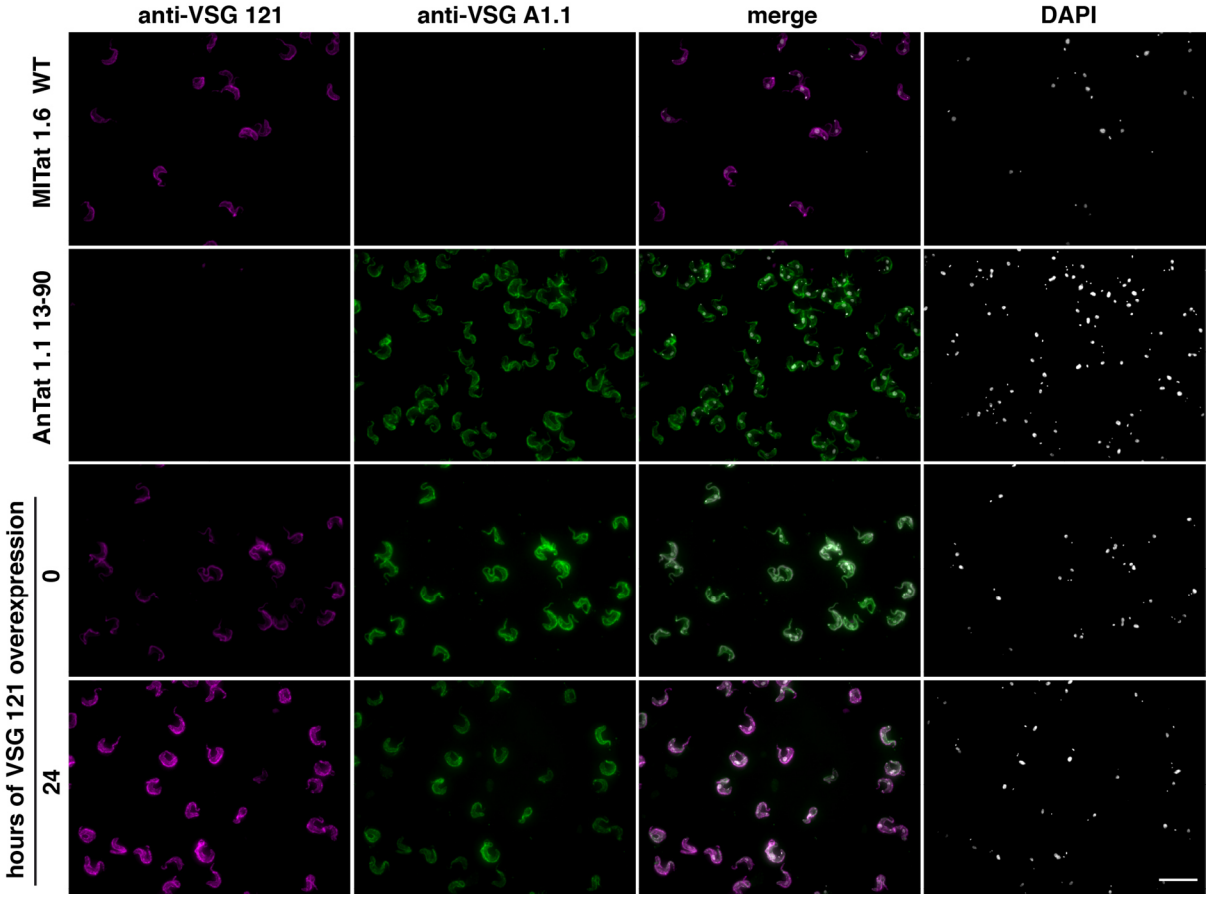

Figure 9: Overexpression of the ectopic VSG 121 causes surface coat exchange. Immunofluorescence analysis of a proliferating clone of the GFP:PAD1$_{UTR}$A1.1^{ES}121^{tet} cell line. Non-induced cells (0 h) and VSG 121 overexpressors induced for 24 hours were stained with antibodies against the ectopic VSG 121 (magenta) and the endogenous VSG A1.1 (green). MITat1.6 wild type cells natively expressing VSG 121 and the parental AnTat1.1 13-90 cells natively expressing VSG A1.1 served as controls for antibody specificity. The DNA was stained with DAPI (grey). Scale bar: 20 µm.

VSG 121 expression was induced in the GFP:PAD1$_{UTR}$A1.1^{ES}121^{tet} cell line for 24 hours and the induced as well as the non-induced cells were simultaneously stained for VSG 121 (magenta) and VSG A1.1 (green). As a control for the specificity of the antibodies, MITat1.6 wild type cells natively expressing VSG 121 and the parental AnTat1.1 13-90 cell line natively expressing VSG A1.1 were stained as well: both showed the expected staining only for the expressed VSG (Figure 9, upper panels). The immunofluorescence data confirmed the Western blot data of Figure 8 B: the ectopic VSG increased and the endogenous VSG decreased upon induction. The parasites exchanged their surface coat within 24 hours of VSG overexpression as exemplified by an immunofluorescence of a proliferating clone (Figure 9,

lower panel). Parasites that reacted not with VSG 121 overexpression to the addition of tetracycline were never observed within the populations, which ruled out that a small subpopulation was in some way resistant to the inducible system.

I also analyzed how stable the exchange of the surface coat was. Therefore, a proliferating clone of the GFP:PAD1$_{UTR}$A1.1^{ES}121^{tet} cell line was induced for seven and 28 days and analyzed using immunostaining as above (Figure 10).

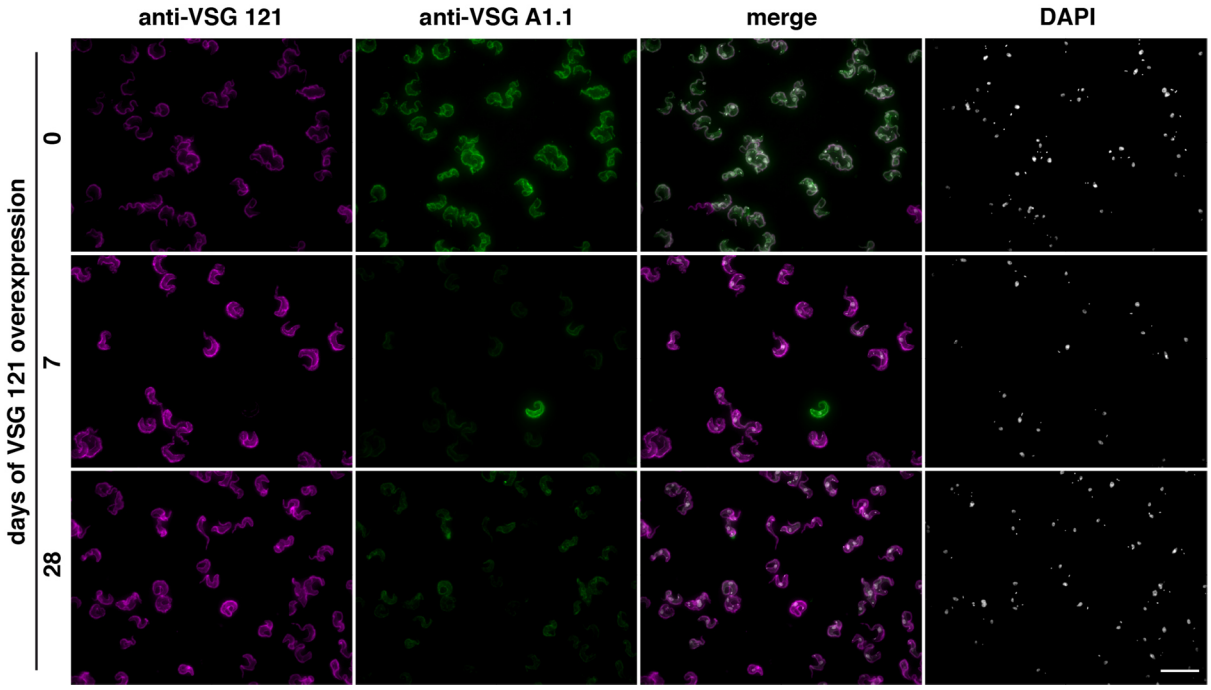

Figure 10: The ectopic VSG 121 is expressed over prolonged periods. Immunofluorescence analysis of a proliferating clone of the GFP:PAD1$_{UTR}$A1.1^{ES}121^{tet} cell line. Non-induced cells (0 h) and VSG 121 overexpressors induced for seven or 28 days were stained with antibodies against the ectopic VSG 121 (magenta) and the endogenous VSG A1.1 (green). The DNA was stained with DAPI (grey). After seven days >95% (in 200 cells) of the parasites expressed the ectopic VSG and after 28 days >93% (in > 250 cells). Scale bar: 20 µm.

The immunofluorescence analyses showed that the cells can express the ectopic VSG over extended periods. Only in a few cases (less than 5% in 200 cells), it was observed that the ectopic VSG did not dominate anymore the cell surface after seven days of induction. However, these cells did not outgrow the VSG 121 overexpressors as illustrated by the comparison of day seven and 28 of induction. Thus, the reverted parasites had no advantage compared to the VSG overexpressors. In summary, the immunofluorescence analysis demonstrated that the VSG coat is exchanged within 24 hours of induction and that the ectopic VSG can be stably expressed over prolongated periods.

3.2 *VSG*-silencing can be uncoupled from ES-attenuation

The previous results have demonstrated that ectopic VSG overexpression caused distinct growth phenotypes, which were not the result of a deficient overexpression system. In both cases, clones that arrested in growth or kept proliferating, the overexpression of VSG 121 resulted in an exchange of surface coats within 24 hours of overexpression. However, the cause for the different growth phenotypes remained unclear. To answer this question, VSG mRNA and protein levels as well as the transcriptional status of the active ES were determined in the different clones during the course of VSG 121 overexpression.

3.2.1 The different growth phenotypes do not result from differences in *VSG*-silencing

Clonal variations in the expression levels upon overexpression of a protein often cause different growth phenotypes. I quantified the mRNA and protein levels of the ectopic VSG in order to compare proliferating and growth-arrested VSG 121 overexpressors. In addition, the expression of VSG A1.1 was measured to determine if the endogenous *VSG* was silenced with similar kinetics in both cases. For this purpose, I used one growth-arrested and one proliferating clone each of the GFP:PAD1$_{UTR}$A1.1^{ES}121^{tet} and of the GFP^{ESpro}A1.1^{ES}121^{tet} cell lines. Total RNA and protein were extracted from non-induced cells (0 h) and from VSG 121 overexpressors induced for up to 48 hours. The VSG mRNA and protein signals were normalized and are given relative to the wild type VSG levels (100%). VSG 121 levels were adjusted to MITat1.6 wild type cells natively expressing VSG 121 and VSG A1.1 levels to the parental AnTat1.1 13-90 cell line expressing VSG A1.1.

The *VSG* mRNA amount of the cells was measured by quantitative Northern blots using dot-blotting and labeling of mRNAs by fluorescent probes (Figure 11). First, I found that the *VSG* levels changed comparably in clones displaying the same phenotype, irrespectively of the parental cell line (GFP:PAD1$_{UTR}$A1.1^{ES} and the GFP^{ESpro}A1.1^{ES}). Thus, clones of both cell lines could be used to compare the *VSG* mRNA levels in growth-arrested (Figure 11 A) and proliferating clones (Figure 11 B). This showed that within four hours of VSG 121 overexpression the *VSG 121* mRNA increased to 82 ± 9% of the wild type levels in growth-arrested and to 99 ± 11% in proliferating clones. In the same time, the endogenous *VSG* mRNA levels decreased to 30 ± 8% in the growth-arrested and to 43 ± 3% in the proliferating clones. The *VSG A1.1* level further decreased within eight hours to approximately 25% of the wild type transcription level in both populations. The *VSG A1.1* levels remained at this low level up to 48 hours. Thus, within eight hours a change in the *VSG* mRNA levels occurred with similar kinetics in both proliferating and growth-arrested clones. Consequently, differences in the initial *VSG* mRNA expression levels cannot explain the different growth phenotypes.

However, after eight hours of induction the *VSG 121* levels started to decrease in the growth-arrested clones, whereas transcript levels remained constant in proliferating ones.

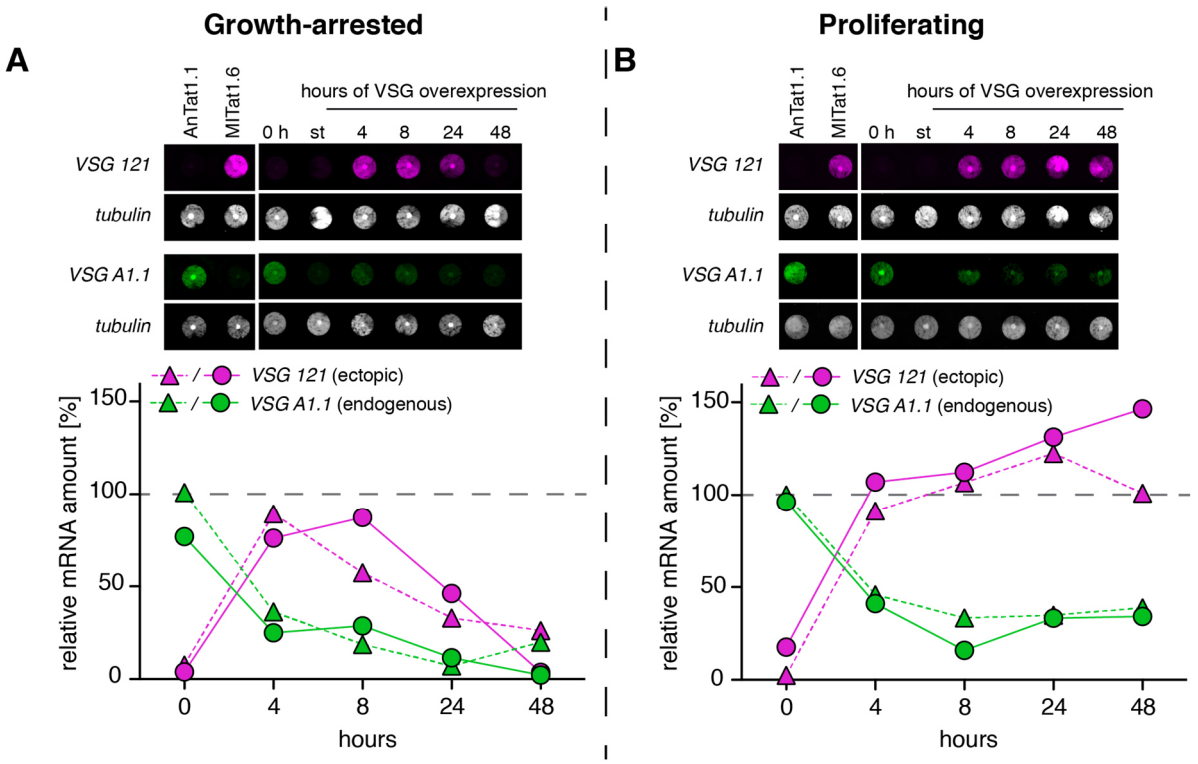

Figure 11: Independent of the growth phenotype, the endogenous *VSG* is down-regulated at the mRNA level upon induction of VSG 121 overexpression. (A, B) The mRNA levels of the endogenous *VSG A1.1* (green) and the ectopic *VSG 121* (magenta) were determined during the course of VSG 121 overexpression. Total RNA samples of **(A)** a growth-arrested and **(B)** a proliferating clone were dot-blotted, stained with fluorescently labeled probes specific to the respective *VSG* and quantified with the Licor Odyssey system (upper panel). Probes either against *VSG 121* (magenta) or *VSG A1.1* (green) were used and the signal was normalized to *tubulin* (grey). Lower panel, quantification of RNA samples of the GFP^{ESpro}A1.1^{ES}121^{tet} (triangles) and GFP:PAD1$_{UTR}$A1.1^{ES}121^{tet} (circles) cell line, respectively. The normalized *VSG 121* mRNA levels (magenta) are given relative to the *VSG* transcript levels of MITat1.6 wild type cells natively expressing VSG 121. The normalized *VSG A1.1* mRNA levels (green) are given relative to the *VSG* transcript levels of the parental AnTat1.1 parasites. The dashed grey line indicates wild type transcript levels (100%).

It has been demonstrated that a reduction of the VSG supply causes a rapid growth arrest in the 2K2N cell cycle stage (Sheader et al., 2005). As the *VSG* mRNA levels dropped after eight hours of induction in growth-arrested clones, I had to analyze if the growth defect is caused by a shortage of the VSG protein. Therefore, the protein levels of the endogenous VSG A1.1 and the ectopic VSG 121 were compared in the different clones (Figure 12). For this purpose, protein samples were dot-blotted on a membrane, which was then stained with antibodies specific for VSG A1.1 or VSG 121 and, as a loading control, histone H3. First, I tested whether

clones derived from different parental cell lines showed similar protein expression kinetics, if they displayed the same growth phenotype upon VSG 121 overexpression. As this was the case (Figure 12), the VSG protein levels could be compared between growth-arrested and proliferating clones.

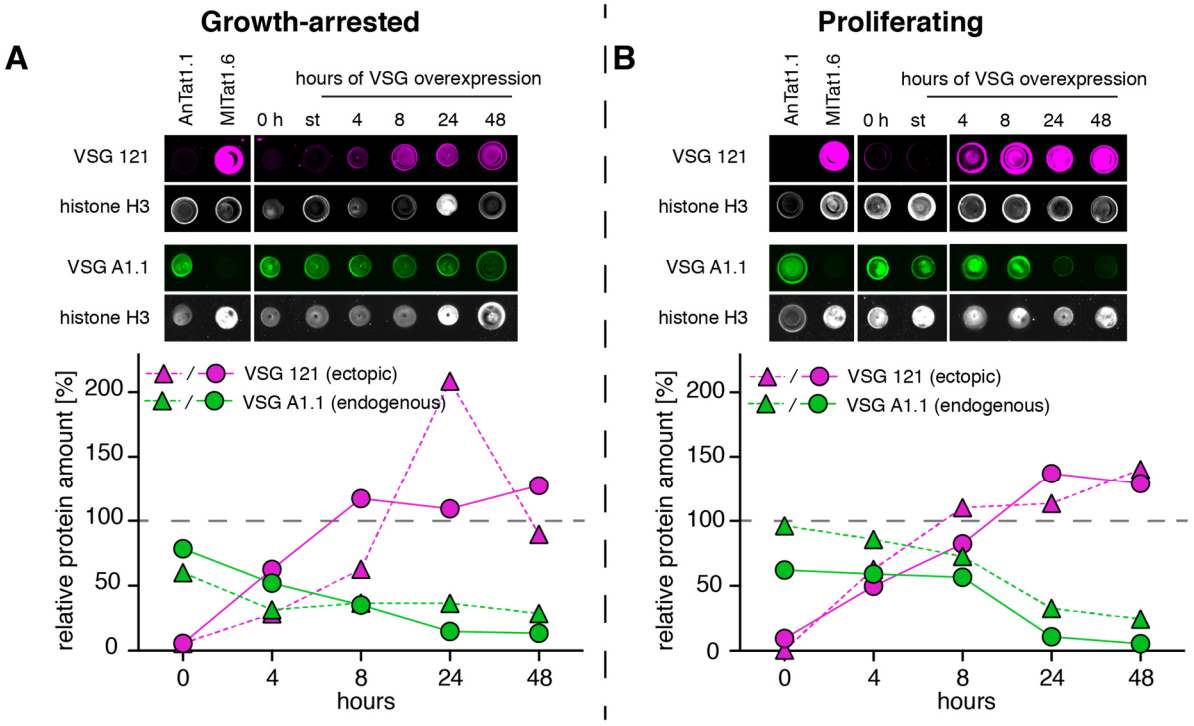

Figure 12: Independent of the growth phenotype, the endogenous VSG is down-regulated at the protein level upon induction of VSG 121 overexpression. (A, B) The protein levels of the endogenous VSG A1.1 (green) and the ectopic VSG 121 (magenta) were determined during the course of VSG 121 overexpression. Protein samples of **(A)** a growth-arrested and **(B)** a proliferating clone were dot-blotted, stained with antibodies and analyzed with the Licor Odyssey system (upper panel). Antibodies either against VSG 121 (magenta) or VSG A1.1 (green) were used and histone H3 (grey) antibodies were used for normalization. Lower panel, quantification of protein samples of the GFP^{ESpro}A1.1^{ES}121^{tet} (triangles) and the GFP:PAD1$_{UTR}$A1.1^{ES}121^{tet} (circles) cell line, respectively. The normalized VSG 121 protein levels (magenta) are given relative to MITat1.6 wild type cells natively expressing VSG 121. The normalized VSG A1.1 protein levels (green) are given relative to the VSG protein levels of the parental AnTat1.1 parasites. The dashed grey line indicates wild type expression levels (100%).

No significant differences between proliferating and growth-arrested clones were observed in the VSG protein levels upon induction of VSG 121 overexpression. Within eight hours of induction, the expression of the ectopic VSG 121 reached approximately 90% of the wild type expression levels irrespectively of the growth phenotype. The VSG 121 levels increased further within 24 hours of induction in all clones. Within the same time, the endogenous VSG decreased to approximately 22% of the wild type expression level. In all clones, the VSG 121

protein levels remained stable at wild type expression levels for up to 48 hours of induction, excluding that a shortage in VSG protein caused the growth arrest. Therefore, variations in the protein expression and hence in the exchange of the surface coat cannot explain the different growth responses upon VSG 121 overexpression.

3.2.2 The transcriptional status of the active ES determines the growth response

Previously, it was shown that ectopic VSG overexpression in monomorphic cells not only caused the silencing of the endogenous *VSG* but also an attenuation of the complete active ES (Batram et al., 2014). It was suggested that the ES-attenuation caused the growth retardation in monomorphic parasites upon induction of ectopic VSG overexpression. Thus, we assumed that differences in the transcriptional status of the active ES could explain the different growth phenotypes of pleomorphic VSG 121 overexpressors. Therefore, the transcriptional activity of the complete active ES of proliferating and growth-arrested clones was analyzed upon induction of VSG overexpression. In accordance with the study of Batram et al., mRNA levels were used a marker for transcriptional activity. This method was chosen for the following reasons: first, direct measurement of transcription for example by nuclear-run on would be difficult in pleomorphic trypanosomes, because high cell numbers are needed (10^9 nuclei/ml), prolonged harvesting may affect transcription and different nuclei preparation cause variability in the transcription levels (Kooter and Borst, 1984; Rudenko et al., 1989). Second, mRNA half-lives are generally short (median half-life of a BSF transcript is 12 min) and thus changes are visible with fast kinetics (Fadda et al., 2014). For the moment, we neglected that changes in mRNA processing or decay could be mistaken for changes in transcription. In the following, the terms ES-activity or transcriptional status will refer to the determined mRNA levels.

Northern blot analysis was used to analyze RNA samples of two clones of the $GFP^{ESpro}A1.1^{ES}121^{tet}$ cell line, which displayed the distinct growth responses upon induction (Figure 13). This cell line has a *GFP* ORF integrated into the promotor region of the active ES. Thus, the amount of *GFP* transcripts can serve as a reporter for the transcriptional status of the complete ES. Results from one quantitative Northern blot showed that the *GFP* mRNA levels decreased within four hours of VSG 121 overexpression in a growth-arrested clone. The *GFP* amount dropped further to less than 50% compared to the level of the non-induced cells within 24 hours of induction (Figure 13 A). An initial decrease in the *GFP* levels was also observed in the proliferating clone, but within 48 hours of VSG 121 overexpression the *GFP* levels remained above 50% of the level of non-induced cells (Figure 13 B). This indicated that the active ES of growth-arrested clones could be less transcribed compared to proliferating VSG 121 overexpressors.

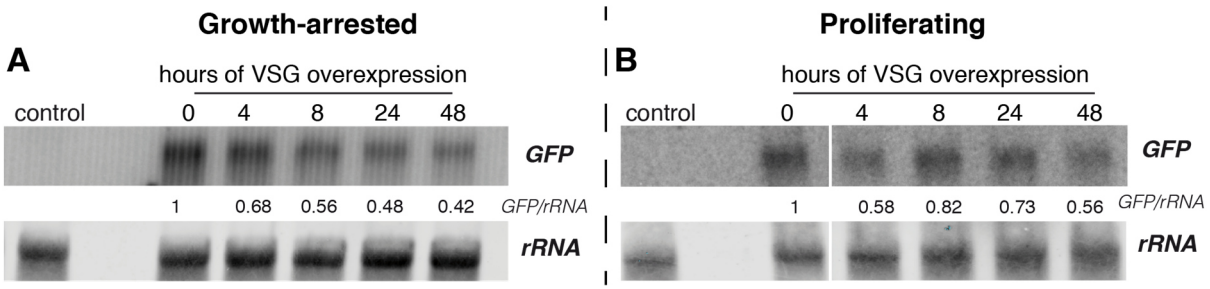

Figure 13: Differences in ES-activity between growth-arrested and proliferating clones during VSG 121 overexpression. **(A, B)** The transcriptional status of the active ES was determined in **(A)** a growth-arrested and **(B)** a proliferating clone of the GFP^{ESpro}A1.1^{ES}121^{tet} cell line. Northern blot analyses were conducted to assess the transcript levels of the *GFP* reporter in the promotor region of the active ES. Total RNA samples of parasites overexpressing VSG 121 for up to 48 hours were analyzed. To detect the *GFP* mRNA, the blots were hybridized with a ^{32}P-labeled probe and the signals were quantified with a phosphorimager. The *GFP* mRNA amounts were normalized to the signal of fluorescently labeled *18s rRNA* quantified with the Licor Odyssey system. The *GFP/rRNA* ratio of the non-induced samples was set to one. The parental AnTat1.1 13-90 cell line, not expressing GFP, served as a control for the specificity of the GFP probe.

Nevertheless, quantifications of Northern blots using radioactive labeling are error prone and display a high variability. Thus, they need to be conducted in replicates for quantitative conclusions. The high effort to cultivate and harvest the large amounts of pleomorphic trypanosomes needed for RNA samples prevented replicates. Consequently, it remained unclear whether the observed differences between growth-arrested and proliferating VSG 121 overexpressors were significant. Besides this, using Northern blot analyses mRNA levels are determined on the population level and variations for example within the cell cycle cannot be excluded. For these reasons, we decided to validated the Northern blot results by a method that requires tenfold less cells and allows the discrimination of different cell cycle stages: mRNA FISH. For this purpose, the highly sensitive single molecule mRNA FISH of the Affymetrix company was used. One drawback of this method is that the number of samples that can be directly compared with each other is limited, as all samples need to be on the same slide.

First, the *GFP* mRNA levels of growth-arrested and proliferating clones of the GFP^{ESpro}A1.1^{ES}121^{tet} cell line were re-quantified upon induction of VSG overexpression (Figure 14 A, B). The *GFP* mRNA levels of cells after 24 and 48 hours of induction of VSG 121 overexpression were compared with the *GFP* levels of non-induced cells of the same cell line (0 h). Density-induced st parasites were analyzed (st) as a negative control because this stage possesses an attenuated active ES (Amiguet-Vercher et al., 2004). In growth-arrested VSG 121 overexpressors, the *GFP* transcripts decreased by 80% after 24 hours of induction and remained at this low level (Figure 14 A). This compared well to the drop of *GFP* mRNA by 90% in the st control. In contrast, the *GFP* mRNA levels did not change significantly in a

proliferating clone within 24 hours of induction and decreased only to 50% within 48 hours of induction (Figure 14 B). Thus, the very sensitive measurements using quantitative *in situ* hybridization confirmed the results obtained from Northern blot analysis: the mRNA levels of the ES-reporter dropped early during the course of VSG 121 overexpression in the growth-arrested clones, whereas changes were less pronounced and occurred later on in the proliferating clones.

Next, we wanted to confirm these results by quantifying an endogenous component of the active ES. As the sequence of the AnTat1.1 ES is unknown, we decided to quantify the transcripts of *ESAG6*, which encodes one subunit of the heterodimeric trypanosome transferrin receptor (Schell et al., 1991). The transferrin receptor is essential for trypanosomes and the encoding gene was present in all functional ESs described to date; it is thus very likely present in the AnTat1.1 ES, too (Hertz-Fowler et al., 2008; Tiengwe et al., 2016). Using density-induced st parasites, we showed that *ESAG6* transcript levels indeed decreased when the active ES was silenced (Figure 14 C). *ESAG6* was reduced by 70% in the st control, which is in accordance with studies from monomorphic parasites demonstrating that approximately 20% of the *ESAG6* transcripts originate from silent ESs (Ansorge et al., 1999). Thus, we concluded that *ESAG6* is indeed part of the active AnTat1.1 ES and quantified its transcription levels in the pleomorphic VSG 121 overexpressors (Figure 14 C, D). In growth-arrested VSG 121 overexpressors, *ESAG6* mRNA dropped to 75% within 24 hours and to 40% within 48 hours, which compares well to the *ESAG6* transcript levels of density-induced st cells (30%) (Figure 14 C). In contrast, no significant changes in the *ESAG6* mRNA could be detected during the course of VSG 121 overexpression in proliferating clones (Figure 14 D).

In summary, the transcription of the active ES differed between growth-arrested and proliferating clones. A fast attenuation of the active ES occurred in growth-arrested clones and the ES-activity decreased to levels similar to those of st parasites possessing a silenced ES. In contrast, the activity of the ES was only mildly decreased in proliferating clones. Thus, we concluded that differences in the transcriptional status of the active ES were responsible for the different growth phenotypes. Interestingly, the endogenous *VSG* was silenced with similar kinetics even though the ES-activity differed between growth-arrested and proliferating clones. Hence, *VSG*-silencing could be uncoupled from ES-attenuation.

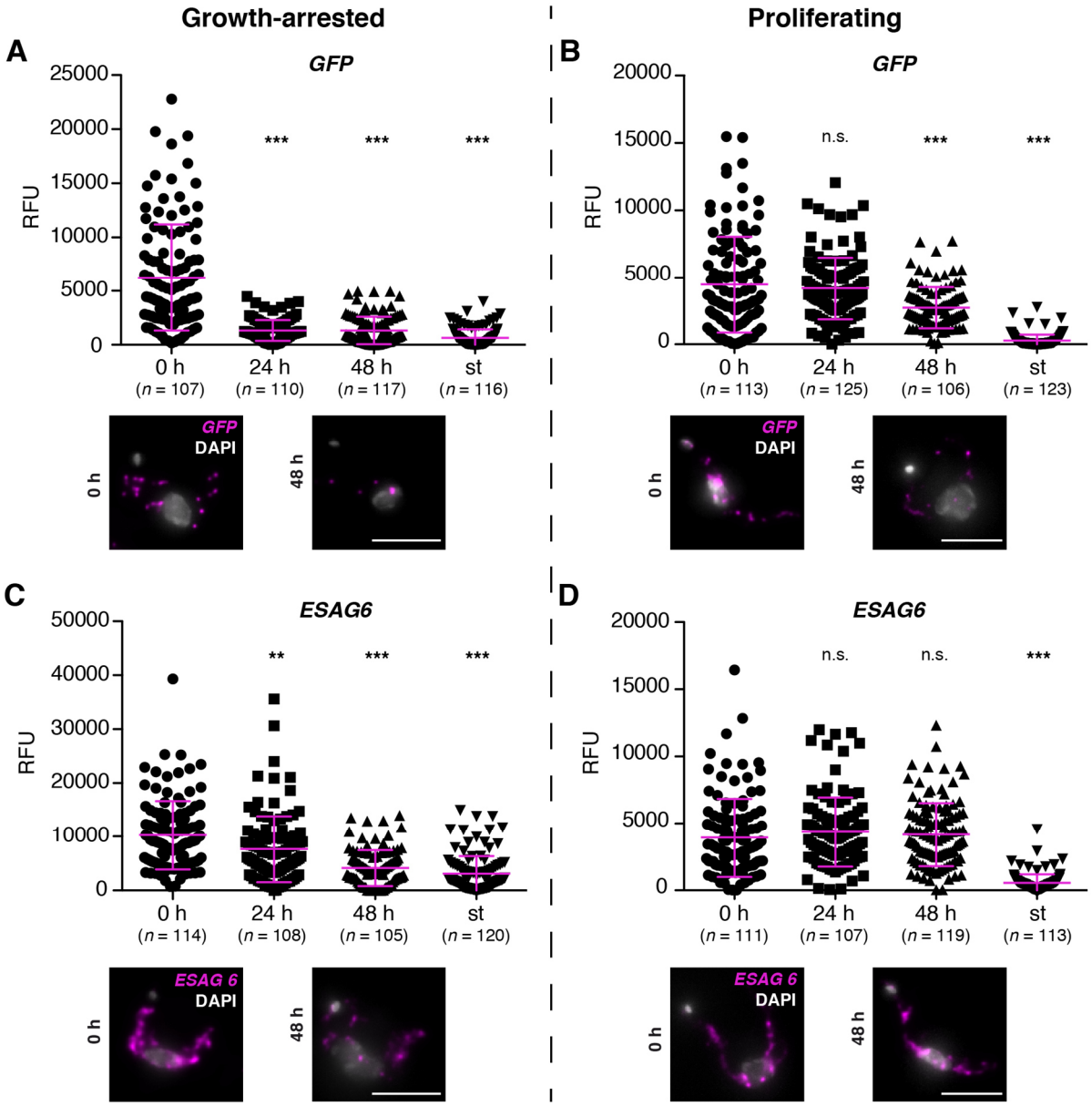

Figure 14: The ES is attenuated in growth-arrested VSG 121 overexpressors only. The transcriptional status of the active ES was determined in **(A, C)** a growth-arrested and **(B, D)** a proliferating clone of the GFP^{ESpro}A1.1^{ES}121^{tet} cell line. **(A, B)** The transcript levels of the *GFP* reporter in the promotor region of the active ES were quantified using mRNA FISH (Affymetrix). **(C, D)** The same method was used to quantify *ESAG6* mRNA levels, as an endogenous component of the active ES. The signal intensity in single cells was measured with ImageJ in deconvolved summed slice projections (100 images, z-step 100 nm) and is shown as arbitrary unit (relative fluorescent unit: RFU). The signal was determined in 1K1N cells only to exclude variations within the cell cycle. The transcript levels were quantified in cells overexpressing VSG 121 for 24 or 48 hours. Non-induced sl or density-induced st cells of the same cell line were analyzed as controls. The magenta bars are means ± SD (n > 100). Statistical analysis was conducted using an unpaired t-test (not significant (n.s.); p-value > 0.05; ** p-value < 0.01; *** p-value < 0.001). Representative microscopy images are shown for non-induced cells and cells induced for 48 hours: the mRNA signal is shown in magenta and the DNA was counterstained with DAPI (grey). Scale bar: 5 µm.

3.3 ES-attenuation triggers differentiation to the short stumpy life cycle stage

It was demonstrated so far that ectopic VSG 121 overexpression in pleomorphic parasites resulted in distinct growth phenotypes. The endogenous *VSG* was silenced in both cases, which resulted in an exchange of the surface coat. However, the clones differed in the transcription of the active ES upon VSG 121 overexpression, which was the cause for the different growth phenotypes. Next, the cell biological consequences of the differently decreased ES-activities were analyzed. A previous study suggested that ES-attenuation caused the development of a parasite stage, which is an intermediate of sl and st parasites (Batram et al., 2014). This analysis was, however, solely based on monomorphic trypanosomes, which are impaired in the differentiation to the st stage. With a pleomorphic model in hand, I now focused on the characterization of the life-cycle stage of the VSG 121 overexpressors. I screened for classical st characteristics such as G1/G0 cell cycle arrest, st specific protein expression, morphological changes and mitochondrial reorganization (reviewed in Fenn and Matthews, 2007; reviewed in MacGregor et al., 2012).

3.3.1 Growth-arrested VSG 121 overexpressors exit the cell cycle and express a stumpy reporter

One characteristics of st cells is a cell cycle arrest in the G1/0 cell cycle phase (Shapiro et al., 1984). I therefore examined, whether cells accumulate in a specific cell cycle stage after VSG 121 overexpression (Figure 15 A, B). For this purpose, growth-arrested and proliferating VSG overexpressors of the GFP:PAD1$_{UTR}$A1.1^{ES}121^{tet} cell line were fixed at 24 and 48 hours after the induction of VSG overexpression and the DNA stained with DAPI. Microscopic analyses of the DAPI-stained cells allowed a precise assignment of the parasites to the different cell cycle phases according to the kinetoplast/nucleus configuration (as shown in Figure 2). Non-induced sl (0 h) and density-induced st parasites of the same cell line were analyzed in the same way as controls. In a non-induced population, 52 ± 1% of the cells were in the G1-phase. In growth-arrested VSG 121 overexpressors, the fraction of cells in G1-phase increased to 72 ± 6 and 86 ± 2% within 24 and 48 hours of VSG 121 overexpression, respectively (Figure 15 A). The number of dividing cells (1K^{d}1N, 2K1N, 2K2N) decreased accordingly. Thus, the growth-arrested VSG 121 overexpressors were arrested in the G1-phase of the cell cycle. This was reminiscent of the st parasites, which are irreversibly arrested in the G1/0-phase (Shapiro et al., 1984).

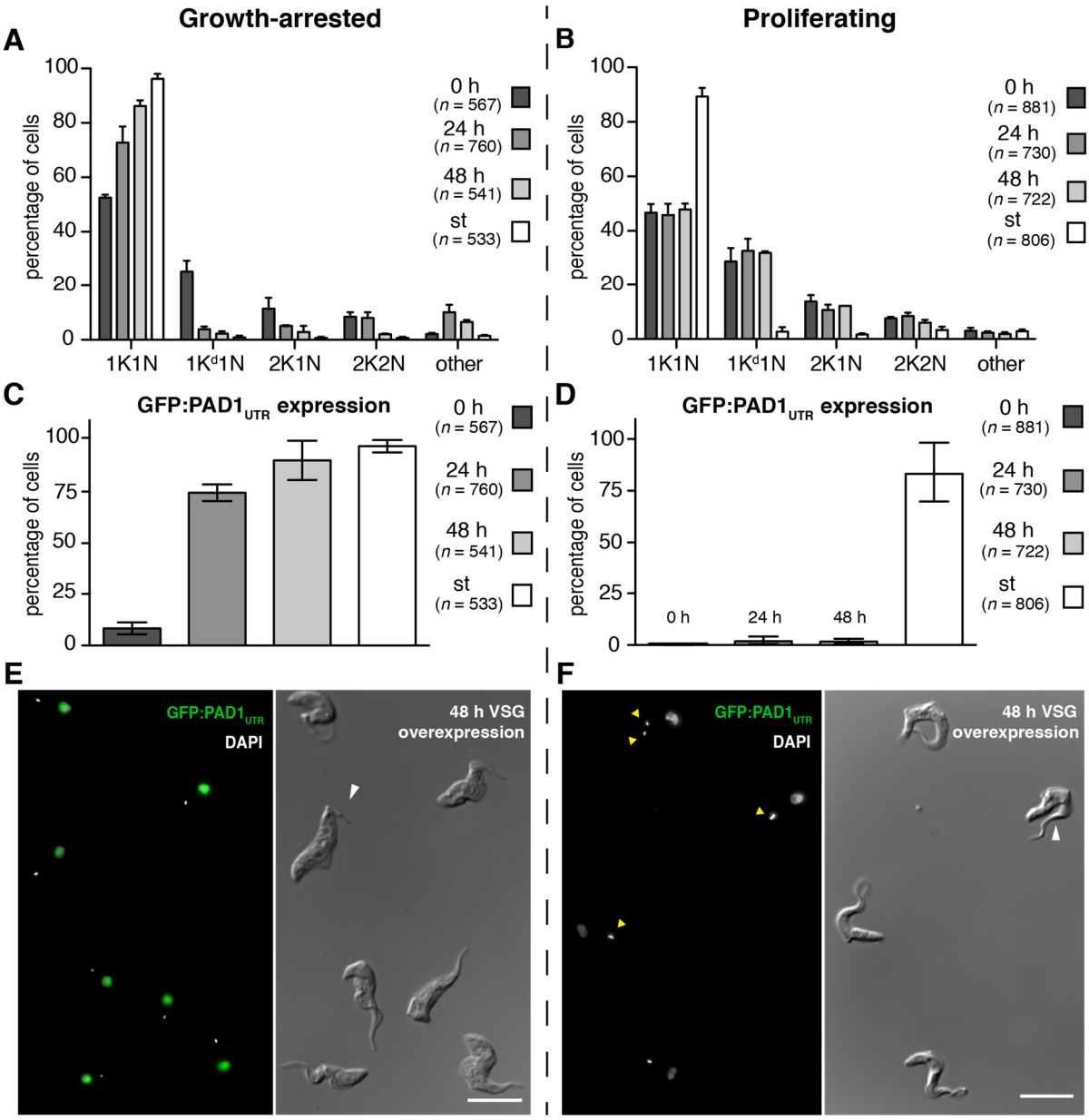

Figure 15: ES-attenuation induces stumpy development. A growth-arrested (left) and a proliferating (right) clone of the GFP:PAD1$_{UTR}$A1.1^{ES}121^{tet} cell line were analyzed. **(A-D)** The analyses were done with parasites overexpressing VSG 121 for 24 and 48 hours. Non-induced sl (0 h) and density-induced st trypanosomes of the same cell line served as controls. **(A, B)** DAPI-stained parasites were microscopically analyzed to determine their kinetoplast (K) and nucleus (N) configuration and thus their position within the cell cycle. Values are given as average percentages (± SD) of two experiments of one clone (total *n* per time point: A > 500; B > 700). **(C, D)** Parasites were microscopically analyzed for the presence of a green fluorescent nucleus (GFP:PAD1$_{UTR}$ reporter). Values are given as average percentages (± SD) of two experiments of one clone (total *n* per time point: C > 500; D > 700). **(E, F)** Representative microscopic images of parasites overexpressing VSG 121 for 48 hours. The nuclear GFP:PAD1$_{UTR}$ reporter is shown in green (left) and the DNA was stained with DAPI (grey, left). The DIC image on the right illustrates the morphology of the VSG 121 overexpressors. **(E)** Growth-arrested trypanosomes had the characteristic stout appearance of st cells with a shortened flagellum (white arrowhead). The trypanosomes were arrested in the 1K1N stage and expressed the GFP:PAD1$_{UTR}$ reporter. **(F)** Proliferating VSG 121 overexpressors had the slim appearance of sl cells with an extended free part of the flagellum (white arrowhead). Different proliferating stages were present (yellow arrowhead) and the st reporter was absent. Scale bar: 10 µm.

Comparison of growth-arrested VSG 121 overexpressors induced for 48 hours and density-induced st parasites showed that indeed a similar amount of cells was in the G1-phase of the cell cycle (48h: 86 ± 2%, st: 96 ± 2%). In contrast, proliferating VSG 121 overexpressors showed no changes in the distribution of the cell cycle phases upon induction (Figure 15 B).

Next, growth-arrested and proliferating clones were analyzed for the presence of the GFP:PAD1$_{UTR}$ reporter, which is exclusively expressed in the st stage. For this purpose, the amount of cells displaying a nuclear GFP:PAD1$_{UTR}$ signal after 24 and 48 hours of VSG 121 overexpression was compared with non-induced sl (0 h) and density-induced st cells of the same cell line. In growth-arrested clones, 74 ± 4% and 90 ± 9% of the cells were GFP:PAD1$_{UTR}$-positive after 24 and 48 hours of VSG 121 overexpression, respectively. This is similar to the 97 ± 3% of GFP:PAD1$_{UTR}$-positive cells in the density-induced st control and significantly higher than the 8 ± 2% GFP:PAD1$_{UTR}$-positive cells in the slender population (Figure 15 C, E). No increase in the number of cells displaying a GFP:PAD1$_{UTR}$ signal was observed during the course of VSG 121 overexpression in the proliferating clone (Figure 15 D, F).

Moreover, the morphology of the growth-arrested VSG 121 overexpressors changed within 48 hours of induction (Figure 15 E). They now had a stout appearance with a shortened flagellum (white arrowhead), which are morphological characteristics of st parasites (Bruce et al., 1912; Robertson, 1912). In contrast, proliferating clones retained their sl appearance upon VSG 121 overexpression (white arrowhead in Figure 15 F) and dividing cells were visible (yellow arrowheads in Figure 15 F). These results indicated that growth-arrested VSG 121 overexpressors differentiated to the st stage, whereas proliferating clones remained sl upon VSG 121 overexpression. This suggested that ES-attenuation induced developmental transition, while the exclusive down-regulation of the endogenous *VSG* was not sufficient.

3.3.2 The mitochondrion is activated in growth-arrested VSG 121 overexpressors

Another hallmark of the developmental transition from the sl to the st stage is the reorganization of the mitochondrion. In sl cells this organelle is a simple single strand and mitochondrial proteins are rarely expressed as this stage produces energy exclusively via glycolysis (reviewed in Michels et al., 2006). However, upon uptake by the tsetse fly vector the availability of glucose dramatically decreases and the parasites now rely on the respiratory system. Therefore, the mitochondrion elaborates and the expression of mitochondrial proteins is initiated (reviewed in Michels et al., 2006; reviewed in Rico et al., 2013). Importantly, pre-adaptation to this severe metabolic change occurs already at late points during sl to st differentiation.

One of the mitochondrial proteins, which is strongly up-regulated during st differentiation, is the lipoamide dehydrogenase (LipDH) (Tyler et al., 1997). Western blot analysis was used to determine the expression of this protein during the course of VSG 121 overexpression (Figure 16 A, B). LipDH expression was assessed in growth-arrested and proliferating VSG 121 overexpressors and compared to the expression levels of non-induced sl (0 h) and density-induced st parasites of the same cell line (st). This demonstrated a 10-fold increase in the LipDH expression in growth-arrested VSG 121 overexpressors after 48 hours of induction compared to the non-induced control (Figure 16 A). This was in accordance with the increase in LipDH expression in density-induced st parasites. In proliferating clones, however, LipDH expression did not increase upon VSG 121 overexpression (Figure 16 B). Moreover, I analyzed the morphology of the mitochondrion of growth-arrested and proliferating clones of the GFP:PAD1$_{UTR}$A1.1^{ES}121^{tet} cell line 24 and 48 hours after the addition of tetracycline (Figure 16 C, D). First, the mitochondrion was stained using mitotracker and, subsequently, the parasites were fixed. Then, the fraction of VSG 121 overexpressors with a branched mitochondrion was counted and, as a control, also in non induced sl cells (0h). Density-induced st parasites served as a positive control. The analysis was restricted to 1K1N cells, to exclude cell cycle specific variations. In growth-arrested VSG 121 overexpressors, 70 ± 9% and 87 ± 5% of the cells had a branched mitochondrion after 24 and 48 hours of induction, respectively (Figure 16 C). This compared well to the density-induced st control, in which 90 ± 4% of the parasites had an elaborated mitochondrion. In contrast, only 27 ± 2% of the non-induced cells displayed a branched mitochondrion. No reorganization of the mitochondrion was observed in proliferating VSG 121 overexpressors (0 h: 28%, 24 h: 24%, 48 h 23%). The elaboration of the mitochondrion into a branched structure in growth-arrested VSG 121 overexpressors is illustrated in Figure 16 E and the slim elongated mitochondrial shape of proliferating clones is shown in Figure 16 F.

In conclusion, the growth-arrested parasites became indistinguishable of the density-induced st control upon induction of VSG 121 overexpression. The parasites displayed early aspects of st development, such as G1/0 cell cycle arrest and PAD1 expression, but also late events like morphological changes or mitochondrial pre-activation (mitochondrial elaboration and LipDH expression). Hence, we termed these parasites ES-induced st cells. The proliferating clones, however, remained sl during the course of VSG 121 overexpression. This suggested that neither the down-regulation of the endogenous *VSG* nor the surface coat exchange caused the developmental transition. Instead, a decrease of the transcription of the active ES appeared to be necessary for the differentiation to st stage.

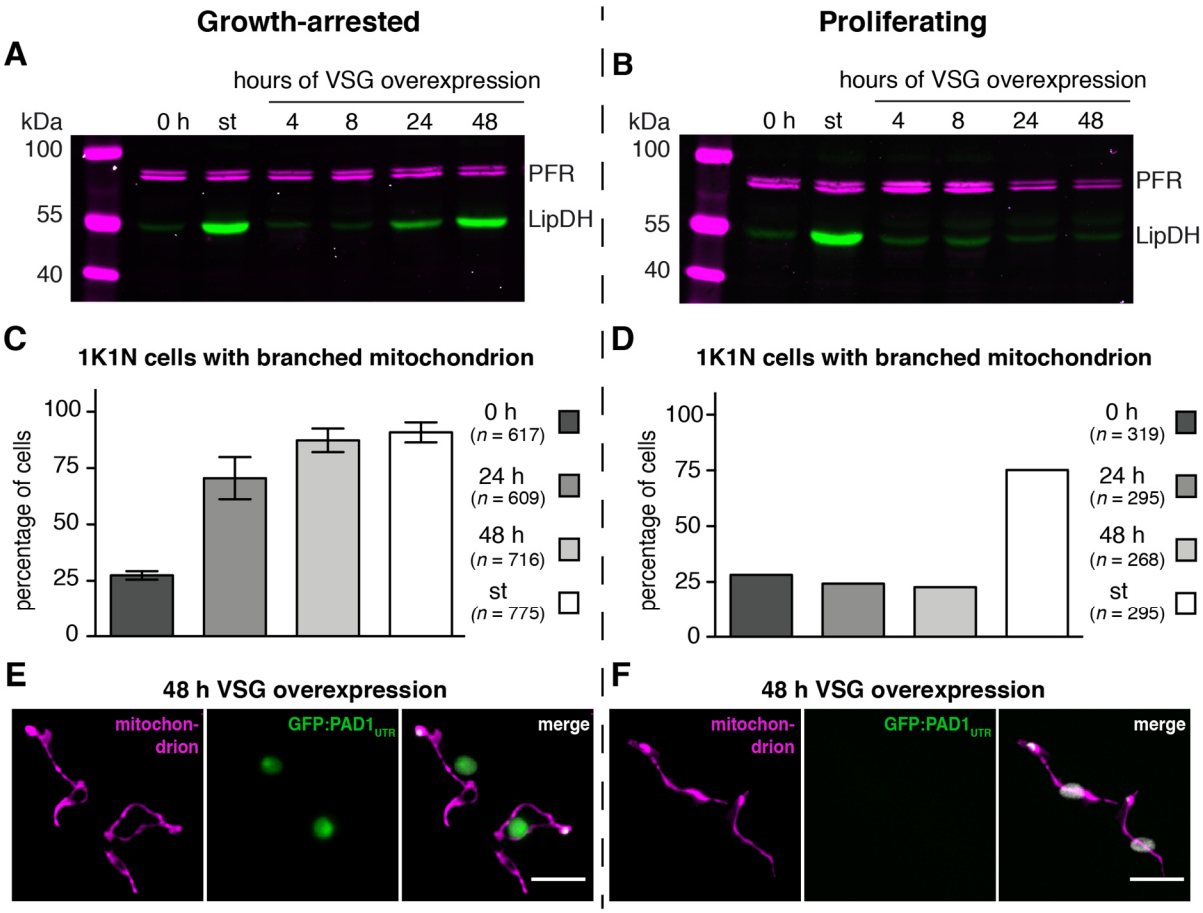

Figure 16: ES-attenuation induces mitochondrial activation. A growth-arrested (left) and a proliferating (right) clone of the GFP:PAD1$_{UTR}$A1.1^{ES}121^{tet} cell line were analyzed. The analyses were done with parasites overexpressing VSG 121 for up to 48 hours. Non-induced sl (0 h) and density-induced st trypanosomes of the same cell line served as controls. **(A, B)** Western blots probed with an antibody against the mitochondrial lipoamide dehydrogenase (LipDH, green), which is up-regulated during density-induced st development. Detection of PFR proteins (magenta) served as a loading control. Using the Western blot analyses, the LipDH level was quantified after 48 hours of induction in two clones of each phenotype, which showed a 10-fold up-regulation in the growth-arrested clones. **(C-D)** Quantification of the fraction of all 1K1N cells with a branched mitochondrion. The mitochondrion was stained with mitotracker (magenta) and the DNA with DAPI. Values are given as average percentages (± SD) of three experiments of one clone (C: total *n* per time point > 600) or of one experiment (D: *n* > 250). **(E, F)** Representative microscopic images of parasites overexpressing VSG 121 for 48 hours. The mitotracker is shown in magenta (left), the nuclear GFP:PAD1$_{UTR}$ reporter in green (middle) and the DNA was stained with DAPI (grey, merged image on the right only). Scale bar: 5 µm.

3.3.3 Proliferating VSG 121 overexpressors can develop to the stumpy stage

The above analyses of st markers demonstrated that growth-arrested VSG 121 overexpressors possessing an attenuated ES differentiated from the proliferative sl to the cell cycle-arrested st stage. In contrast, proliferating VSG 121 overexpressors, which exchanged the surface coat and only mildly down-regulated the ES-activity, remained sl. This suggested that the attenuation of the active ES was necessary to induce st development, whereas the

down-regulation of the endogenous *VSG* was not sufficient. However, it was not excluded so far that the proliferating VSG 121 overexpressors had not lost their developmental potential and thus could not become st anymore. Therefore, st characteristics were analyzed upon density-induced st development in a proliferating clone. As the cells were grown to high densities in the absence of tetracycline, the non-induced trypanosomes were termed according to the phenotype they displayed upon induction of VSG 121 overexpression potentially 'proliferating'. First, the cell cycle and GFP:PAD1$_{UTR}$ expression of density-induced st cells of a potentially 'proliferating' clone was analyzed (st, Figure 15 B, D). This showed that the parasites arrested in the G1-phase of the cell cycle and expressed the fluorescent st marker, suggesting that the potentially 'proliferating' parasites were still developmental competent. Analyses of the pre-activation of the mitochondrion of these cells validated the developmental competence of potentially 'proliferating' parasites as LipDH expression was increased, while a large number of cells (75%) had a branched mitochondrion (Figure 16 B, D). Thus, potentially 'proliferating' VSG 121 overexpressors could still differentiate to the st stage, which demonstrated that indeed the attenuation of the active ES triggered developmental transition in the growth-arrested clones.

Also, a direct comparison of the potentially 'proliferating' and the potentially 'growth-arrested' clones was performed to rule out any differences in their abilities to enter the st stage. The cultures had the same starting cell density (2.5x 10^5 cells/ml) and were cultivated in the absence of tetracycline without dilution to compare the density-induced differentiation to the st stage (Figure 17). The potentially 'proliferating' clone reached a higher cell density (4.9x 10^6 cells/ml) compared to the potentially 'growth-arrested' clone (3.7x 10^6 cells/ml, Figure 17 A), but both cell lines stalled growth and started to die within 72 hours of cultivation. After 93 hours of cultivation without dilution almost no living parasites were observed. This suggested that all non-induced trypanosomes of potentially 'proliferating' and potentially 'growth-arrested' clones differentiated to the stumpy stage within 72 hours of cultivation. The fact that all trypanosomes could differentiate to the st stage with the quorum-sensing trigger was further validated by monitoring the expression of the GFP:PAD1$_{UTR}$ st reporter at different cell densities (indicated by the magenta arrows in Figure 17 A). When the cultures had a density of 5x 10^5 cells/ml and were cultivated without dilution for 48 hours the majority of parasites (>95%) became st (Figure 17 B). Thus, all non-induced trypanosomes of a potentially 'proliferating' and a potentially 'growth-arrested' clone could develop to the st stage. This excluded that the different growth phenotypes observed upon addition of tetracycline were caused by a general deficiency in st development of the proliferating clones.

However, differences in the number of GFP:PAD1$_{UTR}$-positive cells were observed within 24 hours of cultivation. While 15 ± 3% of the non-induced cells of the potentially 'growth-arrested' clone became st, only 8 ± 1% of the potentially 'proliferating' clone expressed the st reporter

at the same time when the same starting cell density was used. This could indicate that the non-induced cells of the potentially 'growth-arrested' clone react earlier with st development than the non-induced parasites of the potentially 'proliferating' VSG 121 overexpressor. This would be in accordance with the results of the growth analyses as the potentially 'proliferating' clone reached higher cell densities before growth was stalled. Nevertheless, the data verified that the different growth phenotypes upon the induction of VSG 121 overexpression were not caused by a loss of the developmental potential of the proliferating VSG 121 overexpressors. Consequently, st development in the growth-arrested clones was caused by the attenuation of the active ES, whereas the down-regulation of the endogenous *VSG* was not sufficient. Interestingly, a reduction of the ES-activity to 50% was observed in the proliferating clones within 48 hours of induction, which suggests that this transcription level is above the critical threshold to induce st development.

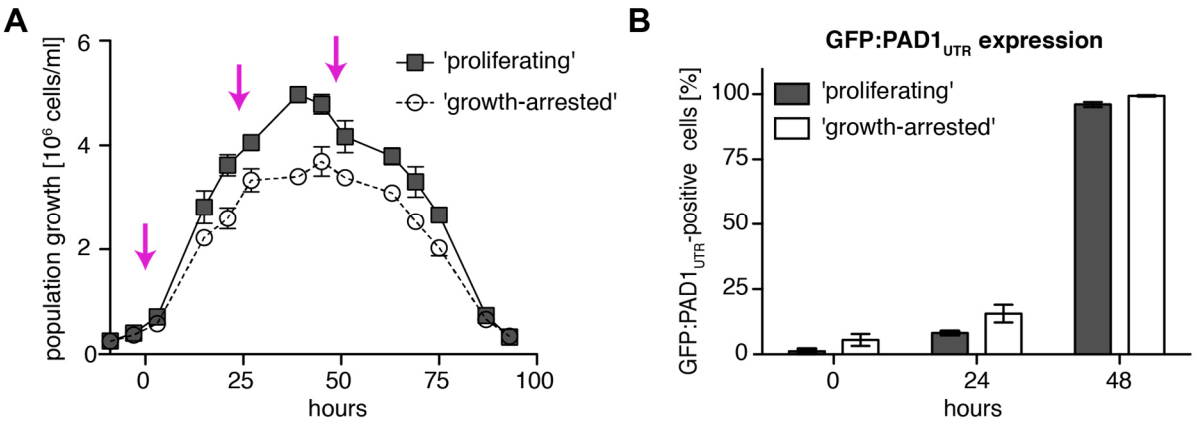

Figure 17: Proliferating VSG 121 overexpressors are developmentally competent. Density-induced st development of non-induced parasites of a potentially 'proliferating' (grey squares) and a potentially 'growth-arrested' (white circles) clone of the GFP:PAD1$_{UTR}$A1.1^{ES}121^{tet} cell line. **(A)** Parasites were cultivated without dilution in the absence of tetracycline and growth was monitored. The starting cell density was 2.5x 10^5 cells/ml for both clones. Note the time point when the parasites had a density of 5x 10^5 cells/ml was defined as zero hours to make the results comparable to the density-induced st parasites in the other experiments. Means (± SD) of triplicate experiments are shown. The magenta arrows indicate the time points at which the amount of GFP:PAD1$_{UTR}$-positive cells was determined. **(B)** The number of parasites expressing the GFP:PAD1$_{UTR}$ st reporter was microscopically analyzed at the indicated time points in A. At zero hours the parasites had a density of 5x 10^5 cells/ml. Values are average percentages (± SD) of triplicate experiments (total *n* per situation > 600 cells).

3.4 ES-induced stumpy trypanosomes are developmentally competent

The results so far demonstrated that the attenuation of the active ES causes the development of cells that were indistinguishable from density-induced st parasites, wherefore we termed these cells ES-induced st trypanosomes. Density-induced st parasites are thought to be the only BSF stage that can infect the tsetse fly vector and complete the parasite life cycle (reviewed in Rico et al., 2013). Therefore, we asked if the ES-induced st parasites posses the same developmental capacity as density-induced ones. To answer this question, ES-induced st parasites were exposed to triggers for procyclic development and used for tsetse flies infections.

3.4.1 ES-induced stumpy cells can differentiate *in vitro*

PCF development of density-induced st parasites can be induced *in vitro* by treatment with *cis*-aconitate and citrate and a drop of temperature to 27°C (CCA-treatment) (Brun, 1981; Engstler and Boshart, 2004; Overath et al., 1986). The developmental progression is accompanied by an exchange of the surface coat (Roditi et al., 1989; Ziegelbauer et al., 1990). The VSG coat is replaced by an invariant EP-procyclin coat within six hours of CCA treatment. Besides this, morphological changes occur such as an elongation of the posterior end of the cell and a repositioning of the kinetoplast, which moves in the vicinity of the nucleus (Matthews et al., 1995). Moreover, G1/0 cell cycle arrest is rescinded and the parasites reenter the cell cycle as procyclics (Matthews and Gull, 1994).

First, it was investigated if ES-induced st parasites posses the same developmental capacity as density-induced st cells *in vitro*. VSG 121 overexpression was induced in a growth-arrested clone for 48 hours (ES-induced st) and the cells were then exposed to the CCA treatment. After zero, six and 24 hours of treatment the parasites were stained with an antibody against the procyclic surface protein EP1. Non-induced sl parasites (0 h) and density-induced st parasites (st) of the same cell line served as controls. Flow cytometry showed that within six hours of CCA treatment ES-induced and density-induced st cells exchanged their surface coat with similar kinetics. After six hours of CCA treatment, 78% of the ES-induced and 80% of the density-induced st parasites expressed EP1 on their surface (Figure 18 and 19). In contrast, only 11% of the sl parasites were EP1-positive within the same time of CCA treatment. After 24 hours of treatment, 95% of the ES-induced and density-induced st parasites were EP1-positive, in contrast to only 57% of the sl cells. Thus, the kinetics in cell surface coat exchange was similar between ES-induced and density-induced st parasites, while sl cells exchanged their cell surface slower.

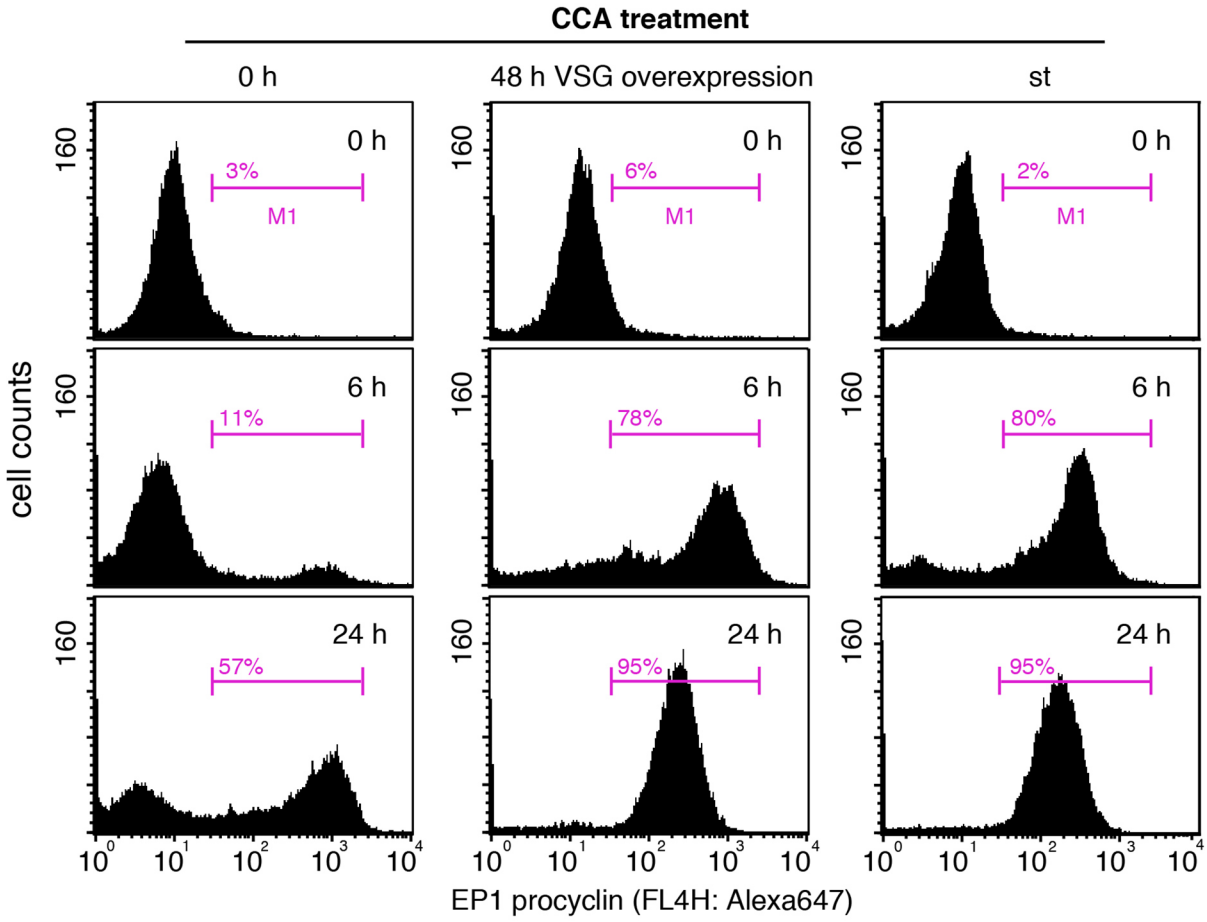

Figure 18: ES-induced stumpy cells are sensitive to triggers for procyclic differentiation *in vitro*. Analyses of the expression of the procyclic surface protein EP1 via flow cytometry. A growth-arrested clone of the GFP:PAD1$_{UTR}$A1.1^{ES}121^{tet} cell line overexpressing VSG 121 for 48 hours was analyzed. Non-induced sl (0 h) and density-induced st parasites of the same cell line were used as controls. The trypanosomes were stained with an EP1 antibody after CCA treatment (3 mM *cis*-aconitate, 3 mM citrate, 27°C) for zero, six or 24 hours. 20,000 cells were analyzed and the M1 region of the plots (indicated by the magenta bar) was defined as EP1-positive.

Next, the EP1-stained ES-induced st parasites were analyzed over a time-course of CCA treatment using fluorescence microscopy (Figure 19). No EP1 was present on the surface without CCA treatment but after six hours of CCA treatment. At this time no morphological changes of the parasites were observed: the cells still had the stout appearance of typical st parasites. Morphological characteristics of the PCF stage became apparent after 24 hours of CCA treatment: the cells had the typical procyclic shape with an elongated posterior end (indicated by white arrowhead in Figure 19) and the kinetoplast in the vicinity of the nucleus. Moreover, 33% of the parasites belonged to the 2K1N or 2K2N cell cycle stage (in >250 cells), demonstrating that the cells had reentered the cell cycle (indicated by yellow arrowhead in Figure 19). Thus, ES-induced st parasites not only responded to CCA treatment with the synchronous expression of EP1 but also changed their morphology and lifted the cell cycle

arrest. Consequently, ES-induced st parasites possessed the same capacity to develop to the PCF stage *in vitro* as density-induced st parasites.

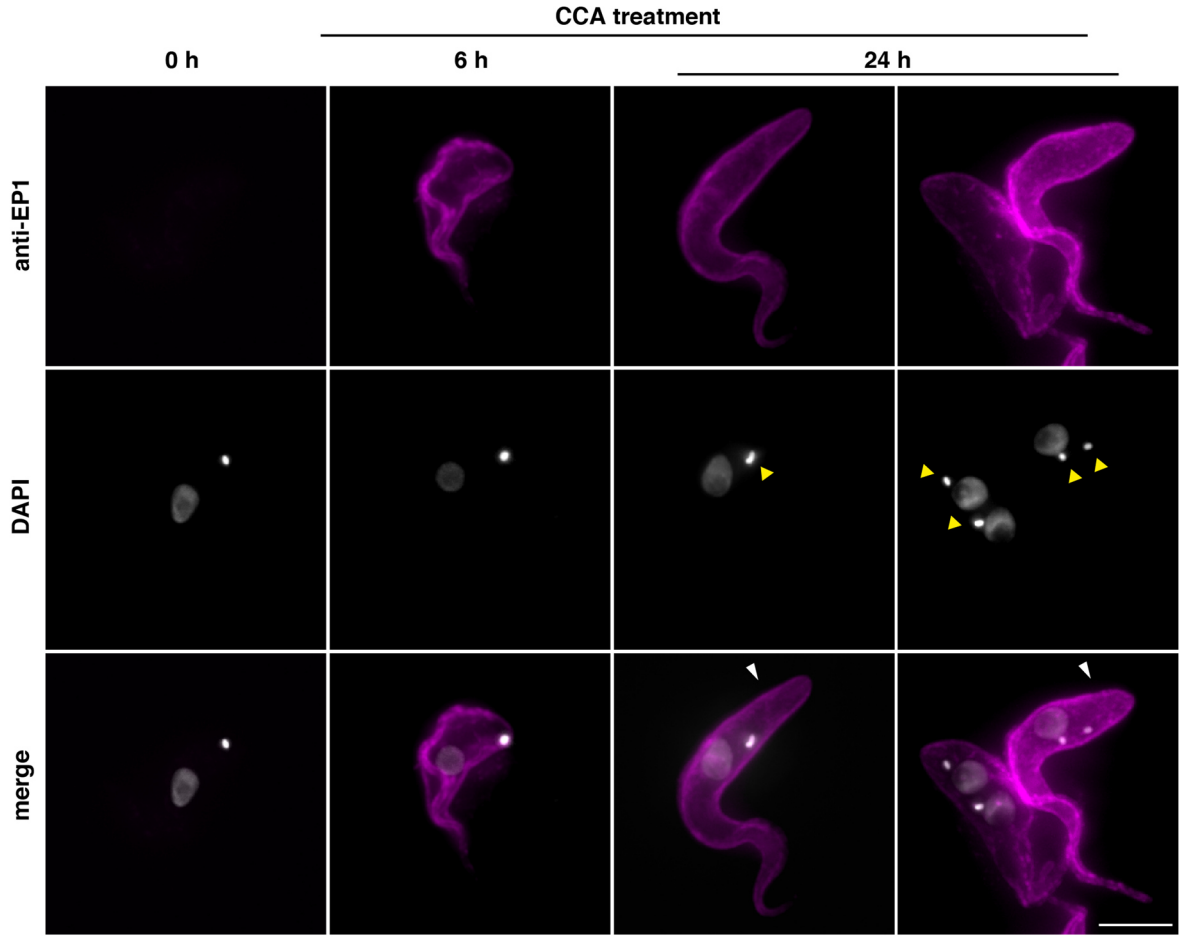

Figure 19: ES-induced stumpy cells differentiate to the procyclic stage *in vitro*. Analysis of the cell shape and the kinetoplast/nucleus configuration during st to procyclic *in vitro* differentiation. A growth-arrested clone of the GFP:PAD1$_{UTR}$A1.1^{ES}121^{tet} cell line overexpressing VSG 121 for 48 hours was treated with CCA (3 mM *cis*-aconitate, 3 mM citrate, 27°C). Parasites were stained with an EP1 antibody (magenta) after zero, six or 24 hours of CCA treatment. The DNA was counterstained with DAPI (grey). The EP1-staining in the representative images shows the procyclic characteristic elongation of the posterior end of the parasites after 24 hours of treatment (white arrowheads). The procyclic characteristic rearrangement of the kinetoplast and the nucleus position as well as the reentry into the cell cycle (yellow arrowheads) is illustrated by the DAPI staining.

3.4.2 ES-induced stumpy cells can complete the parasite cycle *in vivo*

To date, density-induced st parasites are thought to be the only BSF stage, that can complete the parasite life cycle within the tsetse fly vector (reviewed in Rico et al., 2013; reviewed in Sharma et al., 2009). Here, it was investigated if ES-induced parasites were also able to infect tsetse flies and to complete the complex parasite life cycle. For this purpose, ES-induced st

parasites were harvested from the culture at densities below 5x 10^5 cells/ml. The parasites were resuspended in blood at a density of 2x10^6 cells/ml and then fed to 50 flies in total. We included the same amount of density-induced st parasites of the parental GFP:PAD1$_{UTR}$ cell line in the blood meal of another 50 flies as a control. We examined the presence of trypanosomes in the alimentary system of the surviving flies after >50 days of infection. ES-induced parasites were able to infect the salivary glands in 6.4% of flies (*n* = 47) and density-induced st in 22.7% (*n* = 44). Even though the infection rate differed between ES-induced and density-induced st parasites, these results demonstrated that both populations of st parasites were able to establish an infection in the tsetse salivary glands. A greater number of infected flies have to be analyzed to determine whether the observed differences between the transfection rates reflect different infections efficiency. It was also examined if all characteristic developmental stages were present in flies infected with ES-induced st cells. For this purpose, we dissected the flies and fixed the isolated parasites. The different fly stages can be distinguished by morphological criteria such as the shape of the cell, the length of the flagellum and kinetoplast/nucleus configuration (described in chapter 2.3.1). An antibody against a component of the flagellum, the PFR, was used to visualize the positioning and length of the flagellum and the DNA was stained with DAPI. This demonstrated that all expected trypanosome stages were present in flies infected with ES-induced st parasites (Figure 20).

Procyclic and mesocyclic parasites stages, which colonize the midgut of the fly, were identified. In the proventriculus and foregut epimastigote stages, which are defined by the posterior position of the nucleus, were found (described in chapter 2.3.1). In addition to epimastigote cells, we also found short epimastigote parasites, which illustrates that these cells divide as usually in an asymmetric fashion (Van Den Abbeele et al., 1999). The salivary glands of the flies were colonized by attached epimastigote and metacyclic parasites (described in chapter 2.3.1). Metacyclic trypanosomes possess a trypomastigote kinetoplast/nucleus configuration, express a VSG coat and are infective for the mammalian host. Consequently, the ES-induced st parasites were able to complete the life cycle and could now infect a mammalian host (reviewed in Sharma et al., 2009). These results demonstrated that ES-induced st parasites not only differentiate *in vitro* to the procyclic stage but can also complete the trypanosome life cycle in the tsetse fly up to the mammalian infective stage found in the salivary gland. We conclude that ES-induced st trypanosomes possess a similar developmental competence as density-induced parasites.

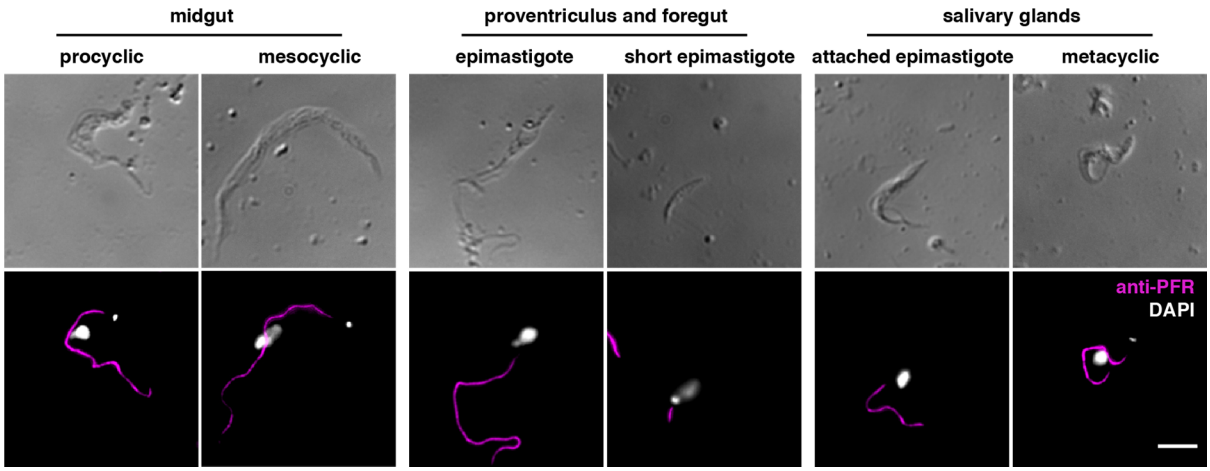

Figure 20: ES-induced stumpy cells can complete the parasite life cycle *in vivo*. ES-induced st parasites were included in the blood meal of 50 tsetse flies ($2x10^6$ cells/ml). After more than 50 days of infection, flies were dissected and parasites derived from the midgut, proventriculus and foregut and the salivary glands were fixed. This showed that all expected trypanosome stages were present in flies infected with ES-induced st parasites. The DIC images (upper panel) illustrate the shape of the different parasites stages. The flagellum of the trypanosomes was stained with a PFR antibody (magenta, lower panel) to visualize the characteristic changes in the length and positioning of the flagellum during developmental progression. DAPI staining of the DNA (grey, lower panel) demonstrated the typical positioning of kinetoplast and nucleus in the different life cycle stages. Scale bar: 5 µm. The different fly stages and their characteristics are explained in chapter 2.3.1.

3.5 Stumpy development is not specific for the overexpression of a distinct VSG variant

The previous results demonstrated that different ES-activity levels caused by the overexpression of VSG 121 resulted in distinct phenotypes. While a mild down-regulation of the ES-activity had no consequences for trypanosomes, the attenuation of the ES triggered the developmental transition to the st stage. These ES-induced st parasites were indistinguishable from density-induced st parasites and possessed a similar developmental capacity. However, the analyses so far were based on the overexpression of VSG 121, which represents only one of more than 2,000 VSG variants (Cross et al., 2014). Therefore, we asked next if the different growth phenotypes or ES-induced st development were specific for the overexpression of VSG 121.

3.5.1 The distinct growth phenotypes are not specific for the overexpression of a distinct VSG variant

Another VSG was overexpressed in pleomorphic trypanosomes to assure that the distinct growth responses observed upon VSG 121 overexpression are not VSG specific. For this purpose, the st reporter cell line was transfected with a construct for VSG 118 overexpression, which yielded the GFP:PAD1$_{UTR}$A1.1^{ES}118^{tet} cell line. The VSG 118 plasmid is similar to pRS.121 but contains the *VSG 118* ORF and 3´UTR instead of the *VSG 121* ORF and 3´UTR (bachelor thesis Henning, 2012).

Induction of VSG 118 overexpression also resulted in distinct growth phenotypes (Figure 21 A, B). In two of five analyzed clones VSG 118 overexpression led to an arrest in growth (growth-arrested clones, Figure 21 A), while in other two clones growth was not affected (proliferating clones, Figure 21 B). The growth-arrested clones doubled only four to six times during eight days of induction and resumed growth after 10 days. In contrast, the growth rate of the proliferating clones remained unchanged upon VSG 118 overexpression. Thus, the ectopic overexpression of two VSGs, VSG 121 and VSG 118, caused the distinct growth phenotypes: proliferating and growth-arrested. Independently of the growth response of the VSG 118 overexpressors, already the non-induced cells displayed an impaired growth (pdt 10 h) compared to the parental AnTat1.1 13-90 (pdt 6.8 h) cell line. The reason for this remains unknown.

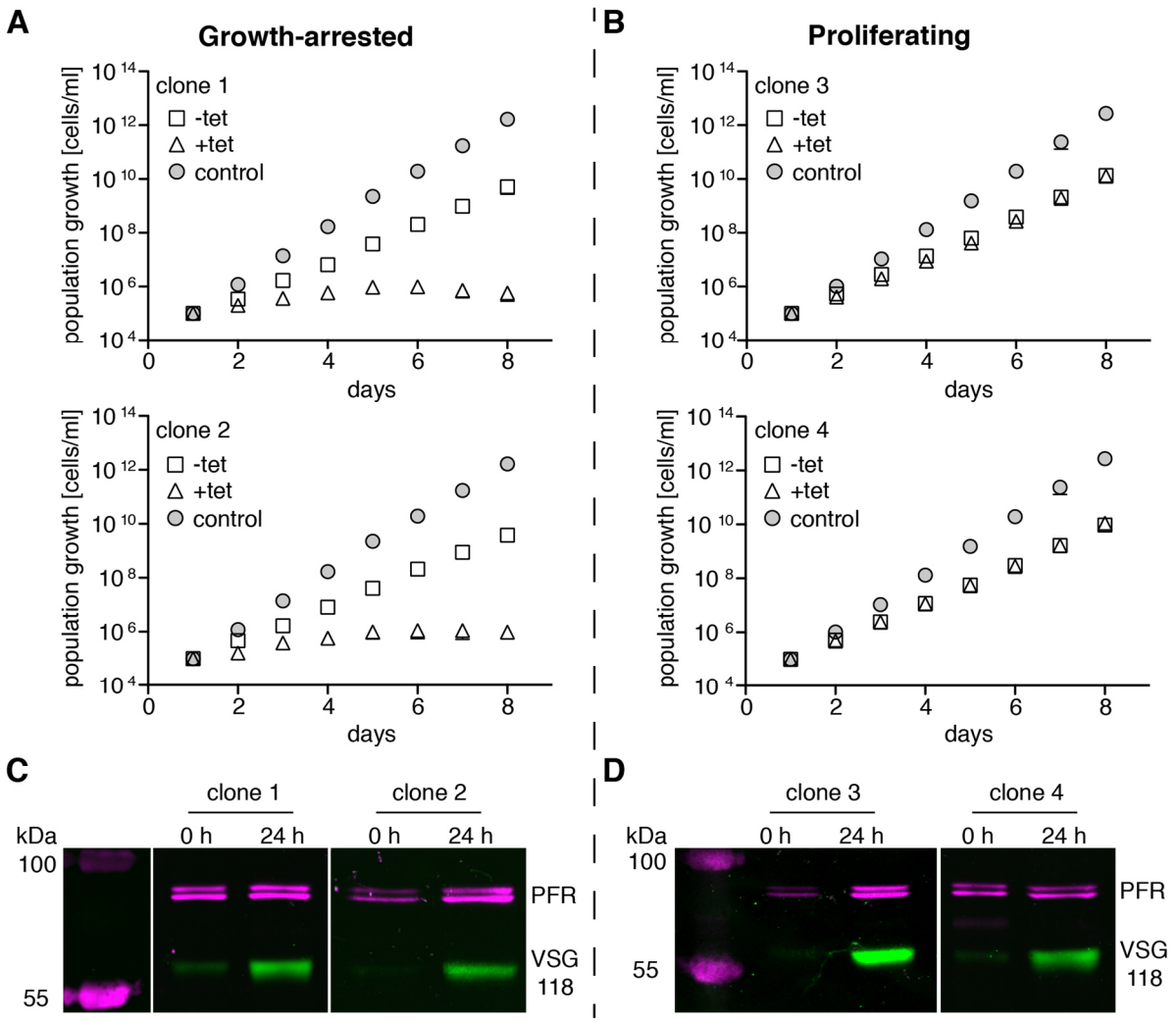

Figure 21: Ectopic overexpression of VSG 118 causes distinct growth phenotypes in pleomorphic trypanosomes. **(A, B)** Growth curves of **(A)** two growth-arrested and **(B)** two proliferating clones of the GFP:PAD1$_{UTR}$A1.1^{ES}118^{tet} cell line. Tetracycline-induced (triangles) and non-induced (squares) parasites were analyzed. The parental AnTat1.1 13-90 cell line (circles) served as a control. For each clone, means (± SD) of three experiments are shown. Due to the small standard deviation the error bars are not visible. (C, D) Western blot analysis of **(C)** the growth-arrested and **(D)** the proliferating clones of the GFP:PAD1$_{UTR}$A1.1^{ES}118^{tet} cell line. Protein samples of non-induced parasites (0 h) and cells induced with tetracycline for 24 hours were analyzed. The Western blots were stained with a VSG 118 antibody (green) and a paraflagellar rod (PFR) antibody (magenta) as a loading control.

Western blot analysis was used to rule out that the different growth phenotypes were caused by a deficient overexpression system (Figure 21 C, D). All clones indeed overexpressed VSG 118 upon addition of tetracycline. The homogeneity of ectopic VSG overexpression was analyzed on the single cell level using immunofluorescence (Figure 22). Non-induced parasites and cells induced for 24 hours of a proliferating clone of the GFP:PAD1$_{UTR}$A1.1^{ES}118^{tet} cell line were stained simultaneously for VSG 118 (magenta) and VSG A1.1 (green). MITat1.5 wild type cells natively expressing VSG 118 and the parental

AnTat1.1 13-90 cell line natively expressing VSG A1.1 were used as a control, demonstrating the specificity of the antibodies (Figure 22, upper panels). The immunofluorescence analyses showed that the majority of the proliferating VSG 118 overexpressors (>98%, *n* = 2, each > 200 cells) expressed the ectopic VSG upon induction, as exemplified by an immunofluorescence of a proliferating clone in Figure 22. Also, the endogenous VSG A1.1 decreased within 24 hours of induction in all cells.

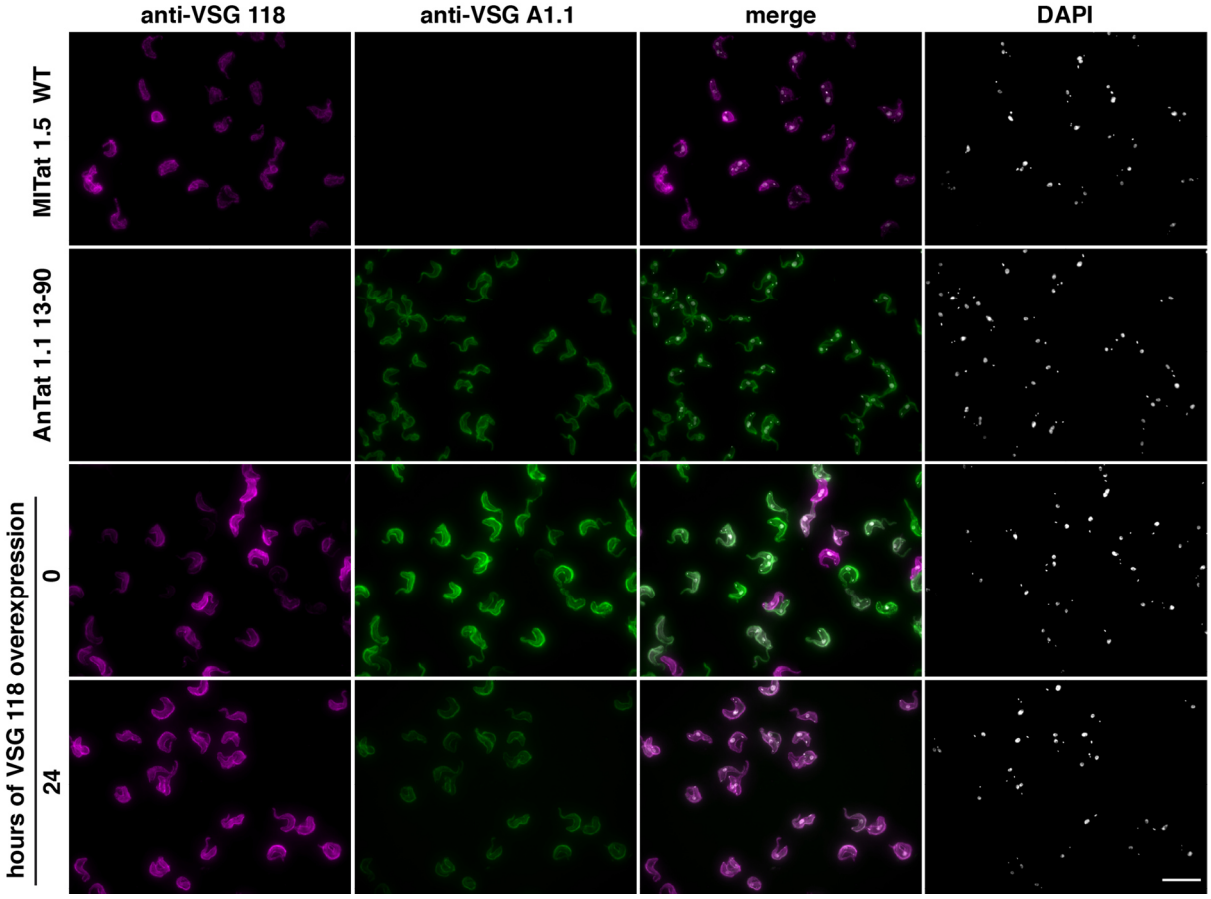

Figure 22: Overexpression of the ectopic VSG 118 causes surface coat exchange. Immunofluorescence analysis of a proliferating clone of the GFP:PAD1$_{UTR}$A1.1^{ES}118^{tet} cell line. Non-induced cells (0 h) and VSG 118 overexpressors induced for 24 hours were stained with antibodies against the ectopic VSG 118 (magenta) and the endogenous VSG A1.1 (green). MITat1.5 wild type cells natively expressing VSG 118 and the parental AnTat1.1 13-90 cells natively expressing VSG A1.1 served as controls for antibody specificity. The DNA was stained with DAPI (grey). 32% of the non-induced cells (*n* > 350 cells) expressed the ectopic VSG and after 24 hours of induction >98% (*n* = 2, each > 200 cells). Scale bar: 20 µm.

The analysis of non-induced cells showed that already in the absence of tetracycline some parasites were strongly VSG 118-positive. The VSG 118-positive cells were observed in non-induced cells of a potentially 'growth-arrested' (12% in >250 cells) and a potentially 'proliferating' clone (32% in >350 cells) and thus most likely did not affect the different growth

responses upon induction. However, the presence of non-induced VSG 118-positive cells could have affected the growth in the absence of tetracycline and explain the slowed growth. The cause for the VSG 118-positive non-induced cells remains unknown. For example it could be that non-induced VSG 118-positive cells express the ectopic VSG at high levels without induction. Thus, non-induced cells would display different leaky VSG 118 expression levels, which can be an indication for non-clonal populations. Alternatively, the non-induced VSG 118-positive cells could have switched the endogenous VSG and expressed now a variant, which was recognized by the VSG 118 antibody. As I could not exclude that the non-induced VSG 118-positive cells would influence the experiments, the analyses in this thesis were mainly conducted using the VSG 121 overexpressors. Nevertheless, the overexpression of VSG 118 in pleomorphic cells demonstrated that the distinct growth responses obtained during ectopic VSG overexpression, proliferating and growth-arrested, were not dependent on the used VSG variant.

3.5.2 VSG overexpression induced stumpy differentiation is not VSG specific

The data above showed that ES-attenuation induced by the overexpression of VSG 121 caused the developmental transition from the sl to st stage. We wanted to assure that the VSG overexpression induced differentiation is not specific to a certain VSG. Therefore, stumpy markers were also analyzed in growth-arrested and proliferating VSG 118 overexpressors.

First the GFP:PAD1$_{UTR}$ expression was monitored because the kinetics of the growth arrest differed slightly between the VSG 118 and the VSG 121 overexpressors (compare Figure 8 and Figure 21). This showed that in growth-arrested VSG 118 overexpressors the expression of the st reporter started later than upon VSG 121 overexpression. The fraction of GFP-positives cells increased from 14 ± 3% in non-induced cells to 18 ± 2, 25 ± 5, 47 ± 2 and 77 ± 2% within 24, 48, 72 and 96 hours of induction, respectively (Figure 23 A). Thus, four days of VSG 118 overexpression were necessary to reach a PAD1-positive level comparable to the one of density-induced st cells, but only one day of VSG 121 overexpression (compare Figure 15). The proliferating VSG 118 overexpressors reacted similar to the proliferating VSG 121 overexpressors and showed no increase in the number of GFP:PAD1$_{UTR}$ expressing parasites (Figure 23 B).

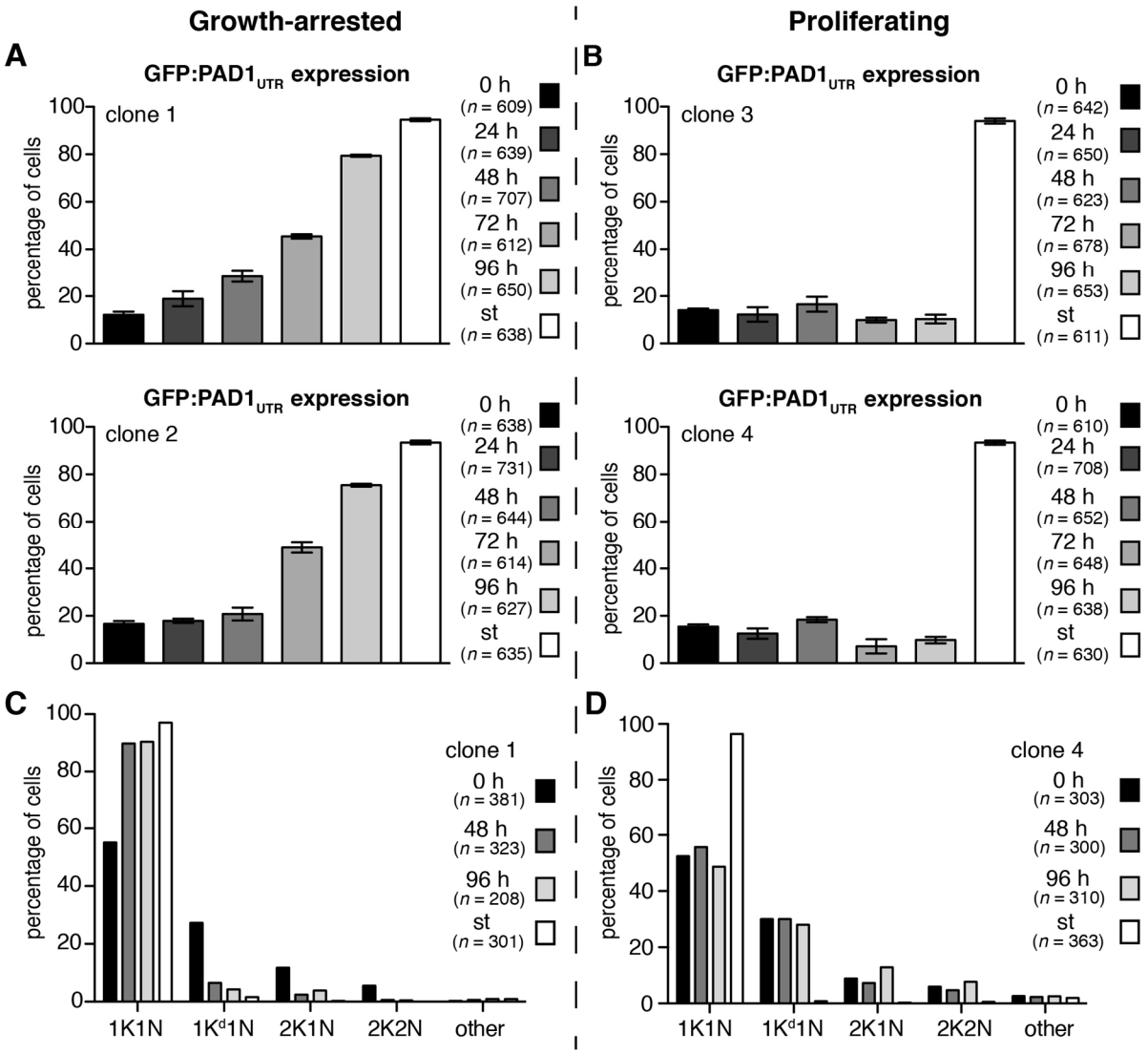

Figure 23: VSG 118 overexpression can induce stumpy development. (A-B) The number of parasites expressing the GFP:PAD1$_{UTR}$ st reporter was microscopically analyzed. Two growth-arrested and two proliferating clones of the GFP:PAD1$_{UTR}$A1.1^{ES}118^{tet} cell line were analyzed over a time-course of VSG 118 expression. Non-induced sl (0 h) and density-induced st trypanosomes of the same cell lines served as controls. For each clone, values are presented as average percentages (± SD) of three experiments (total *n* per time point > 600 cells). **(C, D)** Cell cycle analyses of one growth-arrested and one proliferating clone of the GFP:PAD1$_{UTR}$A1.1^{ES}118^{tet} cell line during the course of VSG 118 overexpression. Parasites overexpressing VSG 118 for 48 and 96 hours were chemically fixed, DAPI-stained and microscopically analyzed to determine their kinetoplast (K) and nucleus (N) configuration. Non-induced sl (0 h) and density-induced st trypanosomes of the same cell lines served as controls. Values are given as percentages of the total number of cells (*n* > 300).

Then, I analyzed the cell cycle of growth-arrested and proliferating parasites after 48 and 96 hours of induction (Figure 23 C, D). This was compared to the cell cycle of non-induced sl (0 h) and density-induced st parasites. In a growth-arrested clone, 89% of the cells were in the G1-phase of the cell cycle after 48 hours of VSG 118 overexpression, in comparison to 55% of the non-induced sl cells (Figure 23 C). After 96 hours, the fraction of 1K1N cells was 90%, which compared well to the 97% 1K1N cells of the density-induced st parasites. The increase of cells

in the G1-phase of the cell cycle was accompanied by a decrease in the number of dividing cells. Thus, the growth arrest of VSG 118 overexpressors was caused by an accumulation of cells in the G1-phase. No changes in the cell cycle were observed in proliferating parasites upon induction of VSG 118 overexpression (Figure 23 D).

The overexpression of both VSG 121 and VSG 118 caused a cell cycle arrest in the G1-phase and the expression of the st reporter PAD1. This suggested that also the growth-arrested VSG 118 overexpressors were ES-induced st parasites. However, VSG 121 overexpression resulted in a nearly uniform st population within 24 hours of induction, whereas 96 hours of induction were required for a similar level of stumpy cells in the VSG 118 overexpressors. This indicated that the critical threshold in ES-activity may be reached later upon VSG 118 overexpression, suggesting that not the kinetics of ES-attenuation is critical for st development but rather the transcriptional status of the ES *per se*.

3.6 Escapers of ES-induced stumpy formation

The results so far have shown that the attenuation of the active ES caused the developmental transition from the sl to the st stage. These ES- induced st cells possessed a similar potential to complete the parasite life cycle as density-induced st trypanosomes. St parasites are irreversible arrested in the G1/0-phase of the cell cycle and thus determined to die, unless they are up-taken by the tsetse fly (MacGregor et al., 2011). However, the growth-arrested VSG overexpressors reproducibly resumed growth (compare Figure 8). Therefore, it remained unclear whether the ES-induced st cells are also doomed to die. Several mechanisms could explain the outgrowth of the growth-arrested VSG overexpressors. First, a small subpopulation of parasites may not respond with growth retardation to the addition of tetracycline and with time, outgrow the growth-arrested VSG overexpressors. Second, a subpopulation of the VSG overexpressors could be resistant to signals for st development and escape ES-induced st development. Third, some parasites could reactivate the complete A1.1 ES and hence lift ES transcription to growth permissive levels. Fourth, a mutation of the T7 polymerase or promotor of the overexpression system could have occurred, causing its defectiveness. Fifth, ES-attenuation did in some parasites not reach the critical threshold to induce st developmental but caused a prolongation of the cell cycle and thus an initial growth retardation.

3.6.1 Outgrowing VSG 121 overexpressors are not resistant to stumpy induction triggers

St parasites are known to have a limited life span of two to three days (MacGregor et al., 2011). Thus, cell death should become apparent in growth-arrested VSG overexpressors at day four of induction. In fact dead cells were observed, but all growth-arrested VSG overexpressors reproducibly resumed growth. The timing of outgrowth differed as growth-arrested VSG 121 overexpressors reentered the cell cycle within four (Figure 8 C) to eight days (Figure 24 A) of induction, whereas growth-arrested VSG 118 overexpressors resumed growth after 10 days. Thus, the question arose what the cause of the outgrowth is. The most obvious explanation would be that the culture contained a small number of parasites that did not respond to VSG overexpression with ES-attenuation and hence growth retardation. These cells would correspond to the proliferating clones, which only mildly adjusted the ES-activity and continued to grow upon VSG overexpression. If we assume that at least one cell of the culture retained a pdt of six to seven hours upon induction, the outgrowth should be observed latest at day five of induction. However, I observed an arrested growth up to eight days (VSG 121) or 10 days (VSG 118) of induction. Therefore, it was excluded that the outgrowth is caused by cells that did not react with growth retardation upon induction.

Another possibility was that some parasites could not differentiate to the st stage. Thus, the cells could escape ES-induced st development. If this is the case, these escapers should also not respond to the classical triggers for st differentiation. Classical triggers for st development are the membrane-permeable cAMP analogue pCPT-cAMP and the stumpy induction factor (SIF). CAMP is known to induce st development similarly to SIF, indicating that cAMP or its hydrolysis products could serve as second messengers to mediate the SIF signal (Laxman et al., 2006; Vassella et al., 1997). PCPT-cAMP is frequently used to induce st differentiation as SIF itself remains elusive to date. SIF is secreted by the parasites themselves and is therefore present in culture medium after the cells were grown to high cell densities (conditioned medium). Based on the conditioned medium a SIF-concentrate, which is x-fold enriched in SIF in comparison to conditioned medium, was generated (kindly provided by I. Subota; described in chapter 5.2.1 Differentiation to the stumpy stage). Hence, st development could not only be induced by pCTP-cAMP, but also with the SIF-concentrate, hereafter referred to as SIF.

If the outgrowth of growth-arrested VSG overexpressors would be caused by a deficiency in st development, outgrown parasites should not react to pCTP-cAMP and SIF. To test this, VSG 121 overexpressors of a growth-arrested clone of the GFP:PAD1$_{UTR}$A1.1^{ES}121^{tet} cell line, that resumed growth after eight days of induction (8 d +tet), were exposed to pCPT-cAMP or to SIF (Figure 24 B). Non-induced cells of the same cell line were treated in the same way using identical cell densities (-tet). To analyze if the cells react with st development, I quantified the number of parasites expressing the GFP:PAD1$_{UTR}$ reporter after 20 and 28 hours of treatment. The number of GFP:PAD1$_{UTR}$-positive cells was also determined in the absence of the triggers as a control (untreated). Neither non-induced nor outgrown cells reacted with st development when pCPT-cAMP and SIF were absent. In the presence of the cAMP analogue 18% of the non-induced cells and 17% of the outgrown VSG 121 overexpressors expressed the st reporter within 20 hours. In the same time, SIF caused st development in 21% of the non-induced cells and in 24% of the outgrown VSG 121 overexpressors. After 28 hours of treatment with pCPT-cAMP, 65% of the non-induced cells and 67% of the overexpressors were st. When treated with SIF, 52% of the non-induced cells and 51% of the outgrown VSG 121 overexpressors became PAD1-positive. Thus, non-induced cells and outgrown VSG 121 overexpressors reacted similarly to the treatment with triggers for st development. This excluded that the outgrowing VSG 121 overexpressors had lost the ability to differentiate to the st stage.

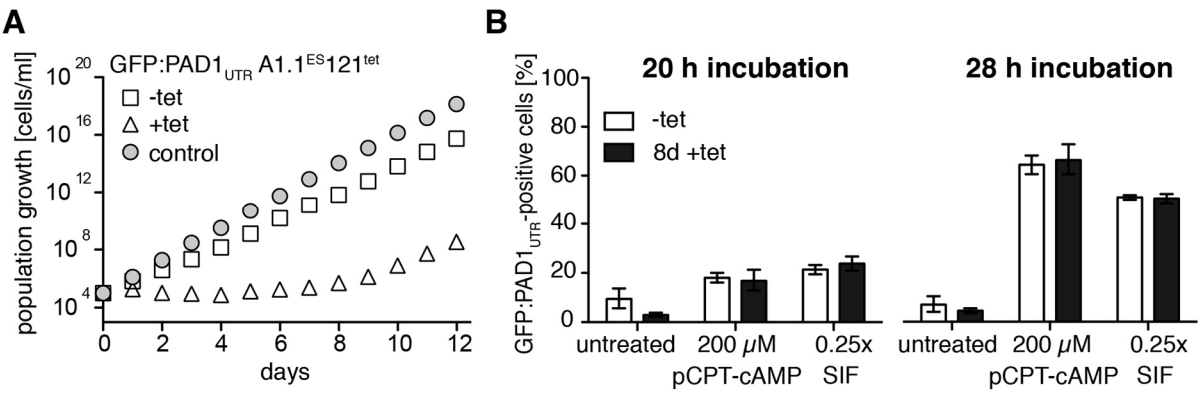

Figure 24: Outgrowing VSG 121 overexpressors can still differentiate to the stumpy stage. (A) Growth curve of a growth-arrested clone of the GFP:PAD1$_{UTR}$A1.1^{ES}121^{tet} cell line that resumed growth after eight days of induction. Tetracycline-induced (triangles) and non-induced (squares) parasites were analyzed. The parental AnTat1.1 13-90 cell line (circles) served as a control. Average values of two experiments of one clonal cell line are shown. **(B)** The parasites were exposed to triggers for st differentiation: either 200 µM pCPT-cAMP or 0.25x SIF. The amount of cells expressing the GFP:PAD1$_{UTR}$ st reporter was quantified after 20 and 28 hours of treatment. Non-induced cells (-tet) of a growth-arrested VSG 121 overexpressor of the GFP:PAD1$_{UTR}$A1.1^{ES}121^{tet} cell line were analyzed as well as VSG 121 overexpressors of the same cell line, that had resumed growth after eight days (8 d +tet) of induction. The amount of cells expressing the st reporter in the absence of the triggers was determined as a control (untreated). Values are presented as average percentages (± SD) of triplicate experiments (total *n* per situation > 600 cells).

3.6.2 Outgrown VSG 121 overexpressors can still express the ectopic VSG

The outgrowth of previously growth-arrested VSG overexpressors could also be explained by a reactivation of the complete A1.1 ES. Thus, the transcriptional status of the active ES would increase and the ESAG levels could return to growth supporting levels. This would also include the reactivation of the expression of the endogenous VSG A1.1. Thus, the outgrowing cells would have exchanged the surface coat once more, now predominantly expressing the original VSG A1.1. To investigate this possibility, immunofluorescence was used to determine which VSG is present on the surface of outgrown VSG 121 overexpressors (Figure 25). Growth-arrested VSG 121 overexpressors of the GFP:PAD1$_{UTR}$A1.1^{ES}121^{tet} cell line induced for seven and 28 days were stained simultaneously with a VSG 121 and a VSG A1.1 antibody. Non-induced cells of the same cell line (0 h) were analyzed in the same way as a control. This demonstrated that even after one month of induction the majority of the outgrown VSG 121 overexpressors (>98% in > 250 cells) still expressed the ectopic VSG 121 on the surface. Thus, a reactivation of the complete A1.1 ES did not occur and could not explain the outgrowth of the growth-arrested VSG overexpressors. In addition, this experiment excluded that the outgrowth is the result of a deficient overexpression system, e.g. a mutation of the T7 polymerase or promotor. If this would be the explanation for the resumed growth, the expression of the ectopic VSG 121 would have stopped. Thus, we conclude that the outgrowth

is neither the result of the reactivation of the complete A1.1 ES nor of a mutation in the overexpression system.

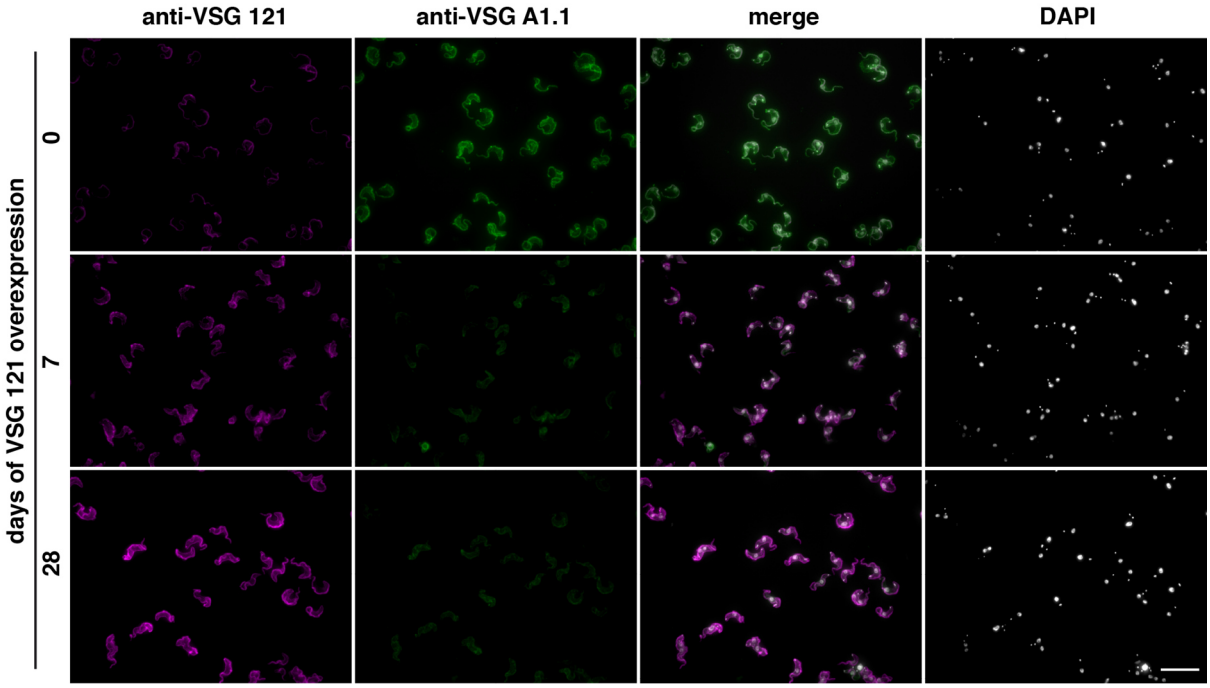

Figure 25: Outgrowing VSG 121 overexpressors can still express the ectopic VSG. Immunofluorescence analysis of a growth-arrested clone of the GFP:PAD1$_{UTR}$A1.1^{ES}121^{tet} cell line. Non-induced cells (0 h) and VSG 121 overexpressors induced for seven or 28 days were stained with antibodies against the ectopic VSG 121 (magenta) and the endogenous VSG A1.1 (green). The DNA was stained with DAPI (grey). After seven days >95% of the parasites expressed the ectopic VSG (*n* = 4, each > 200 cells) and after 28 days >98% (in > 250 cells). Scale bar: 20 µm.

3.6.3 A minor fraction of VSG 121 overexpressors escapes ES-induced stumpy formation

We have so far excluded that the outgrowth is caused by (i) cells that did not respond with growth retardation upon VSG overexpression, (ii) a deficiency in st development, (iii) a reactivation of the complete A1.1 ES and (iv) a deficient overexpression system. Therefore, it was next tested whether all or only a fraction of the VSG overexpressors resumed growth. St parasites are irreversible arrested in the G1/0-phase and can only reenter the cell cycle during the developmental progression to the procyclic stage (Matthews and Gull, 1994; Shapiro et al., 1984). Thus, st trypanosomes have a limited life span in the mammalian host (MacGregor et al., 2011). As the previous results showed that ES-induced cells are *bona fide* st parasites, outgrowth should consequently be caused by a minor fraction of growth-arrested VSG overexpressors, which escaped ES-induced st development. To test this hypothesis, the number of growth-arrested VSG 121 overexpressors that resumed growth was estimated

using serial dilution. For this purpose, I induced VSG 121 overexpression by adding tetracycline and immediately diluted the cultures to 25, 250, 2,500 or 25,000 cells/ml. Each culture was distributed on one 96-well plate, with 200 µl in every well. Thus, each well contained either 5, 50, 500 or 5,000 cells. Non-induced sl cells of the same cell line were seeded at a concentration of five cell per well as a control. In this case, outgrowth was observed in 90% of the wells. However, no growth was observed when induced cells were seeded at the same concentration. This verified the previous suggestion, that ES-induced st parasites are irreversible arrested in the cell cycle. When 50 or 500 induced cells were used per well, outgrowth was observed in 1 and 4% of the wells, respectively. At the highest density (5,000 cells per well) 40% of the wells resumed growth. I assumed that the outgrowth of one well is caused by only one cell to estimate the number of VSG 121 overexpressors that resumed growth. Then, the number of outgrown wells per plate was divided by the total amount of seeded cells per plate. This showed that about one in 10,000 growth-arrested VSG 121 overexpressors resumed growth. We concluded that these cells escaped ES-attenuation induced st development. Nevertheless, the late outgrowth of the growth-arrested VSG overexpressors (discussed above) suggested that these cells initially reacted with growth retardation upon VSG overexpression. Therefore, we assumed that these cells initially did respond to VSG overexpression with ES-attenuation. However, the ES-activity neither fell below the critical threshold to induce terminal st formation nor was sufficient to support growth. Thus, the cells would linger in a prolongated G1-phase of the cell cycle. This state could only be rescinded when the A1.1 ES transcription was re-activated to growth submissive levels. However, not a reactivation of the entire ES would necessarily occur in this case. It would be sufficient if only the *ESAG* transcript levels would be lifted to growth supporting levels, while the endogenous *VSG* could be still silenced. Then, the cells would outgrow as sl parasites still expressing the ectopic VSG 121 on the surface, just as it was the case in our experiments.

3.6.4 VSG 121 overexpression is re-inducible

We also asked if VSG 121 overexpression is re-inducible in the escapers of ES-induced st formation. To answer this question, I induced VSG 121 overexpression for 48 hours in a growth-arrested clone of the GFP:PAD1$_{UTR}$A1.1^{ES}121^{tet} cell line and then removed the tetracycline by washing the cells. The parasites were cultivated in the absence of tetracycline for one week before the drug was re-added. Seven days after the removal of tetracycline and 24 hours after its re-addition the VSG on the cell surface was determined using simultaneous immunostaining for VSG 121 and VSG A1.1 (Figure 26 A). The surface of the parasites was dominated by VSG A1.1 after one week without tetracycline. Upon re-adding the drug, the parasites exchanged their cell surface coat again and now predominantly expressed the

ectopic VSG 121. This demonstrated that VSG 121 overexpression is re-inducible and confirmed that the outgrowth was not caused by a deficient overexpression system.

Next, it was analyzed if the re-induction of ectopic VSG 121 overexpression causes a growth arrest. For this purpose, the parasites were treated as described above and the cultures were split after tetracycline had been removed. One culture was left untreated (tet removed, Figure 26 B) and the other was re-induced with tetracycline (tet re-added, Figure 26 C). This showed that the parasites did not respond any longer with an arrest in growth upon induction of VSG 121 overexpression, even though they expressed the ectopic VSG on the surface. Instead, they now reacted similar to the proliferating clones upon VSG 121 overexpression. However, we had to verify that the altered growth phenotype was indeed a consequence of the escape of ES-induced st formation and not an adaption caused by the prolonged cultivation time. Therefore, non-induced parasites were cultivated for the same period as the washed cultures (-tet, Figure 26 D). At the time VSG 121 overexpression was re-induced in the washed cultures, I also added tetracycline to the non-induced cells (tet added first time, Figure 26 E) and analyzed their growth. VSG 121 overexpression still caused an arrest in growth when the cells were induced for the first time. Thus, the cultivation time was not the cause for the altered growth phenotype upon the re-induction of VSG 121 overexpression. This suggested that the cells do not react any longer with ES-attenuation and subsequent st formation to VSG overexpression once they have escaped ES-induced st development. Thus, in the outgrown, previously growth-arrested, VSG overexpressors the potential to modulate the ES-activity was altered and they now behaved like the proliferating clones. This indicated a high adaptive capacity of the active ES.

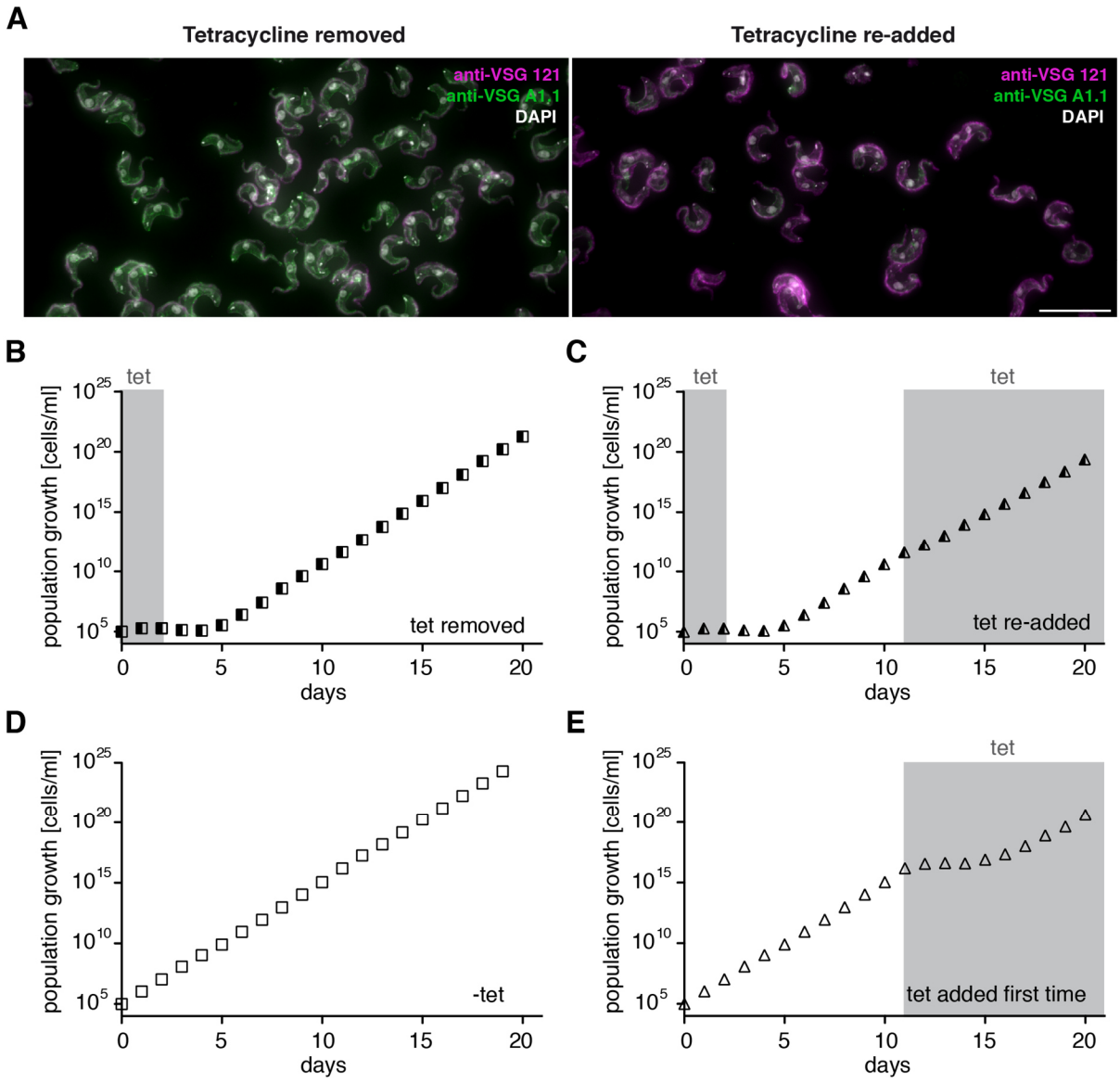

Figure 26: Ectopic VSG 121 overexpression is re-inducible, but the growth arrest is not. VSG 121 overexpression was induced in a growth-arrested clone of the GFP:PAD1$_{UTR}$A1.1^{ES}121^{tet} cell line. After 48 hours of VSG 121 overexpression tetracycline was removed by washing the cells. The cells were cultivated in the absence of tetracycline for one week. The cells were either analyzed in the absence of tetracycline (tet removed) or when the drug was re-added for 24 hours (tet re-added). **(A)** Immunofluorescence analysis of parasites, which were cultivated for one week without tetracycline (Tetracycline removed) and the same parasites after tetracycline re-addition for 24 hours (Tetracycline re-added). The cells were stained with antibodies against the ectopic VSG 121 (magenta) and the endogenous VSG A1.1 (green). The DNA was stained with DAPI (grey). Scale bar: 20 µm. **(B)** Growth curves of parasites that were washed after 48 hours of VSG 121 overexpression and then cultivated without tetracycline (tet removed). **(C)** After nine days without tetracycline the drug was re-added (tet re-added). **(D)** Non-induced parasites of the same cell line (-tet) were cultivated for the same period as the washed cells. **(E)** Then tetracycline was added for the first time (+tet) when the re-addition of the drug was conducted in C. Growth curves of the non-induced and induced parasites are shown. In all growth curves means (± SD) of three experiments of one clone are shown. Due to the small standard deviation the error bars are not visible.

3.6.5 VSG 121 overexpressors are highly adaptive

The re-induction of VSG 121 overexpression indicated a high adaptive potential of the active ES. Therefore, it was analyzed in detail, how the response of growth-arrested VSG 121 overexpressors changes during prolonged cultivation. I thawed a growth-arrested clone of the GFP:PAD1$_{UTR}$A1.1^{ES}121^{tet} cell line and induced VSG 121 overexpression as soon as the non-induced cells doubled normally. Non-induced cells were further cultivated for one or two additional weeks before tetracycline was added. Subsequently, the growth of the induced cells was analyzed and the GFP:PAD1$_{UTR}$ expression quantified after 27 and 51 hours of induction (Figure 27). This demonstrated that the duration of the growth arrest decreased with prolonged cultivation time prior to tetracycline induction (Figure 27 A). The VSG 121 overexpressors doubled only twice until day five when they were induced at the earliest time point (first week). Cells that were cultured for one additional week prior to induction, doubled three times within these five days and parasites that were cultured for two additional weeks prior to induction doubled five times. Consequently, the longer the parasites were cultured prior to induction of VSG 121 overexpression, the higher was the percentage of cells that escaped ES-induced st formation. This was confirmed by the quantification of the GFP:PAD1$_{UTR}$ st reporter (Figure 27 B).

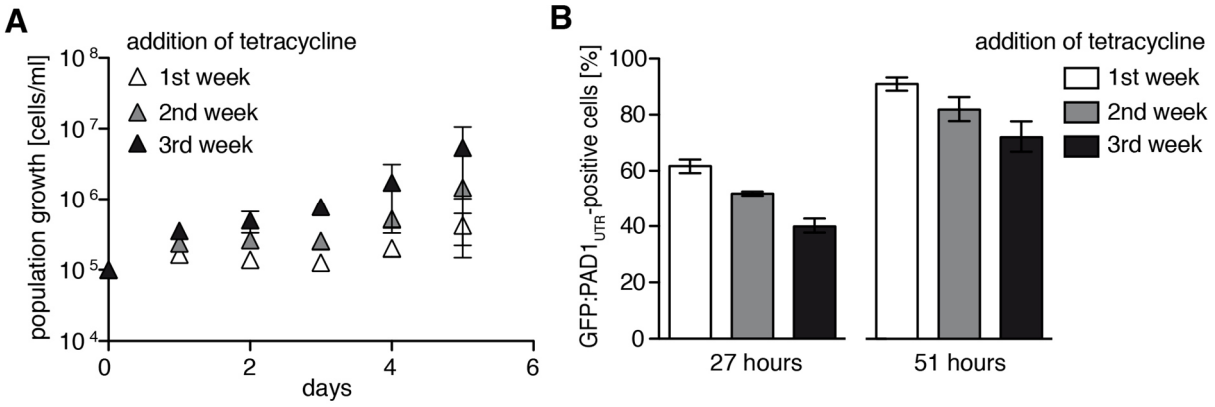

Figure 27: Growth-arrested VSG 121 overexpressors adapt during cultivation. A growth-arrested clone of the GFP:PAD1$_{UTR}$A1.1^{ES}121^{tet} cell line was analyzed in the first, second and third week after thawing. VSG 121 overexpression was induced at a density of 2.5x 10^4 cells/ml **(A)** Growth curves of a growth-arrested VSG 121 overexpressor upon addition of tetracycline (triangles) at different time points after thawing. Means (± SD) of three experiments of one clone are shown. **(B)** Quantification of the amount of parasites expressing the GFP:PAD1$_{UTR}$ st reporter upon addition of tetracycline for 27 and 51 hours. VSG 121 overexpressors were analyzed in the first, second and third week after thawing. Average values (± SD) of three experiments of one clone are shown (total *n* per time point > 600 cells).

Induction at the earliest time point (first week) caused st development in 62% of the parasites within 27 hours of VSG 121 overexpression. When tetracycline was added to cells cultured for

one additional week, 52% of the trypanosomes were GFP:PAD1$_{UTR}$-positive within 27 hours. Within the same time of VSG 121 overexpression, only 40% expressed the st reporter after two additional weeks of cultivation prior to induction. Thus, within two weeks of cultivation the percentage of parasites responding to VSG 121 overexpression with st development decreased by 22%. A similar reduction in st formation was observed after 51 hours of induction. 91% of the parasites expressed the st reporter, when they were induced at the earliest time point of cultivation (first week). After one additional week of cultivation 81% became GFP:PAD1$_{UTR}$-positive within 51 hours of VSG 121 overexpression and after two additional weeks in culture 72%. Thus, with ongoing cultivation fewer parasites differentiated to st sage, indicating that more parasites escape ES-induced st formation. Thus, also the cultivation time influenced the reactivity of the ES, which demonstrated the high adaptive potential of the active ES. Nevertheless, the majority of the parasites still responded with st development to VSG 121 overexpression, though more parasites escaped ES-induced st formation.

Moreover, parasites at densities below 6x 10^5 cells/ml were used for all experiments, which should ensure the predominance of the sl stage as st development is induced *in vitro* at densities above 1x 10^6 cells/ml (reviewed in McCulloch et al., 2004). However, VSG 121 overexpression induced ES-attenuation triggered st formation at densities below the critical SIF (stumpy induction factor) threshold. This suggested that ES-attenuation can act independently of cell density and hence the stumpy induction factor SIF.

3.7 SIF and ES-attenuation feed in the same pathway

The previous results have demonstrated that ES-attenuation caused the development of *bona fide* st parasites. The only naturally occurring trigger known to cause this differentiation was up till now the stumpy induction factor (SIF) (Vassella et al., 1997). The so far elusive factor is secreted by the parasites and accumulates with rising parasitemia (Reuner et al., 1997; Vassella et al., 1997). Once a critical threshold in concentration is reached, the sl trypanosomes differentiate to the st stage and thus SIF acts in a cell density dependent manner. In contrast, ES-attenuation triggered the developmental transition at cell densities, which are *a priori* not sufficient to induce st development. This suggested that ES-attenuation can act independently of cell density and SIF. Thus, our results demonstrated for the first time that another way exists to induce st development besides SIF, namely ES-attenuation. This raised the question, whether SIF and ES-attenuation act on separate pathways or if the pathways intersect and thus the triggers can act in a cooperative manner. To answer this, basically two approaches were pursued. First, the impact of the cell density on the VSG overexpressors was analyzed. Second, parasites were simultaneously challenged with ES-attenuation and defined concentrations of known triggers for st development (SIF and its second messenger cAMP).

3.7.1 ES-induced cell cycle arrest is independent of the cell density

First, the impact of cell density and hence different SIF concentrations on the VSG overexpressors was analyzed. For this purpose, I induced VSG 121 overexpression in a growth-arrested clone at two different starting cell densities: 2.5x 10^5 cells/ml (high density, HD) and 2.5x 10^4 cells/ml (low density; LD) (+tet, Figure 28 A, B). The cultures were then cultivated without dilution in the constant presence of tetracycline. The cultures were diluted again when the cells doubled for the first time after five days of induction and escaped ES-attenuation induced stumpy formation. First, I determined the growth upon addition of tetracycline to analyze the impact of the different cells densities on the VSG 121 overexpressors. This showed that independently of the starting cell density, the VSG 121 overexpressors only divided once after the addition of tetracycline and then arrested in growth (Figure 28 A, B). Thus, the immediate cell cycle arrest of the growth-arrested VSG 121 overexpressors was not influenced by the cell density. Due to the fast kinetics and low cell number the cell cycle the arrest cannot be attributed to SIF. The possible impact of SIF only became apparent at later time points.

HD cultures had a 10-fold higher parasite density than LD cultures and SIF accumulates proportional to the cell number. Thus, the critical SIF threshold should be exceeded earlier in

HD cultures than in LD cultures. Indeed growth was different in HD and LD cultures. While the HD cultures started to die after four days of induction, the LD cultures started to resume growth at day five of VSG 121 overexpression (Figure 28 A, B, +tet). This indicated that in the LD cultures few trypanosomes were present, which could lift the initial growth retardation and escaped ES-attenuation induced stumpy formation (as described in chapter 3.6). Thus, in LD cultures the SIF concentration did not reach the critical threshold to induce st development. In contrast, the death of HD cultures indicated that all parasites, including the escapers, differentiated to the st stage. These results suggested the following scenario: independent of the cell density ES-attenuation triggered st development within the first two days in the majority of cells and only a few parasites could escape. While the ES-induced st parasites were doomed to die approximately three days after developmental transition, the escapers could outgrow them. However, also the escapers would differentiate to the st stage once the critical SIF threshold was reached. Consequently, the death of the st parasites should become apparent at day five of induction as we observed it in the presented experiments. Thus, within four days the SIF concentration could have reached in HD cultures the critical threshold to induce st development also in the escapers. Alternatively, a lack of nutrients or the accumulation of growth-inhibiting conditions due to the constant high amount of cells over several days in HD cultures could have prevented the outgrowth of the escapers.

Then, it was analyzed at which time point SIF possibly reached the critical concentration to induce the developmental transition in all cells (including the escapers). For this purpose, the accumulated SIF in the HD and the LD cultures was removed by washing the parasites after one and two days of induction (washed 1 and 2 days +tet, Figure 28 A, B). The VSG 121 overexpressors were further cultivated in the presence of tetracycline without dilution until the cells started to divide again. This showed that the cells in the HD cultures resumed growth, just like the LD cultures, once the medium was exchanged. It was excluded that the washing procedure influenced the cells as I treated non-induced cells (-tet) and the parental AnTat1.1 13-90 (control) cell line in the same way and did not observe any changes in growth (Figure 28 C, D). This indicated that, within the first two days, the amount of secreted SIF was not sufficient to induce st development in HD and LD cultures. However, ES-attenuation caused the formation of st parasites in the majority of cells in less than one day. These results supported our previous conclusion, that ES-attenuation can induce st development independent of the cell density and SIF.

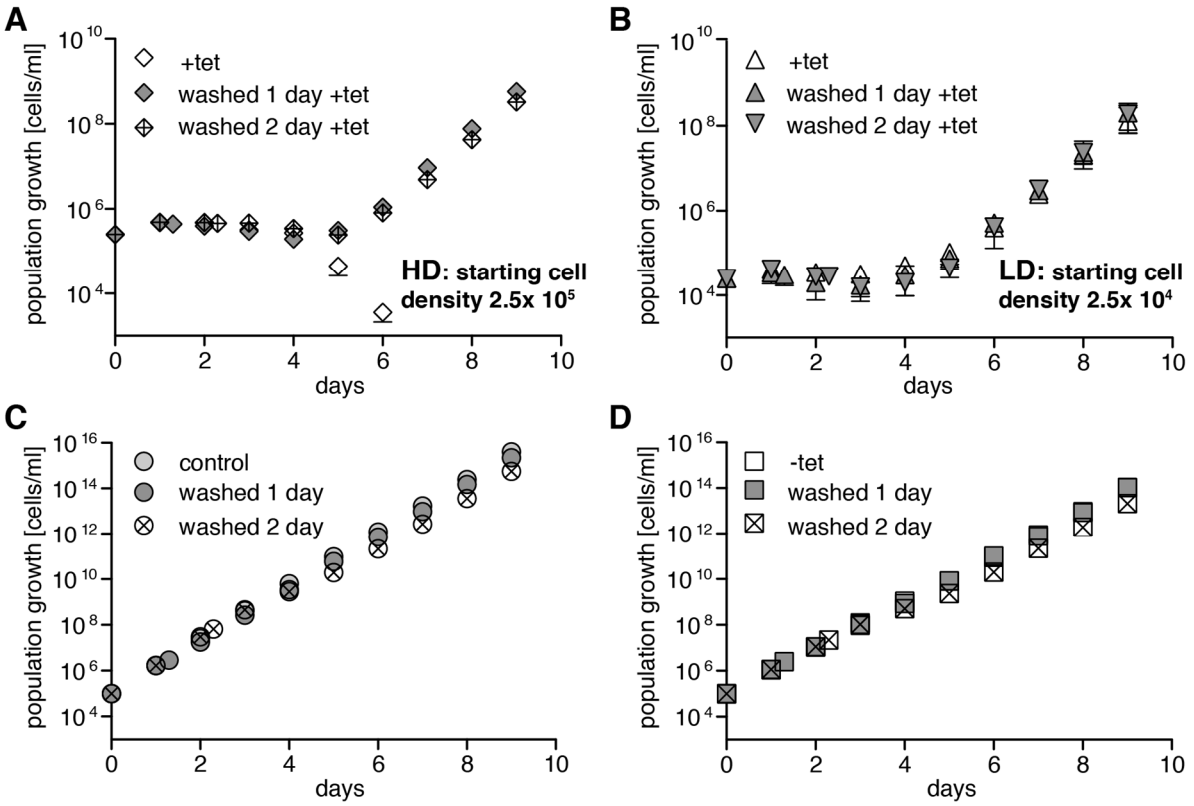

Figure 28: The impact of cell density on ES-induced st formation and its escapers. SIF induces st development in a cell density dependent manner as it is secreted by the parasite itself. To analyze the possible impact of SIF on a growth-arrested clone of the GFP:PAD1$_{UTR}$A1.1^{ES}121^{tet} cell line, VSG 121 overexpression was induced at two different starting cell densities (**A**: HD: 2.5x 10^5 cells/ml and **B**: LD: 2.5x 10^4 cells/ml). The parasites were cultivated without dilution to allow the accumulation of SIF and were diluted again, when the parasites reentered the cell cycle and doubled for the first time. Consequently, in **(A)** SIF should have reached the critical threshold to induce st development earlier than in **(B)**, as the cells had a 10-fold higher concentration. The possible impact of SIF in addition to the VSG 121 overexpression (+tet) was analyzed using cumulative growth curves. SIF was removed by washing the cultures after one and two days of induction (washed 1 or 2 day) to determine at which time point the escapers of ES-attenuation could resume growth. The parasites were further cultivated in the presence of tetracycline. **(C, D)** To control that the washing procedure did not have an impact on the cells, **(C)** the parental 13-90 cell line (control) was washed after one and two days of cultivation as well as **(D)** non-induced cells and their growth was recorded. In all growth curves means (±SD) of three experiments of one clone are presented. Due to the small standard deviation the error bars are not visible.

The experiments indicated that ES-attenuation induced st development, before the SIF concentration reached the critical threshold to influence the parasites. Only the escapers of VSG 121 overexpression induced ES-attenuation were possibly affected by SIF. It remained unclear if SIF had an additional effect during ES-induced st development as we did not know the amount of secreted SIF that had already accumulated at the analyzed time points. Thus, we could not draw any conclusion if SIF and ES-attenuation can act in a cooperative manner and feed in the same pathway. Besides this, it could not been ascertained if indeed an accumulation of SIF in HD cultures hindered the outgrowth of the escapers as the molecular

nature of SIF is unknown. For example, a lack of nutrients or the accumulation of growth-inhibiting conditions could be an alternative explanation for the death of all cells. Also in this case, the escapers could resume growth once new medium was provided. For these reasons, we decided to challenge the VSG 121 overexpressors directly with SIF or its downstream analogue.

3.7.2 SIF and ES-attenuation are acting in a cooperative manner

To analyze if SIF and ES-attenuation act on separate signaling pathways or feed into the same, the parasites were simultaneously challenged with ES-attenuation and defined concentrations of known triggers for st development. It has been demonstrated that membrane permeable and hydrolysable cAMP derivatives like pCPT-cAMP mimic the intracellular SIF-response of the cells and can be considered as its downstream analogue (Laxman et al., 2006; Vassella et al., 1997). Thus, st development can be induced by SIF or due to the addition of pCPT-cAMP. The latter one is frequently used to induce st differentiation as SIF itself remains elusive to date.

The impact of these known triggers during ES-induced st development was analyzed using a growth-arrested clone of the GFP:PAD1$_{UTR}$A1.1^{ES}121^{tet} cell line (Figure 29). The amount of st parasites was determined by quantifying the number of cells expressing the GFP:PAD1$_{UTR}$ st reporter. A starting cell density of 1x 10^5 cells/ml was used to ensure that the cells do not reach densities which are sufficient to induce st development *per se* within 28 hours of treatment. To determine the effect of ES-attenuation alone, I added tetracycline to the cells and cultivated them without any pCPT-cAMP or SIF (+tet untreated, Figure 29). Non-induced cells were also cultivated in the absence of the developmental triggers to ensure that the assay *per se* did not cause st development (-tet untreated, Figure 29). These controls showed that 2% of the non-induced and 20% of the VSG 121 overexpressors expressed the st marker after 20 hours (untreated, Figure 29 A). Within 28 hours of treatment, 4% of the non-induced parasites and 50% of the VSG 121 overexpressors were st (untreated, Figure 29 B). Consequently, the non-induced control was almost devoid of st parasites while the induction of ES-attenuation with tetracycline caused st development in up to 50% of the cells. Thus, the assay was suitable to analyze the interplay between the known st differentiation triggers and ES-induced st development.

For the assay, a concentration of either 100 or 200 µM pCPT-cAMP was chosen based on preliminary tests. These concentrations provided a good time window for the analysis when the amount of st parasites was determined after 20 and 28 hours of treatment (-tet, Figure 29 A, B). Moreover, we wanted to use defined concentrations of the extracellular SIF signal. As the molecule SIF is unknown, we decided to use a SIF-concentrate to induce st

development (kindly provided by I. Subota). 1x of this concentrate corresponds to the source conditioned medium, which had not been concentrated (as described in chapter 5.2.1 Differentiation to the stumpy stage). Initially, I titrated different concentrations of the SIF-concentrate and analyzed its impact on sl trypanosomes by quantifying the amount of GFP:PAD1$_{UTR}$-positive cells. For further analysis, we decided to use a final concentration of 0.25x as this had almost no effect after 20 hours, but was able to induce st differentiation in approximately half of the population within 28 hours (-tet, Figure 29 A, B). Additionally, I decided to use 0.37x as this concentration caused the formation of a nearly uniform st population within 28 hours (-tet, Figure 29 B). Hence, defined concentrations of an intracellular differentiation signal and the extracellular SIF could be used to induce st development (as described in chapter 5.2.1 Differentiation to the stumpy stage).

Next, the influence of the triggers on the parasites alone (-tet) and in combination with ES-attenuation (+tet) were analyzed. Therefore, I either added the different pCPT-cAMP and SIF concentrations to non-induced parasites (-tet) or simultaneous with tetracycline (+tet) to induce ES-attenuation (Figure 29 A, B). This showed that 4% of the non-induced cells expressed the st marker within 20 hours when treated with 100 µM pCPT-cAMP or 16% once the higher concentration of the cAMP analogue was used (-tet, Figure 29 A). In contrast, 34% of the VSG 121 overexpressors became st within the same time due to the addition of 100 µM pCPT-cAMP and 68% in the presence of 200 µM (+tet, Figure 29 A). If the non-induced parasites were treated with 0.25x and 0.37x SIF, 8% and 22% of the trypanosomes were GFP:PAD1$_{UTR}$-positive within 20 hours (-tet, Figure 29 A). In the same time, the addition of 0.25x and 0.37x SIF caused st development in 46% and 59%, respectively, of the VSG 121 overexpressors (+tet, Figure 29 A). After 28 hours, 24% of the non-induced cells were stumpy when the lower cAMP concentration was added and 68% with the higher concentration (-tet, Figure 29 B). However, pCPT-cAMP treatment of the VSG 121 overexpressors resulted in a nearly uniform st population within 28 hours (100 µM: 90%; 200 µM: 99%) (+tet, Figure 29 B). When non-induced parasites were challenged for 28 hours with 0.25x SIF, 43% of the cells expressed the st reporter and 83% once the higher concentration was used (-tet, Figure 29 B). In contrast, nearly all VSG 121 overexpressors developed to the st stage upon the addition of SIF (+tet, Figure 29 B). Thus, the presence of st differentiation triggers caused an increase in the number of st VSG 121 overexpressors.

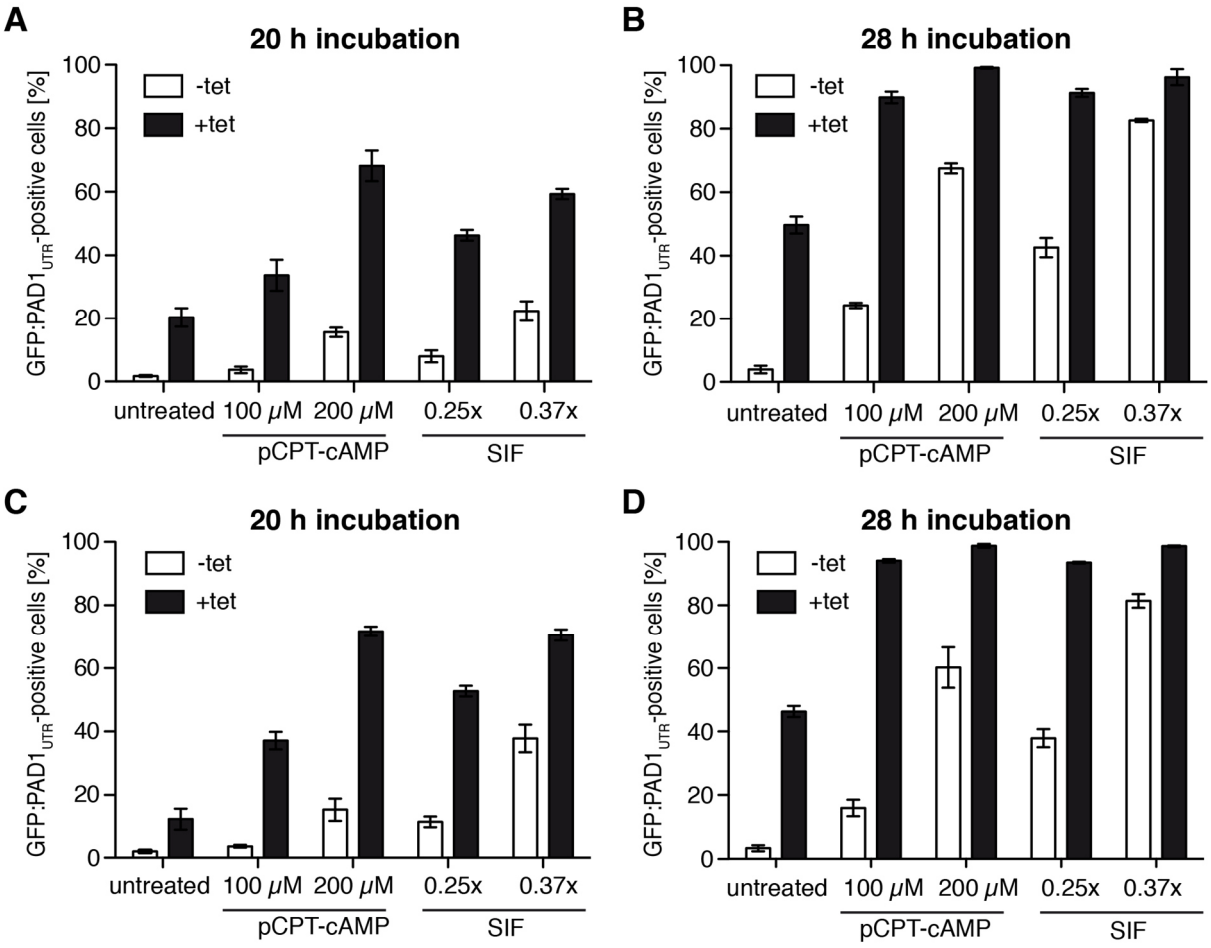

Figure 29: SIF and ES-attenuation act in a cooperative manner. Parasites were simultaneously challenged with ES-attenuation and other triggers for st differentiation to determine the impact of SIF during ES-induced st formation. For this purpose, a growth-arrested clone of the GFP:PAD1$_{UTR}$A1.1^{ES}121^{tet} cell line was used. Either non-induced cells (-tet) or VSG 121 overexpressors were treated simultaneous to the addition of tetracycline (+tet), with two different concentrations of pCPT-cAMP (100 µM, 200 µM) or SIF (0.25x, 0.37x). The number of parasites expressing the GFP:PAD1$_{UTR}$ st reporter was microscopically analyzed to quantify the impact of the triggers after **(A, C)** 20 and **(B, D)** 28 hours of treatment. The amount of GFP:PAD1$_{UTR}$-positive cells was determined in the absence of the triggers as a control (untreated). Values are presented as percentage of cells (± SD) of triplicate experiments (total *n* per situation > 600 cells). After **(A, B)** the first quantification, the experiment was repeated after one week **(C, D)** to validate that the cooperative effect was still present with ongoing cultivation.

As previous experiments showed that more cells can escape ES-induced st development with ongoing cultivation (compare Figure 27), the experiment was repeated after one week to validate the obtained results (Figure 29 C, D). This verified that more cells react with st development, when simultaneously challenged with ES-attenuation and the classical triggers. ES-attenuation alone caused the developmental transition only in 12% of the cells within 20 hours (untreated +tet, Figure 29 C). Between 4% and 38% of the cells expressed the st reporter, when non-induced cells were treated for the same time with SIF or pCPT-cAMP (-tet, Figure 29 C). The mildest effect (4%) was observed with 100 µM cAMP and the strongest

effect with 0.37x SIF (38%). In contrast, when the VSG 121 overexpressors were incubated with the compounds for 20 hours at least 37% of the parasites responded with st formation (100 µM pCPT-cAMP) and at most 72% (200 µM pCPT-cAMP) (+tet, Figure 29 C). After 28 hours, ES-attenuation alone caused the developmental transition in 46% of the cells (untreated +tet, Figure 29 D). In non-induced cells, a nearly uniform st formation (81%) was observed only when 0.37x SIF was used (-tet, Figure 29 D). In contrast, more than 93% of the VSG 121 overexpressors differentiated to the st stage when the additional triggers were added (+tet, Figure 29 D). Thus, the combination of ES-attenuation and the classical triggers caused the developmental transition in more cells than each trigger alone within the same time. This pointed to an additive effect of both triggers.

I could imagine two simplistic scenarios, which could explain how the triggers intertwine. First, both triggers are acting on separate pathways, which would have st development as the same output. Thus, when both triggers are combined st development would be caused in one cell either by SIF or by ES-attenuation and the effect of the triggers should add up. Second, if both triggers feed into the same pathway, st development could be caused in one cell by SIF and ES-attenuation. This could accelerate the developmental transition and the combination of both triggers would lead to the development of more st parasites. A super pulse in st differentiation should be observed in this case, instead of a summation of the effect of both triggers alone. That the combination of ES-attenuation and SIF indeed caused such a super pulse and that the effects did not simply add up is illustrated with two examples. In the first experiment, the cAMP analogue caused the expression of the st marker in 16% and ES-attenuation in 20% of the cells (Figure 29 A). We would expect that the combination of ES-attenuation and 200 µM cAMP would cause st development in approximately 36% of the trypanosomes if the effect of the triggers is additive. However, when 200 µM pCPT-cAMP and ES-attenuation were combined, 68% of all trypanosomes differentiated to the st stage within 20 hours of treatment (Figure 29 A). Thus, almost twofold more cells became GFP:PAD1$_{UTR}$-positive than we would expect from a simple additive effect. In the second experiment, an even more pronounced super pulse was observed. ES-attenuation alone produced 12% st cells, 200 µM cAMP 15% and the combination of both 72% (Figure 29 C). Moreover, the same was true for the combination of ES-attenuation and 0.25x SIF. In the first experiment 46% of the cells expressed the st reporter when exposed to both triggers for 20 hours. Treatment with SIF alone caused the developmental transition in 8% and ES-attenuation in 20% of the cells (Figure 29 A). Likewise, ES-attenuation alone produced 12% st cells in the second experiment, 0.25x SIF 11% and the combination of both 53% (Figure 29 C). Thus, the amount of st cells exposed to the lower SIF concentration and ES-attenuation can also not be explained by a simple additive effect of the triggers. Therefore, we conclude that SIF and ES-attenuation can act in a cooperative manner.

3.7.3 ES-attenuation does not increase SIF sensitivity

The previous experiment indicated that SIF and ES-attenuation act in a cooperative way. This could be explained by two scenarios. First, both triggers act along the same signaling pathway and thus st development is accelerated in the presence of both triggers. Second, ES-attenuation increases the sensitivity of the parasites to act on the SIF trigger. An increased SIF sensitivity would mean that parasites respond with st development to low SIF concentrations, which are not sufficient to induce st development alone. If this is the case, the increased SIF sensitivity would cause developmental transition and not the attenuation of the active ES *per se*. The analyses before suggested that ES-attenuation induces st development independent of SIF as differentiation was triggered at densities that were 40-fold lower (2.5x 10^4 cells/ml) than the assumed critical threshold (1x 10^6 cells/ml). Nevertheless, I wanted to assure further that ES-attenuation does not increase the sensitivity towards SIF.

For this purpose, the same cell line and assay was used as in the previous experiment, but the parasites were treated either with 0.25x SIF or different dilutions of the concentrate (Figure 30). I decided to dilute the SIF-concentrate further 1:10 (0.025x SIF) as ES-attenuation induced developmental transition at 10-fold different cell densities. If ES-induced st development would be triggered by an increased sensitivity towards SIF, treatment of the VSG 121 overexpressors with this concentrate should result in an increased number of st parasites compared to the untreated cells. As ES-induced and density-induced st development occur at cell densities that differ by more than 10-fold, trypanosomes were also treated with the 1:100 diluted SIF-concentrate (0.0025x SIF). Non-induced cells (-tet) were used to determine the impact of the different SIF concentrations alone or the parasites were challenged in parallel with SIF and ES-attenuation. I also analyzed the number of ES-induced st parasites in the absence of additional triggers (untreated +tet, Figure 30). The impact of the triggers was assessed by quantifying the amount of GFP:PAD1$_{UTR}$-positive parasites.

Within 20 hours of treatment, ES-attenuation caused st development in 33% of the parasites (untreated +tet) and 0.25x SIF in 32% (Figure 30 A). When both triggers were combined, 72% revealed a green fluorescent nucleus (+tet, Figure 30 A). Treatment of non-induced parasites with the lower concentrations did not yield an increase in the number of GFP:PAD1$_{UTR}$-positive cells compared to the 10% in the untreated control (-tet, Figure 30 A). Also, the addition of the SIF dilutions to the VSG 121 overexpressors did not change the amount of st parasites as comparable to the induced control (33%) 28% of parasites expressed the st reporter (+tet, Figure 30 A). After 28 hours of VSG 121 overexpression, 58% of the parasites expressed the GFP:PAD1$_{UTR}$ reporter (+tet control, Figure 30 B). In the same time, 52% of the non-induced parasites became st when the cells were exposed to 0.25x SIF (-tet, Figure 30 B). The combination of both triggers produced a nearly uniform st population (+tet, 0.25x SIF: 93%,

Figure 30 B). However, the lower SIF concentrations neither influenced the non-induced parasites nor the VSG 121 overexpressors.

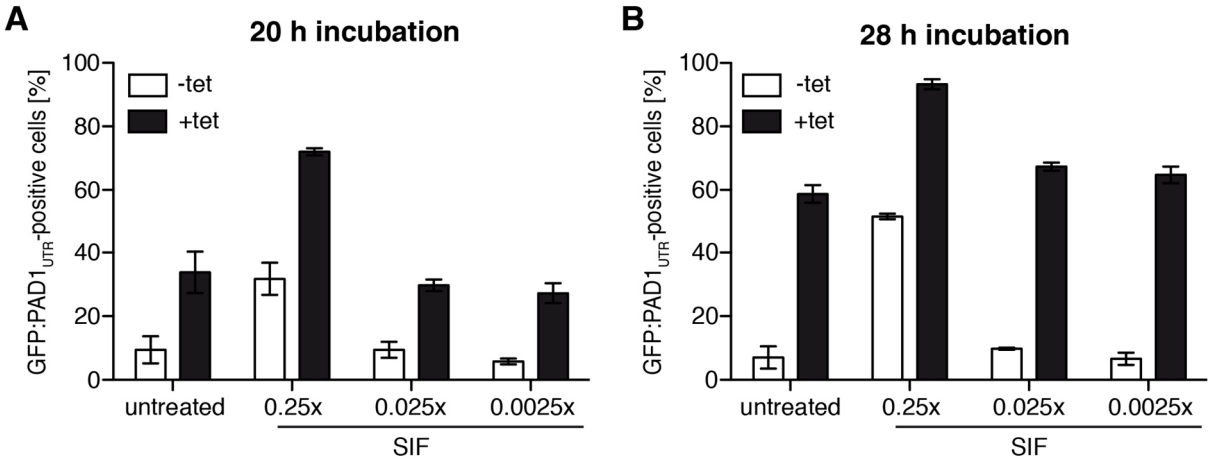

Figure 30: ES-attenuation does not increase SIF sensitivity. Parasites were simultaneously challenged with ES-attenuation and three different SIF concentrations to determine if an increased SIF sensitivity causes ES-induced st development. For this purpose, a growth-arrested clone of the GFP:PAD1$_{UTR}$A1.1^{ES}121^{tet} cell line was used. Non-induced cells (-tet) and VSG 121 overexpressors of the same cell line were treated, immediately after the addition of tetracycline (+tet), with 0.25x, 0.025x or 0.0025x SIF. The number of parasites expressing the GFP:PAD1$_{UTR}$ st reporter was microscopically analyzed to quantify the impact of the triggers after **(A)** 20 and **(B)** 28 hours of treatment. The amount of cells displaying a green fluorescent nucleus in the absence of the triggers was determined as a control. Values are presented as percentage of cells (± SD) of triplicate experiments (total *n* per situation > 600 cells).

Taken together, VSG 121 overexpressors did not display an increased sensitivity to the 10- and 100-fold diluted SIF-concentrate. The factor had only an additional impact during VSG overexpression induced ES-attenuation, when the highest concentration (0.25x SIF) was used. Solely under this condition st development was triggered as well in the non-induced cells. This suggested that SIF only affected the VSG 121 overexpressors when its concentration was sufficient to induce st development without ES-attenuation. This implies that the attenuation of the active ES *per se* caused st development and not an increased SIF sensitivity of the parasites due to ES-attenuation. However, as the parasites are thought to continuously secret SIF, the amount of SIF most likely also increased during the assay, which could have an additional impact. It would be necessary to deplete SIF from the medium to unequivocally demonstrate that ES-attenuation *per se* causes st development, which will be only possible once the molecular nature of SIF is elucidated. Nevertheless, all of the analyses I could conduct to investigate if ES-attenuation acts independent of SIF suggested that this is the case. Thus, we conclude that SIF and ES-attenuation feed into the same pathway, acting in a cooperative manner.

3.7.4 A decreased ES-activity primes trypanosomes for the SIF signal

The previous results showed that ES-attenuation and SIF acted in a cooperative manner in st development, suggesting that both pathways intersect. As ES-attenuation occurs also during density-induced st development, we propose that the transcriptional status of the ES could be a crucial element in the st differentiation pathway. In this scenario, developmental transition could only be induced when the ES-activity falls below a critical threshold. If this hypothesis holds true, a decrease of the ES-activity above the critical threshold for st development should prime the parasites for the SIF signal. These trypanosomes should differentiate faster to the st stage than parasite displaying a higher or full ES-activity. To test this hypothesis, cells which reduced the ES-activity without phenotypic consequences were exposed to classical triggers for st development.

A reduction of the ES-activity to 50% was not sufficient to trigger st development within 48 hours of VSG 121 overexpression in proliferating clones (chapter 3.2 and 3.3). Therefore, parasites induced for 48 hours (+tet) and non-induced cells (-tet) of a proliferating clone of the GFP:PAD1$_{UTR}$A1.1^{ES}121^{tet} cell line were used for the assay. Induced parasites (+tet) and non-induced cells were diluted to a concentration of 5x 10^4 cells/ml and two different concentrations of pCPT-cAMP (100 or 200 µM) or SIF (0.25x or 0.37x) were added (as described in chapter 5.2.1 Differentiation to the stumpy stage). The amount of st parasites was determined after 20 and 28 hours of treatment by monitoring the number of cells expressing the GFP:PAD1$_{UTR}$ reporter (Figure 31). Within 20 hours of incubation, the number of st parasites increased only when the VSG 121 overexpressors were treated with 200 µM pCPT-cAMP (26%, data not shown). Less than 6% of the population became GFP:PAD1$_{UTR}$-positive within the same time when the other conditions were applied (data not shown). If the VSG 121 overexpressors were treated for 28 hours with the lower pCPT-cAMP or SIF concentration, a 6 to 12-fold increase in the number of st parasites was observed (Figure 31 A). Only 1% of the non-induced parasites expressed the reporter with the cAMP treatment, whereas 13% of the induced cells were st. When the parasites were exposed to 0.25x SIF for 28 hours, 2% of the non-induced parasites were GFP:PAD1$_{UTR}$-positive and 12% of the VSG 121 overexpressors. A marked increase in the number of st parasites was observed when treated with 200 µM pCPT-cAMP for 28 hours. In this case, more than 89% of the VSG 121 overexpressors developed to the st stage and only 8% of the non-induced parasites. Thus, 11-fold more st parasites were present, when the ES-activity was mildly down-regulated prior to the treatment. A comparable result was obtained by the exposure of the proliferating VSG 121 overexpressors to the higher SIF concentration. The addition of 0.37x SIF caused the differentiation in almost fourfold more parasites, when tetracycline was present (-tet: 10% versus +tet: 35%).

These results were surprising as the non-induced cells of the potentially 'proliferating' clone reacted to the treatment not in a similar manner as the non-induced cells of a potentially

'growth-arrested' clone (discussed below). Therefore, I wanted to validate if the non-induced cells of the potentially 'proliferating' clone could develop after all to the st within the assay. For this purpose, I decided to analyze the amount of st parasites also after 48 hours of treatment. This was possible as all of the cultures had a density below 5x 10^5 cells/ml after 28 hours of treatment and it was previously shown that the accumulation of the parasite secreted SIF alone would not be sufficient to trigger st development in the following 24 hours (compare Figure 17). After 48 hours of treatment, more than 80% of the non-induced and tetracycline-induced parasites differentiated to the st stage when treated with either of the pCPT-cAMP concentrations (Figure 31 B). In the same time, 35% of the non-induced cells expressed the st reporter when treated with 0.25x SIF and 96% of the VSG 121 overexpressors. Thus, nearly threefold more trypanosomes became st when the ES-activity was decreased prior to the treatment with 0.25x SIF. Also, more VSG 121 overexpressors were GFP:PAD1$_{UTR}$-positive than the non-induced parasites when exposed to the higher SIF concentration (-tet 0.37x: 74%, +tet 0.37x: 100%). Taken together, this showed that the non-induced and induced proliferating VSG 121 overexpressors could differentiate to the stage in the assay, whereby more of the induced cells became st in the same time.

Proliferating VSG 121 overexpressors and non-induced parasites should respond in a similar way to the classical triggers for st development, if a reduced ES-activity does not prime the trypanosomes for st development. However, this was not the case. The represented results demonstrated that more trypanosomes differentiate to the st stage, when the parasites had a reduced ES-activity prior to the treatment. The most striking example was the 11-fold increase in the amount of st parasites after 28 hours of treatment with 200 µM pCPT-cAMP. Beyond that, also the exposure to SIF caused an increase in the number of st VSG 121 overexpressors compared to the non-induced cells. Consequently, these results showed that a reduced ES-activity primed the parasites for the developmental transition.

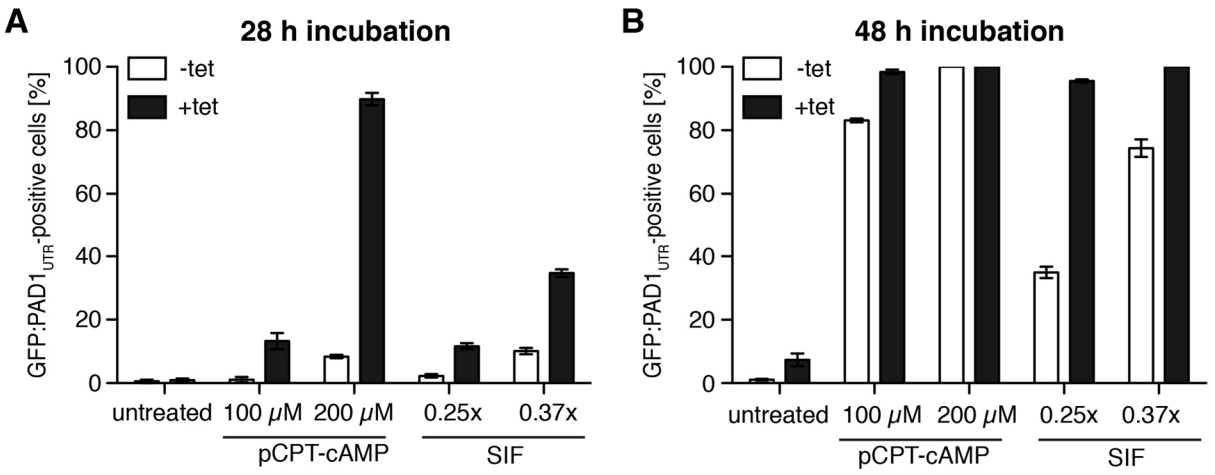

Figure 31: A reduced ES-activity primes trypanosomes for stumpy development. VSG 121 overexpression was induced in a proliferating clone of the GFP:PAD1$_{UTR}$A1.1^{ES}121^{tet} cell line for 48 hours prior to the treatment of the cells. As it was shown previously in this thesis, the ES-activity of proliferating VSG 121 overexpressors is reduced within this time without phenotypic consequence. Non-induced cells of the same cell line (-tet) and the VSG 121 overexpressors (+tet) were treated with two different concentrations of pCPT-cAMP (100 µM, 200 µM) or SIF (0.25x, 0.37x). The number of parasites expressing the GFP:PAD1$_{UTR}$ st reporter was microscopically analyzed to quantify the impact of the triggers after **(A)** 28 and **(B)** 48 hours of treatment. The amount of cells displaying a green fluorescent nucleus in the absence of the triggers was determined as a control (untreated). Values are presented as percentage of cells (± SD) of triplicate experiments (total *n* per situation > 600 cells).

However, the comparison of the results of the non-induced parasites of the potentially 'growth-arrested' and potentially 'proliferating' clones revealed that they responded differently to the classical triggers for st development. When a potentially 'growth-arrested' clone was used, more than 60% of the non-induced parasites differentiated to the st stage within 28 hours of treatment with the higher pCPT-cAMP or SIF concentration (Figure 29 B). When non-induced trypanosomes of a potentially 'proliferating' clone were used, less than 11% of the cells expressed the st reporter under similar conditions (Figure 31 A). It was excluded that this was caused by a general failure in st development in the potentially 'proliferating' VSG 121 overexpressors for two reasons. First, a uniform density-induced st population could be obtained in both cell lines (Figure 17, Figure 31 B). Second, all non-induced trypanosomes responded to pCPT-cAMP and SIF with st development, although the timing at which a uniform population was obtained differed between the clones. This suggested that even in the absence of tetracycline potentially 'proliferating' and potentially 'growth-arrested' clones responded with different kinetics to the triggers for st development. Though it seems unlikely that variations within the set-up like the different starting cell densities or another used batch of the SIF-concentrate caused the discrepancy, this needs to be excluded by analyzing non-induced cells of both clones in one assay in parallel under identical conditions.

3.8 Identification of potential regulators of the ES using RNA sequencing

Overexpression of the ectopic VSG 121 caused the silencing of the endogenous *VSG* and a decrease of the transcriptional status of the active ES in monomorphic and pleomorphic trypanosomes (Batram et al., 2014; Chaper 3.2 of this thesis). Batram et al. have previously shown that the ectopic VSG 121 needs to be expressed at high levels to induce ES-attenuation: low-level expression, achieved by deletions within the 3'UTR, did not cause the attenuation (PhD thesis Batram, 2013). This raised the question, how the ectopic VSG expression is sensed and the signal mediated to attenuate the ES. To identify potential ES regulators, RNA sequencing experiments with monomorphic and pleomorphic VSG 121 overexpressors were conducted to screen for differences in the expression patterns pre- and post-induction.

For monomorphic cells, mRNA levels of VSG 121 overexpressors induced for 4, 8, 24 and 48 hours were analyzed and compared to the transcript levels of non-induced cells. Within four hours of VSG 121 overexpression, the transcript levels of only three genes (*Tb427.08.510, Tb427.10.6200, Tb427.10.13410)* were more than twofold up-regulated (Table 1). All three genes encoded hypothetical proteins with an unknown function and their transcription increased further at later time points (Table 1). A twofold up-regulation was detected for 92 transcripts after 24 hours of VSG 121 overexpression. However, we decided to focus our analysis on genes that displayed an up-regulation within the first four hours, as the attenuation of the active ES initiated within this time. We assumed that knocking-down negative ES regulators, while simultaneously overexpressing an ectopic VSG, should prevent ES-attenuation and thus growth retardation in monomorphic cells. Therefore, it was assessed if the candidates with unknown function are essential for attenuation of the active ES by knocking-down the individual proteins via RNAi in the monomorphic $221^{ES}121^{tet}$ cell line. RNAi cell lines of *Tb427.10.13410* and *Tb427.10.6200* were generated by Matthias Grießmann as part of his bachelor thesis (bachelor thesis Grießmann, 2014). Neither the knockdown of *Tb427.10.13410* nor of *Tb427.10.6200* in parallel to VSG 121 overexpression did alter the VSG 121 overexpression growth phenotype (chapter 7.1 Figure 46). This suggested that these genes are not essential for VSG 121 overexpression induced ES-attenuation. However, we cannot exclude that a different timing in the on-set of VSG 121 overexpression and RNAi or an incomplete down-regulation of the respective candidate via RNAi did obscure a potential function of either candidate during ES-attenuation.

Table 1: Up-regulated transcripts upon VSG 121 overexpression in monomorphic cells. The upper part of the table shows the transcripts that were more than twofold up-regulated within four hours of VSG 121 overexpression in monomorphic cells. The lower part of the table shows three adjacent genes of the strongest regulated transcript, *Tb427.08.510*, that were also up-regulated during the course of VSG 121 overexpression (overview of the gene array in chapter 7.1 Figure 47). Transcripts with FPKM (fragments per kilobase of transcript per million mapped reads) values below one in the non-induced sample were excluded. Presented are the Gene IDs for the corresponding transcripts (TriTrypDB), the FPKM values for the respective transcript in the non-induced cells and the fold regulation during the course of VSG 121 overexpression. Also, a short description of the protein, its conservation and its predicted domains (transmembrane domain: TMD) are given. RNA samples were isolated by C. Batram and the alignment of the data was conducted by N. Siegel.

Gene ID	FPKM	Fold regulation				Description/ Conservation	Domains
	0 h	4 h	8 h	24 h	48 h		
Tb427.10.13410	1.32	2.04	1.29	5.25	5.16	hypothetical protein/ unique for trypanosomes	2x TMD
Tb427.10.6200	1.24	2.45	0.99	2.03	2.72	hypothetical protein/ conserved in kinetoplastids	1x TMD
Tb427.08.510	4.12	2.28	1.26	6.74	20.53	hypothetical protein/ unique for trypanosomes	-
Tb427.08.490	80.62	1.44	1.12	2.60	6.62	hypothetical protein/ unique for trypanosomes	-
Tb427.08.500	18.64	1.22	0.92	2.44	4.36	hypothetical protein/ unique for trypanosomes	-
Tb427.08.520	17.07	1.24	1.10	2.65	4.61	hypothetical protein/ unique for trypanosomes	-

Tb427.08.510 displayed the strongest up-regulation following VSG 121 overexpression, namely 20-fold within 48 hours. Its down-regulation during VSG 121 overexpression via RNAi did not change the initial growth phenotype as the cells stalled growth upon the addition of tetracycline (C. Batram, chapter 7.1 Figure 48), indicating that the protein was not essential for the initiation of the attenuation of the ES. However, 96 hours after tetracycline treatment the cultures started to die instead of growing out. As the reactivation of the *VSG 221* ES occurs at this time point, we suspected that the protein could play a role in this process. The effect of *Tb427.08.510* RNAi alone (in the absence of VSG 121 overexpression) was analyzed to examine whether the RNAi phenotype was connected to the VSG 121 overexpression (C. Batram, chapter 7.1 Figure 48). In this case, no changes in growth were observed upon induction of RNAi indicating that the protein was not essential for BSF parasites but for VSG overexpressors. If the protein directly participates in the reactivation of the ES, it should be present in the nucleus. For this reason, its localization was assessed as a part of the bachelor

thesis of Alessa Gräb. Endogenous tagging of the C-terminus of *Tb427.08.510* with an *eYFP*, however, indicated a mitochondrial positioning of the protein (bachelor thesis Gräb, 2015). Though the localization needs to be further confirmed, it seems unlikely that a mitochondrial protein is a direct ES regulator. Thus, the up-regulation of the *Tb427.08.510* mRNA could be a downstream effect of the ES-attenuation.

Interestingly, detailed analyses of the RNA sequencing data indicated that, besides *Tb427.08.510*, three adjacent genes (*Tb427.08.490, Tb427.08.500, Tb427.08.520*) were more than fourfold up-regulated within 48 hours of VSG 121 overexpression in monomorphic parasites (Table 1). Sequence analyses of these genes showed that *Tb427.08.500* and *Tb427.08.520* neither differed in their UTRs nor in the ORF, wherefore it could not be exclude that the mRNA levels of only one of the candidates' increases. Also no differences in the UTRs of *Tb427.08.490* and *Tb427.08.510* were found and the sequences of the 3' and 5' part of the ORF were similar (for illustrative purposes an overview of this gene array is presented in chapter 7.1 Figure 47). We decided to analyze if the depletion of *Tb427.08.490* alters the growth phenotype of the VSG 121 overexpressors in a similar way to the *Tb427.08.510* RNAi. Sequencing of the *Tb427.08.490* mRNA revealed that the ORF was 54 nucleotides shorter than annotated in the database. A 400 bp long fragment from the middle of the ORF, which did not display similarities to Tb427.08.510, was used for the generation of the RNAi construct. *Tb427.08.490* RNAi during VSG 121 overexpression caused the death of the cells after 48 hours of induction in three of five analyzed clones (chapter 7.1 Figure 48). However, the other two clones displayed the VSG 121 overexpression growth phenotype. The impact *of Tb427.08.490* RNAi in the parental 13-90 cell line was analyzed to control that the growth phenotype was connected to the VSG 121 overexpression. In this case, no effect on growth was observed in two clones, whereas in three other clones growth was stalled after 24 hours of induction for up to 72 hours (chapter 7.1 Figure 48). Thus, the death of the parasites upon RNAi was specific for the VSG 121 overexpressors. However, the results also indicated that the protein was in general important for BSF parasites. Nevertheless, we suggest that the gene array of *Tb427.08.490-08.520* is essential for the parasites to escape ES-induced growth retardation. If the proteins are only essential for the formation of st like cells during VSG 121 overexpression in monomorphic cells or if they are involved in the development of *bona fide* st parasites as well remains elusive.

Preliminary RNA sequencing experiments were also done with a growth-arrested clone of the pleomorphic VSG 121 overexpressor. For this purpose, I used parasites overexpressing VSG 121 for 24 hours and compared the transcript levels to non-induced cells. Unfortunately, no genome sequence for the used pleomorphic EATRO 1125 (AnTat1.1) strain is available. For this reason, the genome of the monomorphic 927 strain was used to align the mRNA sequences, which makes the results error prone: in particular, any mRNA that is unique to the

pleomorphic parasites will be missed. Nevertheless, more than 200 proteins were more than twofold up-regulated (Table 2 shows the 20 transcripts with the strongest up-regulation), including 21 of the proteins that were also up-regulated in monomorphic parasites (shown in chapter 7.1 Table 15).

Table 2: Up-regulated transcripts upon VSG 121 overexpression in pleomorphic cells. The transcripts of >200 proteins were more than twofold up-regulated within 24 hours of VSG 121 overexpression in pleomorphic trypanosomes. Shown are the 20 transcripts that displayed the strongest up-regulation. Transcripts with FPKM values below one in the non induced sample were excluded. Presented are the Gene IDs for the corresponding transcripts (TriTrypDB), the FPKM values for the respective transcript in the non-induced cells and induced cells. The fold regulation within 24 hours of VSG 121 overexpression, the length of the coding DNA sequence (CDS in nucleotides) and a short description of the protein are given. Note the asterisk in the description indicates genes which have been removed in the current version of TriTrypDB (based on other transcriptome analyses) and can be found at http://r28.tritrypdb.org/tritrypdb.b28/. In grey are candidates highlighted that were also up-regulated in monomorphic VSG 121 overexpressors.

Gene ID	FPKM 0 h	FPKM 24 h	Fold regulation	CDS Length	Description
Tb927.9.7460	1.26	19.57	15.50	321	hypothetical protein*
Tb927.6.510	150.02	1115.55	7.44	345	GPEET2 procyclin
Tb927.10.10260	93.15	611.17	6.56	426	EP1 procyclin
Tb927.6.480	1.44	9.30	6.44	372	EP3-2 procyclin
Tb927.10.10250	24.19	153.63	6.35	390	EP2 procyclin
Tb927.6.530	1.04	5.73	5.49	609	procyclin associated gene 3 (PAG3)
Tb927.8.2666	169.36	926.66	5.47	null	tRNA Tryptophan
Tb927.6.520	50.18	255.91	5.10	390	EP3-2 procyclin
Tb927.9.2680	71.14	352.03	4.95	96	hypothetical protein*
Tb927.5.440	1.13	5.35	4.73	2328	trans-sialidase, putative
Tb927.7.6850	24.31	109.94	4.52	2316	trans-sialidase (TS)
Tb927.9.15310	5.28	22.94	4.35	180	hypothetical protein*
Tb927.5.4020	48.89	198.47	4.06	819	hypothetical protein
Tb927.11.17850	9.45	37.99	4.02	885	expression site-associated gene 9 (ESAG9), fragment
Tb927.1.4770	13.83	55.40	4.00	153	hypothetical protein*
Tb05.5K5.270	1.72	6.57	3.83	882	expression site-associated gene 9 (ESAG9), putative
Tb927.9.13410	7.89	30.09	3.81	192	hypothetical protein*
Tb927.9.5940	384.90	1465.65	3.81	117	hypothetical protein*
Tb927.1.2780	1.36	5.06	3.72	225	hypothetical protein
Tb927.7.4270	24.15	88.99	3.69	669	hypothetical protein

The change in expression of the transcripts of the gene array described above was difficult to determine in the transcriptome analyses of the pleomorphic cells, because the transcript level in the non-induced sample were partially below the defined threshold. However, if this threshold is ignored, the up-regulation ranged from 1.4 to 6.6-fold depending on the respective transcript (shown in chapter 7.1 Table 15). Therefore, it is possible that this gene array plays a role either during ES-induced st formation or in the escape of ES-attenuation. However, combining RNA sequencing and VSG 121 overexpression no genes involved in ES-attenuation could be identified so far. Thus, we hypothesized that high VSG expression levels may cause the initiation of a signal cascade that (de)activates positive or negative ES regulators. In this scenario, changes would be observed in the phosphoproteome, or perhaps in the proteome, but there would be no change in the transcriptome. However, the RNA sequencing data need to be considered with care, as analyzes of the monomorphic and the pleomorphic VSG 121 overexpressors were not conducted in replicates. As it will be necessary to analyzes at least three biological replicates to determine if the observed changes in the transcript levels during the course of VSG 121 overexpression are significant, the presented results can be considered only as preliminary at the moment.

3.9 The 16mer is a signal for the integrity of the ES

The previous results have shown that ectopic VSG overexpression causes a decrease of the transcriptional status of the active ES (Batram et al., 2014; chapter 3.2 of this thesis). However, it remained unexplored how the signal for ES-attenuation was triggered and mediated. RNA sequencing in combination with VSG overexpression did not reveal potential ES regulators so far (chapter 3.8). Nevertheless, somehow the ES has to be perceived to get attenuated upon VSG overexpression as well as during a transcriptional switch of the active ES (*in situ* switching). Conserved DNA sequence motifs within the *VSG* ES could serve as signaling hubs to regulate its activity. Binding or releasing of regulatory proteins could trigger a signaling cascade that causes the attenuation of the ES.

Though the composition of all known and sequenced ESs differs, such a motif would have to be present in all ESs (Hertz-Fowler et al., 2008). VSG overexpression induced ES-attenuation initiated at the telomere and propagated towards the promotor, suggesting that the signal for silencing was conveyed at the telomere (Batram et al., 2014). Therefore, we focused on the lowest common denominator of all ESs that is located at their telomeric ends: the *VSG* itself. The *VSG* ORFs differ greatly in their sequence, making it unlikely that a recognition motif is located within the ORF. However, within the 3'UTR of all ES resident *VSGs*, two motifs are 100% conserved in their sequence, namely the 8mer and the 16mer (diploma thesis Batram, 2009; Berberof et al., 1995; M. Engstler, unpublished data). Extensive mutational analyses showed that the 16mer is essential for VSG expression. Deletion of seven nucleotides within the 16mer (Δ 46-52) caused a 10-fold reduction in the amount of the VSG protein (diploma thesis Batram, 2009). Trypanosomes expressing solely a *VSG* with deleted 16mer were not able to build a proper VSG coat: RNAi depletion of the endogenous *VSG 221* led to a pre-cytokinesis cell cycle arrest in stable VSG double expressors expressing *VSG 221* and *VSG 121(Δ 46-52)* (diploma thesis Batram, 2009; Sheader et al., 2005). In contrast, down-regulation of the endogenous *VSG 221* did not cause growth defects when the second *VSG* was coupled to a functional 3'UTR (diploma thesis Batram, 2009; Smith et al., 2009). The 16mer motif appears to be critical for the formation of an RNA stem loop, which stabilizes the mRNA and thus contributes to the long half life of the *VSG* mRNA (diploma thesis Batram, 2009, PhD thesis 2013). The function of the 8mer remained unexplored so far as no changes in VSG expression were detected upon its inversion. Besides their role in mRNA integrity, these motifs could also serve as protein binding sites at the ES DNA regulating its activity. Thus, if one of these motifs is essential for initiating ES-attenuation, its deletion should prevent this process.

3.9.1 Integration of a *GFP* with a defective 16mer in its 3'UTR downstream of the endogenous *VSG* causes switching

If the 16mer motif is essential for ES-attenuation, ectopic VSG overexpression should not trigger this process once the motif is defective in the endogenous *VSG* 3'UTR. However, the mutation of the 16mer within the 3'UTR of the endogenous *VSG* would considerably reduce the amount of *VSG* mRNA. Thus, not enough VSG protein would be present to build a functional coat and the cells would enter a pre-cytokinesis arrest (diploma thesis Batram, 2009; Sheader et al., 2005). Therefore, we decided to integrate a *GFP* reporter gene coupled to the *VSG 121* 3'UTR downstream of the endogenous *VSG 221* (Figure 32 A, B). For this purpose, a modified pbRn6 construct, which contains targeting sequences for integration into the regions downstream of *VSG 221*, was used (Horn and Cross, 1997). The plasmid contained a blasticidin resistance cassette flanked by *tubulin* UTRs, that was followed by a *GFP* ORF (Janzen et al., 2004). C. Batram replaced the *GFP* ORF with a *GFP* ORF flanked by the *VSG 121* 5' and 3'UTR. The latter one was either a complete *VSG 121* 3'UTR with an intact 16mer (pbRn6 GFP 198, Figure 32 A) or contained a 16mer with nucleotides 46-52 of the 3'UTR being deleted (pbRn6 GFP Δ, Figure 32 B). Consequently, parasites transfected with these constructs should have enough VSG 221 to support growth and their active ES would contain a reporter with an intact or defective 16mer. In a next step, we planned to transfect these reporter cell lines with the VSG 121 overexpression construct to be able to induce ES-attenuation and, subsequently, monitor changes in the activity of the ES. After transfecting the BSF 13-90 cell line with the pbRn6 GFP 198 and GFP Δ constructs, the resulting reporter cell lines, $GFP^{EStel}{}_{198}221^{ES}$ and $GFP^{EStel}{}_{\Delta}221^{ES}$, were characterized first (Figure 32 A, B).

The parasites with a *GFP* with a functional *VSG* 3'UTR ($GFP^{EStel}{}_{198}221^{ES}$) had a pdt of 6.3 hours and thus a similar growth rate as the parental BSF 13-90 parasites (pdt 6.1 h, Figure 32 C). In contrast, clones of the cell line with a *GFP* with a defective 16mer ($GFP^{EStel}{}_{\Delta}221^{ES}$) grew slower than the parental cell line as their pdt ranged from 9 to about 20 hours during cultivation (Figure 32 C). Next, flow cytometric analysis was used to monitor the GFP intensity and thus to determine the expression of the telomere-proximal *GFP* in the different cell lines (Figure 32 D). The comparison to the GFP-negative parental cell line showed that clones with an intact 16mer in the 3'UTR ($GFP^{EStel}{}_{198}221^{ES}$) did not express GFP at detectable levels, while the majority of parasites with a mutated 16mer ($GFP^{EStel}{}_{\Delta}221^{ES}$) displayed a strong GFP signal.

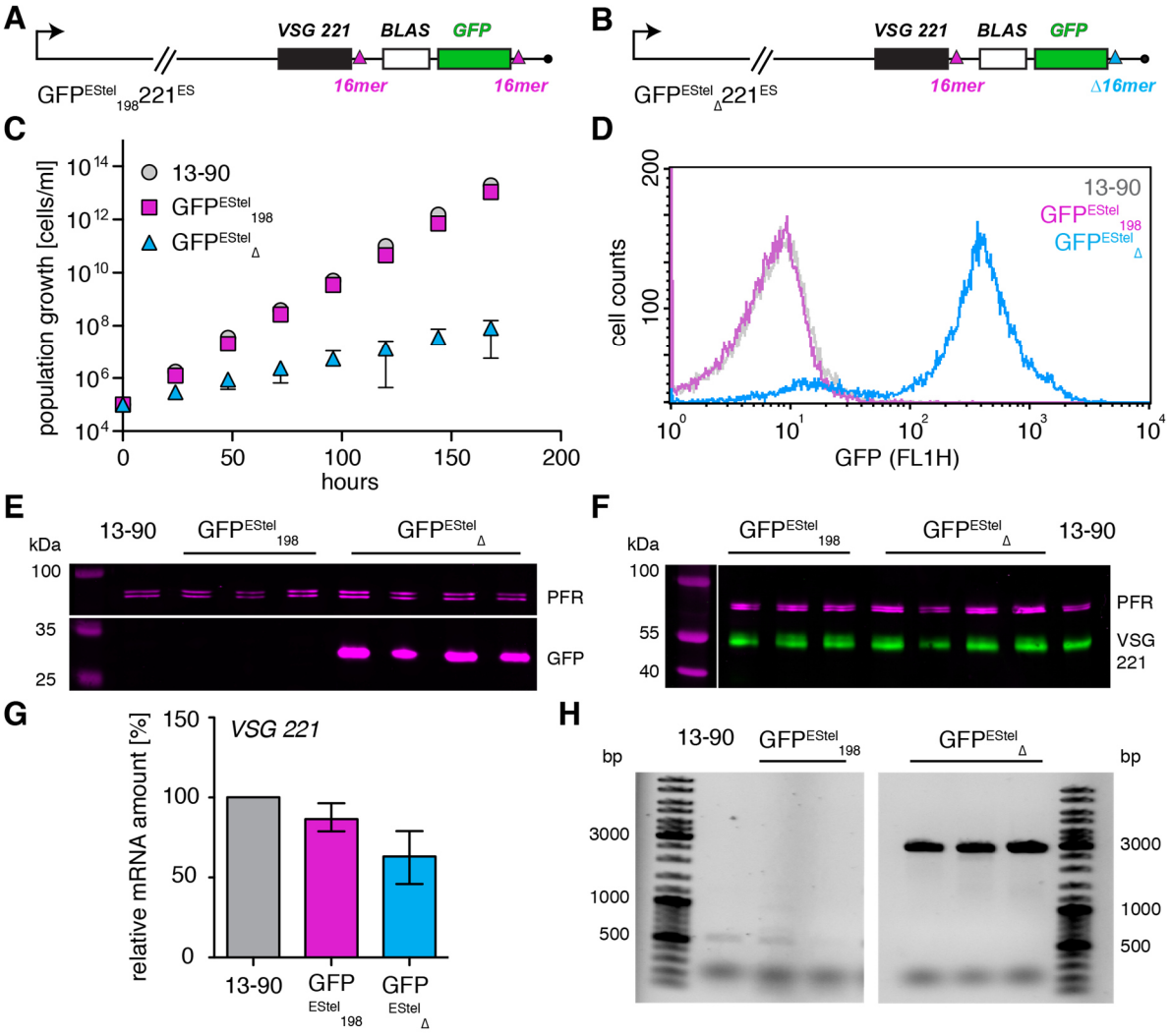

Figure 32: Integration of a *GFP* with a functional or a defective *VSG* 3'UTR downstream of the endogenous *VSG*. Transfection of BSF 13-90 parasites with pbRn6 GFP 198 or pbRn6 GFP Δ generated the cell lines GFP$^{EStel}{}_{198}$221ES and GFP$^{EStel}{}_{\Delta}$221ES, respectively. **(A, B)** Schematic representation of the modified *VSG 221* ES. The telomere-proximal *GFP* was either coupled **(A)** to a functional *VSG 121* 3'UTR (complete 16mer, magenta triangle) or **(B)** to a defective *VSG 121* 3'UTR (nucleotide 46-52 deleted, Δ16mer blue triangle). **(C)** Growth curves of the GFP$^{EStel}{}_{198}$221ES (magenta squares) and the GFP$^{EStel}{}_{\Delta}$221ES cell line (blue triangle). The parental BSF 13-90 cell line (circles) served as a growth control. Means (± SD) are shown (GFP$^{EStel}{}_{198}$221ES: five clones; GFP$^{EStel}{}_{\Delta}$221ES: six clones). **(D)** Analyses of the GFP expression via flow cytometry. Representative flow cytometric profiles of one clone of the GFP$^{EStel}{}_{198}$221ES (magenta) and the GFP$^{EStel}{}_{\Delta}$221ES (blue) cell line are presented. The parental BSF 13-90 cell line (grey) served as a negative control. 20,000 cells were counted. **(E, F)** Western blot analyses of the GFP and the VSG 221 expression in different clones of both cell lines. The blots were stained **(E)** with a GFP antibody (magenta) or **(F)** a VSG 221 antibody (green). Detection of PFR proteins (magenta) served as a loading control. **(G)** Quantification of the mRNA levels of the endogenous *VSG 221* in the GFP$^{EStel}{}_{198}$221ES (magenta) and the GFP$^{EStel}{}_{\Delta}$221ES (blue) cell line. The *VSG 221* transcript levels were normalized to *tubulin* and are given relative to the levels of the parental BSF 13-90 cell line (100%). Means (± SD) of three clones of the GFP$^{EStel}{}_{198}$221ES cell line and of four clones of the GFP$^{EStel}{}_{\Delta}$221ES cell line are shown. **(H)** Validation of the integration of the pbRn6 GFP construct in the *VSG 221* ES using PCR. A forward primer binding to the *VSG 221* ORF (outside of the integration site) and a reverse primer binding within the pbRn6 construct were used. A PCR-product with the size of 2,980 bp would be obtained only if the plasmid was integrated in this ES. Each lane represents one clone of the indicated cell lines. The PCRs were exemplarily validated for one clone of each cell line by Southern blot analysis (data not shown).

The results of the flow cytometric analyses were further confirmed by Western blot analyses using an antibody against GFP (Figure 32 E): clones with a defective 16mer expressed the reporter, whereas no signal was detected in the clones containing a *GFP* with an intact 16mer. These results were surprising as the *GFP* mRNA with a defect 16mer should be less stable compared to the one with an intact 16mer. Consequently, parasites transfected with the *GFP* reporter coupled to an intact *VSG* 3'UTR ($GFP^{EStel}{}_{198}221^{ES}$) should display a considerably higher GFP level than cells with a defective one ($GFP^{EStel}{}_{\Delta}221^{ES}$). Western blot analyses using a VSG 221 antibody showed that both cell lines expressed the endogenous VSG 221 (Figure 32 F), indicating that not a switch of the active ES was responsible for these unexpected results. Next, the *VSG 221* mRNA amounts were measured in the two cell lines by quantitative Northern blots to accurately compare the *VSG* levels (Figure 32 G). Transfectants with a *GFP* coupled to a functional *VSG* 3'UTR ($GFP^{EStel}{}_{198}221^{ES}$) transcribed *VSG 221* at only slightly lower levels as the parental cell line (87 ± 8%), while, the *VSG* transcript levels were decreased in the clones with a defective 16mer ($GFP^{EStel}{}_{\Delta}221^{ES}$: 63 ± 15%). To sum up, the normally doubling $GFP^{EStel}{}_{198}221^{ES}$ parasites were GFP-negative and expressed VSG 221 at wild type levels. Parasites of the $GFP^{EStel}{}_{\Delta}221^{ES}$ cell line had, in contrast, an impaired growth, a reduced amount of VSG 221 and were GFP-positive.

One possible reason for these observed differences could be a wrong integration of one of the plasmids. To investigate this, genomic DNA was prepared from clones of both cell lines and analyzed by analytical PCR. One primer was chosen to bind within the sequence derived from the plasmid (CB80) and the other primer was designed to bind to a sequence outside of the integration site of the construct (*VSG 221* ORF, HZ43). Consequently, a PCR product (in this case 2,800 bp) would be obtained only if the construct was integrated downstream of *VSG 221*. No PCR product was obtained for two clones with a *GFP* coupled to a functional *VSG* 3'UTR ($GFP^{EStel}{}_{198}221^{ES}$), indicating that the construct was not integrated in the active *VSG 221* ES. In contrast, integration in the *VSG 221* ES was successful in three clones of the GFP reporter cell line with a defective 16mer ($GFP^{EStel}{}_{\Delta}221^{ES}$). Thus, the absence of a detectable GFP signal in the $GFP^{EStel}{}_{198}221^{ES}$ clones was caused by a failed integration of the construct. It remains unclear why the construct did not integrate when the 16mer was intact, though the same construct did integrate when the 16mer was defective. The most likeliest explanation would be that the functional 16mer causes such high GFP expression levels, that these are toxic to the cell. Consequently, the cells would not be viable with the pbRn6 GFP 198 construct integrated in the active ES. Only cells with a more unstable *GFP* mRNA, which express the protein at a lower level, could survive. This was the case, when the GFP construct with a defective 16mer integrated in the *VSG 221* ES.

However, it remained unclear why the cells with a defective 16mer in the 3'UTR of the *GFP* reporter did not grow normally. 22-32% of the population had an aberrant kinetoplast/nucleus

configuration with more than two nuclei and two kinetoplasts, indicating a problem in cell division (each *n* > 250 cells for three clones; illustrated in Figure 33 A). At the population level a reduced amount of *VSG 221* transcripts was observed in the GFP reporter cell line with a mutated 16mer. This could be explained either by a similar reduction of the VSG in all cells or by some parasites, which did not express VSG 221. Analyzes of the VSG 221 expression at the single cell level by immunofluorescence showed that depending on the analyzed clone 1-8% of the population were VSG 221-negative (*n* > 250 cells for each of the three clones, examples of VSG-negative cells are marked in Figure 33 A by yellow arrowheads). Detection of the GFP signal revealed that these VSG 221-negative cells were also GFP-negative (yellow arrowhead, Figure 33 A). The presence of a small proportion of parasites not expressing the reporter was also obvious in the previous flow cytometric analyses of the reporter cell line (Figure 32 D). In six analyzed clones, 8-17% of the population was GFP-negative (each *n* = 20,000 cells). Together, this suggested that parasites of the $GFP^{ESTel}{}_{\Delta}221^{ES}$ reporter cell line are trying to switch the active ES.

During such a transcriptional switch of the ES (termed *in situ* switching), the active ES gets attenuated while a new one is activated. Once the *VSG 221* ES is silenced, the expression of all ES located genes would stop. This includes the expression of the *GFP* reporter and the *VSG* 221, but also the expression of the selection marker (*BLAS*) of the pbRn6 GFP Δ construct. Consequently, parasites trying to switch the active ES would become sensitive towards the selection and die. Cells could only grow if they do not complete the switch and keep the *VSG 221* ES active at levels supporting resistance against the selection. This scenario would explain why (i) the $GFP^{ESTel}{}_{\Delta}221^{ES}$ clones displayed an impaired growth in the presence of the selection, (ii) a minor fraction of the cells was GFP-negative and (iii) the *VSG 221* levels were slightly reduced. Thus, it was hypothesized that the integration of the *GFP* with a defective 16mer downstream of the *VSG* triggers a switch in the actively transcribed ES, a so called *in situ* switch. To investigate this hypothesis, the selection was removed by washing the cultures and VSG/GFP expression was monitored at the single cell level. The removal of the selection should allow the cells to switch the active ES completely. Flow cytometric analyses of VSG 221-stained trypanosomes were conducted to quantify the amount of VSG 221 and GFP-positive cells in the presence and absence of the drug (Figure 33 B). The parental BSF 13-90 cell line served as a positive control for the VSG staining (GFP-/VSG 221+) and the N50 cell line expressing VSG M1.13 as a negative control (GFP-/VSG-).

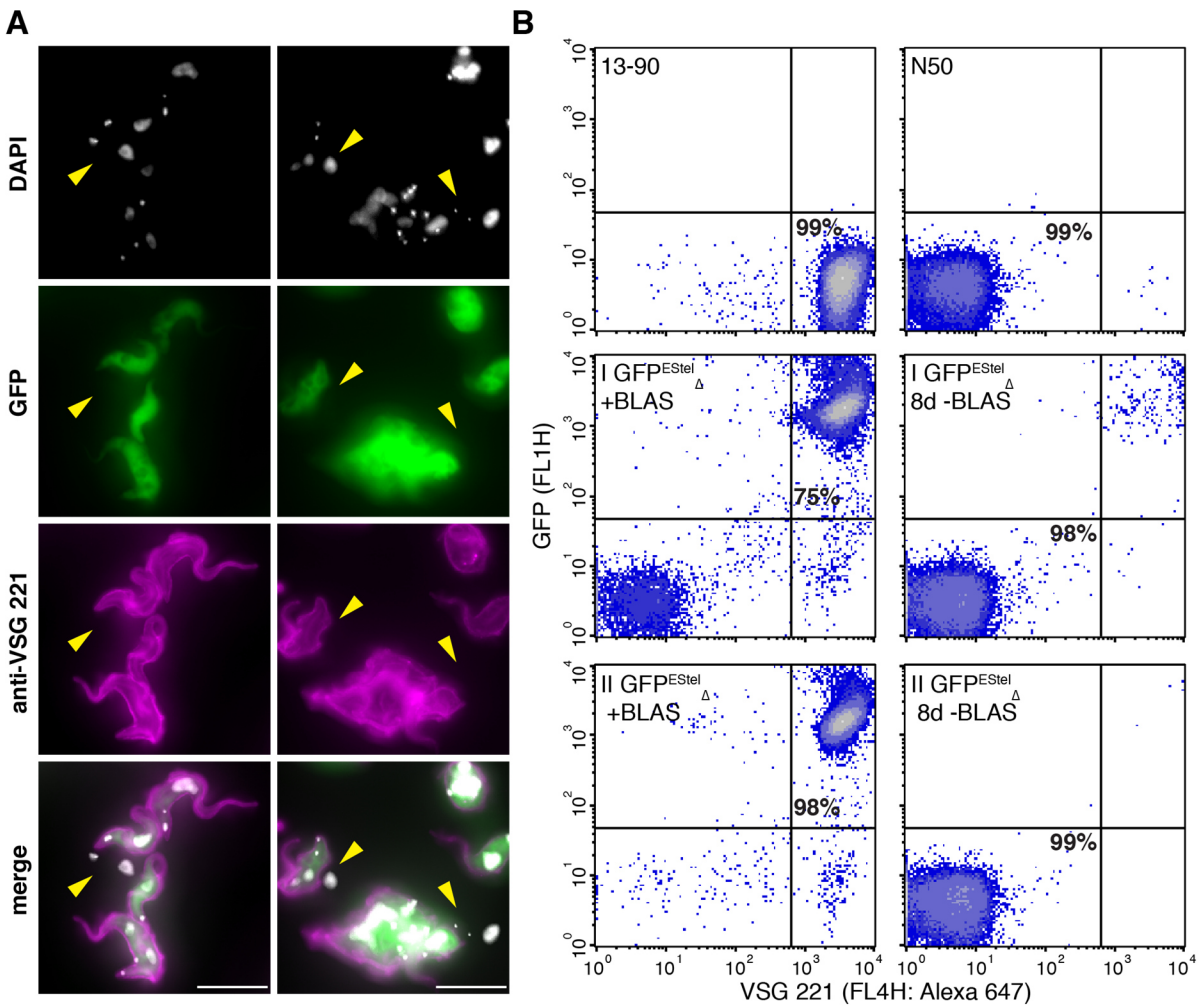

Figure 33: Integration of a *GFP* with a defective *VSG* 3'UTR in the active ES triggers ES switching. (A) Immunofluorescence analysis of a clone with a telomere-proximal *GFP* with defective 16mer (GFP$^{EStel}{}_{\Delta}221^{ES}$ cell line) in the presence of the selection (BLAS). Chemically fixed cells were stained with an antibody against the endogenous VSG 221 (magenta).The DNA was stained with DAPI (grey) and the GFP signal is shown in green. Yellow arrowheads indicate GFP− and VSG 221-negative parasites. Scale bar: 10 µm. **(B)** Analyses of the VSG 221 and GFP expression of a clone with a telomere-proximal *GFP* with defective 16mer (GFP$^{EStel}{}_{\Delta}221^{ES}$ cell line) using flow cytometry. The parasites were cultivated in the presence of the selection (+BLAS) or the selection was removed by washing and the cells were further cultivated without BLAS for eight days before they were analyzed (8d -BLAS). Parasites of the parental 13-90 cell line were analyzed as a positive control for VSG 221 expression and cells expressing VSG M1.13 (N50) served as a negative control. The living trypanosomes were stained with a rabbit anti-VSG 221 and, subsequently, with an Alexa647 conjugated anti-rabbit antibody. The manual set threshold for VSG 221-positive cells is indicated by the vertical line and the threshold for GFP-positive cells by the horizontal line. 20,000 cells were analyzed and the percentage of cells being GFP/221-positive or -negative is given for the most abundant fraction of the population.

VSG staining combined with flow cytometric analyzes showed that the majority of cells (75% in experiment I and 98% in experiment II) of the GFP$^{EStel}{}_{\Delta}221^{ES}$ cell line expressed the GFP and VSG 221 in presence of the drug (left column middle and lower panel, Figure 33 B). No

reproducible results were obtained when the selection was removed for only 24 or 48 hours (data not shown). If the parasites with a defective 16mer ($GFP^{EStel}{}_{\Delta}221^{ES}$) were cultivated for eight days in the absence of the antibiotic the vast majority (>98%) became VSG 221- and GFP-negative (right column, middle and lower panel, Figure 33 B). This suggested that the integration of a *GFP* with a defective 16mer downstream of the endogenous *VSG* does indeed trigger transcriptional ES switching. However, it remained unclear if all cells conducted a switch or if the switching frequency was increased. In the latter case, the switchers would outgrow the parasites, which did not switch the expressed VSG. In both cases, the result would be the same: a VSG 221- and GFP-negative population once the selection was removed.

3.9.2 The position of the defect 16mer determines switching

The previous results suggested that integration of a *GFP* with a defect 16mer downstream of the endogenous *VSG 221* causes *in situ* switching. As integration of a construct containing a *GFP* with a full length *VSG* 3'UTR failed, it remained unclear if switching was induced: (i) by the deleted 16mer, (ii) by the expression of the GFP protein in high amounts, or (iii) by the integration of the construct *per se*. It was also uncertain if the presence of the *GFP* mRNA with the defective 16mer *per se*, or rather its position within the genome would cause the switching.

To answer these questions, the GFP 198 and the GFP Δ constructs were integrated into two different genomic loci: (1) downstream of the promotor of the active *VSG 221* ES, to maintain the genomic context of the ES while changing the site of integration (Figure 34); (2) in the tubulin locus, as it is transcribed by another polymerase (RNA polymerase II) and transcription occurs at lower rates compared to the active ES (Figure 35). In order to create these constructs, the complete insert between the two regions of the pbRn6 construct that target the genomic integration (*tubulin* 5'UTR-*BLAS* ORF-*tubulin* 3'UTR-*VSG* 5'UTR- *GFP* ORF-*VSG* 3'UTR) was mobilized using the enzymes HindIII and BamHI. Then, the overhangs of the restriction sites were removed from the insert. Next, backbones containing only the suitable integration sites were generated. For this purpose, the insert of the pLF12 construct, which targets the promotor region of the ESs, was removed by digestion with XhoI and SmaI (Figueiredo et al., 2008). The insert of the pTub vector, which targets the tubulin locus, was removed by digestion with XhoI and PaeI (PhD thesis Günzel, 2010). The backbones were blunted and ligated with the BLAS/GFP insert containing either a functional or defective 16mer. Thus, the complete insert of the pbRn6 GFP 198 and GFP Δ construct remained intact, while the integration site was exchanged.

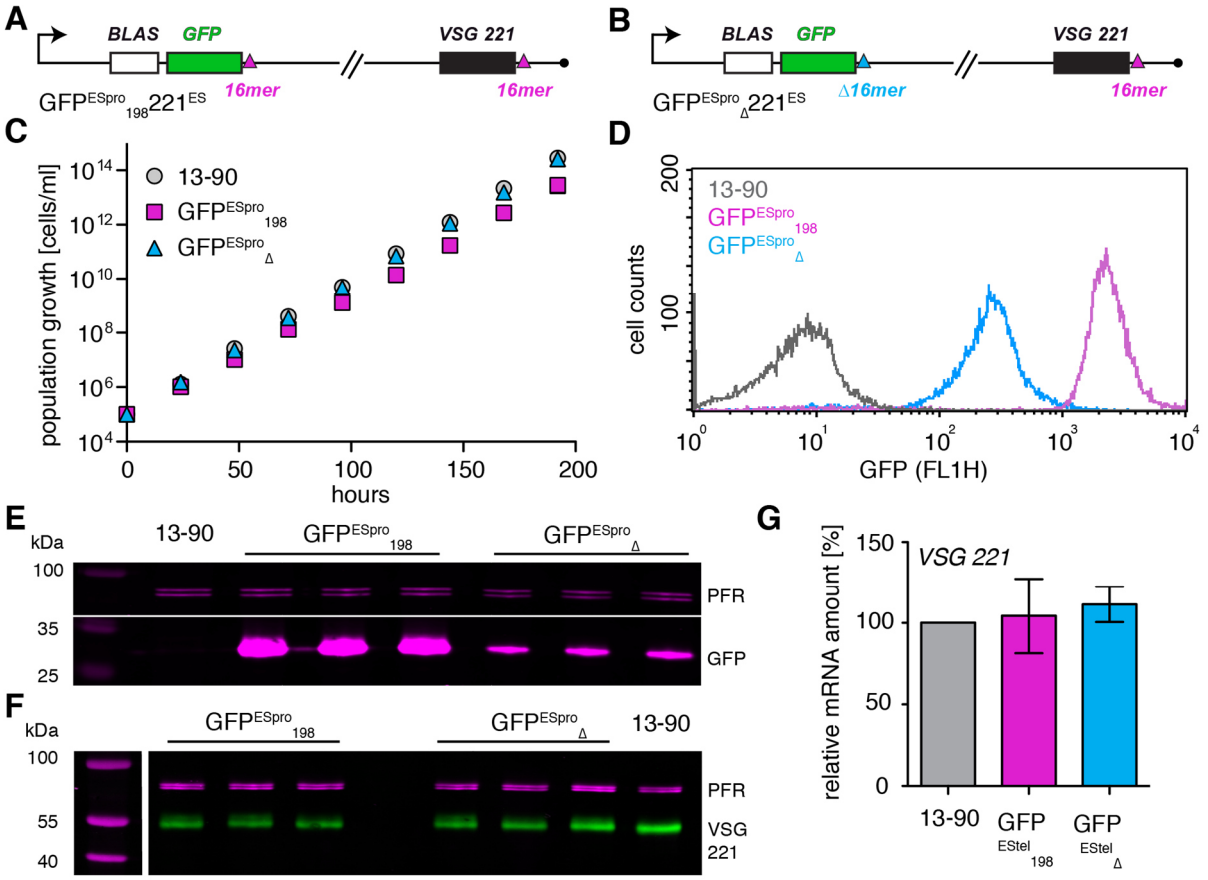

Figure 34: Integration of a *GFP* with a functional or a defective *VSG* 3'UTR in the promotor region of the active ES. Transfection of the BSF 13-90 cell line with pLF12 GFP 198 or pLF12 GFP Δ generated the cell lines GFP$^{ESpro}{}_{198}$221ES and GFP$^{ESpro}{}_{\Delta}$221ES, respectively. **(A, B)** Schematic representation of the modified *VSG 221* ES. The promotor-proximal *GFP* was either coupled **(A)** to a functional *VSG 121* 3'UTR (complete 16mer, magenta triangle) or **(B)** to a defective *VSG 121* 3'UTR (nucleotide 46-52 deleted, Δ16mer blue triangle). **(C)** Growth curves of the GFP$^{ESpro}{}_{198}$221ES (magenta squares) and the GFP$^{ESpro}{}_{\Delta}$221ES cell line (blue triangle). Means (± SD) of six clones are shown for each cell line. Due to the small standard deviation the error bars are not visible. The parental BSF 13-90 cell line (circles) served as a growth control. **(D)** Analyses of the GFP expression via flow cytometry. Representative flow cytometric profiles of one clone of the GFP$^{ESpro}{}_{198}$221ES (magenta) and the GFP$^{ESpro}{}_{\Delta}$221ES (blue) cell line are presented. The parental BSF 13-90 cell line (grey) served as a negative control. 10,000 cells were counted. **(E, F)** Western blot analyses of the GFP and the VSG 221 expression in three clones of the GFP$^{ESpro}{}_{198}$221ES and the GFP$^{ESpro}{}_{\Delta}$221ES cell line. Blots were stained **(E)** with a GFP antibody (magenta) or **(F)** a VSG 221 antibody (green). Detection of PFR proteins (magenta) served as a loading control. (**G)** Quantification of the mRNA levels of the endogenous *VSG 221* in the GFP$^{ESpro}{}_{198}$221ES (magenta) and the GFP$^{ESpro}{}_{\Delta}$221ES (blue) cell line. The *VSG 221* transcript levels were normalized to *tubulin* and are given relative to the *VSG* transcript levels of the parental BSF 13-90 cell line (100%). Means (± SD) of three clones are shown.

The integration of the *GFP* with a functional *VSG* 3'UTR into the promotor region of the active ES (GFP$^{ESpro}{}_{198}$221ES, Figure 34 A) did only slightly change population growth. The clones displayed a pdt of 7 hours, in comparison to 6.1 hours of the parental BSF 13-90 cell line (Figure 34 C). Transfection of BSF 13-90 with the pLF12 GFP Δ construct (GFP$^{ESpro}{}_{\Delta}$221^{E}, Figure 34 B) did not affect growth as the cells doubled every 6.2 hours (Figure 34 C). Flow

cytometric analysis showed that the cells with an intact 16mer ($GFP^{ESpro}{}_{198}221^{ES}$) expressed 9.3-fold more GFP than the cells with a mutated 16mer ($GFP^{ESpro}{}_{\Delta}221^{ES}$; Figure 34 D). The higher GFP expression in the presence of a functional *VSG 121* 3'UTR was further confirmed by Western blots using a GFP antibody (Figure 34 E). Western blot analysis using a VSG 221 antibody also validated that all clones still expressed VSG 221 (Figure 34 F). Next, the amount of the *VSG 221* mRNA was determined for both cell lines to compare the *VSG* transcript levels (Figure 34 G). This demonstrated that they possessed a similar amount of *VSG 221* mRNA, that did not differ from the parental 13-90 cell line ($GFP^{ESpro}{}_{198}221^{ES}$: 104 ± 22%; $GFP^{ESpro}{}_{\Delta}221^{ES}$:111 ± 10%). The integration of the *GFP* reporters with either intact or mutated *VSG* 3'UTR into the promotor region of the active ES did not affect growth and did not change the expression of VSG 221 protein or mRNA and thus did not cause an *in situ* switch.

Next, it was analyzed if the integration of a *GFP* with a functional *VSG 121* 3'UTR ($GFP^{tub}{}_{198}221^{ES}$, Figure 35 A) or a defective one ($GFP^{tub}{}_{\Delta}221^{ES}$, Figure 35 B) in the tubulin locus causes *in situ* switching. Growth analyses demonstrated that neither construct altered the doubling times of the parasites (Figure 35 C). Flow cytometric analyses of the GFP signal showed that the reporter was only weakly expressed in cells with a mutated 16mer ($GFP^{tub}{}_{\Delta}221^{ES}$). The GFP signal could barely be discriminated from the GFP-negative parental BSF 13-90 cell line. The GFP expression was approximately 4 times higher when the *VSG 121* 3'UTR contained the complete 16mer (GFP 198) than when it was defective (GFP Δ) (Figure 35 D). The higher GFP expression in the presence of a functional *VSG 121* 3'UTR was further confirmed by Western blots using a GFP antibody (Figure 35 E). Western blot analysis using a VSG 221 antibody demonstrated that the clones of both cell lines expressed the ES-resident *VSG* (Figure 35 E, F). (Figure 35 G) Quantitative Northern blot analysis showed no differences in the amount of *VSG 221* transcripts between the two cell lines and the parental 13-90 cell line ($GFP^{tub}{}_{198}221^{ES}$: 116 ± 6%; $GFP^{tub}{}_{\Delta}221^{ES}$: 123 ± 8%).

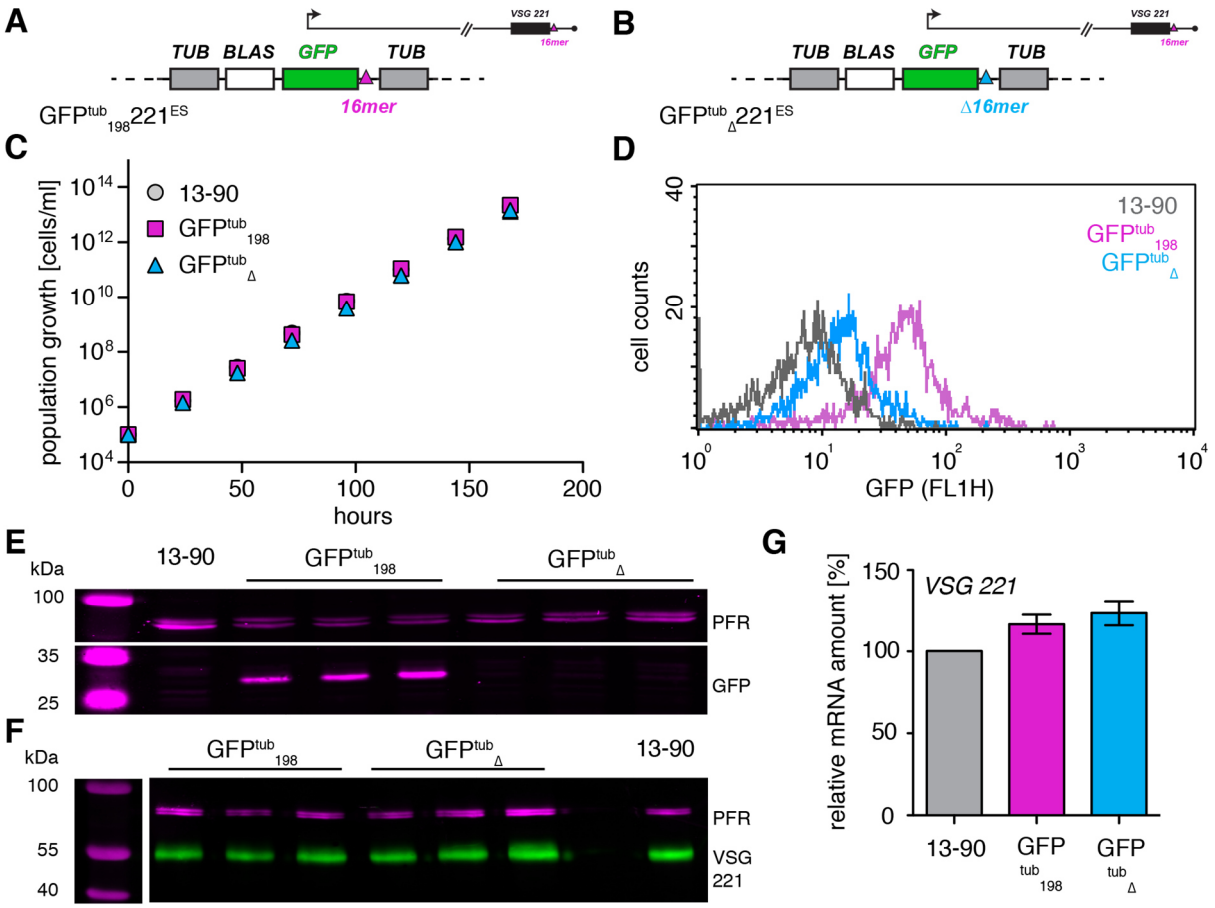

Figure 35: Integration of a *GFP* with a functional or a defective *VSG* 3'UTR in the tubulin locus. Transfection of the BSF 13-90 cell line with pTub GFP 198 or pTub GFP Δ generated the cell lines GFP$^{tub}_{198}$221ES and GFP$^{tub}_{\Delta}$221ES, respectively. **(A, B)** Schematic representation of the modified tubulin locus. **(A)** The *GFP* was either coupled to a functional *VSG 121* 3'UTR (complete 16mer, magenta triangle) or **(B)** to a defective *VSG 121* 3'UTR (nucleotide 46-52 deleted, Δ16mer blue triangle). **(C)** Growth curves of the GFP$^{tub}_{198}$221ES (magenta squares) and the GFP$^{tub}_{\Delta}$221ES cell line (blue triangle). Means (± SD) of three clones are shown for each cell line. Due to the small standard deviation the error bars are not visible. The parental BSF 13-90 cell line (circles) served as a growth control. **(D)** Analyses of the GFP expression via flow cytometry. Representative flow cytometric profiles of one clone of the GFP$^{tub}_{198}$221ES (magenta) and the GFP$^{tub}_{\Delta}$221ES (blue) cell line are presented. The parental BSF 13-90 cell line (grey) served as a negative control. 2,000 cells were counted. **(E, F)** Western blot analyses of the GFP and the VSG 221 expression levels in three clones of the GFP$^{tub}_{198}$221ES and the GFP$^{tub}_{\Delta}$221ES cell line. The blots were stained **(E)** with a GFP antibody (magenta) or **(F)** a VSG 221 antibody (green). Detection of PFR proteins (magenta) served as a loading control. **(G)** Quantification of the mRNA levels of the endogenous *VSG 221* in the GFP$^{tub}_{198}$221ES (magenta) and the GFP$^{tub}_{\Delta}$221ES (blue) cell line. The *VSG 221* transcript levels were normalized to *tubulin* and are given relative to the *VSG* transcript levels of the parental BSF 13-90 cell line (100%). Means (± SD) of three clones are shown.

In summary, these results confirmed that a reporter gene was expressed at higher levels when the *VSG* 3'UTR was complete (GFP 198) than when parts of the 16mer were deleted (GFP Δ) (diploma thesis Batram, 2009). These differences in expression levels were observed independent of the genomic location of the constructs and thus supported the results of C.

Batram that the 16mer is essential for high VSG expression levels. Comparison of the GFP intensities showed that the $GFP^{ESpro}{}_{198}221^{ES}$ cell line, which expressed VSG 221 at wild type levels and had a normal growth, expressed almost 5-fold more GFP than the $GFP^{EStel}{}_{\Delta}221^{ES}$ cell line. Thus, neither the impaired growth nor the switching of the latter cell line, containing a telomere-proximal *GFP* coupled to a defective 16mer, was caused by high GFP expression levels. Also, no signs of switching were observed in the $GFP^{ESpro}{}_{\Delta}221^{ES}$ and the $GFP^{tub}{}_{\Delta}221^{ES}$ cell lines: the cells doubled normally and expressed the endogenous VSG 221 at wild type levels. Consequently, only the integration of a *GFP* with a defective 16mer downstream of the endogenous *VSG* triggered switching. This suggested that the telomere-proximal 16mer was used to monitor the integrity of the active ES and that the 16mer must be recognized at the DNA level. If the presence of a defective 16mer within the mRNA would be the signal for VSG switching, this should also occur when the construct was integrated at different genomic locations. Therefore, we concluded that the 16mer motif in the DNA served as a signal for the integrity of the ES. However, the functionality of the ES seemed to be assessed only by controlling the presence of the telomere-proximal 16mer in the ES.

3.9.3 Integration of a *VSG* with a defective 16mer downstream of the endogenous *VSG* causes switching

We showed that a defective 16mer triggers ES *in situ* switching using a *GFP* reporter gene with either the wild type or mutated *VSG* 121 3'UTR. In these experiments, switching was clearly dependent on the genomic location of the transgene; it was only observed when the defective 16mer was located downstream of the endogens *VSG* in the active ES. Neither the integration into the ES promotor region nor into the PolII transcribed tubulin locus led to detectable higher switching frequencies. This suggested that the 16mer is a DNA motif that serves as a signal for the functionality of the active ES.

Unfortunately, high levels of the GFP protein seem to be toxic for trypanosomes and I failed to generate a cell line with the GFP 198 reporter downstream of the endogenous *VSG*. Consequently, it could not be excluded that the *GFP* reporter gene itself, independent of its 3'UTR, would trigger ES *in situ* switching when it is integrated at this locus. Therefore, the experiments were repeated with the *VSG 121* ORF as reporter gene. *VSG 121* is a well-known, ES-resident *VSG*, and many stable double-expressor cell lines have been generated using the combination of *VSG 221* ES and the *VSG 121* with its wild type UTRs as ectopic transgene (Muñoz-Jordán et al., 1996).

First, the *GFP* ORF had to be replaced with the ORF of the *VSG 121* in the respective plasmids, pbRn6 GFP 198 and GFP Δ. For this purpose, the *GFP* ORF including parts of the *VSG* UTRs was subcloned into a pJet1.2 vector (pJet1.2 GFP VSG UTR). The *VSG 121* ORF

was amplified from the pRS.121 plasmid via PCR using the primers HZ30 and HZ31. Then, the *GFP* ORF was removed of the pJet1.2 plasmid by digestion with PacI and PaeI and replaced by the blunted VSG 121 PCR product. Next, the *VSG 121* ORF with the UTRs was transferred from the pJet VSG 121 plasmid to the pbRn6 GFP 198/Δ plasmids generating the plasmids pbRn6 VSG 121 198 and pbRn6 VSG 121 Δ. These constructs were completely identical to pbRn6 GFP 198/Δ except that the *GFP* ORF was now replaced by the *VSG 121* ORF. Thus, transfection of BSF 13-90 cells with the constructs should yield cell lines, which have integrated the *VSG 121* with a complete ($121^{ESTel}{}_{198}221^{ES}$) or a defective *VSG* 3'UTR ($121^{ESTel}{}_{\Delta}221^{ES}$) downstream of the endogenous *VSG 221* (Figure 36 A, B).

The clones of the $121^{ESTel}{}_{198}221^{ES}$ cell line grew slightly slower (pdt 8 h) than the parental BSF 13-90 parasites (pdt 6.1 h), whereas growth was severely impaired in the $121^{ESTel}{}_{\Delta}221^{ES}$ cell line (Figure 36 C). The pdt of five out of seven analyzed clones (termed $121^{ESTel}{}_{\Delta}1$) ranged from 9 to about 400 hours. However, two clones (termed $121^{ESTel}{}_{\Delta}$ 2) showed a pdt similar to the parental cell line (6.6 hours). Western blot analyses using either a VSG 121 or VSG 221 antibody showed that the clones with *VSG 121* coupled to its wild type 3'UTR ($121^{ESTel}{}_{198}221^{ES}$) expressed high levels of VSG 121 and only minor amounts of VSG 221 (Figure 36 D). In contrast, the growth affected clones with a defective 16mer ($121^{ESTel}{}_{\Delta}1$) showed only weak expression of both, VSG 121 and VSG 221. The two normally growing clones with a defective 16mer ($121^{ESTel}{}_{\Delta}$ 2) showed an inconsistent VSG 121/221 expression pattern: clone 1 was VSG 121-negative and VSG 221-positive, whereas clone 2 expressed high levels of VSG 121 and nearly no VSG 221. Quantitative Northern blot analyses confirmed the above observations on the mRNA level (Figure 36 E). Clones with a functional 16mer ($121^{ESTel}{}_{198}221^{ES}$) had *VSG 121* mRNA at wild type levels (95%), whereas mRNA of the endogenous *VSG 221* was barely detectable (5%). Only a small amount of *VSG 121* and *VSG 221* mRNA was present in the growth affected parasites with a defective 16mer ($121^{ESTel}{}_{\Delta}1$: *VSG 221:* 8 ± 3%; *VSG 121*: 4 ± 3%). The mRNA quantification also supported the results for the $121^{ESTel}{}_{\Delta}$ transfectants that had normal growth: clone 1 expressed *VSG 221* mRNA at wild type levels (93%), but had no *VSG 121* mRNA (0.1%), while clone 2 had wild type transcript levels of *VSG 121* (94%) and only 4% of *VSG 221* mRNA.

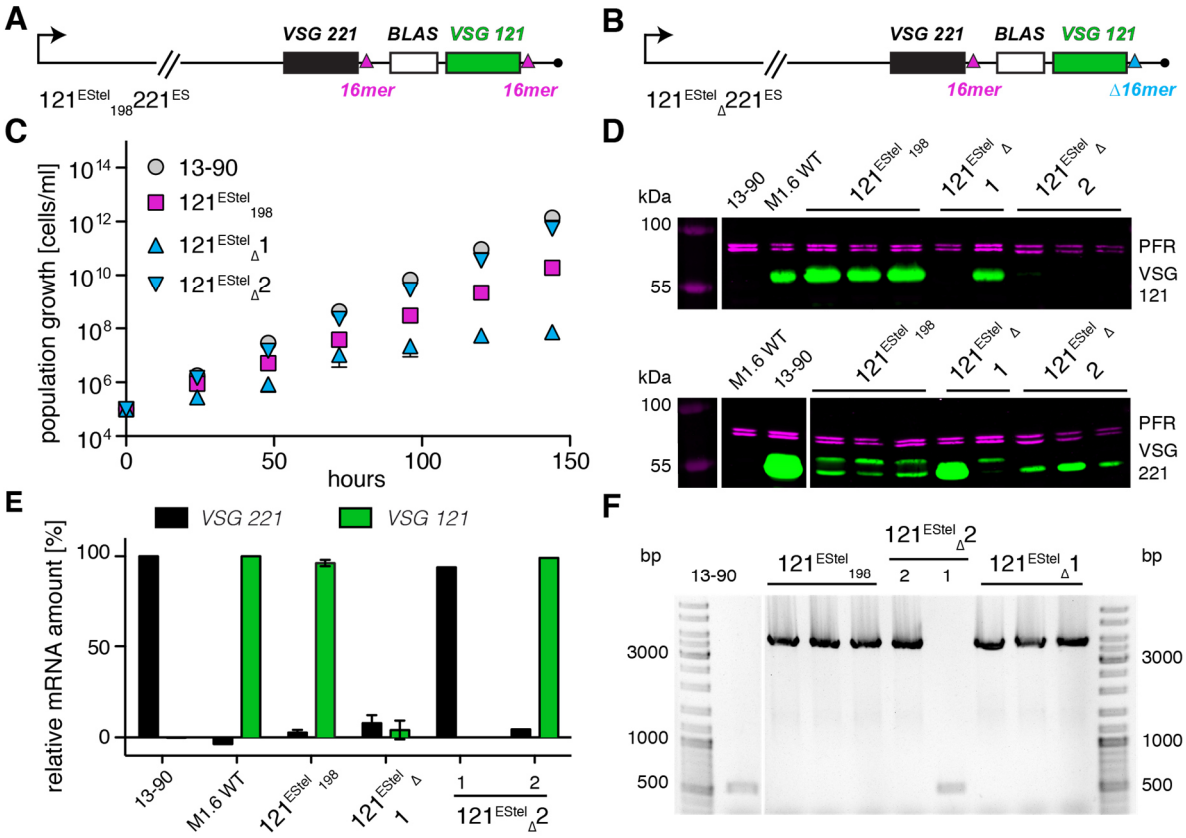

Figure 36: Integration of *VSG 121* with a functional or a defective *VSG* 3'UTR downstream of the endogenous *VSG*. Transfection of the BSF 13-90 cell line with pbRn6 VSG 121 198 or pbRn6 VSG 121 Δ generated the cell lines $121^{ESTel}{}_{198}221^{ES}$ and $121^{ESTel}{}_{\Delta}221^{ES}$, respectively. **(A, B)** Schematic representation of the modified *VSG 221* ES. The telomere-proximal *VSG 121* was either coupled **(A)** to a functional *VSG 121* 3'UTR (complete 16mer, magenta triangle) or **(B)** to a defective *VSG 121* 3'UTR (nucleotide 46-52 deleted, Δ16mer blue triangle). **(C)** Growth curves of the $121^{ESTel}{}_{198}221^{ES}$ (magenta squares) and the $121^{ESTel}{}_{\Delta}221^{ES}$ cell line (blue triangle). The parental BSF 13-90 cell line (circles) served as a growth control. Means (± SD) of three clones of the $121^{ESTel}{}_{198}221^{ES}$ cell line, five clones of the $121^{ESTel}{}_{\Delta}$ cell line with impaired growth (1) and two clones of the $121^{ESTel}{}_{\Delta}$ cell line with normal growth (2) are shown. Due to the small standard deviation the error bars are not visible. **(D)** Western blot analyses of the VSG 121 (upper panel) and the VSG 221 (lower panel) expression. Three clones of the $121^{ESTel}{}_{198}$ cell line and five clones of the $121^{ESTel}{}_{\Delta}221^{ES}$ cell line were analyzed. The blots were stained with a VSG 121 antibody (green, upper panel) or VSG 221 antibody (green, lower panel). Detection of PFR proteins (magenta) served as a loading control. Protein samples of MITat1.6 wild type cells natively expressing VSG 121 and the parental 13-90 cells natively expressing VSG 221 served as controls for antibody specificity. **(E)** Quantification of the mRNA levels of *VSG 121* (green) and the endogenous *VSG 221* (black). The *VSG* transcript levels were normalized to *tubulin* and are given relative to the *VSG* transcript levels of the parental BSF 13-90 cell line or MITat 1.6 wild type parasites expressing natively VSG 121 (100%). Means (± SD) of three clones are presented for $121^{ESTel}{}_{198}$ and $121^{ESTel}{}_{\Delta}1$ (clones with impaired growth). The two clones of the $121^{ESTel}{}_{\Delta}$ cell line with normal growth (2) are shown separately. **(F)** Validation of the integration of the pbRn6 VSG 121 construct in the *VSG 221* ES using PCR. A forward primer binding to the *VSG 221* ORF (outside of the integration site of the pbRn6 construct) and a reverse primer binding within the pbRn6 construct were used. A PCR-product with the size of 3,850 bp (arrow) will be only obtained if the plasmid is correctly integrated in the *VSG 221* ES. Each lane represents one clone of the indicated cell lines and 13-90 parasites served as a negative control.

As the growth affected clones expressed very low levels of both VSGs and the non-impaired clones showed an inconsistent VSG 121/221 expression, the correct integration of the pbRn6 construct in the *VSG 221* ES was controlled in all clones (Figure 36 F). For this purpose, an integration PCR was performed as described above. This validated that the pbRn6 construct was integrated in all clones expressing *VSG 121* with its wild type 3'UTR ($121^{EStel}{}_{198}221^{ES}$). The same was true for the clones with defective 16mer that displayed an impaired growth and neither expressed VSG 221 nor VSG 121 ($121^{EStel}{}_{\Delta}1$). In the normally growing VSG 221-positive clone 1 ($121^{EStel}{}_{\Delta}$ 2-1), the construct was not integrated in the active ES. Thus, this clone differed from the others with a defective 16mer because integration of the construct failed. In the other normally doubling clone, which was VSG 121-positive ($121^{EStel}{}_{\Delta}$ 2-2), the construct was correctly integrated. The latter result was inconsistent with our previous observations that deletions in the 16mer lead to decreased expression levels. VSG 121 levels should not reach wild type expression in the $121^{EStel}{}_{\Delta}221^{ES}$ clones if the 16mer was indeed defective.

DNA recombination events are very frequent within the trypanosome ES (reviewed in McCulloch et al., 2015). Thus, it was assumed that the deleted 16mer could have been replaced by a functional one through DNA recombination in the clone 2 ($121^{EStel}{}_{\Delta}$ 2-2). To target this question, the 3'UTR of *VSG 121* was sequenced. I prepared genomic DNA and amplified the integration site of pbRN6, including the *VSG 121* 3'UTR, using the primers HZ43 and CB80. The PCR product was cloned in the pJet1.2 vector and sequenced. This revealed that the *VSG 121* ORF was followed by a 3'UTR with a complete 16mer in clone 2 ($121^{EStel}{}_{\Delta}$ 2-2). Thus, the defective 16mer was most likely exchanged by a functional one via recombination. Also the *VSG 121* 3'UTR of a clone with impaired growth ($121^{EStel}{}_{\Delta}1$) was sequenced as control, which showed that in these cells the defective 16mer was still present. In summary, the combination of integration PCR and sequencing showed that the defective 16mer is only present in the $121^{EStel}{}_{\Delta}1$ clones that are affected in growth and express neither VSG 121 nor VSG 221 at high levels.

Nevertheless, it remained unclear why the parasites of the $121^{EStel}{}_{\Delta}1$ clones had an impaired growth. It has been demonstrated using RNAi that trypanosomes arrest in the cell cycle and die, once the VSG supply decreases (Sheader et al., 2005). As the $121^{EStel}{}_{\Delta}1$ parasites expressed neither VSG 121 nor VSG 221, one possible explanation for the growth phenotype of the cells was that they suffered of a VSG shortage. Therefore, it was investigated if the parasites express another VSG variant using SDS-page combined with Coomassie Blue staining of all proteins (Figure 37 A). The $121^{EStel}{}_{\Delta}1$ cells had no dominant band at the size of VSG 121 or VSG 221, but one with higher molecular weight. This indicated that the cells indeed express another VSG and thus did not suffer of a lack of the major surface protein. To investigate which VSG was expressed, cDNA was synthesized from RNA of two clones and

used for a PCR amplifying all *VSG* transcripts using a primer that binds to a sequence present in all *VSGs* (http://tryps.rockefeller.edu/Protocols /VSG_cloning_from_mRNA_lf.pdf). Subsequently, the PCR products were cloned into a pJet1.2 plasmid and sequenced. For one clone, transcripts of *VSG M1.9* and for the other, transcripts of *VSG M1.11* were identified. Thus, a VSG shortage was most likely not the reason for the impaired growth of the $121^{EStel}{}_{\Delta}1$ clones. Another explanation for the growth defect could be that the cells are trying to switch the active ES like the $GFP^{EStel}{}_{\Delta}$ parasites described above. The $121^{EStel}{}_{\Delta}1$ parasites were cultivated with drug selection for the *VSG 221* ES, but during an *in situ* switch the *VSG 221* ES is silenced. Thereby, the expression of the resistance cassette would stop and the parasites would get sensitive towards the selection and die. Therefore, it was tested whether the drug selection for the *VSG 221* ES was responsible for the growth phenotype (Figure 37 B). Growth analyses demonstrated that when the selection was removed the $121^{EStel}{}_{\Delta}1$ parasites resumed a normal growth within 24 hours (-BLAS pdt 7.1 h, Figure 37 B). The clones only displayed decreased doubling times in the presence of the antibiotic (+BLAS pdt 46 h).

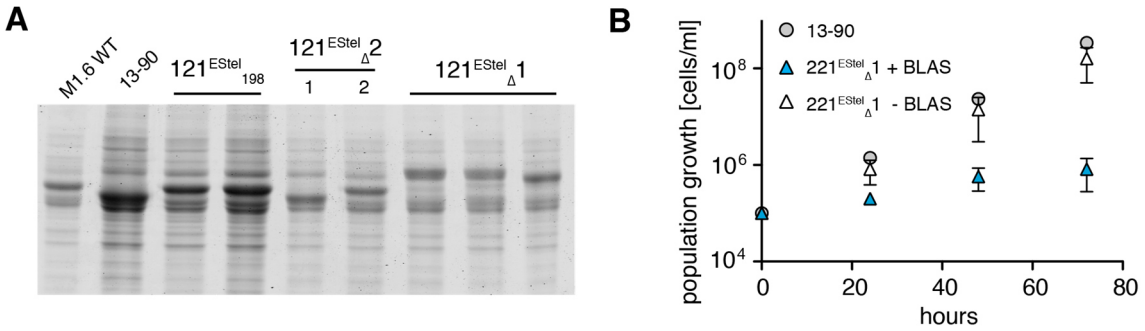

Figure 37: Integration of *VSG 121* with defective *VSG* 3'UTR downstream of the endogenous *VSG* triggers switching. (A) Visualization of the expressed VSGs using a Coomassie Blue stained SDS-gel. Protein samples of three clones of the $121^{EStel}{}_{198}221^{ES}$ cell line and five clones of the $121^{EStel}{}_{\Delta}221^{ES}$ cell line were analyzed. A sample of the parental BSF 13-90 cell line is used as a marker for VSG 221 and a sample of MITat 1.6 wild type for VSG 121. **(B)** Growth curves of the clones of the $121^{EStel}{}_{\Delta}221^{ES}$ cell line with impaired growth (1) in the presence of the selection (+BLAS, blue triangle) and in the absence of the drug (-BLAS, white triangle). The parasites were washed to remove the antibiotic and, subsequently, the growth of the cells in the absence of the selection was recorded. Means (± SD) of four clones are presented. The parental BSF 13-90 cell line (circles) served as a control.

Taken together these results suggested that the $121^{EStel}{}_{\Delta}1$ clones were trying to switch the active ES. In the presence of the antibiotic, the *VSG 221* ES had to remain partially open as its complete silencing would render the parasites sensitive towards the antibiotic and thus cause their death. Nevertheless, the activation of a new ES had already been initiated as the presence of other VSGs clearly showed. Consequently, the switch could only be completed once the antibiotic was removed and the cells resumed growth. Moreover, this phenotype was

specific for the integration of the defective 16mer. When the *VSG 121* ORF with a functional *VSG* 3'UTR was integrated downstream of *VSG 221*, the cells doubled every 8 hours and mainly expressed VSG 121. Thus, no signs of switching were observed in this cell line, which excluded that the switching was caused by the integration of the pbRn6 construct *per se*. However, it remained unclear why the endogenous *VSG 221* was down-regulated to 5% in the $121^{ESTel}{}_{198}221^{ES}$ cell line and had levels of 63 ± 15% in the $GFP^{ESTel}{}_{\Delta}221^{ES}$ cell line. Nevertheless, overall the results of the 121^{ESTel} cell line were identical to the results obtained with the GFP reporter cell lines. We conclude that the 16mer has a role in the stabilization of mRNA, but in addition, it serves as a DNA recognition motif. It is most likely used to assess the functionality of the active ES, whereby only the telomere-proximal 16mer in the *VSG* UTR serves as signal.

3.10 A *trans*-regulation of the VSG expression

During overexpression of an ectopic *VSG* with its wild type 3'UTR in monomorphic or pleomorphic trypanosomes the total amount of *VSG* mRNA seemed to be balanced (Batram et al., 2014; Chapter 3.2.1 of this thesis). Also when a second *VSG* with wild type 3'UTR was integrated upstream of the native *VSG* in the active ES the total mRNA amount of both *VSGs* did not exceed the *VSG* amount of cells expressing a single *VSG* (diploma thesis Fey, 2011; Smith et al., 2009; diploma thesis Uhl, 2009). Moreover, depletion of one of the *VSGs* using RNAi caused an increased expression of the other *VSG* to wild type levels (Smith et al., 2009). This suggested that a *VSG* counting mechanism could operate to determine and control the *VSG* mRNA amount. Such a mechanism could trigger a feedback loop, which controls the activity of the ES (PhD thesis Batram, 2013). However, the *VSG* mRNAs have to be somehow recognized to get counted. Therefore, a conserved motif would need to be present in all *VSGs*. It was likely that such a motif is either the conserved 8mer or 16mer within the 3'UTRs of the *VSGs* as the remaining mRNA sequence differ greatly between the *VSG* variants.

C. Batram investigated this hypothesis by overexpressing a *GFP* with *VSG 121* 3'UTR ($221^{ES}GFP^{tet}$) from the ribosomal spacer and monitoring the *GFP* as well as the *VSG 221* mRNA levels (PhD thesis Batram, 2013). Induction of the GFP overexpression caused a decrease of the VSG *221* mRNA to 60% within 8 hours. However, the amount of *VSG 221* mRNA returned back to its original level within 24 hours and the cells died during the course of GFP overexpression, perhaps due to the toxicity of the protein (PhD thesis Batram, 2013; Liu et al., 1999). However, the *GFP* was most likely translated in the cytosol, whereas the VSG is suggested to get co-translational imported into the ER. If a *VSG* counting mechanism would operate at the ER during translation, the cytosolic *GFP* could have escaped the *trans*-regulation mechanism. This hypothesis was investigated by C. Batram by overexpressing a *GFP* with *VSG 121* 3'UTR that was coupled to an ER import signal from the ribosomal spacer ($221^{ES}LS{:}GFP^{tet}$) (PhD thesis Batram, 2013). Induction of overexpression of an ER-targeted GFP caused a decrease in the *VSG 221* mRNA levels to 20% within two hours. However, the cells started to die already within four hours of overexpression. Thus, it remained unclear whether the presence of the *VSG* 3'UTR at the ER was responsible for the down-regulation of the endogenous *VSG 221*, or perhaps the accumulation of the toxic GFP in the ER (PhD thesis Batram, 2013).

3.10.1 VSG overexpression causes a reduced expression of a *GFP* with a *VSG* 3'UTR

The aim of this project was to continue the work of C. Batram and further investigate the hypothesis that the *VSG* mRNA levels are regulated *in trans*. First, we needed to distinguish whether the down-regulation of the *VSG 221* mRNA upon overexpression of the *GFP* with *VSG* 3'UTR was caused by the toxicity of the GFP or indeed by a sequence motif in the *VSG* 3'UTR. For this, a *GFP* with *VSG* 5' and 3'UTRs was constitutively expressed at non-toxic levels from a genomic location outside the ES: the tubulin intergenic region. It was shown earlier in the present thesis that this cell line grows normally and expresses the endogenous VSG 221 as well as low levels of GFP protein (Figure 35). Then, a *VSG* with its wild type UTRs was overexpressed in this cell line and the GFP as well as the VSG 221 levels were monitored. If the hypothesis holds true that the *VSG* is regulated *in trans*, VSG overexpression should result in the down-regulation of both: the endogenous VSG 221 and the GFP expressed with the *VSG* 3'UTR. VSG 118 was used for ectopic overexpression ($GFP^{tub}{}_{198}221^{ES}118^{tet}$, Figure 38 A) as in previous studies with monomorphic cells only a minor deceleration in growth was observed upon induction, suggesting that no general transcriptional shut-down should occur (bachelor thesis Henning, 2012). Consequently, any change in GFP expression upon induction of VSG 118 overexpression should be the result of a *trans*-regulation mechanism and not of a transcriptional shut-down.

Growth analyses of the clones of the $GFP^{tub}{}_{198}221^{ES}118^{tet}$ cell line showed that the non-induced cells had growth rates similar to the ones of the BSF 13-90 cell line (-tet: pdt 6.7 h; BSF 13-90: pdt 6.1 h; Figure 38 B). The growth was slightly affected upon induction of VSG 118 overexpression as the cells had a pdt of nine hours (Figure 38 B). Quantification of the *VSG 118* and *VSG 221* mRNA from Northern blots showed that the endogenous *VSG 221* mRNA was down-regulated within eight hours of induction (Figure 38 C). In the same time, the ectopic *VSG 118* mRNA reached wild type transcript levels. Thus, the *VSG* transcripts were exchanged with similar kinetics as previously observed for the mono- and pleomorphic VSG 121 overexpressors (Batram et al., 2014; chapter 3.2.1 of this thesis). Analyses of the GFP signal by fluorescence microscopy showed that the GFP was equally distributed throughout the cytoplasm in both non-induced and induced cells (Figure 38 D). The total GFP signal, however, appeared reduced upon the addition of tetracycline (Figure 38 D). This was confirmed by quantitative Western blot and flow cytometry analyses: the GFP was down-regulated at the protein level within 24 hours of VSG 118 overexpression (Figure 38 E, F)

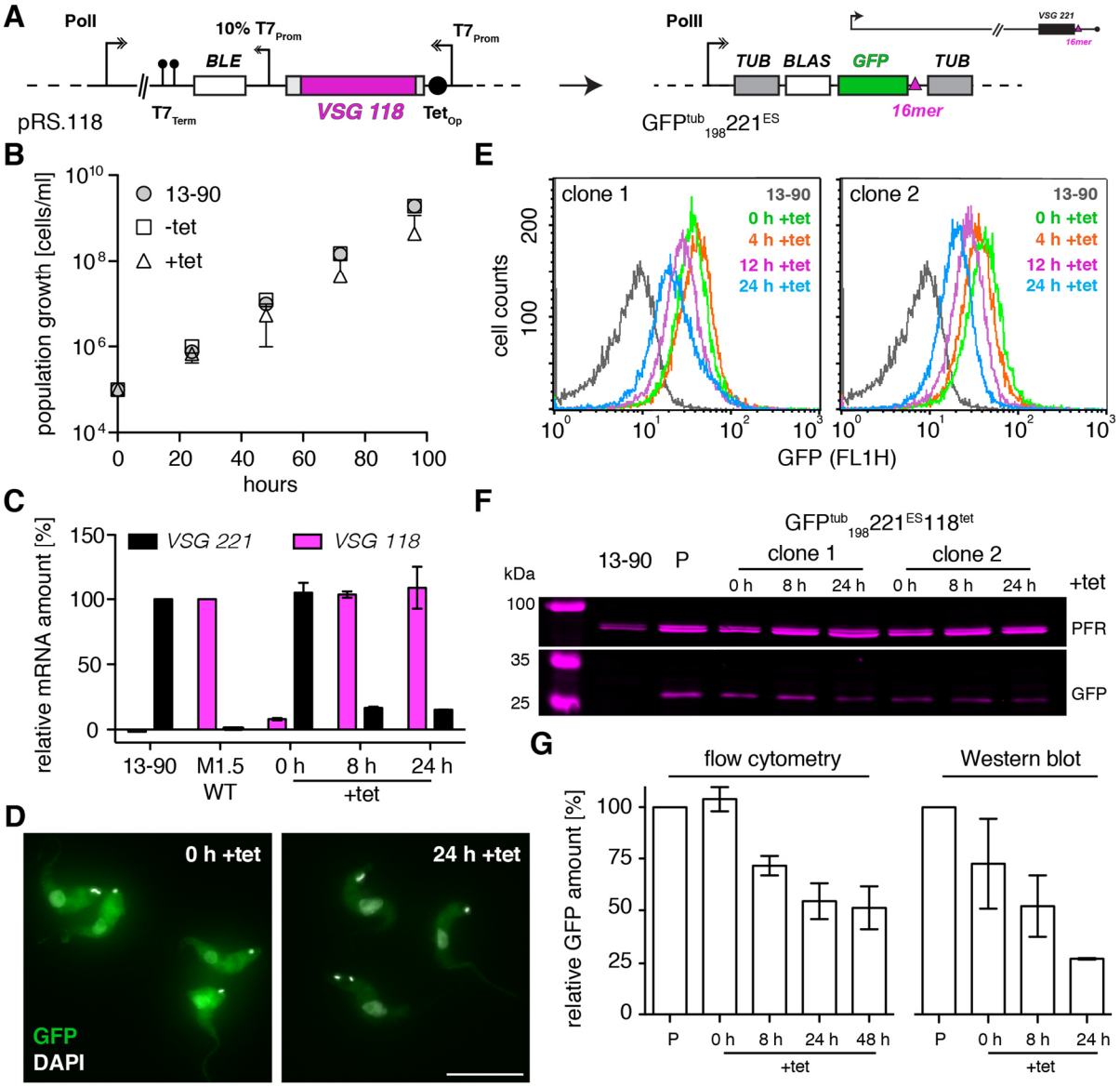

Figure 38: VSG overexpression causes the down-regulation of a GFP expressed with *VSG* 3'UTR. Parasites constitutively expressing a *GFP* with functional *VSG* 3'UTR from the tubulin locus were transfected with the construct for ectopic VSG 118 overexpression ($GFP^{tub}{}_{198}221^{ES}118^{tet}$). All shown analyses were conducted with this cell line. **(A)** Schematic representation of the VSG overexpression construct (pRS.118) and the modified tubulin locus. **(B)** Growth curves of tetracycline-induced (triangles) and non-induced (squares) parasites. Means (± SD) of four clones are shown. The parental BSF 13-90 cell line (circles) served as a growth control. **(C)** The *VSG 118* (magenta) and the *VSG 221* (black) mRNA amount was determined during the course of VSG overexpression. The normalized *VSG 118* levels are given relative to MITat1.5 wild type cells natively expressing VSG 118. The normalized *VSG 221* levels are given relative to the *VSG* transcript levels of BSF 13-90 cells. Means (± SD) of two clones are shown. **(D)** Fluorescence microscopic images of the parasites in the absence (0 h +tet) or presence of tetracycline (24 h +tet). The GFP signal is shown in green and the DAPI-stained DNA in grey. Scale bar: 10 µm. **(E)** Analyses of the GFP expression during the course of VSG 118 overexpression via flow cytometry. Representative flow cytometric profiles of two clones. The parental BSF 13-90 cell line (grey) served as a negative control. 20,000 cells were counted. **(F)** Western blot analysis of the GFP expression during the course of VSG 118 overexpression using a GFP antibody (magenta). Detection of PFR (magenta) served as a loading control. **(G)** Quantification of the GFP signal from flow cytometry in E and Western blots in F. Values are given relative to the GFP expression level of the parental cell line. Means (± SD) of two clones are shown.

Quantification of the flow cytometric analyses showed that the GFP levels decreased to 54 ± 8% of the levels in the parental cell line ($GFP^{tub}{}_{198}221^{ES}$) within 24 hours of VSG overexpression and remained at this level within 48 hours of induction (GFP: 51 ± 10%; Figure 38 G). Quantification of the Western blot analysis showed that the GFP expression decreased to 26% of the parental cell line ($GFP^{tub}{}_{198}221^{ES}$) within 24 hours of VSG overexpression, whereby the GFP signal was already weaker in the non-induced cells. Unfortunately, the *GFP* mRNA levels were too low to be detected on an RNA dot blot using fluorescently labeled oligonucleotides.

In summary, the overexpression of VSG 118 in trypanosomes constitutively expressing a cytosolic *GFP* with *VSG* 3'UTR ($GFP^{tub}{}_{198}221^{ES}118^{tet}$) supported the hypothesis that the VSG expression is regulated *in trans*. The expression of the *GFP* with *VSG* UTRs decreased upon induction of VSG overexpression, but between 25 and 50% of the GFP protein levels were still observed after 24 hours. This suggested that some mRNAs could escape the regulation mechanisms, perhaps because the counting mechanism is operating at the ER.

3.10.2 VSG overexpression causes a reduced expression of a *GFP* with a *VSG* 3'UTR that localizes to the endoplasmic reticulum

The previous results supported the hypothesis that a *trans*-regulation mechanism adjusts the *VSG* levels to wild type levels in trypanosomes. However, the data also suggested that some mRNAs escaped this regulation as the down-regulation of a cytoplasmic GFP expressed with *VSG* 3'UTR was only partial. This was in agreement with the previous suggestion of C. Batram that a VSG *trans*-regulation mechanism could operate at the ER (PhD thesis Batram, 2013). Therefore, a reporter cell line with a *GFP* with *VSG* 3'UTR coupled to an ER import signal was generated. For this purpose, the LS:GFP was cut out of the plasmid pLew82v4:LS:GFP 198 with the enzymes EcoRI and BserI. The *GFP* ORF was removed from the previously generated pJet1.2 GFP VSG UTR plasmid by digestion with PaeI and BserI. The overhangs of the EcoRI cuts of the insert and the PaeI cuts of the backbone were blunted prior the ligation of the fragments. The resulting pJet1.2 LS:GFP VSG UTR plasmid as well as the pTub GFP 198 construct were digested with PacI and Ppu21I. Ligation of the generated LS:GFP insert with the pTub backbone yielded the pTub LS:GFP 198 plasmid (Figure 39 A).

Transfection of the BSF 13-90 cell line with the pTub LS:GFP 198 plasmid yielded a reporter cell line, which constitutively expressed an ER-targeted *GFP* with *VSG* 3'UTR ($LS:GFP^{tub}{}_{198}221^{ES}$). Clones of this cell line did not display any changes in growth (Figure 39 B), but flow cytometry analyses revealed differences in the GFP expression levels between the different clones (Figure 39 C). Clone 1 ($LS:GFP\text{-}1^{tub}{}_{198}$) expressed the GFP at levels comparable to the GFP signal without ER localization. However, the GFP was barely

detectable in all other clones (clone 2-5), as illustrated by the comparison of the flow cytometric profiles of clone 2 and 3 (LS:GFP$^{tub}_{198}$-2 and -3) to the GFP-negative 13-90 cell line in Figure 39.

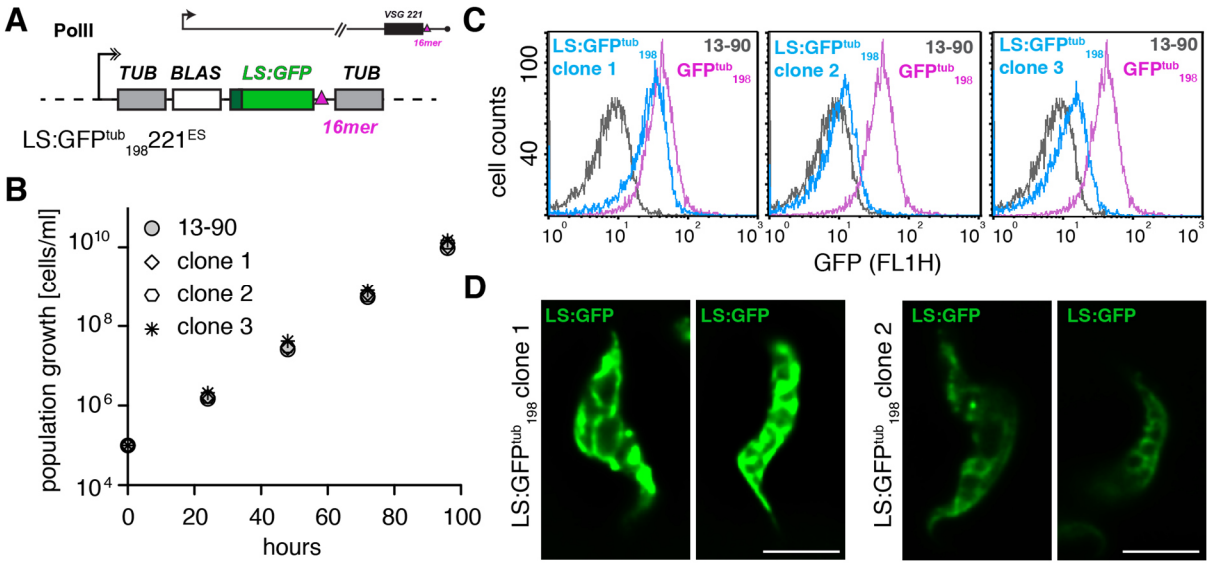

Figure 39: Different protein levels of an ER-targeted *GFP* with *VSG* 3'UTR. Transfection of the BSF 13-90 cell line with the pTub LS:GFP 198 construct generated the LS:GFP$^{tub}_{198}$221ES reporter cell line. **(A)** Schematic representation of the modified tubulin locus. **(B)** Growth curves of three different clones of the reporter cell line. The parental BSF 13-90 cell line (circles) served as a growth control. **(C)** Analyses of the expression levels of the ER-targeted GFP by flow cytometry. Flow cytometric profiles of three clones of the reporter cell line (blue). The parental BSF 13-90 cell line (grey) served as a negative control. Parasites constitutively expressing a cytosolic *GFP* with *VSG* 3'UTR (GFP$^{tub}_{198}$221ES cell line; magenta) were used as a positive control. 10,000 cells were counted. **(D)** Fluorescence microscopic images of clone 1 and clone 2 of the reporter cell line. The GFP signal of gelatine-embedded living cells is shown in green. Presented are single slices of deconvolved Z-stacks to visualize the branch-like structure of the ER. Scale bar: 10 µm.

Quantification of the GFP intensity by flow cytometry indicated that clone 1 expressed almost three times more GFP than clone 2 or 3. One explanation for this difference could be that in clone 1 the GFP was not targeted to the ER. However, microscopic analyses showed that the GFP localized to the branched structure that is characteristic for the ER in all clones, independent of the GFP expression level (Figure 39 D).

Another explanation for the different GFP expression levels could be that clone 1 had a defect in the *trans*-regulation mechanism. Thus, the targeting of the *GFP* to the ER caused in the majority of clones (four of five analyzed clones) a down-regulation via the *trans*-regulation mechanism, whereas clone 1 could not regulate the GFP expression anymore. If this holds true, clone 1 should also display altered kinetics in the regulation of the *VSG* transcripts upon induction of VSG overexpression and no down-regulation of the GFP should be observed in

this case. To test this hypothesis, the ectopic VSG 118 was overexpressed in clone 1 and as a control also in clone 2, one of the clones with a weak GFP signal.

Overexpression of VSG 118 in clone 1 (LS:GFP-1$^{tub}{}_{198}221^{ES}118^{tet}$; Figure 40 A) caused a delay in growth. The non-induced parasites (-tet) doubled every seven hours, whereas the doubling time increased to 13.3 hours upon the addition of tetracycline (Figure 40 B). No changes in the kinetics of the regulation of the *VSG* transcript levels were observed upon induction of VSG 118 overexpression (Figure 40 C). Within four hours of VSG overexpression, the endogenous *VSG* decreased to 25 ± 10% of wild type expression levels and remained at this level for up to 24 hours (18 ± 1%). The ectopic *VSG* was up-regulated to 85% ± 0.3% of the wild type levels within four hours and increased within 24 hours to 102 ± 1%. Using flow cytometry, a decrease in the GFP levels during the course of VSG 118 overexpression was observed (Figure 40 D). Within 24 hours, the GFP signal decreased to 58 ± 1% of the signal of the parental cell line (LS:GFP-1$^{tub}{}_{198}221^{ES}$) and remained at this level for at least another 24 hours (56 ± 4%) (Figure 40 E).

Western blot analysis confirmed the decrease in GFP expression. The GFP levels reached 22 ± 6% of the levels in the parental cell line (LS:GFP-1$^{tub}{}_{198}221^{ES}$) after 24 hours of VSG overexpression (Figure 40 E). Thus, clone 1 with the strong ER-localized GFP signal regulated the *VSG* transcript and the GFP expression upon VSG 118 overexpression (LS:GFP-1$^{tub}{}_{198}221^{ES}118^{tet}$), like the VSG overexpressor with the constitutively expressed cytoplasmic GFP (GFP$^{tub}{}_{198}221^{ES}118^{tet}$; Figure 38). The previous assumption, that a defect in the VSG *trans*-regulation mechanism was responsible for the higher GFP levels in clone 1, is therefore wrong.

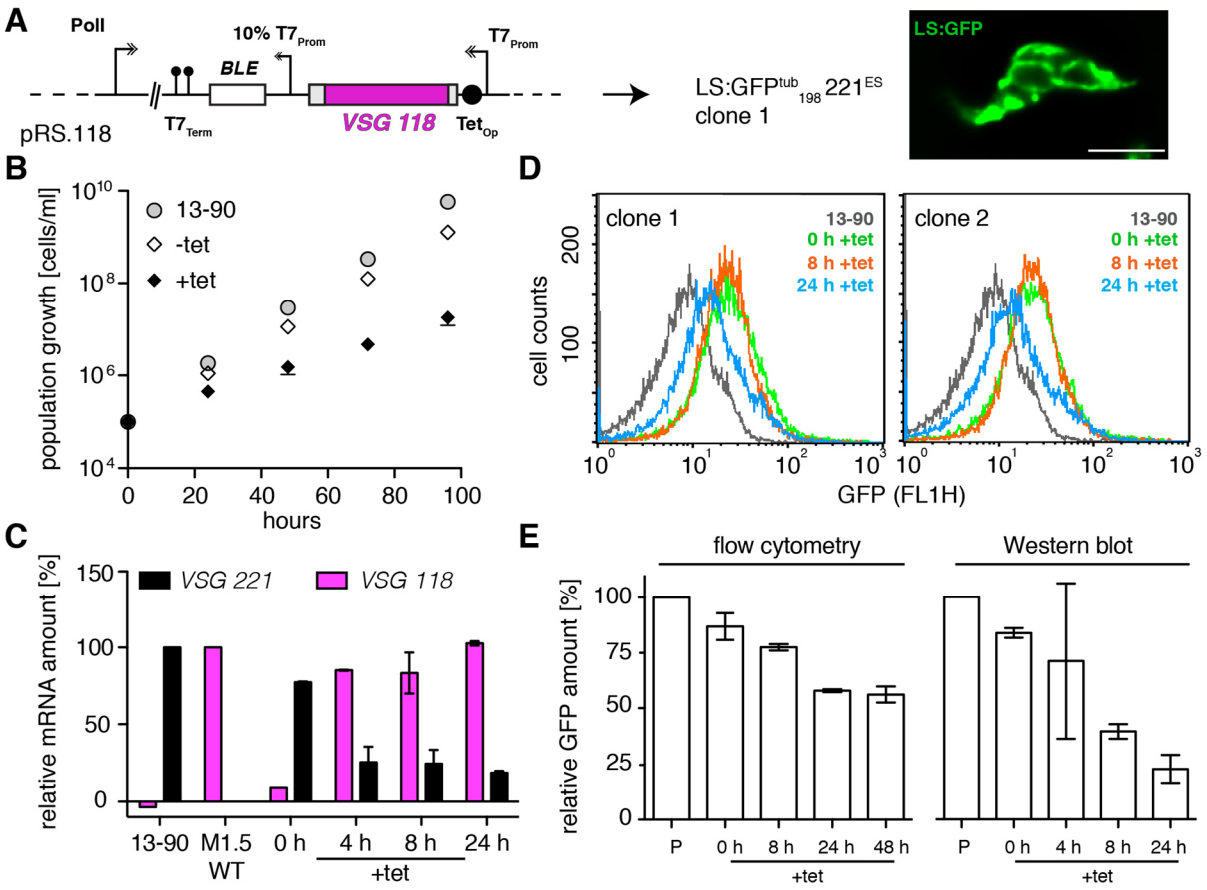

Figure 40: VSG overexpression causes the down-regulation of a strongly expressed ER-targeted *GFP* with *VSG* 3'UTR. Clone 1, which strongly expressed an ER-targeted *GFP* with *VSG* 3'UTR (LS:GFP-1$^{tub}{}_{198}$221ES), was transfected with the construct for ectopic VSG 118 overexpression (LS:GFP-1$^{tub}{}_{198}$221ES118^{tet}). All analyses shown here were done with this cell line. **(A)** Schematic representation of the VSG overexpression construct (pRS.118) and a fluorescent image of clone 1 (LS:GFP-1$^{tub}{}_{198}$221ES). **(B)** Growth curves of tetracycline-induced (black diamonds) and non-induced (white diamonds) parasites. Means (± SD) of five clones are shown. Due to the small standard deviation the error bars are not visible. The parental BSF 13-90 cell line (circles) served as a growth control. **(C)** The mRNA levels of the ectopic *VSG 118* (magenta) and the endogenous *VSG 221* (black) were determined during the course of VSG overexpression. The normalized *VSG* levels are given relative to the *VSG* transcript levels of cells natively expressing VSG 118 or VSG 221. Means (± SD) of two clones are shown. **(D)** Analyses of the GFP expression during the course of VSG 118 overexpression via flow cytometry. Representative flow cytometric profiles of two clones: non-induced cells (0 h +tet, green) and cells overexpressing VSG 118 for 8 or 24 hours (8 h +tet, orange; 24 h +tet, blue). The parental BSF 13-90 cell line (grey) served as a negative control. 20,000 cells were counted. **(E)** Quantification of the GFP signal determined by the flow cytometric analyses in D (left panel). The GFP expression was also quantified via Western blot analysis using antibodies against GFP and PFR (right panel). The GFP signal was normalized to PFR. For both quantifications the values are given relative to the GFP expression level of the parental cell line. Means (± SD) of two clones are shown.

VSG 118 overexpression in clone 2, the one with the weak ER-localized GFP signal (LS:GFP-$2^{tub}{}_{198}221^{ES}118^{tet}$, Figure 41 A) had no effect on growth (Figure 41 B). In the absence of tetracycline the cells doubled every seven hours and when the drug was present every 7.5 hours. The *VSG 221* transcripts decreased to 28 ± 6% within four hours of VSG 118 overexpression, while the ectopic *VSG* increased to wild type levels (87 ± 12%; Figure 41 C). Thus, the *VSG* transcripts were regulated in a similar manner compared to the other analyzed VSG 118 overexpression cell lines (compare Figure 38 C and Figure 40 C). Quantification of the GFP expression levels using Western blot analysis showed no change in GFP protein level within 8 hours of VSG 118 overexpression (90 ± 12%; Figure 41 D, E). Within 24 hours of induction, the GFP expression levels varied between the analyzed clones. The GFP levels decreased to 70% of the parental cell line in clone one (LS:GFP-$2^{tub}{}_{198}221^{ES}$) and to 33% in the other clone. Unfortunately, these results could not be confirmed by flow cytometry as the GFP expressing parasites could not be distinguished from the GFP-negative BSF 13-90 cell line (illustrated in Figure 41 F).

Together, the data showed that the expression of a *GFP* with *VSG* 3'UTR was down-regulated during VSG 118 overexpression, independent on whether it localized to the cytoplasm or to the ER. The ER-localized GFP should decrease either faster or to a lower level or both upon induction of VSG overexpression compared to a cytosolic GFP, if a VSG *trans*-regulation mechanism would operate at the ER. This was not observed, indicating that the *trans*-regulation mechanism does not operate at the ER as previously suggested. It remained unclear (i) why clone 1 expressed nearly threefold more of the ER-localized GFP than the other clones and (ii) why neither the cytoplasmic nor the ER-localized GFP disappeared completely during VSG overexpression. Do some mRNA molecules escape the *trans*-regulation mechanism and if this is the case, how? Or has this mechanism a lower threshold?

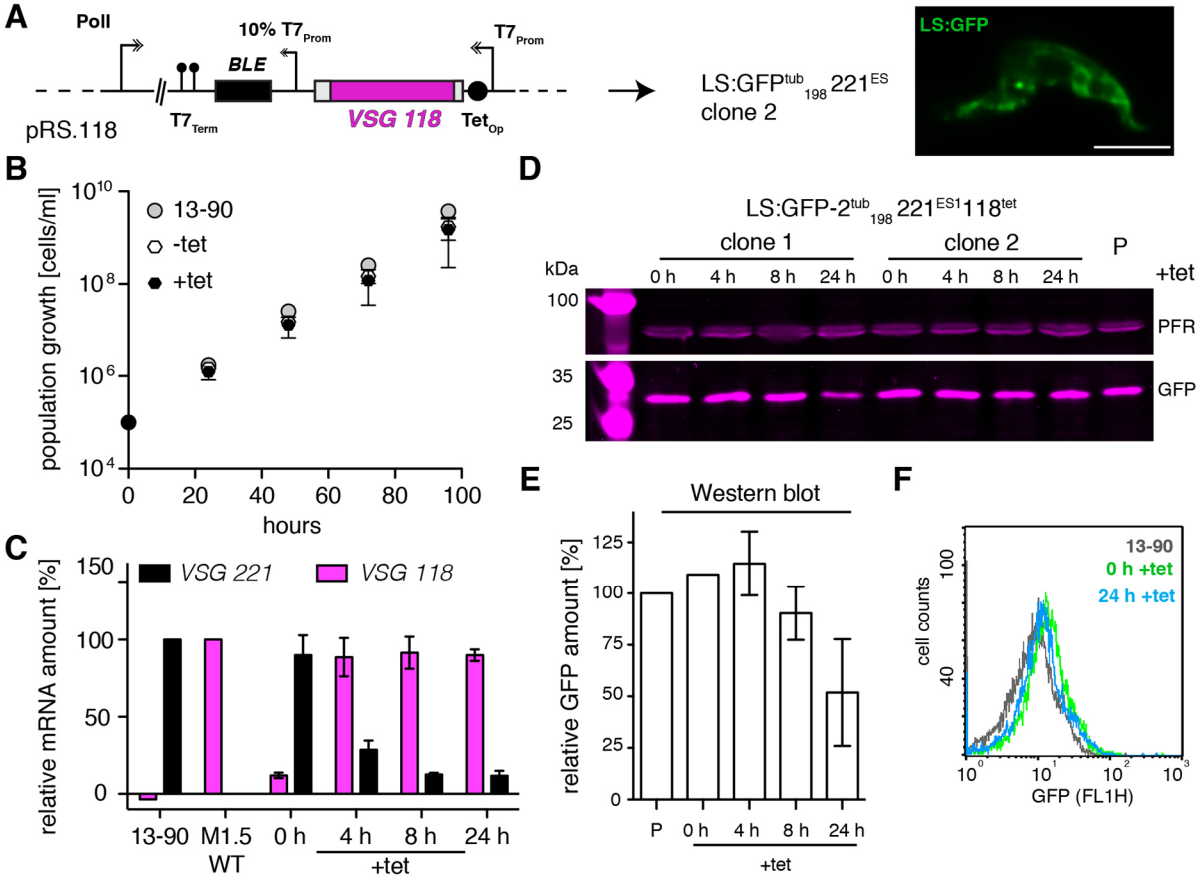

Figure 41: VSG overexpression causes a slight down-regulation of a weakly expressed ER-targeted *GFP* with *VSG* 3'UTR. Clone 2, which weakly expressed an ER-targeted *GFP* with *VSG* 3'UTR (LS:GFP-2$^{tub}{}_{198}$221ES), was transfected with the construct for ectopic VSG 118 overexpression (LS:GFP-2$^{tub}{}_{198}$221ES118^{tet}). All analyses shown here were done with this cell line. **(A)** Schematic representation of the VSG overexpression construct (pRS.118) and a fluorescent image of clone 2 (LS:GFP-2$^{tub}{}_{198}$221ES). **(B)** Growth curves of tetracycline-induced (black hexagons) and non-induced (white hexagons) parasites. Means (± SD) of five clones are shown. The parental BSF 13-90 cell line (circles) served as a growth control. **(C)** The mRNA levels of the ectopic *VSG 118* (magenta) and the endogenous *VSG 221* (black) were determined during the course of VSG overexpression. The normalized *VSG* levels are given relative to the *VSG* transcript levels of cells natively expressing VSG 118 or VSG 221. Means (± SD) of two clones are shown. **(D)** Western blot analysis of the GFP expression levels of two clones during the course of VSG 118 overexpression. The blot was stained with a GFP antibody (magenta). Detection of PFR proteins (magenta) served as a loading control. **(E)** Quantification of the GFP signal determined by the Western blot analysis in D. GFP values were normalized to PFR and are given relative to the GFP expression level of the parental cell line. Means (± SD) of two clones are shown. **(F)** Representative flow cytometric profile of one clone: non-induced cells (0 h +tet, green) and cells overexpressing VSG 118 for 24 hours (24 h +tet, blue). The parental BSF 13-90 cell line (grey) served as a negative control. 10,000 cells were counted.

3.10.3 GFP expression is less influenced by VSG overexpression if the transcript contains a *PFR* UTR

The results so far supported the idea that a *trans*-regulation mechanism based on the *VSG* 3'UTR operates to regulate the *VSG* levels, albeit there is no evidence for a connection to the ER. However, it was necessary to control that the down-regulation of the expression of the *GFP* was indeed dependent on the *VSG* 3'UTR. For this purpose, we decided to generate a GFP reporter cell lines with the *PFR* 3'UTR instead of a *VSG* 3'UTR. First, the *VSG 121* 3'UTR of the pTub GFP 198 and the pTub LS:GFP 198 plasmid was removed by enzymatic digestion with HindIII and PacI. The HindIII restriction site was blunted to generate a suitable backbone. The *PFR* 3'UTR was amplified from the plasmid p4676 with the primers HZ47 and HZ48 via PCR and cloned into a pJet1.2 plasmid. Next, the *PFR* 3'UTR insert was obtained by enzymatic digestion with the enzymes PdiI and PacI. Ligation of the digested pTub GFP 198 or pTub LS:GFP 198 backbones with the *PFR* 3'UTR insert yielded the pTub GFP:PFR_{UTR} and pTub LS:GFP:PFR_{UTR} plasmids. Transfection of BSF 13-90 parasites with the plasmids generated reporter cell lines with a cytoplasmic *GFP* with *PFR* 3'UTR ($GFP^{tub}{}_{PFR}221^{ES}$; Figure 42 A) or with an ER-targeted *GFP* with *PFR* 3'UTR ($LS:GFP^{tub}{}_{PFR}221^{ES}$; Figure 42 B).

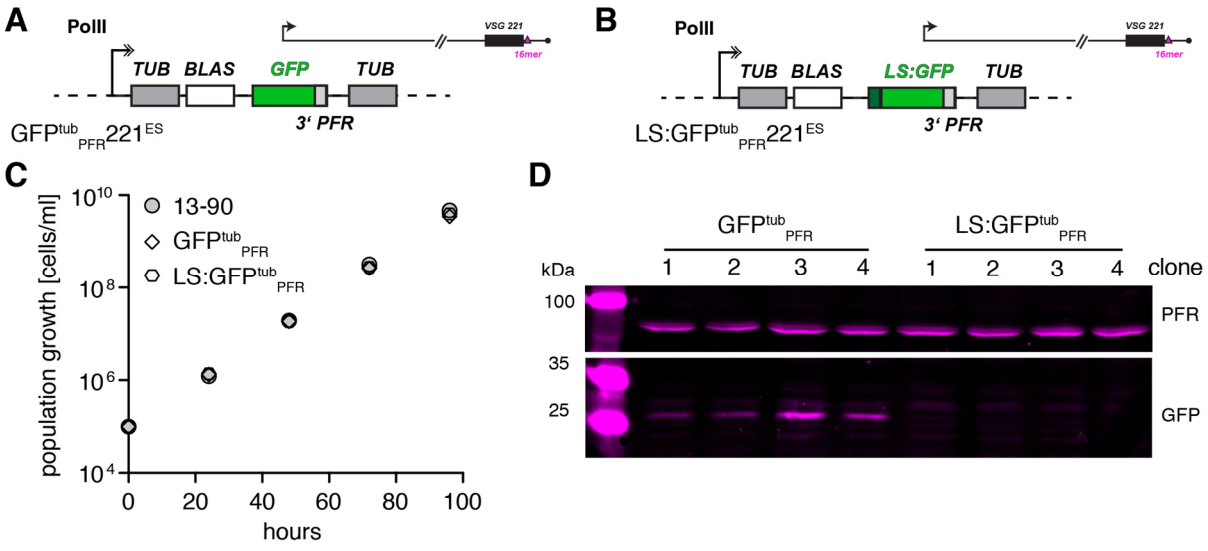

Figure 42: Targeting of a *GFP* with *PFR* 3'UTR to the ER causes a decrease in its expression. **(A, B)** Transfection of the BSF 13-90 cell line with **(A)** pTub GFP:PFR_{UTR} or **(B)** pTub LS:GFP:PFR_{UTR} generated the cell lines $GFP^{tub}{}_{PFR}221^{ES}$ and $LS:GFP^{tub}{}_{PFR}221^{ES}$, respectively. **(C)** Growth curves of cells with a cytosolic GFP ($GFP^{tub}{}_{PFR}221^{ES}$; white diamonds) and an ER-targeted GFP ($LS:GFP^{tub}{}_{PFR}221^{ES}$; white hexagons). Means (± SD) of five clones are shown for each cell line. Due to the small standard deviation the error bars are not visible. The parental BSF 13-90 cell line (circles) served as a growth control. **(D)** Western blot analyses of the GFP expression levels of four clones of each cell line. The blot was stained with a GFP antibody (magenta) and detection of PFR proteins (magenta) served as a loading control.

Growth analyses showed that neither the cytoplasmic GFP ($GFP^{tub}_{PFR}221^{ES}$) nor the ER-targeted GFP ($LS:GFP^{tub}_{PFR}221^{ES}$) altered the growth of the trypanosomes (Figure 42 C). Fluorescence microscopy showed a faint GFP signal in both cell lines (data not shown). However, the ER targeted signal was even weaker than the cytosolic GFP so that its correct localization to the ER could not be confirmed by fluorescence microscopy. Western blot analysis confirmed the differences in GFP expression between the two reporter cell lines (Figure 42 D). A weak GFP expression was observed in the clones expressing a cytoplasmic *GFP* with *PFR* 3'UTR ($GFP^{tub}_{PFR}221^{ES}$), whereas no GFP signal could be detected when the *GFP* was targeted to the ER ($LS:GFP^{tub}_{PFR}221^{ES}$).

Thus, VSG 118 was only overexpressed in a clone of the cytoplasmic GFP reporter cell line ($GFP^{tub}_{PFR}221^{ES}118^{tet}$, Figure 43 A). Induction of VSG overexpression caused a delay in growth as the cells doubled every 11 hours in the presence of tetracycline, whereas the non-induced cells displayed a pdt of 6.5 hours (Figure 43 B). Western blot analysis using a VSG 118 antibody confirmed that all clones overexpressed the ectopic VSG within 24 hours of induction (Figure 43 C). Next, Western blot analysis was used to determine if the expression of the cytosolic *GFP* with *PFR* 3'UTR decreased upon VSG overexpression (Figure 43 D). This indicated that there could be a reduction in the GFP levels at least in some clones as the GFP expression ranged from 37% to 82% of the non-induced expression levels within 24 hours of VSG overexpression (Figure 43 E). However, these data need to be considered with care, as the detection of the GFP expressed with *PFR* 3'UTR was already difficult in the non-induced cells due to the low expression levels. Thus, slight differences in the loading or the blotting of the samples could have a substantial impact on the quantification of the GFP expression. For this reason, it will be inevitable to analyze different samples in replicates. Moreover, it will be necessary to compare the *GFP* transcript levels of this cell line with the others to get unambiguous results regarding the GFP regulation upon the addition of tetracycline.

Nevertheless, comparison of the protein levels of the cytosolic *GFP* expressed with *VSG* 3'UTR or with *PFR* 3'UTR during VSG 118 overexpression suggested that the reporter was regulated dependent on its 3'UTR. The expression of the *GFP* with *VSG* 3'UTR was down-regulated in all four clones to 23 ± 11% within 24 hours, whereas the expression levels of the *GFP* with *PFR* 3'UTR remained in average at 67 ± 18%. Thus, *GFP* expression seems to be regulated *in trans* dependent on the 3'UTR, albeit further analyses will be necessary to strengthen this conclusion.

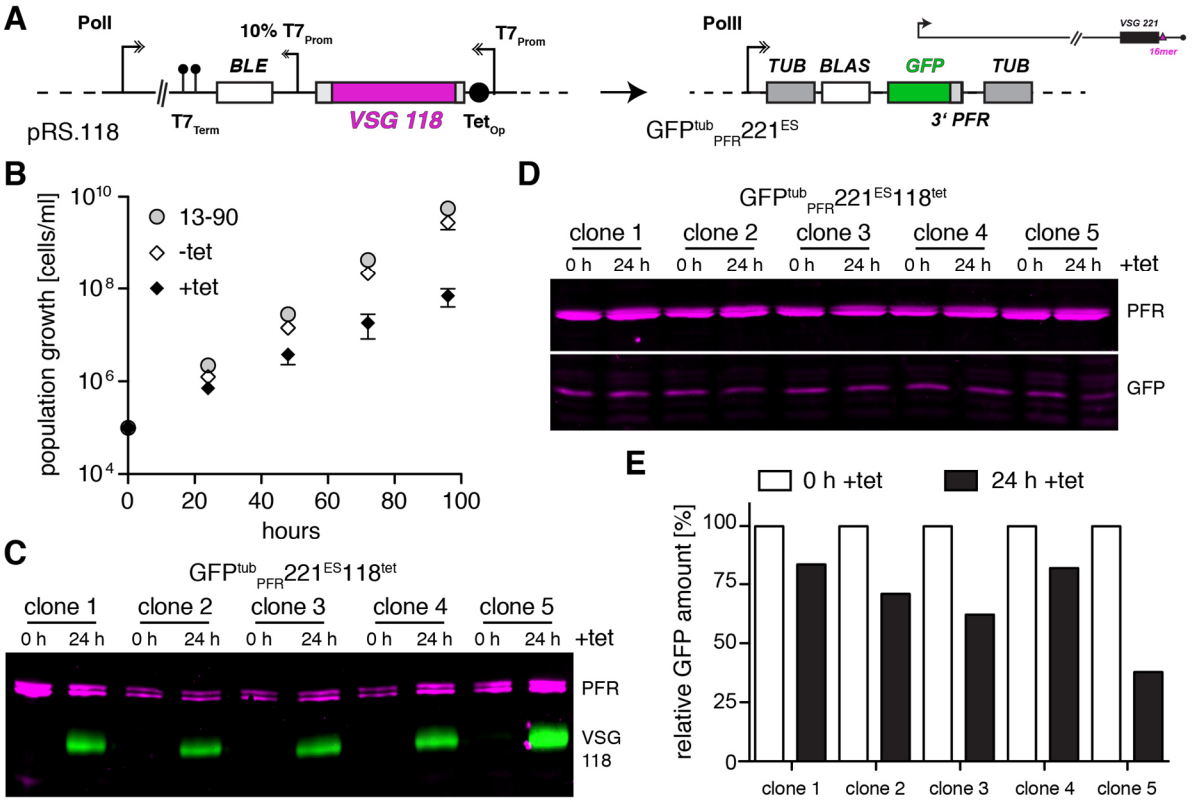

Figure 43: The expression of a *GFP* with *PFR* 3'UTR is only mildly affected by VSG overexpression. Parasites constitutively expressing a *GFP* with a *PFR* 3'UTR from the tubulin locus ($GFP^{tub_{PFR}}221^{ES}$ cell line) were transfected with the construct for ectopic VSG 118 overexpression ($GFP^{tub_{PFR}}221^{ES}118^{tet}$). All analyses shown here were done with this cell line. **(A)** Schematic representation of the VSG overexpression construct (pRS.118) and the modified tubulin locus. **(B)** Growth curves of tetracycline-induced (black diamonds) and non-induced (white diamonds) parasites. Means (± SD) of five clones are shown. The parental BSF 13-90 cell line (circles) served as a growth control. **(C, D)** Western blot analyses of the VSG 118 and the GFP expression levels of five clones. Protein samples of non-induced (0 h) parasites or cells induced for 24 hours were analyzed. The blots were stained **(C)** with a VSG 118 antibody (green) or **(D)** with a GFP antibody (magenta). Detection of PFR proteins (magenta) served as a loading control. **(E)** Quantification of the GFP signal determined by the Western blot analyses in D. GFP values were normalized to PFR and the values after 24 hours of VSG 118 overexpression are given relative to the values of the non-induced parasites of the corresponding clone (100%).

Taken together the results support the idea that a *trans*-regulation mechanism operates to control *VSG* expression, although no evidence for the mechanism to operate at the ER was found. Quantifications of the *GFP* mRNA levels will be essential in the future to provide substantial proof for the made suggestions.

4 Discussion

4.1 The control of the activity status of the ES

During an in *situ switch* the active ES is silenced and transcription initiates at a new ES (Bernards et al., 1984; Michels et al., 1984). The order of the events during an *in situ* switch is unknown as well as the underlying molecular mechanisms (reviewed in: Borst and Ulbert, 2001; Günzl et al., 2015; Pays et al., 2004). In principal, either (i) transcription of the active ES is stalled before a new one is activated or (ii) transcription of a new ES is initiated before the active ES is silenced. Batram recently provided support for the (ii) scenario using the inducible overexpression of an ectopic VSG (Batram et al., 2014). This system simulated the activation of an incomplete ES as only a VSG was overexpressed and not the other ES-components, the *expression site associated genes* (*ESAGs*) (Hertz-Fowler et al., 2008). Thus, it was assumed that the VSG overexpression mimicked an unsuccessful *in situ* switch. Nevertheless, VSG overexpression was sufficient to induce the attenuation of the complete active ES, suggesting that the activation of a second ES would result in the silencing of the old one (Batram et al., 2014). The VSG overexpression system could provide an exceptional possibility to identify proteins involved in the initiation of ES-attenuation and/or *VSG*-silencing during *in situ* switching, albeit no potential ES-regulators could be identified so far using transcriptome analysis of VSG overexpressors (chapter 3.8).

However, the active ES needs to be recognized somehow to get attenuated, suggesting that a distinctive feature has to be present in all ESs to identify them and mediate their silencing. The general architecture of the known ESs is similar but they differ in their composition as the presence as well as number of *ESAGs* varies (Hertz-Fowler et al., 2008). We suggested that the distinctive ES-feature could be provided by the *VSG* itself as the attenuation of the ES is initiated at the telomeric end, where the *VSG* is located in all ESs (Batram et al., 2014; Hertz-Fowler et al., 2008). As the sequence of the *VSG* genes differ as well, it seems unlikely that a recognition motif is located within the ORF (Cross et al., 2014). However, two 100% conserved motifs have been identified within the 3'UTR of all *VSGs*: the 8mer and the 16mer (Berberof et al., 1995 M. Engstler, unpublished data). RNA structure predictions and mutational analyses suggested that the 16mer and the 8mer are essential to form an RNA stem loop, which is critical to stabilize the *VSG* mRNA (diploma thesis Batram, 2009, PhD thesis 2013). The formation of the stem loop seems not to be the reason for the preservation of the 8mer and the 16mer motif as substitutions within the loop region did not alter the VSG expression levels (diploma thesis Batram, 2009). We propose that the motifs could have a second role as a high selective pressure has to be present to keep a sequence motif conserved. Given the location of the *VSG* within the ES, the second role could be associated with the recognition or the silencing of the ESs.

To investigate this suggestion, a *GFP* reporter coupled either to a complete functional *VSG* 3'UTR ($GFP^{EStel}{}_{198}221^{ES}$) or to a defective *VSG* 3'UTR with an incomplete 16mer ($GFP^{EStel}{}_{\Delta}221^{ES}$) was integrated downstream of the endogenous *VSG*. Unfortunately, integration of the *GFP* with functional *VSG* 3'UTR failed, most likely as the GFP expression reaches toxic levels (PhD thesis Batram, 2013; Liu et al., 1999). Although the integration of the *GFP* with defective *VSG* 3'UTR was successful, the growth of the trypanosomes was impaired and 22-32% of the cells displayed an abnormal DNA content. This was not the cause of toxic GFP expression levels as growth was not affected when fivefold more of the protein was expressed in a cell line with a promotor-proximal *GFP* ($GFP^{ESpro}{}_{198}221^{ES}$). The parasites that expressed a telomere-proximal *GFP* reporter with a defective *VSG* 3'UTR had reduced *VSG 221* transcript levels. Immunofluorescence analyses showed that 1-8% of the parasites switched the expressed VSG even in the presence of the selection. Impaired growth and loss of VSG 221 expression was even more pronounced when another *VSG* coupled to a defective *VSG* 3'UTR was integrated in the same locus. The growth defect was not caused by the presence of a second *VSG* in the ES as expression of two *VSGs* from the same ES does not impair the viability of trypanosomes (diploma thesis Fey, 2011; Muñoz-Jordán et al., 1996). These VSG double expressors with a defective telomere-proximal 16mer expressed neither the endogenous *VSG 221* nor the transgenic *VSG 121*, but another variant as shown by an SDS-page stained with Coomassie. The expressed VSG can be either switched by a recombinational exchange of the *VSG* gene or by a transcriptional change of the actively transcribed ES (reviewed in Horn and McCulloch, 2010; reviewed in Taylor and Rudenko, 2006). If the *VSG* is replaced via gene conversion, the cells should maintain drug resistance as long as the resistance cassette is not deleted together with *VSG 221* (Kim and Cross, 2010). In contrast, trypanosomes will become sensitive to the drug during an *in situ* switch as transcription of the resistance cassette will be terminated when the active ES gets attenuated (Kim and Cross, 2010). PCR using a primer binding to the *VSG 221* ORF and a primer binding to the defective *VSG* 3'UTR demonstrated, however, that the *VSG 221* ORF and the resistance cassette were still present in the parasites with a telomere-proximal *GFP* or *VSG 121*. This suggested that the cells with a defective 16mer downstream of *VSG 221* were trying to change the actively transcribed ES but could not complete the switch in the presence of the selection.

This hypothesis was confirmed in a first experiment by measuring the VSG 221 and the GFP expression upon removal of the selection for the *VSG 221* ES. Flow cytometric analyses demonstrated that the parasites silenced the *VSG 221* ES in the absence of the drug as the majority of cells (>98%) became GFP- and VSG 221-negative. Second, the VSG double expressors with a defective *VSG* 3'UTR resumed growth in the absence of the drug demonstrating that the impaired growth was caused by a loss of resistance. Third, sequencing of the *VSG* mRNA molecules of this cell line showed that transcripts of *VSG M1.9* were present

in one clone, whereas transcripts of *VSG M1.11* were detected in another clone. Interestingly, both *VSG* genes are located in other ESs: *VSG M1.9* is located in ES 2 and *VSG M1.11* in ES 15 (Hertz-Fowler et al., 2008). Taken together, these results supported the previous suggestion that the trypanosomes with a defective 16mer downstream of the endogenous *VSG* are trying to switch the transcribed ES but can only complete the switch in the absence of the selection. The *in situ* switch could be triggered either (i) by the position of the defective 16mer in the active ES or (ii) by the presence of transcripts containing a defective 16mer.

If transcripts with a defective 16mer would be the cause for the switching, this effect should be also observed when the construct is expressed from a different genomic location. However, expression of a *GFP* with a defective *VSG* 3'UTR from the promotor region of the active ES (GFP^{ESpro}) or the tubulin locus (GFP^{tub}) did not alter growth or VSG 221 expression. Besides this, in previous studies no signs of switching were observed when the *VSG 121* ORF coupled to a defective or functional *VSG* 3'UTR was integrated upstream of *VSG 221* (diploma thesis Batram, 2009). Also, upon integration of the same constructs in a knock-out cell line of the histone methyltransferase DOT1B, which trimethylates histone H3, no indications for switching were observed in preliminary analyses (chapter 7.1 Figure 49). Consequently, the telomere-proximal position of the defective 16mer was necessary to trigger *in situ* switching, whereas the presence of mRNA molecules with a defective 16mer was not sufficient.

So far it was not excluded that the integration of the construct downstream of the endogenous *VSG* already triggered the switching. This was investigated by the integration of the *VSG 121* ORF with a functional *VSG* 3'UTR downstream of the endogenous *VSG* ($121^{EStel}{}_{198}221^{ES}$). No signs of a switch in ES transcription were observed in this cell line as growth was not impaired and the transgenic *VSG* was expressed at wild type levels. This was in accordance with previous studies, which did not report switching when the same integration site was used to target a *GFP* or a resistance cassette downstream of *VSG 221* (Horn and Cross, 1997; Janzen et al., 2004). Taken together, this excluded that the integration of the construct *per se* triggered switching and verified that the *in situ* switching was the results of the telomere-proximal position of the defective 16mer. Interestingly, integration of the transgenic *VSG 121* with a functional 3'UTR downstream of the endogenous *VSG* resulted in wild type transcript levels of the transgene (95%), whereas the endogenous *VSG* was barely expressed (5%). This differed from the ratio of VSG expression in previously described VSG double expressor cell lines, in which the endogenous VSG and the transgene were expressed at comparable levels (diploma thesis Fey, 2011; Muñoz-Jordán et al., 1996; Smith et al., 2009). The high expression levels of promotor-proximal *VSG* transgenes exclude that the decreased expression of the endogenous VSG in the present study was caused by the increased space to the telomere (Smith et al., 2009). Alternatively, the decreased VSG expression could be caused by the close proximity of the *VSG* genes (1,700 nucleotides). Glover and colleagues observed such a *cis*-

regulation effect when two reporter genes with the same UTR were integrated in immediate vicinity, albeit the expression of the telomere-proximal gene was decreased and not the more distal one as in this study (Glover et al., 2016). Nevertheless, the cause for the different expression levels of VSG 121 and VSG 221 in the VSG double expressors with functional *VSG* 3'UTRs remains unknown.

Based on the presented results, we propose that the telomere-proximal 16mer in the 3'UTR of the *VSG* serves as a distinctive feature for the active ES. It is used to determine the functionality of the ES as switching occurs once it is incomplete. The ES-integrity is assessed by the telomere-proximal 16mer as switching was dependent on its position within the ES. The 16mer motif seems to be specifically used to determine the functionality of the ES as preliminary analyses indicated that inversion of the conserved telomere-proximal 8mer did not cause switching (data not shown). But how can the integrity of the ES be assessed by the 16mer motif? The high conservation of the sequence implies that it serves as a recognition motif for a DNA-binding protein. The 16mer-binding protein could be somehow associated with the telomere of the active ES as switching occurred only once the telomere-proximal 16mer was defective. For example, it could be that the protein itself recognizes the TTAGGG repeats of the telomere and binds to them or that it is part of a telomere-binding protein complex. We assume that the interaction of the 16mer motif and a telomere associated DNA-binding protein, which is sequestered at the active ES, is essential to maintain the active state of the ES. The protein cannot longer bind to the 16mer motif once parts of it are deleted. In this case, the active ES is considered as non-functional, gets silenced and a new one has to get activated.

The shelterin complex has been identified in mammalian cells as the core telomere protein complex (reviewed in de Lange, 2005). It consists of six proteins (TRF1, TRF2, TIN2, RAP1, TPP1, and POT1), which together protect the chromosome ends from DNA damage. In trypanosomes, three homologues of the complex have been identified: TbRAP1, TbTRF, TbTIF2 (Jehi et al., 2014a; Li et al., 2005; Yang et al., 2009). The latter two suppress VSG switching as they are essential to maintain the telomere structure. Depletion of either protein via RNAi caused an increase in the switching frequency, predominantly via a recombinational exchange of the *VSG* gene (Jehi et al., 2014a, 2014b, 2016). This phenotype is, however, clearly different from the presented results as the telomere-proximal defective 16mer caused exclusively *in situ* switching. Derepression of silent ESs was observed when RAP1 was depleted in trypanosomes, which suggests that this protein is essential for the silencing of inactive ESs (Yang et al., 2009). This phenotype is also distinct from the effect of the defective 16mer as the expression of previous silent ES-resident *VSGs* increases during derepression, while the active ES is still expressed. Integration of a defective 16mer downstream of the endogenous *VSG 221* triggered *in situ* switching and low level expression of the *VSG 221* ES was maintained only when selection for this ES was applied. Besides the shelterin complex,

some other proteins are thought to associate with telomeres in trypanosomes (reviwed in Lira et al., 2007). For example, the KU70–KU80 heterodimer is involved in the regulation of telomere length and maintenance, but has no impact on VSG switching or ES-silencing (Conway et al., 2002; Janzen et al., 2004). None of the so far identified telomere-binding proteins were directly involved in maintaining the active state of the ES to our knowledge suggesting that the 16mer-binding protein has not been characterized so far.

Silent ESs are tightly packed in heterochromatin, whereas the active ES is depleted of nucleosomes (Figueiredo and Cross, 2010; Stanne and Rudenko, 2010). In the recent years, evidence has accumulated that the formation of heterochromatin at silent ESs is critical to maintain their inactive state (reviewed in Duraisingh and Horn, 2016). For example, disruption of heterochromatin formation due to the depletion of histone H3 and H1 caused derepression of silent ESs (Alsford and Horn, 2012; Pena et al., 2014; Povelones et al., 2012). Similarly, down-regulation of chromatin remodelers and modifiers like TbISWI, NLP, FACT and others (described in chapter 2.5.2) resulted in the expression of previously silent ESs (Denninger and Rudenko, 2014; Denninger et al., 2010; Hughes et al., 2007; Narayanan et al., 2011; Stanne et al., 2015). Thus, it seems likely that the active state of the ES could be maintained if the binding of an ES sequestered protein to the 16mer motif would inhibit the formation of heterochromatin. In all of these studies, the most prominent effect was observed at the promotor region of the inactive ESs, indicating that regulation occurred predominantly within this region. In contrast, the position dependent effect of the 16mer deletions suggests that the proximity to the telomere is essential for the motif to be recognized. Thus, it seems likely that the potential 16mer-protein complex would prevent the formation of heterochromatin at the telomere-proximal region of the ES. In fact, TDP1 has been suggested to counteract the formation of heterochromatin at the active ES as it facilitated transcription by replacing histones at these loci (Narayanan and Rudenko, 2013). TDP1 maintained, however, the open chromatin structure in general at PolI transcribed regions and not specifically at the telomeric regions of the active ES as it would be the case for a potential 16mer-protein complex.

It was first shown in *Drosophila* and yeast that the formation of heterochromatin at the telomere is involved in the silencing of telomere-proximal genes (Gottschling et al., 1990; Levis et al., 1985). This phenomenon of the vigorous regulation of telomere-proximal genes compared to more distant genes is termed telomere positioning effect (TPE) (reviewed in Blasco, 2007). Due to the telomere-proximal position of the *VSG*, it has been suggested that TPE could play a role for *VSG*-silencing in trypanosomes. The strongest support for TPE in trypanosomes was provided by a study of Glover and Horn, where *de novo* assembled telomeres repressed PolI transcription (Glover and Horn, 2006). It has been suggested that in yeast TPE is based on the recruitment of the silent information regulator (Sir) proteins to the telomere via RAP1 (reviewed in Blasco, 2007). Then, Sir2 can deacetylate histone H3 and H4 at the telomere,

which promotes the formation of heterochromatin. Controversially, the Sir2 homologue of trypanosomes is involved in telomeric silencing, but not *VSG*-silencing (Alsford et al., 2007). In contrast, RAP1 is essential for *VSG*-silencing as its depletion caused the derepression of silent ESs (Yang et al., 2009). Likewise, down-regulation of TbPIP5-Pase, a potential interaction partner of RAP1, resulted in the expression of silent ESs (Cestari and Stuart, 2015). In both cases, ES-derepression had the most prominent effect at telomere-proximal regions, suggesting that RAP1 and TbPIP5-Pase maintain the silent state of the ESs directed from the telomere. Consequently, it seems possible that the 16mer motif and its binding protein could be an antagonist of TPE mediated *VSG*-silencing in trypanosomes. Binding of the protein to the motif could counteract the formation of heterochromatin at the telomeric end of the ES and thus maintain its active state. The open chromatin structure would change once the interaction of the 16mer motif and the protein is interrupted and the active ES would get silenced. The survival of the individual parasite would depend on the degree of silencing as a VSG shortage causes a rapid pre-cytokinesis arrest (Sheader et al., 2005). Only those parasites would survive that have activated a previously silent ES and express a VSG at sufficient amounts. This scenario is supported by several studies demonstrating that a reduced VSG supply, for example due to VSG RNAi, the inducible block of ES transcription or the replacement of the ES promotor, gives predominantly rise to *in situ* switchers (Aitcheson et al., 2005; Aresta-Branco et al., 2015; Navarro et al., 1999).

To provide proof for the above made suggestions, it will be crucial to further validate that the 16mer motif serves as a DNA-binding motif. In a first step, the *VSG 121* ORF coupled to the *VSG* 3'UTR with 16mer substitutions should be integrated downstream of the endogenous *VSG*. The UGA46-48ACU substitution seems to be the best choice as it was previously shown that this substitution does not influence VSG expression, suggesting that the stem-loop formation is not affected (diploma thesis Batram, 2009, PhD thesis 2013). If switching would also occur in this case, it would demonstrate that the sequence of the 16mer motif is critical for the recognition and not the formation of the stem loop. Nevertheless, it will be inevitable to identify the interaction partner of the 16mer motif. Once potential 16mer-binding proteins are identified, it will be essential to determine the switching frequencies and the underlying switching mechanism upon depletion of the candidates. Moreover, analyses of the interaction of the candidates with the 16mer motif for example using electrophoretic mobility shift assay (EMSA) or chromatin immunoprecipitation (ChIP) will be necessary. The role of the ORF coupled to the *VSG* 3'UTR also deserves further considerations. If a *GFP* with a defective 16mer was integrated downstream of *VSG 221*, the parasites still expressed the endogenous *VSG*. In contrast, *VSG 221* was completely down-regulated upon integration of the *VSG 121* with a defective 16mer at the same loci. This could imply that the presence of a *VSG* ORF in front of the 3'UTR with the defective 16mer could have a greater impact. This could be

analyzed by deleting parts or the complete *VSG 121* ORF in the $121^{ESTel}{}_{\Delta}221^{ES}$ cell line. Moreover, it seems reasonable to try to rescue the 'defective 16mer phenotype' by integrating a second *VSG* 3'UTR containing a functional 16mer downstream of the defective one. Though several experiments have to be done to further investigate the role of the 16mer motif and its potential interaction partner, this thesis provides the first evidence that the 16mer motif has a dual role at the mRNA and DNA level. Besides being essential to stabilize the *VSG* mRNA, it serves as a distinctive feature of the active ES, which is critical to maintain the active state.

4.2 The control of the VSG expression

It was implied that a VSG homeostasis exists in trypanosomes as several studies showed that VSG levels are balanced around wild type levels. When a second *VSG* was integrated in the active ES, the expression levels of both added up to wild type VSG levels (100%) (diploma thesis Fey, 2011; Muñoz-Jordán et al., 1996). Down-regulation of one of the VSGs via RNAi caused an increased expression of the other VSG (Smith et al., 2009). The VSG amount was also maintained at wild type level when the endogenous *VSG* was down-regulated upon inducible overexpression of an ectopic *VSG* with its wild type UTRs (Batram et al., 2014). It was implied that the VSG controls its own expression as only high ectopic VSG expression levels were sufficient to trigger the down-regulation of the endogenous *VSG* (PhD thesis Batram, 2013). Batram suggested that this VSG homeostasis is achieved via a *trans*-regulation mechanism. Trypanosomes would have to detect and measure the VSG levels to ensure that such a mechanism would work. For this, all of the 2,000 different VSG variants would have to be recognized as VSGs. As the variants differ greatly in their sequence, it was assumed that the two conserved motifs in the *VSG* 3'UTR (the 8mer and the 16mer) could represent a distinctive feature to identify *VSG* transcripts (PhD thesis Batram, 2013; Berberof et al., 1995; Cross et al., 2014). It was proposed that the *VSG* mRNA levels are controlled by 'counting' the *VSG* 3'UTR and thus the VSG homeostasis is regulated *in trans* (PhD thesis Batram, 2013).

The inducible expression of a *GFP* reporter with *VSG* 3'UTR provided support for this hypothesis as its induction caused a transient down-regulation of the endogenous *VSG* (PhD thesis Batram, 2013). However, the results were ambiguous as high GFP levels are thought to be toxic and the GFP overexpression caused the death of the parasites (PhD thesis Batram, 2013; Liu et al., 1999). For this reason, this thesis further investigated if *VSG* levels in trypanosomes are balanced via the proposed *trans*-regulation mechanism. First, a *GFP* reporter coupled to a *VSG* 3'UTR was constitutively expressed from the tubulin locus at low non-toxic levels (GFP^{tub}_{198}). Then, a second *VSG* with its wild type 3'UTR was overexpressed in this cell line. If a *trans*-regulation mechanism exists in trypanosomes, overexpression of the ectopic VSG should not only cause the down-regulation of the endogenous VSG 221 but also of the GFP. The levels of the endogenous VSG decreased upon overexpression of the ectopic VSG just as previously reported (Batram et al., 2014; bachelor thesis Henning, 2012). A decrease in the GFP protein levels by 50-75% was also observed within 24 hours of VSG overexpression, suggesting that the expression was regulated *in trans*. To control if the down-regulation of the GFP protein was linked to the *VSG* 3'UTR, it was replaced by a *PFR* 3'UTR (GFP^{tub}_{PFR}) and the ectopic VSG was overexpressed in the generated reporter cell line. Preliminary quantifications of the GFP signal upon induction of VSG overexpression indicated that the GFP expression was differently affected within the analyzed clones and thus did not

provide unambiguous results. Nevertheless, the comparison of the GFP protein levels upon induction of VSG overexpression showed that the GFP expression was influenced to a greater extent when the gene was coupled to a *VSG* 3'UTR. Consequently, these results support our hypothesis that a *trans*-regulation mechanism of the *VSG* based on its 3'UTR is present in trypanosomes.

However, the following points need to be considered when interpreting the data: First, quantifications of the GFP signal in the cell line with the *PFR* 3'UTR could be error prone as GFP protein levels were at the detection limit. Second, the presented preliminary data of five clones of the cell line with the *PFR* 3'UTR are based on a single analysis. For these reasons, it will be crucial to conduct the experiments in replicates and to use additional methods to quantify the GFP levels. Third, the attenuation of the active ES due to the overexpression of VSG 121 caused in monomorphic trypanosomes growth retardation and subsequently a reduction of the RNA-synthesis (Batram et al., 2014). In the present study, the VSG 118 overexpression system was used as only a minor deceleration in growth was observed in previous studies, suggesting that no shut-down of the RNA synthesis occurs (bachelor thesis Henning, 2012). Nevertheless, it will need to be ensured that the down-regulation of the GFP is not the consequence of a global down-regulation of transcript levels, especially as the clones analyzed in this study did not slow growth identically.

In the study of Batram, the *VSG* was not completely silenced and the down-regulation was only transient upon overexpression of a *GFP* with *VSG* 3'UTR (PhD thesis Batram, 2013). Similarly, the cytosolic GFP expressed with the *VSG* 3'UTR did not completely decrease and the minimal expression was observed within 24 hours of VSG 118 overexpression in the present study. This could indicate that either a threshold cannot be undershot via the proposed *trans*-regulation mechanism or that the mechanism operates at a certain compartment of the cell. Batram suggested that the *VSG trans*-regulation mechanism could operate at the ER as the nascent VSG polypeptides are thought to be co-translationally translocated into this organelle (reviewed in Manna et al., 2014). This hypothesis was supported by the overexpression of a *GFP* with *VSG* 3'UTR that was coupled to an ER-import signal (LS:GFP^{tet}). The endogenous *VSG 221* mRNA decreased to 20% within two hours of induction of GFP overexpression, but within four hours the cells started to die. Thus, it remained unclear if the *VSG* was down-regulated due to (i) a stress-response of the ER (ii) the high and toxic GFP levels or (iii) a *trans*-regulation mechanism operating at the ER.

To investigate further if the VSG *trans*-regulation mechanism operates at the ER, the *GFP* with *VSG* 3'UTR was coupled to an ER import signal and constitutively expressed from the tubulin locus in the present study (LS:GFP$^{tub_{198}}$). While the majority of clones expressed almost 4-fold less of the ER localized GFP compared to the cytosolic GFP with the same UTRs, one clone expressed the GFP to a similar extent. The different GFP protein levels of the transfectants

could reflect clonal variations as it is known that expression levels can vary when a construct integrates in different regions within the tubulin gene array (http://tryps.rockefeller.edu/trypsru2_genetics). Another explanation could be that the LS:GFP was secreted to the medium with different efficiencies as other studies showed that ER-imported proteins without retention signal can get exocytosed (Bangs et al., 1996). Consequently, it remains elusive why different intensities of the LS:GFP were observed between the clones and why the signal is decreased in the majority of the clones. Therefore, VSG 118 was overexpressed in one clone displaying a weak LS:GFP signal and in the one with the strong signal. If the *VSG* levels are controlled by 'counting' the *VSG* 3'UTR at the ER, the ER targeted GFP should decrease compared to the cytosolic GFP either faster or to a greater extent or both upon induction of VSG overexpression. However, at the protein level no clear differences were observed during VSG 118 overexpression in all cell lines. The strong LS:GFP signal was comparably down-regulated to the cytoplasmic GFP (LS:GFP 22%; GFP 26%) and the weak GFP signal remained at approximately 50% of the non-induced levels. This suggests that the potential VSG *trans*-regulation mechanism does not operate at the ER. Unfortunately, the GFP was barely visible at the microscope and could not be detected using Western blot analyses when the *GFP* with *PFR* 3'UTR was targeted to the ER. Thus, we could not control if the regulation of the ER targeted GFP upon VSG overexpression was also specific for the *VSG* 3'UTR.

In summary, the results support the hypothesis that the *VSG* levels could be balanced using a *trans*-regulation mechanism. A similar mechanism was proposed by Glover and colleagues, who integrated two reporter genes with the same UTR in immediate vicinity and observed a repression of the telomere-proximal gene (Glover et al., 2016). However, this observation is clearly distinct from our findings for three reasons: (i) the reporter genes were not coupled to a *VSG* 3'UTR but to an *aldolase* 3'UTR; (ii) the regulation occurred when the reporters were integrated in close vicinity on the same chromosome, suggesting a *cis*-regulation; (iii) down-regulation of the telomere-proximal reporter was complete. In contrast, in the present study regulation occurred between different genomic loci dependent on the *VSG* 3'UTR. Therefore, we propose that *VSG* levels are detected and measured by 'counting' *VSG* mRNA molecules using the *VSG* 3'UTR. However, that such a mechanism operates at the ER could not be further validated as independent of the place of translation the GFP expressed with *VSG* 3'UTR was down-regulated in a similar manner. Thus, the counting mechanism seems to be based rather on a cytosolic RNA-binding protein than an ER-membrane bound one as previously speculated.

How could a cytosolic RNA-binding protein 'count' *VSG* transcripts and thereby balance the VSG expression? RNA-binding proteins have various functions in trypanosomes for example in mRNA decay, stability or translation initiation and thus can enhance translation (reviewed in

Clayton, 2013). Consequently, when two *VSGs* are transcribed, the transcripts bound to the protein could be translated more often. Thereby, the VSG homeostasis would shift towards the expression of the protein bound transcripts and the VSG would control its own expression. However, a limited amount of the RNA-binding protein would have to be present in the cell to ensure that a basis VSG level and not an excess of VSG is produced. An RNA-binding protein could for example increase the translation when its binding enhances the stability of the mRNA molecule directly or prevents the binding of proteins promoting degradation (Archer et al., 2009; Droll et al., 2013). Alternatively, association of the protein and the transcript could be essential for translation or promote its initiation as indicated for Alba3 in trypanosomes (Mani et al., 2011). In all cases, transcripts bound to the limited protein would be translated more often than the unbound ones and thus the VSG levels would be balanced. Nevertheless, an additional layer of control would have to be present to ensure that during an *in situ* switch one *VSG* is completely down-regulated once a second ES is activated.

The results so far suggest that indeed an RNA-binding protein increases the stability of the *VSG* mRNA molecules. First, ectopic VSG overexpression caused the down-regulation of the endogenous VSG at the mRNA and protein level. Second, the transcripts of the endogenous *VSG 221* were transiently down-regulated upon overexpression of a *GFP* with *VSG* 3'UTR (PhD thesis Batram, 2013). Further evidence could be provided by measuring the *GFP* transcript levels upon induction of VSG 118 overexpression in the cell lines generated as part of this study. For this purpose, the best method would be the highly sensitive Affymetrix system as already single mRNA molecules within single cells can be detected. A potential recognition motif for an RNA-binding protein is the 8mer/16mer RNA stem-loop, as mutations causing a deletion or destruction of the hairpin caused a 10-fold decrease in VSG expression (diploma thesis Batram, 2009, PhD thesis 2013; Berberof et al., 1995). In contrast, substitutions within the 16mer, which retain the loop formation, did not affect the VSG expression levels. This suggests that not the primary sequence of the 8mer or 16mer is recognized by an RNA-binding protein, but the mRNA stem-loop (reviewed in Marzluff et al., 2008). We speculate that in trypanosomes a protein recognizes the RNA-stem loop in the *VSG* 3'UTR. Its binding to the cytosolic *VSG* transcripts increases their stability and thus balances VSG expression at a basis level *in trans* (as discussed above). However, to prove the made suggestions it will be inevitable to identify the RNA-binding protein. One promising approach could be the MS2-BioTRAP method, where the mRNA of interest is tagged with a MS2 stem-loop and a tagged bacteriophage MS2 protein is co-expressed in the cell (Tsai et al., 2011). The tagged MS2 protein will tightly associate with the MS2 stem-loop and thus allow the affinity purification of the RNA-protein complexes.

4.3 The dynamic regulation of the ES during *in situ* switching

The attenuation of the active ES due to the overexpression of an ectopic VSG caused a prolongation of the G1-phase of the cell cycle and thus growth retardation in monomorphic trypanosomes (PhD thesis Batram, 2013; Batram et al., 2014). The VSG overexpressors with an attenuated ES had an enhanced developmental competence towards triggers for PCF development. However, this state was reversible as the VSG overexpressors resumed growth when the old ES was reactivated. For this reason, it was considered that the VSG overexpressors reflect an intermediate stumpy-like stage, which can either develop to the PCF in the presence of the appropriate triggers or reenter the cell cycle as slender (sl) parasites. However, the experiments were conducted with monomorphic trypanosomes, which have lost the capacity to complete the parasite cycle as they cannot differentiate anymore to the stumpy (st) stage (reviewed in Fenn and Matthews, 2007). Therefore, it remained unexplored how and to what extent ES-attenuation and st development are linked. For example, another explanation for the obtained results could be that ES-attenuation is an alternative trigger for st development, which could not be completed as the used strain was developmentally deficient. These possibilities were further investigated in this thesis using the VSG overexpression system in a pleomorphic trypanosome strain that reacts to the stumpy induction factor (SIF) with st differentiation and can complete the parasite cycle.

Pleomorphic trypanosomes displayed a surprising phenotypic plasticity upon induction of VSG overexpression as two distinct phenotypes were observed. In some clones, the parasites doubled only one time before growth was stalled (growth-arrested), while in others VSG overexpression only minimally affected the doubling time (proliferating). This was clearly different from the monomorphic cells, where VSG 121 overexpression exclusively caused growth retardation. Moreover, the phenotypes were not VSG specific as overexpression of another variant also caused the distinct growth responses: growth-arrested and proliferating. At first sight, the growth-arrested clones were reminiscent to the monomorphic VSG 121 overexpressors. In both cases, the active ES was attenuated, which caused an accumulation of cells in the G1-phase of the cell cycle and thus growth retardation. However, the majority of pleomorphic VSG overexpressors were in contrast to the monomorphic cells irreversibly arrested as only one in 10,000 growth-arrested parasites could escape the growth retardation. The different phenotypes of the pleomorphic VSG overexpressors were not caused by a deficient overexpression system or by different kinetics in the VSG coat exchange. In both cases, the ectopic *VSG* was highly expressed within eight hours of induction and the endogenous *VSG* was down-regulated. Instead, differences in the attenuation of the active ES were responsible for the distinct growth phenotypes of pleomorphic VSG 121 overexpressors. In growth-arrested clones, a fast attenuation of the complete active ES occurred as the ES-activity decreased to 20% within 24 hours. In contrast, in proliferating clones the ES-activity

remained above 50% within 48 hours of VSG 121 overexpression. Thus, the irreversible arrest in the G1-phase of the cell cycle was triggered once the ES-activity fell below a critical threshold, whereas the down-regulation of the endogenous *VSG* was not sufficient. We conclude that one or more ESAGs are essential to support growth and that the parasites arrest in the cell cycle when an ESAG shortage occurs.

These results also showed that the down-regulation of the endogenous *VSG* was independent of the transcriptional status of the ES. In proliferating VSG 121 overexpressors, the ectopic VSG dominated the surface for many generations, while the endogenous one was silenced and the ES remained active. Thus, the VSG of the surface coat does not have to originate from the active ES and the ES-resident *VSG* can be silenced without complete ES shut-down. This suggests that distinct mechanisms are responsible for *VSG*- and ES-silencing and that these mechanisms can be uncoupled. This questions the role of the expression site body (ESB), an extranucleolar accumulation of PolI at the active ES. It has been suggested that the ESB is essential for the monoallelic transcription of the active ES as it excludes the silent ESs (Landeira and Navarro, 2007; Navarro and Gull, 2001). However, the results in this thesis showed that a *VSG* can be transcribed in a sufficient amount outside of the ESB. The situation in the presented experiments was not a natural one, but we suggest that it corresponds to a newly activated ES during an *in situ* switch. This leads to the question whether the ESB would release the old ES during an *in situ* switch when the endogenous *VSG* gene is silenced. The presented results indicate that this does not have to occur as in the proliferating clones the endogenous *VSG* was down-regulated, while the active A1.1 ES remained open. This implies that the ESB did not release the A1.1 ES and thus suggests that the ESB rather marks the active ES as physical unit than controlling monoallelic expression of the *VSG*.

In a genetic screen for defects in monoallelic expression, recently the factor VSG exclusion 1 (VEX1) was identified as a regulator of ES transcription (Glover et al., 2016). This factor accumulates at the active ES in the vicinity of the ESB and is duplicated during the cell cycle. Interestingly, in a small proportion of the cells also two VEX-1 foci were detected during the G1-phase of the cell cycle. A simultaneous expression of both VSGs was observed in some clones when Glover and colleagues assembled a telomere-mediated chromosome-fragmentation construct containing another *VSG* gene within the genome of trypanosomes. In these cases, an increase in the number of cells displaying two VEX-1 foci was observed, while only one ESB was present. These findings are in accordance with our conclusion that two ESs can be active at the same time, whereby one provides the ESAGs and the other the VSG. This questions the commonly accepted hypothesis that only one ES is active at any given time as this was based on the detection of a single VSG variant on the surface of the parasites.

The results demonstrate further that during an *in situ* switch the ES transcript levels would determine whether the cells keep proliferating or arrest in the cell cycle. However, it remained

unclear what determines the level to which the ES-activity is down-regulated upon VSG overexpression. Our data suggest that the reactivity of the ES is heritable as the different phenotypes upon VSG overexpression were reproducible for more than one week, reflecting 20 parasite generations. Thus, the different phenotypes could mirror an initial phenotypic plasticity in the capability to down-regulate the ES-activity, which could to our knowledge only be explained by epigenetic modifications. Chromatin modifying enzymes were shown to play an important role during switching and monoallelic expression (reviewed in Duraisingh and Horn, 2016; reviewed in Figueiredo et al., 2009). It was previously shown in monomorphic VSG overexpressors, that in the absence of the histone methyltransferase DOT1B, which trimethylates histone H3, VSG overexpression-induced ES-attenuation is prevented (Batram et al., 2014). In this thesis, no differences in the trimethylation levels between proliferating and growth-arrested clones could be detected using Western blot analyses (chapter 7.1 Figure 50). This suggests that the proliferating clones are no natural DOT1B knock-out cells and that the methyltransferase is still functional. Nevertheless, as the trimethylation of all histone H3s is detected in the Western blot analyses, it remains possible that differences in the trimethylation levels of the ESs are responsible for the different ES-activities upon VSG overexpression. Alternatively, the ES could be differently affected in the clones due to the leaky VSG 121 expression in the non-induced cells. Though the latter case seems unlikely as the clones had similar leaky VSG 121 expression levels, it can formally not be excluded.

That an initial phenotypic plasticity in the ES-reactivity could cause the different phenotypes upon VSG overexpression is supported by the high adaptive potential of the ES-activity. Limiting dilutions demonstrated that one in 10,000 trypanosomes escaped ES-attenuation induced cell cycle arrest. In contrast to the majority of the growth-arrested VSG 121 overexpressors, these parasites could reenter the cell cycle and thus caused the outgrowth of the culture. Growth analyzes suggested that these escapers also displayed an initial phase of growth retardation, which could be the result of a prolongation of the G1-phase of the cell cycle caused by reduced ESAG levels. We assume that the ES-activity of these cells with a prolongated G1-phase can either drift towards ES-attenuation and growth arrest or can be rescinded to growth supporting levels allowing the reentry into the cell cycle. However, the cells did not respond to VSG 121 overexpression with growth arrest anymore once they have escaped ES-attenuation as demonstrated by the re-induction experiments. This suggested that the escapers could not down-regulate the ES-activity any longer to levels causing a prolongation of the G1-phase and thus the ES-reactivity was changed. Such changes could be caused by alterations in epigenetic modifications as they can determine the transcriptional status of DNA sections. Upon removal of tetracycline, the surface of the escapers was dominated by the endogenous VSG within one week. However, the ectopic VSG dominated the surface again upon the re-addition of tetracycline for 24 hours, supporting the hypothesis

that the presence of the second VSG interferes with the expression of the endogenous one (discussed in chapter 4.2). In accordance with this, the endogenous *VSG* remained silenced in the escapers in the constant presence of tetracycline, whereas the ES had to be rescinded to growth supporting levels. Thus, the ES-activity could be dynamically regulated while the *VSG*-silencing was efficiently maintained. This further supports the hypothesis that the two processes of ES-and *VSG*-silencing are mechanistically distinct.

In summary, the presented results show that ES-attenuation can be uncoupled from *VSG*-silencing and indicate that both process are most likely mechanistically distinct. While *VSG*-silencing seems to adopt the principle of 'all or nothing', the regulation of the ES is highly dynamic. This implies a surprising capability to regulate the transcription of the active ES, when a new one is turned on during an *in situ* switch. We propose that the ES-activity can have three states during an *in situ* switch (Figure 44): (1) a mildly down-regulated ES-activity supporting growth; (2) ES-attenuation causing growth arrest; (3) an intermediate state of ES-activity provoking a prolongation of the G1-phase, which drifts towards either ES-attenuation or reactivation.

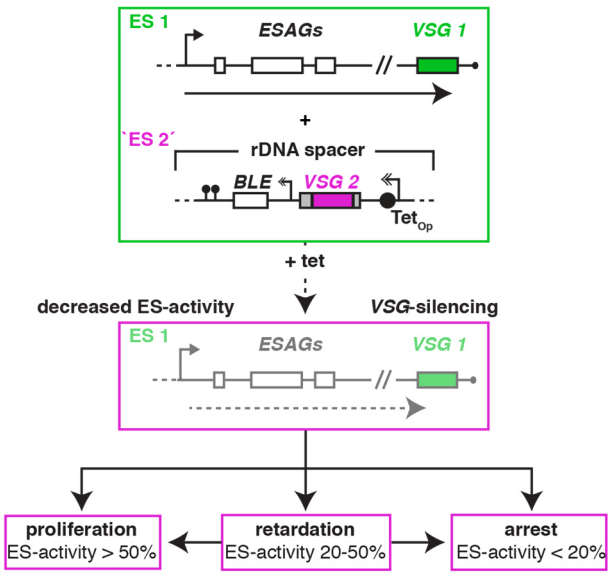

Figure 44: Model of the dynamic regulation of the active ES. Non-induced cells transfected with a construct for VSG overexpression express the complete ES 1 (upper panel). Upon addition of tetracycline, the ectopic VSG 2 (magenta) is expressed, which corresponds to the activation of an incomplete ES ('ES 2'). This causes the silencing of the endogenous *VSG 1* and a decrease of the activity of ES 1 (middle panel). The transcriptional status of the ES can adapt three states (lower panel). If the ES-activity is above 50%, ESAGs are present at growth supporting quantities. When the ES-activity falls below 20%, the cells terminally arrest in the G1-phase of the cell cycle. If the ES-activity is between 20-50%, the G1-phase of the cell cycle is prolongated and retardation in growth occurs. This state can either drift towards ES shut-down or be rescinded to growth supporting levels.

This highly dynamic way of ES-regulation during an *in situ* switch would provide a high flexibility for the parasites. We can only speculate about the biological advantages of this state, but it could be beneficial in several situations for the parasite. Trypanosomes can be found in a wide range of hosts as the tsetse fly vector feeds on various species and transmits the parasites

among them. When metacyclic trypanosomes are transmitted to the host, they express a metacyclic *VSG* (*mVSG*) from a metacyclic ESs (mES) without any *ESAGs* (Pedram and Donelson, 1999). Subsequently, the expression is switched to an ES containing *ESAGs*, when the metacyclic parasites differentiate to the BSF stage in the mammalian host. ESAGs derived from different ESs support growth in different host species, suggesting that the activation of a certain ES is advantageous for the survival within a certain species (Bitter et al., 1998; reviewed in Pays, 2006; reviewed in Pays et al., 2001; Van Luenen et al., 2005). Trypanosomes are not only heterogeneously distributed in the circulatory system of their host but also invade different organs, tissue spaces and fat (Capewell et al., 2016; Losos and Ikede, 1972; Trindade et al., 2016; Turner et al., 1986). Knowing that different ESAGs are beneficial for the survival in certain hosts, it is possible that they could also provide advantages for the survival in different tissues. Thus, the uncoupling of *VSG* and ES transcription could allow the parasites to probe for the most advantageous ES once they are transmitted and during every *in situ* switch. Besides this, the flexibility of the ES-activity could be a considerable advantage in late infections, where the amount of cells expressing so called mosaic *VSGs* increases, which are assembled from at least two different *VSGs* or *VSG* pseudogenes (Marcello and Barry, 2007). Up till now, it is not proven if mosaic *VSG* genes are formed within active or silent ESs and how they are controlled for functionality (Marcello and Barry, 2007). However, the transient expression of two ESs could allow the parasites to check for VSG functionality.

The aforementioned scenarios have considered the advantages of the dynamic ES regulation during an *in situ* switch in general including successful switching events. During an unsuccessful *in situ* switch (newly activated ES is non-functional), the dynamic ES regulation could also allow the parasites to stall ES-attenuation before the transcriptional status falls below the critical threshold to induce cell cycle arrest. Thus, the old ES would remain active, the parasites could keep proliferating and their survival would be ensured. Nevertheless, even if the ES-activity falls below the critical threshold, the ES-induced irreversible cell cycle arrest is in fact not a dead end for the trypanosomes.

4.4 The function of the transcriptional status of the active ES during stumpy development

So far, the dynamics of ES regulation during *in situ* switching and its advantages for the parasites were discussed. However, once the ES-activity fell below a certain threshold an ESAG shortage occurred and the parasites irreversibly arrested in the G1/0-phase of the cell cycle. At a first glance, this is a dead end for the trypanosomes but the experiments in this thesis unambiguously demonstrate that terminally growth-arrested VSG overexpressors are *bona fide* stumpy (st) parasites.

Upon VSG overexpression-induced ES-attenuation, the flagellum of the pleomorphic cells shortened and the parasites adapted a stout appearance just like density-induced st cells (reviewed in MacGregor et al., 2012; reviewed in Rico et al., 2013). They arrested in the G1-phase and expressed the GFP:PAD1$_{UTR}$ reporter, which is exclusively transcribed upon developmental transition from the sl to st stage (Dean et al., 2009; MacGregor and Matthews, 2012; Shapiro et al., 1984). Besides this, the mitochondrion was pre-activated like in density-induced st parasites: the organelle elaborated and the expression of the mitochondrial protein LipDH increased (Brown et al., 1973; reviewed in Rico et al., 2013; Tyler et al., 1997). Thus, in every single analyzed aspect of st development, the growth-arrested VSG overexpressors were indistinguishable from density-induced st parasites. For this reason, the growth-arrested pleomorphic VSG overexpressors were termed ES-induced st cells. It was further demonstrated that ES-induced st parasites differentiate to the PCF *in vitro* with identical kinetics as density-induced ones (Brun, 1981; Ziegelbauer et al., 1990). Moreover, infection of tsetse flies with ES-induced st parasites verified that these cells can passage through the tsetse fly and are able to complete the parasite cycle. Consequently, ES-attenuation does not cause the differentiation of a st-like stage with enhanced developmental competence as the results of monomorphic VSG overexpressors indicated (PhD thesis Batram, 2013; Batram et al., 2014). Instead, this thesis ascertained that ES-attenuation causes the development of *bona fide* st cells, which can complete the parasite cycle.

The only trigger known to induce st development in nature was so far the elusive stumpy induction factor (SIF). This factor is secreted by the trypanosomes and accumulates with rising parasitemia (Reuner et al., 1997; Vassella et al., 1997). A signaling cascade is initiated once a threshold in its concentration is reached, which triggers the development of st cells. Thus, st development is initiated in a cell density dependent manner using a quorum sensing like mechanism (Reuner et al., 1997). During st differentiation an increase in the intracellular cAMP level can be detected and developmental transition can be induced *in vitro* by the addition of hydrolysable and membrane-permeable cAMP analogues (Vassella et al., 1997). Therefore, it

was generally accepted that cAMP is the second messenger in the SIF signaling cascade until evidence arose that its hydrolysis products AMP or adenosine transmit the signal instead (Laxman et al., 2006). Besides the chemical nature of SIF and its imminent second messenger, also the pathway *per se* is still not completely understood (reviewed in Mony and Matthews, 2015). However, the presented results demonstrate now that a SIF-independent way exists to induce the development of fly transmissible st parasites. ES-attenuation caused the development of *bona fide* st parasites within 24 hours of induction independent of the cell density and hence critical SIF concentration.

As ES-attenuation could induce st development independent of SIF, we asked if and how the triggers could interact. When the parasites were simultaneously exposed to 0.25x SIF or 200µM pCPT-cAMP and ES-attenuation, a nearly twofold increase in the number of st cells occurred compared to the sum of the triggers alone. Thus, the effect of SIF and ES-attenuation was not simply additive, but cooperative. The most likely explanation for the cooperative effect would be that the pathways intersect at some point in the signal transduction cascade and thus st development was triggered in one cell by SIF and ES-attenuation. In this case, ES-attenuation has to trigger st development downstream of the quorum sensing factor as the SIF signal is extracellular (Reuner et al., 1997; Vassella et al., 1997). If the conclusion that ES-attenuation acts downstream of SIF along the same signaling pathway is correct, a mild down-regulation of the ES-activity should prime the cells for the signals of the SIF pathway. This was tested by the treatment of proliferating VSG 121 overexpressors, which have a reduced ES-activity that does not affect growth, with triggers for st development. The proliferating VSG 121 overexpressors with a reduced ES-activity responded faster towards the trigger for st development than the non-induced cells. Thus, a reduction in ES transcription, that was not sufficient to cause st development alone, primed the trypanosomes for the SIF signal. This substantially reinforced our conclusion that SIF and ES-attenuation feed into the same pathway.

Interestingly, it is known that during SIF-induced st development the active ES is silenced (Amiguet-Vercher et al., 2004). This was assumed to be part of the general transcriptional down-regulation during st development, which is thought to occur as an adaption to the cell cycle arrest (Amiguet-Vercher et al., 2004; reviewed in Pays, 2005). However, the presented results show that both, ES-attenuation and SIF, are triggers for st development and that they can act in a cooperative manner. While ES-attenuation alone is sufficient to trigger st development, a decrease of the ES-activity primes trypanosomes for the SIF signal. This suggests that the transcriptional status of the ES could be part of the SIF pathway and that st development is in general triggered once an ESAG shortage occurs. This hypothesis is supported by the identification of TbISWI, a chromatin remodeler with a function in ES regulation, in a screen for components of the SIF pathway (Hughes et al., 2007; Mony et al.,

2013). We propose a model, which integrates the transcriptional status of the active ES for st differentiation (Figure 45). We assume that developmental transition is triggered once ES-activity falls below the critical threshold, which can be induced during an *in situ* switch, SIF or the interaction of both triggers.

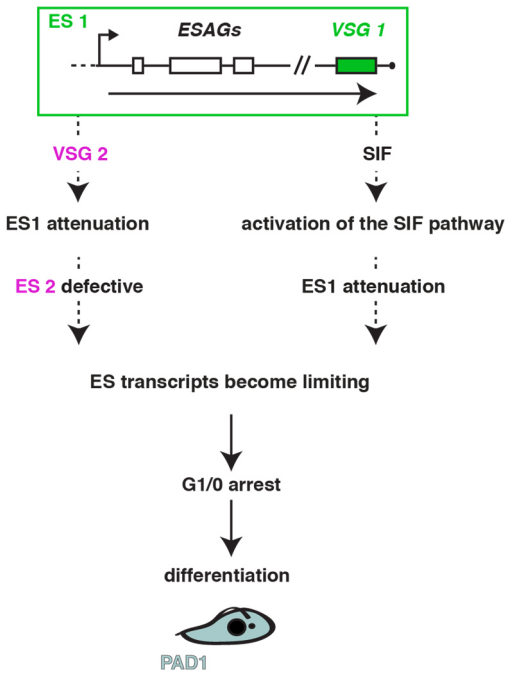

Figure 45: Model of the cooperative effect of SIF and ES-attenuation for stumpy development. The transcriptional status of the active ES decreases either during an *in situ* switch or due to the activation of the SIF pathway. If a new VSG (VSG 2) is expressed, the attenuation of the old ES (ES 1) is triggered. Thus, the ES transcripts decrease and become limiting if the new ES is defective. This causes the arrest of the parasites in the G1/0-phase of the cell cycle and, subsequently, the differentiation to the st stage. The active ES (ES 1) is also silenced during SIF-induced st development. We assume that the resulting ESAG shortage is part of the SIF signaling cascade, which triggers st differentiation. Consequently, ES-attenuation during an *in situ* switch and SIF would act in a cooperative manner.

The comparison of SIF-treated non-induced cells of potentially 'growth-arrested' and potentially 'proliferating' VSG 121 overexpressors supported the previous notion that the different growth phenotypes could be caused by an initial phenotypic plasticity. While the majority of non-induced cells of a potentially 'growth-arrested' clone responded to SIF with st development within 28 hours of treatment, less than 10% of the non-induced cells of a potentially 'proliferating' clone developed to the st stage when treated in a similar way. This could reflect either a different capability to attenuate the ES or an initial difference in the ES-activity between the clones as st development is triggered once the ES-activity falls below a critical threshold. To investigate these hypotheses, the transcriptional status of the ES has to be compared in non-induced cells and during the course of SIF treatment. However, to provide proof for the assumed initial phenotypic plasticity, it will be necessary to conduct limiting dilutions with the parental cell line, then analyze the responsiveness of the resulting clones towards SIF and determine their ES-activity.

ES-attenuation induces the development of *bona fide* st parasites, but how relevant would this mechanism be during an infection with trypanosomes? St development will be induced once the ESAGs level drop below a certain level. This could happen when ES transcription is

switched to a new but non-functional ES during an *in situ* switch. The ES would be non-functional if one or more *ESAGs* are missing or if they are defective. ESs are large transcriptional units, which are subjected to frequent recombination events e.g. the recombinational change of the *VSG* via gene conversion or telomere exchange (reviewed in McCulloch et al., 2015). This suggests that the telomeric ESs are prone to mutation, which could affect their functionality and would contribute to 'unsuccessful switching' events. According to the host range hypothesis, it is also possible that an ES is non-functional if the ESAGs are not suitable for the survival within the respective host (Bitter et al., 1998; Van Luenen et al., 2005).

In the monomorphic strain Lister 427 only 15 ESs are present, which would limit the capacity of the parasites to conduct *in situ* switches (Hertz-Fowler et al., 2008). However, the number of ESs was determined so far only in this strain and is thought to vary between different subspecies as well as strains (Hertz-Fowler et al., 2008). Thus, the capacity to conduct *in situ* switching could be elevated in the natural situation. In addition, an *in situ* switch most likely does not only happen between ESs but also between an ES and a metacyclic ES (mES). This was indicated by studies demonstrating that depletion of certain proteins or sequences caused derepression of BSF and metacyclic *VSGs* (Glover et al., 2016; Hovel-Miner et al., 2016; Pena et al., 2014; Schulz et al., 2015). MESs are monocistronic transcription units that do not contain any functional *ESAGs* but only a metacyclic *VSG* (Pedram and Donelson, 1999). Consequently, the switch to a mES would be unsuccessful in any case as an ESAG shortage could not be functionally completed. Thus, switching to mESs would as well contribute to the rate of unsuccessful switching events. As it is suggested that at least five mESs are present in the genome of trypanosomes, unsuccessful *in situ* switching could occur between approximately 20 ESs (Cross et al., 2014; Turner et al., 1988).

But how often would such an unsuccessful *in situ* switch happen? In general, pleomorphic trypanosomes have a higher switching frequency (10^{-2}-10^{-3} switches per cell per generation) than the monomorphic cells (10^{-4}-10^{-6} switches per cell per generation) (Aitcheson et al., 2005; Turner and Barry, 1989). Thus, it seems likely that the overall switching frequency, including successful and unsuccessful switching, is higher during non-artificial infections. However, to which extent each switching mechanism (*in situ* switchers, gene conversion and telomere exchange) contributes to the switching frequency is controversial as the proportion of *in situ* switching ranged from 2% to 77% between different studies (Aitcheson et al., 2005; Devlin et al., 2016; Kim and Cross, 2010, 2011). As only the rate of the successful switching events can be detected, the rate of all *in situ* switching events would always be underestimated. Anyway, ES-induced st formation would generate a constant background rate of st differentiation, which is independent of the cell density and SIF, as VSG switching occurs stochastically.

In fact, such a SIF independent rate for st development has been previously proposed by Savil and Seed. They showed that a density-dependent model for st development, like it would be the case for the SIF-induced st formation, can explain several aspects of the experimental data sets (Savill and Seed, 2004). However, st parasites are also present within the population, when the SIF concentration is below its critical threshold (MacGregor et al., 2011; Savill and Seed, 2004; Trindade et al., 2016). As this cannot be explained by a density-dependent model alone, a stochastic background rate of st development was proposed. This is in accordance with the presented results as st development was observed in 1-5% of the population although the parasites were cultivated at low densities. Given that VSG switching occurs stochastically and ES-attenuation is sufficient to induce st development, we presume that ES-induced st development during unsuccessful *in situ* switching represents the proposed background rate.

Such a SIF independent stochastic background rate of st formation could explain how transmissibility is ensured at low parasitemia. During trypanosome infections of natural hosts, like goat or cattle, only a few parasites can be detected in the blood (Goodwin, 1970). In these cases, the parasite secreted SIF should accumulate to effective concentrations only in tissue spaces. A stochastic background rate of st development would guarantee developmental transition also outside of tissue spaces at low parasitemia. Interestingly, it was recently shown that sl parasites can re-invade the skin of their host and built a reservoir in this region while parasitemia diminishes in the blood (Capewell et al., 2016). St parasites were observed in variable proportions in this 'skin reservoir', which can be rather explained by a stochastic background rate of st development than by SIF as a local accumulation of the quorum sensing factor should cause st development in all parasites within the region. A constant background rate would guarantee st development also at early time points of mammalian infections and thus ensure re-transmissibility early on.

We conclude that the activity status of the ES is the interface of antigenic variation and development, which links two key aspects for the persistence of trypanosomes: immune evasion and transmissibility.

5 Materials and Methods

5.1 Materials

5.1.1 Antibodies, fluorescent probes and dies

Table 3: Primary antibodies used for Western blot or protein dot blot analyses. Indicated are the names of the used antibodies, the host species of the antibodies (organism), the used dilutions and references for the antibodies (origin).

Antibody	Organism	Dilution	Origin
anti-GFP	Mouse	1:1,000-1:500	Roche, Rotkreuz (CH), Cat. No. 11814460001
anti-H3	Rabbit	1:10,000	(Gassen et al., 2012)
anti-H3	Guinea pig	1:5,000	(Dindar et al., 2014)
anti-H3K76me3	Rabbit	1:2,000	(Janzen et al., 2006)
anti-LipDH	Rabbit	1:10,000	(Roldan et al., 2011)
anti-PFR (L13D6)	Mouse	1:300-1:20	(Kohl et al., 1999)
anti-VSG AnTat1.1 (A1.1)	Rat	1: 20,000	(Engstler and Boshart, 2004)
anti-VSG 121	Rabbit	1:1,000	(Batram et al., 2014)
anti-VSG 221 first bleed	Rabbit	1:5,000	N. Jones, Würzburg (DE)

Table 4: Secondary antibodies used for Western blot or protein dot blot analyses. Indicated are the names of the used antibodies, the fluorophore they are conjugated with (IRDye800CW or 680LT), the host species of the antibodies (organism), the used dilutions and references for the antibodies (origin).

Antibody	Organism	Dilution	Origin
anti-guinea pig IgG IRDye800CW	Goat	1: 10,000	LI-COR Bioscience, Lincoln (USA), Cat. No. 926-32411
anti-mouse IgG IRDye680LT	Goat	1: 10,000	LI-COR Bioscience, Lincoln (USA), Cat. No. 926-68020
anti-rabbit IgG IRDye680LT	Goat	1: 10,000	LI-COR Bioscience, Lincoln (USA), Cat. No. 926-68023
anti-rabbit IgG IRDye800CW	Goat	1: 10,000	LI-COR Bioscience, Lincoln (USA), Cat. No. 926-32211
anti-rat IgG IRDye800CW	Goat	1: 10,000	LI-COR Bioscience, Lincoln (USA), Cat. No. 926-32219

Table 5: Primary antibodies used for immunofluorescence analyses. Indicated are the names of the used antibodies, the host species of the antibodies (organism), the used dilutions and references for the antibodies (origin).

Antibody	Organism	Dilution	Origin
anti-EP TRBP1/247	Mouse	1: 500	Cedarlane Laboratories, Burlington (CAN)
anti-PAD1	Rabbit	1:100	(Dean et al., 2009)
anti-PFR (L8C4)	Mouse	1:20	(Kohl et al., 1999)
anti-VSG 121*	Rabbit	1:500	N. Jones, Würzburg (DE)
anti-VSG 118	Rabbit	1:500	M. Carrington, Cambridge (GB)
anti-VSG 221	Rabbit	1: 1,000	N. Jones, Würzburg (DE)
anti-VSG 221	Rabbit	1: 500	(Figueiredo et al., 2008)
anti-VSG AnTat1.1 (A1.1)	Rat	1: 4,000	(Engstler and Boshart, 2004)

***** The antibody cross-reacted with VSG A1.1 in immunofluorescence analyses. Thus, the antibody was depleted on fixed AnTat1.1 13-90 parasites. After controlling that the depleted antibody did not recognize VSG A1.1 anymore, it was used for the shown immunostainings with the indicated dilution.

Table 6: Secondary antibodies used for immunofluorescence analyses. Indicated are the names of the used antibodies, the fluorophore they are conjugated with, the host species of the antibodies (organism), the used dilutions and references for the antibodies (origin).

Antibody	Organism	Dilution	Origin
anti-mouse IgG Alexa594	Goat	1:500	Thermo Fisher Scientific, Waltham (USA), Cat. No. A11005
anti-mouse IgG Alexa647	Goat	1:500	Thermo Fisher Scientific, Waltham (USA), Cat. No. A21235
anti-rat IgG Alexa488	Goat	1:500	Thermo Fisher Scientific, Waltham (USA), Cat. No. A11006
anti-rabbit IgG Alexa594	Goat	1:500	Thermo Fisher Scientific, Waltham (USA), Cat. No. A11012
anti-rabbit IgG Alexa647	Goat	1:500	Thermo Fisher Scientific, Waltham (USA) Cat. No. 111-605-003

Table 7: Probes to visualize RNA molecules bound to a nitrocellulose membrane. Indicated are the names of the used RNA probes and thus what kind of mRNA they recognize. Also, the fluorophore conjugated with the probe (DY-682 or DY-782) and the sequences of the probes are given. All probes had a stock concentration of 100 µM and were obtained from MWG-Biotech, Ebersberg (DE).

Name	Fluorophore	Sequence (5'-3')
18s rRNA	DY-682	CAACCAAACAAATCACTCCACCGACCAAAA
Tubulin	DY-782	ATCAAAGTACACATTGATGCGCTCCAGCTGCAGGTC
VSG 118	DY-682	TCTTTCTCTCCTGTTGCTTGGTTTTTCTGT
VSG 121	DY-682	GGCTGCGGTTACGTAGGTGTCGATGTCGAGATTAAG
VSG 221	DY-682	CAGCGTAAACAACGCACCCTTCGGTTGGTCGTCTAG
VSG AnTat1.1 (A1.1)	DY-682	GTCTTTCTCTTCTTTCCCTTTGCACTTTTC

Table 8: Probes to visualize single mRNA molecules within individual cells (Affymetrix). Indicated are the names of the used RNA probes and thus what mRNA they recognize. Also, the fluorophore conjugated with the probe (red = type 1) and the sequences of the probes are given. All probes were obtained from Affymetrix, Santa Clara (USA).

Name	Fluorophore	Sequence
ESAG6	red = type 1	antisense to nucleotides 107-1206 Tb427.BES40.3
GFP	red = type 1	full antisense ORF

Table 9: Fluorescent dyes used in this work. Indicated are the names of the used fluorescent dyes and the supplier they were obtained from (origin). Also, the used concentrations and what the dyes stain (target) are given.

Fluorescent dyes	Origin	Concentration	Target
MitoTracker Red CMXRos	Thermo Fisher Scientific, Waltham (USA)	50 nM	mitochondrion
DAPI	AppliChem, Darmstadt (DE)	1 µg/ml	DNA

5.1.2 Buffers and solutions

DNA analyses

10x DNA loading buffer: 0.1 M EDTA (pH 8.0), 0.05% (w/v) bromphenol blue, 0.05% (w/v) xylene cyanol, 40% (w/v) sucrose

Elution buffer: 10 mM TRIS-HCl (pH 8.5)

Extraction buffer: 10 mM TRIS (pH 8.0), 10 mM NaCl, 10 mM EDTA (pH 8.0), 0.5% (w/v) SDS

TAE buffer: 40 mM TRIS, 40 mM concentrated acetic acid, 1 mM EDTA (pH 8.0)

TE buffer: 10 mM TRIS-HCl (pH 8.0), 1 mM EDTA (pH 8.0)

***E. coli* cultivation**

Agar plates: 1.5% agar in LB-Medium, 100 µg/ml ampicillin

LB-Medium (for 1 l): 10 g Bacto-Tryptone, 5 g yeast extract, 10 g NaCl, pH 7.4 (autoclaved)

TSS buffer: LB Medium containing 10% PEG 3350, 5% DMSO, 50 mM $MgCl_2$

Light microscopy analyses

8% (w/v) pFA: 8 g pFA, 100 ml 0.1 M Hepes (pH 7.2)

Gelatin solution 10% (w/v): type-A gelatine (from porcine skin, Sigma-Aldrich (St. Louis, USA)) in TDB, pH 8.0

Phosphate buffered saline (PBS): 10 mM Na_2HPO_4, 1.7 mM KH_2PO_4, 137 mM NaCl, 2.7 mM KCl, pH 7.4

Protein analyses

Blotting buffer: 25 mM TRIS, 192 mM glycine, 0.1% (w/v) SDS, 20% (v/v) methanol

Laemmli running buffer (1x): 25 mM TRIS, 192 mM glycine, 0.1% (w/v) SDS

Resolving gel buffer: 1.5 M TRIS-HCl (pH 8.8), 0.4% (w/v) SDS

Resolving gels:

12.5% (5 gels): 10 ml acrylamide/bis-acrylamide 30:0.8, 7.5 ml resolving gel buffer, 12.5 ml ddH_2O, 100 µl 10% (w/v) APS, 20 µl TEMED

20% (5 gels): 16 ml acrylamide/bis-acrylamide 30:0.8, 7.5 ml resolving gel buffer, 6.5 ml ddH_2O, 100 µl 10% (w/v) APS, 20 µl TEMED

Sample buffer (2x): 120 mM TRIS-HCl (pH 6.8), 20% (v/v) glycerol, 4% (w/v) SDS, 0.004% (w/v) bromphenol blue, 2% (v/v) β-mercaptoethanol

Stacking gel buffer: 0.5 M TRIS-HCl (pH 6.8), 0.4% (w/v) SDS

Stacking gel (5 gels): 1.95 ml acrylamide/bis-acrylamide 30:0.8, 3.75 ml stacking gel buffer, 9.15 ml H2O, 75 µl 10% (w/v) APS, 15 µl TEMED

Coomassie staining solution: 0.25 g/l Coomassie Blue R250, 10% (v/v) isopropanol, 5% (v/v) acetic acid

Coomassie destaining solution: 10% (v/v) isopropanol, 5% (v/v) acetic acid

RNA analyses

Denhardts solution (DEN, 50x): 1% (w/v) Ficoll 400, 1% (w/v) polyvinylpyrolidone, 1% (w/v) bovine serum albumin (BSA)

Glyoxal solution: 75.4% (v/v) DMSO, 21.5% (v/v) Glyoxal (deionised), 15 mM NaH_2PO_4 (pH 6.9)

Northern blot hybridization solution: 5x SSC, 5x DEN, 0.1% (w/v) SDS, 0.1% (w/v) tetrasodium pyrophosphate, 0.01% (w/v) heparin

Northern blot washing solution: 0.1% (w/v) SDS, 0.1x SSC

RNA buffer (50x): 0.5 M NaH_2PO_4 (pH 6.9)

SSC (20x): 3 M NaCl, 0.3 M trisodium citrate, pH 7.0

Trypanosoma brucei cultivation

2x freezing mix: 80% (v/v) HMI-9, 20% (v/v) glycerol (sterile filtered, stored at -20°C)

HMI-9 medium (1x for 1 l or 1.6x for 0.625 l) after Hirumi (Hirumi and Hirumi, 1989) : 17.6 g 'Iscove's modified Dulbecco's medium' (IMDM, pH 7.5), 3 g sodium bicarbonate, 136 mg hypoxanthine, 28.2 mg bathocuproine sulfonate, 14 µl β-mercaptoethanol, 39 mg thymidine, 100.000 U penicillin, 100 mg streptomycin, 182 mg cysteine and 10% (v/v) heat inactivated fetal calf serum (FCS; Sigma-Aldrich, St. Louis, USA) (pH 7.5, sterile filtered, stored at -20°C)

HMI-9 medium containing 1.1% methylcellulose:

To prepare the methylcellulose, 11 g Me-cellulose (Cat. No. 94378-500G; Sigma-Aldrich, St. Louis, USA) in 366 ml water were autoclaved in a 1 l bottle with a magnetic stirrer inside. Then, the methylcellulose was stirred for at least 24 hours at 4°C until it became transparent. After thawing a bottle of 1.6x HMI-9 (625 ml), the medium was poured into the prepared methylcelluloses, stirred for at least 24 hours at room temperature and then stored at 4°C while constantly stirring.

Trypanosoma dilution buffer (TDB): 20 mM Na_2HPO_4, 2 mM NaH_2PO_4 (pH 7.7), 20 mM glucose, 5 mM KCl, 80 mM NaCl, 1 mM $MgSO_4$, pH 7.6 (sterile filtered)

5.1.3 Equipment and devices

Cell culture

Airstream Class II BSC	Esco global, Hoyland (UK)
Amaxa NucleofectorTM 2b Device	Lonza, Basel (CH)
CO_2 Incubators	Binder, Tuttlingen (DE)
Bottle top filter unit	Carl Roth, Karlsruhe (DE)
Neubauer chamber	Marienfeld, Lauda-Königshofen (DE)

Centrifuges, rotors and shakers

BioVortex V1	Biosan, Riga (LV)
Centrifuge 6-16 K, rotors: 12169, 12170	SIGMA Laborzentrifugen, Osterode (DE)
Centrifuge Mikro 200	Hettich, Bäch (CH)
Centrifuge Z 216 MK, rotor: 220.87	HERMLE Labortechnik, Wehingen (DE)
Centrifuge Z 383 K	HERMLE Labortechnik, Wehingen (DE)
Shaker Certomat-S	B. Braun Melsungen, Melsungen (DE)
Shaker KS-15	Edmund Bühler, Hechingen (DE)
Shaker celltron	Infors, Bottmingen (CH)
Stirrer	Phoenix Instrument, Garbsen (DE)
SpectrafugeTM Mini centrifuge	Labnet International, Edison (USA)

Chemicals

The used chemicals were obtained from Carl Roth (Karlsruhe, DE), AppliChem (Darmstadt, DE) or Sigma-Aldrich (St. Louis, USA) if not other stated in the text.

Consumables

24 and 96-well tissue culture plates; cryo, falcon and PCR tubes; pasteur and serological pipettes.	Sarstedt, Nümbrecht, (DE)
Vented cell culture flasks	Greiner Bio-One, Frickenhausen (DE)
Circular (MN 615 Ø 50 mm) and pleated filters (MN 615 ¼ Ø 185 mm)	Macherey-Nagel, Düren (DE)
Cover slips and Eppendorf tubes	A. Hartenstein, Würzburg (DE)
Steriflip and Steritop filter	Merck, Darmstadt (DE)
Object and poly-L-lysine slides	Thermo Fisher Scientific, Waltham (USA)

DNA, RNA and protein analyses

Amersham Protran Supported 0.45 NC	GE Healthcare, Little Chalfont (UK)

Amersham Hybond-N	GE Healthcare, Little Chalfont (UK)
Bachofer UV-table, 302	Vilber Lourmat, Eberhardzell (DE)
GEL iX Imager	Intas Science Imaging Instruments, Göttingen (DE)
GeneRuler™ DNA Ladder mix	Thermo Fisher Scientific, Waltham (USA)
MiniFold dot blotter	GE Healthcare, Little Chalfont (UK)
Mini Protean® Tetra Cell	Bio-Rad Laboratories, Munich (DE)
Odyssey Infrared Imaging System	LI-COR Bioscience, Lincoln (USA)
PageRuler™ Prestained Protein Ladder (10-180 kDa)	Thermo Fisher Scientific, Waltham (USA)
Primus 25	PEQLAB Biotechnologie, Erlangen (DE)
Storage Phosphor Screen	GE Healthcare, Little Chalfont (UK)
T-100 Thermal cycler	Bio-Rad Laboratories, Munich (DE)
Tecan Infinite M200 NanoQuant	Tecan Group, Männerdorf (CH)
Transfer blot chamber	A. Hartenstein, Würzburg (DE)

Enzymes

All used enzymes (including CIAP, PNK, Klenow fragment, Phusion High-Fidelity DNA Polymerase, restriction enzymes, T4-ligase) were obtained from Thermo Fisher Scientific (Waltham, USA) if not other stated in the text.

Microscopes and cameras

DMI6000 wide-field microscope	Leica, Wetzlar (DE)
Eclipse TS100 microscope	Nikon, Tokio (JP)
FACScalibur Flow Cytometer	BD Biosciences, Franklin Lakes (USA)
iMIC	FEI-TILL Photonics, Gräfelfing (DE)
PCO Sensicam qe	PCO, Kelheim (DE)
Leica DFC 365 FX	Leica, Wetzlar (DE)

Kits

Amaxa Basic Parasite Nucleofector Kit 1	Lonza, Basel (CH)
CloneJET PCR Cloning Kit	Thermo Fisher Scientific, Waltham (USA)
DecaLabel DNA labeling Kit	Thermo Fisher Scientific, Waltham (USA)
High Pure PCR Template Preparation Kit	Roche Diagnostics, Rotkreuz (CH)
NucleoBond PC 100	Macherey-Nagel, Düren (DE)
NucleoSpin Gel and PCR clean-up Kit	Macherey-Nagel, Düren (DE)
NucleoSpin Plasmid Kit	Macherey-Nagel, Düren (DE)
QuantiGene ViewRNA ISH Cell Assay Kit	Affymetrix, Santa Clara (USA)

RevertAid First Strand cDNA Synthesis Kit	Thermo Fisher Scientific, Waltham (USA)
RNase-Free DNase Set	QIAGEN, Venlo (NL)
RNeasy Mini Kit	QIAGEN, Venlo (NL)

5.1.4 Oligonucleotids

Table 10: Oligonucleotides used for PCR. Represented are the names of the oligonucleotides and their sequences. Within the given nucleotide sequences small letters indicate added overhangs, bold letters added restriction sites and capital letters the annealing sequence. Also, the restriction enzyme (RE) recognizing the indicated restriction site is given as well as the sequence that can be amplified using the primer. Abbreviations are explained below.

Name	Sequence (5'-3')	RE	Anneals with
CB80 VSG121 3'UTR HindIII rev	**aagctt**CCTCCTACCTAGCTACCTAC	HindIII	*VSG 121* 3'UTR
CB82 427.08.510 neu HindIII fwd	**aagctt**ATGAAAACCATAG	HindIII	*427.08.510/490*
CB83 427.08.510 neu HindIII rev	**aagctt**ACCGTCATACAAC	HindIII	*427.08.510/490*
CB87 121 3'UTR fwd paci	**ttaattaa**ttggatcTTAATTTTCC	PacI	*VSG 121* 3'UTR
HZ2 oligo54 spliced leader fwd	g**actAGT**TTCTGTACTAT	BcuI	spliced leader
HZ3 oligo42 VSGall rev	ccg**ggtacc**GTGTTAAAATATATC	KpnI	*VSG* 3'UTR
HZ16 GFP ISCEI HindIII fwd	cgcc**aagctttagggataacagggtaat**ATGG TGAGCAAGGGCGAG	HindIII I-SceI	*GFP*
HZ30 M16 fwd c	cATGGCCGTGCACAGAGC	-	*VSG 121*
HZ31 M16 rev attaa	a**ttaaTTAA**AAAAGCAAGGCCACA	PacI	*VSG 121*
HZ32 121 UTR Hind rev	ggcg**AAGCTT**CCTCCTACCT	HindIII	*VSG 121* 3'UTR
HZ35 VSG221 UTR Mva fwd	cgccACA**AGCATT**CTATACGTAAA	Mva1269I	*VSG 221* 5'UTR
HZ43 M1.2 fwd 3	CGACTATACTTGCCTATTAC	-	*VSG 221*
HZ47 PFR 3UTR PacI Space fwd	**ttaattaa**ttggatcttaaCGCTGCGCTTAA	PacI	*PFR* 3'UTR
HZ48 PFR 3UTR HindIII rev	ggcg**aagctt**TGATGCTTTATTGCT	HindIII	*PFR* 3'UTR
JJ44 Act 5'UTR Hind rev	tgc**aagctt**GCTTATTTTATGG	HindIII	*actin* 5'UTR

CB, primer was designed by Christopher Batram; fwd, forward primer; HZ, primer was designed by Henriette Zimmermann; JJ, primer was designed by Jamin Jung; rev, reverse primer; PFR, paraflagellar rod; RE, restriction enzyme; UTR, untranslated region; VSG, variant surface gylcoprotein

5.1.5 Organisms

Bacterial strains

Escherichia coli (*E. coli*) Top 10

Genotype: F-mcrA Δ(mrr-hsdRMS-mcrBC) Φ80lacZΔM15 ΔlacX74 recA1 araD139 Δ(araleu)7697galU galK rpsL(StrR) endA1 nupG

Competent bacteria were generated using the method of Chung et al. as described below (Chung et al., 1989).

Trypanosomes

Wild type strains

Following monomorphic parasites of the *Trypanosoma brucei brucei* strain Lister 427 were used (Cross, 1975):

MITat 1.2 wild type (referred to as M1.2 WT)

Molteno Insitut Trypanozoon Antigen Typ 1.2, blood stream form (BSF), expressing VSG 221 (also known as MITat1.2).

MITat 1.6 wild type (referred to as M1.6 WT)

Molteno Insitut Trypanozoon Antigen Typ 1.6, blood stream form (BSF), expressing VSG 121 (also known as MITat1.6).

MITat1.5 wild type (referred to as M1.5 WT)

Molteno Insitut Trypanozoon Antigen Typ 1.5, blood stream form (BSF), expressing VSG 118 (also known as MITat1.5).

Following pleomomorphic parasites of the *Trypanosoma brucei brucei* strain EATRO 1125 (serodeme AnTat1.1) were used (Delauw et al., 1985).

AnTat1.1 (referred to as $A1.1^{ES}$)

Antwerp Insitut Trypanozoon Antigen Typ 1.1, blood stream form (BSF), expressing VSG AnTat1.1 (abbreviated as VSG A1.1).

Transgenic cell lines

MITat 1.2 13-90 (referred to as 13-90 or 221^{ES})

Trypanosomes of the monomorphic MITat1.2 wild type cell line were transfected with the pLew13 (Addgene plasmid 24007, G. Cross) and with the pLew90 plasmid (Addgene plasmid 24008, G. Cross). The first one encodes a T7 RNA-polymerase as well as a Tet-repressor and the latter one a Tet-repressor under the control of T7-promotor.

Consequently, MITat 1.2 13-90 parasites constitutively express a T7-RNA polymerase and a tetracycline repressor (Wirtz et al., 1999). This enables the tetracycline inducible expression of other transfected plasmids, if they are under the control of a Tet-operator and a T7-promotor. Selection: 5 µg/ml hygromycin and 2.5 µg/ml neomycin (G-418).

MITat 1.2 SM

This cell line is based on the MITat 1.2 13-90 trypanosomes. The hygromycin resistance cassette was deleted and thus the cell line is referred to as 'single marker' (SM). Selection: 2.5 µg/ml neomycin (G-418) (Wirtz et al., 1999).

MITat 1.2 PN221 (abbreviated as N50)

This cell line is based on the MITat 1.2 SM. A neomycin resistance cassette was integrated in the inactive ES 17 (Figueiredo et al., 2008). Trypanosomes, which have switched the expression to ES 17 were selected, due to the addition of the drug. The parasites express now VSG M1.13. Selection: 10 µg/ml neomycin (G-418).

MITat1.2 DOT1B$^{-/-}$ (abbreviated as ΔDOT1B)

This cell line is based on the MITat 1.2 SM. Both alleles encoding for the histone methyltransferase DOT1B were replaced with the resistance cassettes for hygromycin and for phleomycin (Janzen et al., 2006). Selection: 2.5 µg/ml neomycin (G-418).

AnTat1.1 13-90 (referred to as A1.1^{ES})

Trypanosomes of the pleomorphic AnTat1.1 wild type cell line were transfected with the pLew13 (Addgene plasmid 24007, G. Cross) and with the pLew90 plasmid (Addgene plasmid 24008, G. Cross), just like the MITat 1.2 13-90. Thus, transfected plasmids containing the gene of interest under the control of a Tet-operator and a T7-promotor can be inducibly expressed upon the addition of tetracycline in this cell line (Engstler and Boshart, 2004). Selection: 2.5 µg/ml hygromycin and 1.25 µg/ml neomycin (G-418).

5.1.6 Plasmids

Table 11: Plasmids used during this work. Represented are the labels of the plasmids used for transfection of *T. brucei* (vector and name). The references for the plasmid (origin) are given as well as the locus, where the plasmid integrates into the genome of *T. brucei*. Also, the expression of the introduced gene (constitutive or inducible) and the resistance cassette present in the construct are indicated. Abbreviations are explained below.

Vector	Name	Origin	Locus	Expression	Resistance
p2T7-177	p2T7	(Wickstead et al., 2002)	177bp-Region, MC	inducible	*PURO*
p4231	GFP:PAD1$_{UTR}$	M. Carrington	β-tubulin	constitutive	*BLAS*
pbRn6	ES^{tel}	(Horn and Cross, 1997)	*VSG 221* ES	constitutive	*BLAS*
pKD4	-	(Muñoz-Jordán et al., 1996)	*VSG 221* ES	constitutive	*NEO*
pLF12	ES^{pro}	(Figueiredo et al., 2008)	ES	constitutive	*PURO*
pLew82v4	pRS	Addgene plasmid 24009, G. Cross	RS	inducible	*BLE*
pTub	pTub	M. Günzel	β-tubulin	constitutive	*BLAS*

BLE, phleomycin resistance*; BLAS*, blasticidin resistance; ES, bloodstream form expression site; GFP, green fluorescent protein; MC, minichromosomes; *NEO*, neomycin (G-418) resistance; PAD1, protein associated with differentiation 1; pro, promotor-proximal; *PURO*, puromycin resistance; RS, ribosomal spacer; tel, telomere-proximal; tub, tubulin; UTR, untranslated region

5.1.7 Software

Adobe Illustrator Creative Suite 6	Adobe Systems Incorporated, San Jose (USA)
CellQuest Pro	BD Biosciences, Franklin Lakes (USA)
CLC Main Workbench 6	CLC bio, Venlo (NL)
Huygens Essential	Scientific Volume Imaging B. V., Hilversum (NL)
iControl	Tecan, Männedorf (CH)
ImageJ 64	National Institute of Health (USA)
Image studio Lite	LI-COR Bioscience, Lincoln (USA)
LA Aquisition	FEI-TILL Photonics, Gräfelfing (DE)
Leica Application suite AF	Leica, Wetzlar (DE)
Microsoft office	Microsoft, Redmon (USA)
Mendeley	Mendeley Ltd., London (UK)
Prism 5	GraphPad Software, La Jolla (USA)

5.2 Methods

5.2.1 Working with *Trypanosoma brucei*

Cultivation of monomorphic trypanosomes

Monomorphic BSF trypanosomes were cultured in liquid HMI-9 medium, supplemented with 10% (v/v) fetal bovine serum, at 37°C and 5% CO_2 (Hirumi and Hirumi, 1989). The parasites were kept at densities below 1x 10^6 cells/ml to ensure their logarithmic growth. Therefore, the density of trypanosomes was determined regularly using a Neubauer chamber and the cultures were diluted to an appropriate number with pre-warmed HMI-9 (37°C). Addition of suitable antibiotics guaranteed the maintenance of transgenic cell lines. The parasites were harvested via centrifugation at 1,400x *g* for 10 minutes at 4°C if not other stated.

Cultivation of pleomorphic trypanosomes

Pleomorphic BSF trypanosomes were cultivated in viscous HMI-9, supplemented with 10% (v/v) fetal bovine serum and 1.1% (w/v) methylcellulose (Sigma-94378), at 37°C and 5% CO_2 (Hirumi and Hirumi, 1989; Vassella et al., 2001). The parasites were strictly kept at densities below 6x 10^5 cells/ml to ensure the predominance of the slender (sl) stage. The differentiation to the density-induced stumpy (st) stage is triggered *in vitro* at cell densities above 1x 10^6 cells/ml (reviewed in McCulloch et al., 2004). Therefore, the number of the parasites was counted daily using a Neubauer chamber. Then, the cultures were diluted to an appropriate number with pre-warmed medium (37°C) and suitable antibiotics were added. Drops in the temperature were avoided during the handling of pleomorphic BSF trypanosomes as this can affect the sl cells as well.

The methylcellulose had to be removed from the cultures for harvesting the cells. For this reason, the cultures had to be diluted with pre-warmed TDB (37°C) at least 1:4 and then filtered under sterile conditions. For filtration, a sterile bottle top filter unit (Carl Roth, DE) and autoclaved filters were used (MN 615 1/4; Macherey-Nagel, DE). The diluted culture was stepwise filtered into pre-warmed (37°C) and sterile bottles. The filtered cells were stepwise centrifuged at 1,400x *g* for 15 minutes at 37°C. The remaining filtrate was stored at 37°C and 5% CO_2 during centrifugation. After each centrifugation step, the supernatant was discarded up to 5 ml, the cells carefully resuspended and new filtrate added to the centrifuged cells. For the last centrifugation step, the cells were unified in one falcon and washed additionally with pre-warmed TDB (37°C), if needed. If a certain amount of cells is required, it needs to be considered that approximately one third of the cells will be lost during harvesting.

Generating and thawing cryo-stabilates of trypanosomes

Trypanosomes can be stored for long periods in cryo-stabilates. One cryo-stabilate contains ideally 5x 10^6 cells in HMI-9 supplemented with 10% glycerol. For freezing, the parasites were harvested as described above and resuspended in an appropriate volume of pre-cooled HMI-9 (500 µl for one cryo-stabilate). Then, the same volume of the pre-cooled 2x freezing mix (20% glycerol, 80% HMI-9) was carefully added and the mixture was evenly divided into pre-cooled cryo tubes (one cryo-stabilate containing 1 ml). The resulting cryo-stabilates were immediately placed on ice and frozen at -80°C. For long term storage, the cryo-stabilates were transferred to -150°C.

The cryo-stabilate was quickly thawed in a 37°C warm water bath to cultivate the cells again. Immediately afterwards, the cells were transferred into 10 ml ice-cold HMI-9 and centrifuged (1,400x *g*, 10 min, 4°C). Then, the supernatant was discarded, the cells resuspended in 500 µl pre-warmed HMI-9 (37°C) and transferred into the appropriate pre-warmed medium (37°C). After one hour of cultivation, the number of parasites was determined, the culture diluted and the suitable antibiotics added.

When handling pleomorphic parasites, the following deviations were made. For the generation of cryo-stabilates, parasites were harvested at 37°C and placed on ice for three minutes before the freezing mix was added. The cryo-stabilates may contain a lower amount of cells due the loss of cells while harvesting. Thus, the culture can have a low density after thawing and a proportion of the cells might differentiate to the st stage due to the treatment. Consequently, pleomorphic cells need more time until they resume normal growth after thawing compared to monomorphic parasites.

Generation of transgenic trypanosomes cell lines

The *Amaxa Nucleofector II* and the *Amaxa Basic Parasite Nucleofector Kit 1* (Lonza, CH) were used to generate stable transgenic trypanosome cell lines. For transfection, 3x 10^7 BSF cells were harvested at room temperature via centrifugation (essentially as described above). The trypanosomes were carefully resuspended in 100 µl *Basic Parasite Solution 1* and added to the linearized DNA (10 µg). Next, the parasites were transferred into a cuvette and transfected via electroporation using the program X-001 of the *Amaxa Nucleofector II*. Immediately afterwards, the parasites were transferred into 30 ml pre-warmed HMI-9 (37°C) containing the parental selection and serially diluted (1:5, 1:10, 1:50 and 1:100). Each dilution was plated in a 24-well plate, with each well containing 1 ml. Then, the cells were cultivated again at 37°C and 5% CO_2. After six hours of cultivation, 1 ml medium containing the parental selection (1x) and the new selection (2x) was added to each well. Isogenic clones were obtained after five to seven days of incubations.

The following deviations were made when pleomorphic parasites were transfected. Ideally, a higher cell number (5x 10^7 cells) was used for transfection, as fewer cells survive the treatment with the transfection solution and a proportion of the remaining parasite might respond with st development. More than three centrifugation steps were avoided and the cells were kept as warm as possible in order to keep the stress low and hence prevent st differentiation. After transfection, the parasites were transferred into 5 ml pre-warmed HMI-9 (37°C), which was subsequently added to 35 ml pre-warmed medium (37°C) supplemented with methylcellulose (pool) and thoroughly mixed. Only 1:5 and 1:10 serial dilutions were carried out and the pool was plated as well. The remaining volume of the pool and the dilutions was transferred into cell culture flasks. After six hours, the appropriate selection was added. Growing trypanosomes became visible in the flasks or wells after four to eight days. The cultures had to be analyzed on a Neubauer chamber to identify clones before they reached high cell densities and develop to the st stage.

Generated cell lines

Table 12: Monomorphic and pleomorphic trypanosomes lines generated during this work. Represented are the labels of the generated cell lines, the trypanosome line and the plasmid used for transfection. The selection used for the cultivation of the respective cell line is shown and the selection for the newly integrated constructed is underlined. Addition of tetracycline (1 µg/ml) induced the expression of the pRS and the p2T7-177 constructs. Cell lines containing the pRS construct were cultivated upon addition of tetracycline with 4 µg/ml BLE. Abbreviations are explained below.

Name	Parental cell line	Plasmid	Selection (µg/ml)
GFP:PAD1$_{UTR}$A1.1^{ES}	AnTat1.1 13-90 (A1.1^{ES})	p4231	5 BLAS, 2.5 HYG, 1.25 NEO
GFP:PAD1$_{UTR}$A1.1^{ES}121^{tet}	GFP:PAD1$_{UTR}$A1.1^{ES}	pRS.121	5 BLAS, 2.5 HYG, 1.25 NEO, 1 BLE
GFP:PAD1$_{UTR}$A1.1^{ES}118^{tet}	GFP:PAD1$_{UTR}$A1.1^{ES}	pRS.118	5 BLAS, 2.5 HYG, 1.25 NEO, 1 BLE
GFP^{ESpro}A1.1^{ES}	AnTat1.1 13-90 (A1.1^{ES})	pLF12 GFP	1 PURO, 2.5 HYG, 1.25 NEO
GFP^{ESpro}A1.1^{ES}121^{tet}	GFP^{ESpro}A1.1^{ES}	pRS.121	1 PURO, 2.5 HYG, 1.25 NEO, 1 BLE
GFP$^{EStel}{}_{198}$221ES	MITat 1.2 13-90 (221ES)	pbRn6 GFP 198	5 BLAS, 5 HYG, 2.5 NEO
GFP$^{EStel}{}_{\Delta}$221ES	MITat 1.2 13-90 (221ES)	pbRn6 GFP Δ(45-51)	5 BLAS, 5 HYG, 2.5 NEO
121$^{EStel}{}_{198}$221ES	MITat 1.2 13-90 (221ES)	pbRn6 VSG 121 198	5 BLAS, 5 HYG, 2.5 NEO

121$^{ESteI}{}_{\Delta}$221ES	MITat 1.2 13-90 (221ES)	pbRn6 VSG 121 Δ(45-51)	5 BLAS, 5 HYG, 2.5 NEO
121$^{ESteI}{}_{inv8mer}$221ES	MITat 1.2 13-90 (221ES)	pbRn6 VSG 121 inv(28-35)	5 BLAS, 5 HYG, 2.5 NEO
GFP$^{ESpro}{}_{198}$221ES	MITat 1.2 13-90 (221ES)	pLF12 GFP 198	5 BLAS, 5 HYG, 2.5 NEO
GFP$^{ESpro}{}_{\Delta}$221ES	MITat 1.2 13-90 (221ES)	pLF12 GFP Δ(45-51)	5 BLAS, 5 HYG, 2.5 NEO
GFP$^{tub}{}_{198}$221ES	MITat 1.2 13-90 (221ES)	pTub GFP 198	5 BLAS, 5 HYG, 2.5 NEO
GFP$^{tub}{}_{\Delta}$221ES	MITat 1.2 13-90 (221ES)	pTub GFP Δ(45-51)	5 BLAS, 5 HYG, 2.5 NEO
GFP$^{tub}{}_{198}$221ES118^{tet}	GFP$^{tub}{}_{198}$221ES	pRS.118	5 BLAS, 5 HYG, 2.5 NEO, 1 BLE
LS:GFP$^{tub}{}_{198}$221ES	MITat 1.2 13-90 (221ES)	pTub LS:GFP 198	5 BLAS, 5 HYG, 2.5 NEO,
LS:GFP-1$^{tub}{}_{198}$221ES118^{tet}	LS:GFP$^{tub}{}_{198}$221ES clone 1	pRS.118	5 BLAS, 5 HYG, 2.5 NEO, 1 BLE
LS:GFP-2$^{tub}{}_{198}$221ES118^{tet}	LS:GFP$^{tub}{}_{198}$221ES clone 2	pRS.118	5 BLAS, 5 HYG, 2.5 NEO, 1 BLE
GFP$^{tub}{}_{PFR}$221ES	MITat 1.2 13-90 (221ES)	pTub GFP:PFR$_{UTR}$	5 BLAS, 5 HYG, 2.5 NEO
GFP$^{tub}{}_{PFR}$221ES118^{tet}	GFP$^{tub}{}_{PFR}$221ES	pRS.118	5 BLAS, 5 HYG, 2.5 NEO, 1 BLE
LS:GFP$^{tub}{}_{PFR}$221ES	MITat 1.2 13-90 (221ES)	pTub LS:GFP:PFR$_{UTR}$	5 BLAS, 5 HYG, 2.5 NEO
ΔDOT1B.121$^{DEX}{}_{198}$221ES	ΔDOT1B 221ES	pKD4 VSG 121 198	30 NEO
ΔDOT1B.121$^{DEX}{}_{\Delta}$221ES	ΔDOT1B 221ES	pKD4 VSG 121 Δ(45-51)	30 NEO
Tb427.08.490^{RNAi}221ES	MITat 1.2 13-90 (221ES)	p2T7-177 Tb427.08.490	5 HYG, 2.5 NEO, 0.1 PURO
Tb427.08.490^{RNAi}221ES121^{tet}	221ES121^{tet}	p2T7-177 Tb427.08.490	5 HYG, 2.5 NEO, 1 BLE, 0.1 PURO

Δ, nucleotides 45-51 of the *VSG 121* 3'UTR were deleted; 118, VSG 118; 121, VSG 121; 198, complete *VSG 121* 3'UTR; 221, VSG 221; A1.1, VSG AnTat1.1; BLE, phleomycin; BLAS, blasticidin; ES, bloodstream form expression site; DEX, double expressor; GFP, green fluorescent protein; HYG, hygromycin; inv8mer, nucleotide 28-35 of the *VSG 121* 3'UTR were inverted; LS, leader sequence for ER import; NEO, neomycin (G-418); ORF, open reading frame; PAD1, protein associated with differentiation 1; pro, promotor-proximal; PURO, puromycin; RS, ribosomal spacer; tet, inducible expression upon addition of tetracycline; tel, telomere-proximal; tub, tubulin; UTR, untranslated region, VSG, variant surface glycoprotein.

Serial dilutions of trypanosomes

If phenotypes were not homogenous in assumed isogenic clones of monomorphic parasites, limiting dilutions were used for subcloning. For this purpose, 0.5 parasites per well were plated in a 96-well plate, each well containing 200 µl. Up-coming parasites were further cultivated as described above.

Serial dilutions with pleomorphic cells were used to determine the number of outgrowing VSG overexpressors. For this aim, the trypanosomes were diluted to a concentration of 25, 250, 2,500 or 25,000 cells/ml and VSG overexpression was induced due to the addition of tetracycline. Immediately afterwards, each dilution was plated in a 96-well plate. As each well contained 200 µl, approximately 5, 50, 500 or 5,000 cells were present in one well. Non-induced cells were seeded at the lowest concentration as control. The medium shift from pink (alkaline) to orange (acidic) at high parasite densities enabled the identifications of outgrown wells after 18 days of incubation.

Differentiation to the stumpy stage

For the generation of density-induced st parasites, a culture at a density of 5x 10^5 cells/ml was cultivated without dilution. After 48 hours, the accumulated stumpy induction factor (SIF) caused the developmental transition from the sl to the st stage.

Either pCPT-cAMP or a SIF-concentrate, generated by Ines Subota, was used in order to analyze the impact of classical triggers for st development on the VSG overexpressors (Laxman et al., 2006; Vassella et al., 1997). For the generation of the SIF-concentrate, first conditioned medium was obtained by growing monomorphic trypanosomes to maximum cell densities (0.7-1x 10^7 cells/ml). After the removal of the cells from the medium via filtration, the proteins were depleted from the cell free conditioned medium using methanol precipitation. Then, the cell and protein free conditioned medium was concentrated via lyophilization. After resuspension, the solution had an x-fold SIF concentration (one batch of the SIF-concentrate 37x and the other 43x). 1x corresponded to conditioned medium without further concentration steps.

For the assay, classical triggers for st differentiation were diluted in pre-warmed TDB (pCPT-cAMP: 400 and 800 µM and the SIF-concentrate: 1x and 1.5x) and kept warm until usage. The trypanosomes were diluted to a concentration of 0.5 or 1x 10^5 cells/ml in HMI-9 supplemented with methylcelluloses (potentially 'proliferating' clones: 5x 10^4 cells/ml: potentially 'growth-arrested' clones: 1x 10^5 cells/ml). Either cells in which VSG overexpression was induced for the first time due to the addition of tetracycline or cells induced for longer periods were used. Then, 1.5 ml of the cell suspension were transferred to one well of a 24-well plate and 500 µl of one of the diluted compounds were added to the well. Thus, the VSG overexpressors were exposed to a final concentration of either 100 or 200 µM pCPT-cAMP (0.25x or 0.375x SIF).

Additionally, 500 µl TDB alone was added to one well containing 1.5 ml of the same cell suspension to analyzed the impact of tetracycline alone (untreated). Non-induced cells were treated in the same way as a control. All treatments were conducted for non-induced cells and induced VSG overexpressors in triplicates within one assay. The parasites were incubated at 37°C and 5% CO_2 on a shaker (180 rpm). To determine the impact of the compounds during ES-induced st development, the amount of cells expressing the GFP:PAD1$_{UTR}$ st reporter was determined by microscopic analyses after 20, 28 or 48 hours of treatment.

Differentiation to the procyclic stage

Non-induced sl cell, density-induced st parasites or trypanosomes overexpressing VSG 121 for 48 hours were harvested from the viscous medium as described above. The cells were resuspended in DTM to a density of 2x 10^6 cells/ml and 3 mM *cis*-aconitate as well as 3 mM citrate were added to trigger the differentiation to the PCF (Brun, 1981; Overath et al., 1986). After 0, 6 and 24 hours of CCA treatment, the parasites were harvested and fixed for at least two hours at 4°C with 2% paraformaldehyde and 0.05% glutaraldehyde. The procyclic surface protein EP1 was stained and detected as described below.

5.2.2 Maintenance, infection and dissection of flies

Tsetse flies *(Glossina morsitans morsitans)* were kept at a relative humidity of 70% at 27°C. The flies were infected with cultured parasites during their first blood meal, which was provided to them after a maximum of 48 hours of post-eclosion. For the infections, the pleomorphic trypanosomes were harvested as described above and washed two times with pre-warmed TDB (37°C) in order to remove the antibiotics. Subsequently, the cells were resuspended in sheep blood containing 60 mM *N*-acetylglucosamine to a density of 2x 10^6 cells/ml. In total we fed 50 flies with ES-induced st parasites overexpressing VSG 121 for 56 hours and the same amount of flies with density-induced st parasites of the parental GFP:PAD1$_{UTR}$A1.1^{ES} cell line. The infected flies were fed twice a week with defibrinated sterile sheep blood (ACILA, DE) through a silicone membrane over a period of at least 50 days. Before dissecting the flies, they were starved for at least 24 hours. As described by Rotureau et al., 2011, the salivary glands were isolated in the first place. Subsequently, the whole alimentary tract was dissected in a drop of PBS and microscopically analyzed for the presence of trypanosomes. If parasites were detected, the salivary glands as well as the alimentary tract were transferred to a poly-l-lysine coated slide, where the foregut and proventricle were separated from the midgut. After releasing the parasites from the tissue in distinct drops of PBS, the slides were air-dried and immunostaining was performed. Infections of tsetse flies and their dissection were conducted by Ines Subota.

5.2.3 Working with *E. coli*

Generation of chemically competent *E. coli*

For the generation of chemically competent *E. coli* Top10, 100 ml LB-medium were inoculated with 1 ml bacteria suspension of an overnight culture. The bacterial culture was incubated at 37°C on a shaker (150-200 rpm) until the OD_{600} was between 0.3 and 0.4. Subsequently, the bacteria were harvested (900x *g*, 10 min, 4°C), the supernatant discarded and the pellet resuspended in 2.5 ml TSS. 200 µl of the suspension were transferred into pre-cooled eppendorf tubes and frozen in liquid nitrogen. The chemically competent bacteria were stored at -80°C until usage.

Transformation of chemically competent *E. coli*

Chemically competent *E. coli* Top10 were thawed on ice for transformation. Then, the pure plasmid (10 ng for re-transformation) or the ligation mixture of the plasmid (10-20 µl) was added to the bacteria and incubated on ice for 30 minutes. Next, the bacteria were exposed to a heat shock (42°C, 30 sec) and 1 ml LB-medium was added. After incubation for one hour on a shaker (150-200 rpm), the bacteria were harvested and the supernatant was discarded up to 100 µl, in which the cells were resuspended. Then, the suspension was spread on agar plates containing ampicillin (100 µg/ml) and incubated over night at 37°C.

Liquid bacteria cultures

LB-medium with ampicillin (100 µg/ml) was inoculated with one colony from an agar plate and incubated over night on a shaker (150-200 rpm) in order to isolate plasmid DNA from a liquid culture. Different volumes of liquid cultures and different methods were used, depending on the needed amount and quality of DNA.

5.2.4 Molecular biological methods

5.2.4.1 DNA analyses

Isolation of plasmid DNA from bacteria

Small amounts of plasmid DNA with low purity were sufficient for analytical digestions and subsequent sequencing (sequencing was carried out by GATC Biotech AG, DE). In this case, plasmid DNA was extracted from a bacterial overnight culture (1 ml) by means of alkaline lysis. If the DNA quality was important, 5 ml LB-medium were inoculated for small-scale preparations and 50 ml for large-scale preparations. Then, the plasmid DNA was extracted using the *NucleoSpin Plasmid Kit* or *NucleoBond PC 100 Kit* (Macherey-Nagel, DE), essentially following the manufacturer's instructions. DNA concentration and purity was determined by measuring

the absorption of the solution at 260 nm and 280 nm using the *Tecan Infinite M200* reader (Tecan Group, CH). The plasmid DNA was stored at -20°C.

Isolation of genomic DNA from trypanosomes

If small amounts of genomic DNA were sufficient for analyses, 5x 10^6 trypanosomes were harvested and the DNA isolated using the *High Pure PCR Template Preparation Kit* (Roche Diagnostics, CH), essentially following the manufacturer's instructions. If, however, higher amounts were needed as for Southern blot analyses, genomic DNA was isolated via phenol/chloroform extraction. For this purpose, at least 10^7 cells were harvested, transferred into a 2 ml eppendorf tube and the pellet stored at -20°C until the extraction was continued. Then, 500 µl extraction buffer containing 0.1 mg Proteinase K was added to the cell pellet without resuspending and incubated over night at 37°C. The next day, 1 ml phenol was pipetted on the sample and rotation on an overhead shaker for ten minutes ensured the mixture of the solution. Subsequently, the aqueous phase was separated from the phenolic phase via centrifugation (21,000x *g*, 3 min, 4°C) and transferred into a new eppendorf tube. Next, the procedure was repeated with a 1:1 phenol chloroform mixture and then with pure chloroform. Afterwards, the genomic DNA was isolated from the aqueous phase via isopropanol precipitation. The aqueous phase was transferred to a new eppendorf tube, the same volume of isopropanol was added as well as 3 M sodium acetate (1/10x the total volume). Subsequently, the mixture was centrifuged (14,000x *g*, 30 min, 4°C), the supernatant discarded and the pellet washed with 500 µl 70% ethanol (14,000x *g*, 10 min, 4°C). Then, the pellet was air dried and dissolved in 100 µl TE buffer over night at 4°C. The genomic DNA was stored at 4°C.

Agarose gel electrophoresis and gel extraction of DNA

Agarose gel electrophoresis was conducted to separate PCR products or DNA fragments after digestion. Fragments larger than 500 bp were resolved using 0.8% agarose (Sigma-Aldrich, USA) in TAE and smaller fragments with 2% agarose (Sigma-Aldrich, USA) in TAE. The samples were mixed with a 10x loading dye prior loading and the *GeneRuler DNA Ladder Mix* (Thermo Fisher Scientific, USA) was used as standard for the size of DNA. The DNA was stained in an ethidium bromide bath (3 µg/ml), visualized with UV light (312-350 nm) and recorded using a gel documentation system. If a DNA fragment should be isolated from the gel, it was exposed to a low radiant intensity to minimize DNA damage, while cutting out. Subsequently, the *NucleoSpin Gel and PCR clean-up Kit* (Macherey-Nagel, DE) was used to extract the DNA from the gel piece according to the manufacturers' protocol. The amount of isolated DNA was determined via gel electrophoresis using the *GeneRuler DNA Ladder Mix* (Thermo Fisher Scientific, USA) as standard for DNA concentration.

Polymerase chain reaction

DNA fragments were amplified from genomic or plasmid DNA using the Phusion High-Fidelity DNA Polymerase (Thermo Fisher Scientific, USA). The general conditions and programs are shown in table 13. The PCR products were first separated via electrophoresis and then cleaned up using the *NucleoSpin Gel and PCR clean-up Kit* (Macherey-Nagel, DE). The fragments were either directly digested and used for further cloning steps or ligated into the pJET1.2 cloning vector using the *CloneJET PCR Cloning Kit* (Thermo Fisher Scientific, USA).

Table 13: Protocol for PCRs using the Phusion High-Fidelity DNA Polymerase (25 µl total volume). A general assay and program for the conducted PCRs is given.

PCR-assay	
5 µl	5x HF/GC buffer
0.5 µl	forward primer (100 µM)
0.5 µl	reverse primer (100 µM)
0.5 µl	dNTPs (10 µM)
0-10%	DMSO (depending on the PCR)
0.5 µl	Phusion High-Fidelity DNA Polymerase (2 U/µl)
10 ng 1 µg	plasmid DNA or genomic DNA
add to 25µl	ddH_20

PCR-program			
initial denaturation	95 °C	2 min	
denaturation	95 °C	10 sec	25-35x
annealing	depending on primer	30 sec	
elongation	72 °C	15 sec per 1 kbp	
final elongation	72 °C	10 min	

Restriction enzyme digestion and modification of DNA

Restriction enzyme digestion was used to linearize plasmids for transfection, to analyze the correct integration of an insert into a vector after transformation and to generate suitable overhangs of DNA fragments for the ligation of insert and backbone. The digestion was conducted according to the manufacturer's instructions. If the restriction site overhangs of insert and backbone were not compatible for subsequent cloning, 5' overhangs were filled up or 3' overhangs removed. For this purpose, the Klenow fragment (Thermo Fisher Scientific, USA) was used, essentially following the manufacturer's protocol. In order to avoid the religation of the digested backbone, the phosphate groups were removed with the thermosensitive alkaline phosphatase CIAP (Thermo Fisher Scientific, USA). PCR fragments

were phosphorylated prior to the ligation into a backbone using the T4 Polynucleotide Kinase (PNK*;* Thermo Fisher Scientific, USA). Both enzymes, CIAP and PNK, were used according to the manufacturer's instructions. For cloning, the generated and modified DNA fragments were separated via gel electrophoresis, extracted and the DNA content determined as described above. Subsequently, the T4-ligase (Thermo Fisher Scientific, USA) was used to ligate the fragment into the linearized plasmid with complement overhangs and/or blunt ends. For this purpose, 50 ng of the backbone plasmid were used and the molar ratio of insert to backbone amounted 3:1. Ligation was preferentially performed over night at 16°C or for two hours at room temperature. Then, the ligation mixture was directly used for transformation as described above.

Isopropanol precipitation of DNA

DNA can be isolated from aqueous solutions via isopropanol precipitation. For this purpose, the same volume of isopropanol is added to the solved DNA as well as 3 M sodium acetate (1/10x of the total volume). After mixing the components by inverting the tube, the samples were centrifuged (20,000x *g*, 20 min, 4°C) and the supernatant discarded. Then, the DNA pellet was washed two times with 1 ml 70% ethanol (20,000x *g*, 5 min, 4°C), air-dried and eluted in an appropriate volume of water or TE-buffer. If the precipitated DNA was used for the transfection of trypanosomes, the ethanol was discarded after the last washing step under sterile conditions and the dried pellet eluted in 10 µl of sterile water.

Southern blot analyses

Phenol/chloroform extracted genomic DNA of trypanosomes (10 µl) was digested with appropriate enzymes. The samples were separated on a 0.8% agarose gel together with the *GeneRuler DNA Ladder Mix* (Thermo Fisher Scientific, USA) as standard for DNA size. The ethidium bromide stained gel was documented with a gel documentation system and washed with distilled water. Afterwards, the gel was depurinated in 0.25 M HCl for 15 minutes and the DNA denaturated with 0.5 M NaOH/ 1.5 M NaCl for 30 minutes. Subsequently, the gel was incubated for 30 minutes in 1 M Tris-HCl (pH 7.4)/1.5 M NaCl for neutralization. Then, the DNA was transferred from the agarose gel to a membrane (Amersham Hybond-N; GE Healthcare, UK) over night in 20x SSC by capillary forces. The DNA was fixated to the membrane via UV-crosslinking (Stratalinker 1800, Stratagene, USA; autocrosslink function: 1200x100 µJ/cm^2) and subsequent incubation at 80°C for one hour. The DNA fragments were detected with radioactive labeled probes as described below (chapter 5.2.4.2 Detection of RNA (or DNA) on membranes). Then, DNA was visualized via autoradiography. For this purpose, the membrane was placed on an x-ray film, which was developed after at least one week of exposure.

5.2.4.2 RNA analyses

Isolation of RNA from trypanosomes

Trypanosome total RNA was isolated from 1x10^8 cells using the *RNeasy Mini Kit* (QIAGEN, NL). For this purpose, the cells were harvested as described above and washed once in 2 ml FCS-free HMI-9 (1,400x *g*, 10 min, 4°C). The medium was discarded and the cell pellet thoroughly resuspended in a volume of 20-50 µl. Immediately afterwards, the samples were frozen in liquid nitrogen and stored at -80°C until the RNA extraction was performed.

For RNA extraction, 600 µl RLT buffer containing 6 µl β-mercaptoethanol were added to one frozen sample and mixed by pipetting up and down at 37°C. Next, the sample was mixed with 600 µl 70% ethanol, the lysate was loaded on a column of the *RNeasy Mini Kit* (QIAGEN, NL) and centrifuged (8,000x *g*, 30 sec, RT). The flow-through was collected in a 15 ml falcon and stored at 4°C to precipitate the proteins later on (chapter 5.2.4.3 Isolation of protein extracts from trypanosomes). Then, the column was washed once with 350 µl *RW1 buffer* and two times with 500 µl *RPE buffer* (8,000x *g*, 30 sec, RT). The column was dried via centrifugation (8,000x *g*, 1 min, RT) and the RNA eluted two times with 30 µl RNAse free H_2O (8,000x *g*, 1 min, RT). RNA concentration and purity was determined by measuring the absorption of the solution at 260 nm and 280 nm using the *Tecan Infinite M200* reader (Tecan Group, CH). The RNA samples were stored at -80°C.

For RNA sequencing, residual DNA was removed using the *RNase-Free DNase Set* (QIAGEN, NL) essentially following the manufacturer's instructions. RNA samples (1 µg) of non-induced parasites and cells induced for 24 hours of a growth-arrested clone of the $GFP^{ESpro}A1.1^{ES}121^{tet}$ cell line were analyzed. GATC Biotech AG (Konstanz, DE) carried out the library construction and the sequencing (50bp read length, single end, at least 30 million reads). The mRNA sequences were aligned to the genome of the monomorphic *T. brucei brucei* strain TREU 927 by Frank Förster.

cDNA synthesis

Single stranded cDNA was synthesized using total RNA as template to analyze via PCR if specific mRNAs are expressed and to determine their sequence. For this purpose, the cDNA was generated using the *RevertAid First Strand cDNA Synthesis Kit* (Thermo Fisher Scientific, USA) according to the manufacturer's instructions.

Northern blot analyses

RNA samples were analyzed via Northern blotting and radioactive labeling for the quantifications of mRNAs with a low abundance. In this case, 7.2 µl glyoxal mixture were added to 4 µg total RNA in a volume of 4 µl H_2O. The samples were incubated at 50°C for 40 minutes in order to denaturate the RNA. Subsequently, the RNA samples were separated via

gel electrophoresis according to their size. For this purpose, 1.4 g agarose (Ultra Pure Agarose; Thermo Fisher Scientific, USA) were dissolved in 100 ml H_2O and cooled down on a shaker to 50°C. Then, 2 ml 50x RNA buffer were added to the liquid agarose, thoroughly mixed and poured into a gel chamber. The loaded samples were separated in 1x RNA buffer for 90 minutes at a potential of 10 V/cm. The RNA was transferred from the agarose gel to a nitrocellulose membrane (Amersham Hybond-N; GE Healthcare, UK) over night in 20x SSC by capillary forces. The RNA was fixated to the membrane via UV-crosslinking (Stratalinker 1800, Stratagene, USA; autocrosslink function: 1200x100 µJ/cm^2) and subsequent incubation at 80°C for one hour.

RNA dot blot analyses

RNA samples were analyzed via dot blotting and fluorescent labeling for the quantifications of highly abundant mRNAs. For this purpose, a nitrocellulose membrane (*Amersham Hybond-N*; GE Healthcare, UK) was placed in a dot blot apparatuses (MiniFold dot blotter; Schleicher und Schuell, DE) and 200 µl 10x SSC were loaded to each well. Then, a vacuum was applied to suck the buffer through the membrane. The samples containing 3 µg total RNA were prepared as for Northern blot analyses. Then, each samples was mixed with 40 µl 10x SSC and one sample was loaded to one well of the dot blotter. The vacuum was applied again to suck the samples through the membrane and each well was washed afterwards with 200 µl 10x SSC. Subsequently, the RNA was fixated to the membrane as described for the Northern blot analyses.

Detection of RNA (or DNA) on membranes

For the visualization of mRNAs with a low abundance (or DNA), the probes were labeled with ^{32}P(α)dCTP using the *DecaLabel DNA labeling Kit* (Thermo Fisher Scientific, USA) according to the manufacturer's instructions. The probes for radioactive labeling were enzyme digested DNA fragments of a plasmid, which were extracted from an agarose gel. The membranes were incubated at 65°C for one hour with the hybridization solution under vertical rotation prior staining. After the generation of the radioactive labeled probes, they were directly added to the hybridization solution. Then, the radioactive labeled probe and the membrane were incubated over night at 65°C under vertical rotation. Afterwards, the membranes were washed two times with the North blot washing solution and dried between two whatman papers. The dried membrane was placed on a phosphor imaging plate for at least four days and then documented with a phosphor imager. The rRNA was stained with an infrared labeled probe as a loading control.

For the fluorescent labeling of highly abundant mRNAs, the membranes were incubated at 42°C for one hour with the hybridization solution under vertical rotation prior staining. Then, 10 nM of the fluorescently labeled probe was added and incubated with the membrane

overnight at 42°C. The next day, the blots were washed two times for 20 minutes with the Northern blot washing solution at room temperature. The stained blots were dried between two whatman paper, wrapped in aluminum foil and stored at room temperature. The dried blots were documented with the *LI-COR Odyssey* scanner and analyzed with the corresponding software (*Image studio Lite*; LI-COR Bioscience, USA). For quantification, the signal of the mRNA of interest was normalized to the signal of the loading control. To compare *VSG* transcript levels, the normalized values are given relative to the normalized *VSG* levels of parasites natively expressing this variant (100%).

Single cell mRNA FISH

The *QuantiGene ViewRNA ISH Cell Assay Kit* (Affymetrix, USA) was recently implemented in trypanosomes by Susanne Kramer to detect single mRNA molecules within individual cells (Fritz et al., 2015). Using this method, mRNAs with a low abundance can be accurately quantified in different cell cycle stages. For the assay, 1x 10^7 trypanosomes were harvested per sample as described above and washed two times with TDB. The cells were fixed in 4% pFA for ten minutes at room temperature on a rotary table. The fixed trypanosomes were washed two times with PBS (1,400x *g*, 5 min, RT) and resuspended in 100 µl PBS. Subsequently, the trypanosomes were spread on a poly-l-lysine-coated slide (within hydrophobic circles) and allowed to settle for 30 minutes. Next, the slides were washed once with PBS and 50 µl *detergent solution QC* was added to each sample. After incubation for five minutes at room temperature, the slides were washed twice for five minutes with PBS. Then, 100 µl of a protease solution (1:1,600 in PBS) was added to each circle and incubated for 15 minutes at 25°C. After washing the slides three times for three minutes with PBS, 100 µl of the probes (diluted 1:100 in the *Probe Set Diluent*) were added to each sample and incubated for three hours at 40°C in a humid chamber. Then, the slides were washed three times for five minutes with 0.1x SSC/0.1% (w/v) SDS and once for two minutes with the Affymetrix wash buffer. Afterwards, the signal was amplified using first the *PreAmplifier Mix solution*, second the *Amplifier Mix solution* and finally labeled with the *Label Probe Mix solution*. For each step, 100 µl of the solutions was added to one sample and incubated for half an hour at 40°C in a humid chamber. After each incubation step, the slides were washed three times for five minutes with 0.1x SSC/0.1% (w/v) SDS and once for two minutes with the Affymetrix wash buffer. Next, 100 µl DAPI (1 µg/ml) was added to each circle and incubated for five minutes at room temperature. Then, the slides were washed three times for five minutes with PBS and embedded with *Prolong Gold antifade* (Thermo Fisher Scientific, USA). After drying over night at room temperature, the slides were stored at 4°C in the dark until the acquisition of the images was conducted.

Using the above described protocol, following points need to be taken into consideration for the experimental set-up. Protease digestion may vary between the slides and the experiments,

wherefore only samples from the same slide can be compared with each other. Moreover, on one slide only one probe or probe combination can be applied as the pap pen will vanish during the assay and thus the probe distributes between the different samples.

5.2.4.3 Protein analyses

Isolation of proteins extracts from trypanosomes

Trypanosomes were harvested as described above to generate protein extracts. The cells were washed two times with TDB and resuspended in 1x sample buffer to a concentration of 1x or 2x 10^5 cell equivalents/µl. The protein samples were boiled at 100°C for five minutes and stored at -80°C until the analyses were conducted.

In order to isolate total proteins after RNA isolation, 5 ml ice cold acetone was added to the collected flow-through and incubated at -20°C for 30 minutes. Next, the solution was centrifuged (20,000x *g*, 10 min, 4°C), the supernatant discarded and the protein pellet air dried at room temperature. Then, the pellet was resuspended in 1x sample buffer to a concentration of 2x 10^5 cell equivalents/µl and boiled at 100°C for five minutes. The protein samples were stored at -80°C until the analyses were conducted.

Discontinuous SDS polyacrylamide gel electrophoresis

Discontinuous SDS polyacrylamide gel electrophoresis (SDS PAGE) with 1x Lämmli buffer as running buffer was used to separate proteins according to their molecular weight in a one dimensional gel. Gels containing 12.5% acrylamid/bisacrylamid were used to resolve proteins with a size between 20-150 kDa (VSG/PFR or LipDH/PFR). Proteins with a size between 5-70 kDa were separated on a 20% SDS gel (Histone/PFR). If the gel was subsequently stained with Coomassie Blue to visualize all proteins, 1x 10^6 cells per lane were separated on a 12.5% SDS gel. If specific proteins were analyzed via Western blotting, the amount of loaded cells depended on the abundance of the analyzed proteins. For highly abundant proteins like VSGs, 5x 10^5 cell equivalents were loaded, 2x 10^6 cell equivalents were used for proteins with a lower abundance and when the protein was barely detectable 5x 10^6 cell equivalents. The *PageRuler™Prestained Protein Ladder* (Thermo Fisher Scientific, USA) was used as standard for the size of the proteins.

Staining of proteins in SDS gels

Total proteins separated via SDS PAGE were stained with Coomassie Blue. For this purpose, the gels were incubated with the staining solution for 20 minutes. Next, the gels were incubated in the destaining solution until no background staining was visible and documented with the *LI-COR Odyssey* scanner (LI-COR Bioscience, USA).

Western blot analyses

For the analyses and the quantification of specific proteins, total proteins were first transferred from the SDS gel to a nitrocellulose membrane (*Amersham Protran 0.45 µm NC*; GE Healthcare, UK) using a semi-dry transfer technique. For this purpose, 12 whatman papers at the size of the SDS gel were soaked with blotting buffer (1x Lämmli buffer containing 20% methanol). The blot was assembled as followed (cathode to anode): 6x soaked whatman paper, membrane, gel, 6x soaked whatman paper. The transfer was conducted at a current intensity of 0.8 mA/ (cm^2 of the gel) for 90 minutes. Subsequently, specific proteins could be detected via antibody staining as described below.

Protein dot blot analyses

Protein dot blotting was used to immobilize proteins on a membrane without separating them according to the size. This direct transfer of proteins on a membrane has the advantage that no changes in the protein concentration due to an inaccurate transfer can occur. For this purpose, 3 µl of a protein sample containing 6x 10^5 cell equivalents were boiled for five minutes at 100°C and afterwards pipetted on a nitrocellulose membrane and air dried at room temperature. Subsequently, specific proteins could be detected via antibody staining as described below.

Detection of proteins on nitrocellulose membranes

In order to detect specific proteins via antibody staining, unspecific binding sites of the membranes were in general blocked with 5% (w/v) milk powder in PBS over night at 4°C or for one hour at room temperature. Subsequently, the blots were incubated with the primary antibodies, which were appropriately diluted in 1% (w/v) milk powder/ 0.1% (v/v) Tween-20 in PBS, for one hour at room temperature. Then, the membranes were washed three times for ten minutes with 0.2% (v/v) Tween-20 in PBS. Next, the infrared-labeled secondary antibodies were diluted 1:10,000 in 1% (w/v) milk powder/ 0.1% (v/v) Tween-20 in PBS and the dilution was added to the membranes. After incubation for one hour at room temperature, the blots were washed three times for ten minutes with 0.2% (v/v) Tween-20 in PBS. The following deviations were made for the detection of H3K76me3: membranes were blocked with 3% (w/v) BSA in PBS and antibodies were diluted 0.1% (v/v) Tween-20 in PBS. The stained membranes were dried between two whatman paper, wrapped in aluminum foil and stored at room temperature. The dried blots were documented with the *LI-COR Odyssey* scanner and analyzed with the corresponding software (*Image studio Lite*; LI-COR Bioscience, USA). For quantification, the signal of the protein of interest was normalized to the signal of the loading control. To compare VSG levels, the normalized values are given relative to the normalized VSG levels of parasites natively expressing this variant (100%).

5.2.5 Light microscopy analyses

Immobilization of trypanosomes

Parasites were immobilized via embedding in gelatine to visualize the ER. For this purpose, 5x 10^6 cells were harvested, washed with TDB and resuspended in 10 µl TDB. Then, 3 µl of the cell suspension were gently mixed with 5 µl 10% preheated gelatine (37°C). The mixture was pipetted on a cover slip (placed in a sample holder) and then a second cover slip was placed on top. Subsequently, the apparatus was liquid impermeable sealed and water was added. The sample holder was cooled down to 20°C for at least 15 minutes before the image acquisition was initiated.

Fixation of trypanosomes

Trypanosomes were fixated using three different methods. For methanol fixation, cells (obtained from tsetse flies) were spread on a poly-l-lysine-coated slide (within hydrophobic circles) and air-dried. Subsequently, the slides were submerged for 30 seconds in ice cold methanol and washed once with PBS. After rehydrating the parasites for ten minutes in PBS, immunostaining with an antibody against PFR was performed as described below. Cultured parasites were harvested as described above, washed two times with TDB and carefully resuspended prior the addition of the fixative. Trypanosomes were either fixated with paraformaldehyde alone or with 2% (w/v) paraformaldehyde and 0.05% (v/v) glutaraldehyde. Except for the fixation of PAD1, the cells were washed afterwards two times with PBS and carefully resuspended in an appropriate volume of PBS. The used fixation conditions are shown in table 14 for each application.

Table 14: Fixation conditions used in this work. Represented are different fixation conditions, which were used to visualize certain structures or proteins. The used fixative, temperature and duration of fixation are given. It is also indicated when and how the parasites were stained. Abbreviations are explained below.

Structure/Protein	Fixative	Temperature	Duration	Staining
mitochondria	2% pFA, 0.05% GA	RT	15 min	pf in culture
GFP	2% pFA, 0.05% GA	RT	15 min	-
EP1	2% pFA, 0.05% GA	4°C	at least 2 h	af in tube
VSG	2% pFA	RT	15-30 min	af in tube/ on slide
PFR	methanol	-20°C	30 sec	af on slide
PAD1	3% pFA	RT	10 min	af on slide

Af, after fixation; GA, glutaraldehyde in % (v/v); h; hours; min, minutes; PAD1, protein associated with differentiation 1; pf, prior fixation; pFA, paraformaldehyde in % (w/v); PFR, paraflagellar rod; RT, room temperature; sec, seconds; VSG, variant surface glycoprotein

Fluorescent staining

In order to stain the mitochondria, 50 nM *MitoTracker® Red CMXRos* (Thermo Fisher Scientific, USA) were added directly to the culture and incubated in the dark for 20 minutes at 37 °C. Subsequently, the parasites were harvested and fixated as described above.

To detect the VSGs via flow cytometry, 1x 10^6 parasites were harvested and stained alive with an appropriate antibody against VSG 221 (Figueiredo et al., 2008). During the assay, the cells were always kept cold to avoid the internalization of the antibody bound VSGs. First, the harvested trypanosomes were incubated with the primary antibody diluted in HMI-9 for one hour at 4°C on a rotary table. Then, the cells were washed two times with pre-cooled HMI-9. Subsequently, the parasites were incubated for ten minutes with the secondary antibody (1:2,000 in HMI-9 diluted). Next, the stained cells were washed two times and analyzed with the flow cytometer (*BD Bioscience FACSCalibur*, BD Biosience, USA).

Immunostaining was conducted in suspension to be able to use the stained cells for flow cytometric analyses as well as microscopic analyses. For this purpose, at least 2x 10^7 cells were harvested and fixated as described above. The washed fixated cells were blocked with 1% (w/v) bovine serum albumin (BSA) in PBS for one hour at room temperature on a rotary table. Then, the cells were washed one time with 0.1% (w/v) BSA in PBS and carefully resuspended in a residual volume as small as possible. The primary antibodies were appropriately diluted in 0.1% (w/v) BSA in PBS and added to the cells. After incubation for one hour at room temperature on a rotary table, the cells were washed two times with 0.1% (w/v) BSA in PBS and carefully resuspended in a residual volume as small as possible. Then, the secondary antibodies (anti-rabbit or anti-mouse IgG Alexa647 or Alexa594) were diluted 1:500 in 0.1% (w/v) BSA in PBS and incubated with the cells for one hour at room temperature on a rotary table. Subsequently, the cells were washed two times with PBS and stored in 1 ml PBS in the dark at 4°C until the flow cytometric or microscopic analyses was conducted.

Immunostaining was directly conducted on slides for the detection of VSGs. For this purpose, the fixated cells were resuspended in PBS to a density of 3x 10^4 cells/ml. Next, 100 µl were spread on a poly-l-lysine-coated slide within hydrophobic circles. The following steps were performed in a humid chamber to avoid the drying of the samples. The slides were incubated for 15 minutes at room temperature to allow the parasites to settle. Then, the slides were washed once with PBS and incubated with 1% (w/v) BSA in PBS for 30 minutes in order to prevent unspecific binding of the antibodies. The primary antibodies were appropriately diluted in 0.1% (w/v) BSA in PBS and added to the samples after the removal of the blocking agent. After one hour of incubation at room temperature, the slides were washed three times for five minutes in PBS. Then, the samples were incubated in the dark with the Alexa488 and/or Alexa594 conjugated secondary antibodies (diluted 1:500 in 0.1% (w/v) BSA in PBS) for one

hour at room temperature. Next, the slides were washed three times for five minutes with PBS. After the second wash, the samples were incubated for three minutes with DAPI (1 µg/ml) to stain the DNA. Finally, the samples were mounted with *Vectashield* (BIOZOL; DE). For the PFR staining of methanol fixated cells, the same protocol was used starting with the incubation of the samples with the primary antibody in a humid after the rehydration step.

The detection of PAD1 was conducted on a slide essentially as described by Dean et al. 2009. For this, the harvested cells were resuspended in one volume vPBS (PBS containing 45.9 mM sucrose und 10 mM glucose) and the same volume of 6% (w/v) pFA was added. After ten minutes fixation at room temperature, at least 5 ml vPBS was added to the trypanosomes to wash them (1,400x *g*, 10 min, 4°C). Then, the cells were resuspended in vPBS to a density of $3x10^4$ cells/µl and 100 µl was added to a poly-l-lysine-coated slide. The parasites were allowed to adhere to the slide for 20 minutes in a humid chamber. After washing the slide once with PBS, the cells were permeabilized with 0.05% Triton X-100 in PBS for 20 minutes. Subsequently, the slides were washed two times with PBS for five minutes and incubated with 20% (v/v) FCS in vPBS in order to prevent unspecific binding of the antibody. Then, the primary antibody diluted in 20% (v/v) FCS in vPBS was added to the cells and incubated for one hour at room temperature. After washing the slides two times for five minutes with PBS, the samples were incubated in the dark with the Alexa594 conjugated secondary antibody (diluted 1:500 in 20% (v/v) FCS in vPBS). Lastly, the samples were washed, DAPI- stained and embedded as described above.

Acquisition of fluorescently stained cells and data analyses

Images were recorded with the automated *iMIC* wide field fluorescence microscope (FEI-TILL Photonics, DE). This microscope was equipped with a CCD camera (Sensicam qe, pixel size 6.45 µm, PCO, DE) and the filter cubes *ET-mCherry-Texas-Red*, *ET-GFP* and *DAPI* (Chroma Technology CORP, USA). Either 100x (NA 1.4) or 60x (NA 1.45) objectives (Olympus, DE) were used for the acquisition of Z-stacks, which was controlled with the *'Live acquisition*' software (TILL Photonics, DE). For each stack, 100 Z-planes were recorded at a step size of 100 nm. Afterwards, the analyses of the stacks were performed using the *ImageJ* software (National Institutes of Health, USA). For illustrative purposes, the method 'Max Intensity' was used to project the slices to one plane. Prior signal quantification and image processing, stacks were deconvolved with the *Huygens Essential* software (Scientific Volume Imaging B. V., NL). Then, the deconvolved slices were projected to one plane with the method 'Sum Slices' of *ImageJ*. The fluorescence intensity of single cell was determined using the same software. To calculate the relative fluorescence intensity (RFU), the background was measured as well and subtracted from the value of the individual cells. For this purpose, the background signal was measured for the same area as for the corresponding cell in a non-fluorescent section in its vicinity. Otherwise, images were recorded with the *DMI6000B* wide field fluorescence

microscope (LEICA microsystems, DE), which was equipped with a *DFC365FX* camera (pixel size 6.45 µm, LEICA microsystems, DE). At 100x magnification, 100 Z-planes were acquired at a step size of 67 nm. Fluorescent images are shown as maximum intensity projections of 20-100 planes and differential interference contrast (DIC) images as average projections of 10-20 planes. All images were false colored (green in green, red in magenta and blue in grey) with *ImageJ*, in order to make color information's available as well for people with color vision deficiencies. To normalize the images of the VSG or EP1 immunofluorescence analyses, the minimal and maximal intensity values of the images in one figure were set to the same level in ImageJ (except in Figure 10 for the 7 days induction). Likewise, the signal of the green fluorescent stumpy reporter (GFP:PAD1$_{UTR}$) was set to same values using *ImageJ* in the images of one figure.

Flow cytometric analyses were conducted with a *BD Bioscience FACSCalibur* Flow Cytometer. Either the GFP signal of living cells, antibody-stained VSGs of living parasites or antibody-stained EP1 of fixated trypanosomes were detected (staining was conducted as described above). The number of counted parasites is given within the results section in the respective figure legends. The data were analyzed with the *BD CellQuest Pro Software* (BD Biosience, USA).

6 Bibliography

Acosta-Serrano, A., Vassella, E., Liniger, M., Renggli, C.K., Brun, R., Roditi, I., and Englund, P.T. (2001). The surface coat of procyclic *Trypanosoma brucei*: Programmed expression and proteolytic cleavage of procyclin in the tsetse fly. Proc. Natl. Acad. Sci. *98*, 1513–1518.

Aitcheson, N., Talbot, S., Shapiro, J., Hughes, K., Adkin, C., Butt, T., Sheader, K., and Rudenko, G. (2005). VSG switching in *Trypanosoma brucei*: antigenic variation analysed using RNAi in the absence of immune selection. Mol. Microbiol. *57*, 1608–1622.

Akol, G.W., and Murray, M. (1982). Early events following challenge of cattle with tsetse infected with *Trypanosoma congolense*: development of the local skin reaction. Vet. Rec. *110*, 295–302.

Aksoy, E., Vigneron, A., Bing, X., Zhao, X., O'Neill, M., Wu, Y., Bangs, J.D., Weiss, B.L., and Aksoy, S. (2016). Mammalian African trypanosome VSG coat enhances tsetse's vector competence. Proc. Natl. Acad. Sci. *113*, 6961–6966.

Alsford, S., and Horn, D. (2012). Cell-cycle-regulated control of *VSG* expression site silencing by histones and histone chaperones ASF1A and CAF-1b in *Trypanosoma brucei*. Nucleic Acids Res. *40*, 10150–10160.

Alsford, S., Kawahara, T., Isamah, C., and Horn, D. (2007). A sirtuin in the African trypanosome is involved in both DNA repair and telomeric gene silencing but is not required for antigenic variation. Mol. Microbiol. *63*, 724–736.

Amiguet-Vercher, A., Pérez-Morga, D., Pays, A., Poelvoorde, P., Van Xong, H., Tebabi, P., Vanhamme, L., and Pays, E. (2004). Loss of the mono-allelic control of the *VSG* expression sites during the development of *Trypanosoma brucei* in the bloodstream. Mol. Microbiol. *51*, 1577–1588.

Angara, T.-E.E., Ismail, A.A., and Ibrahim, A.M. (2014). An overview on the economic impacts of animal trypanosomiasis. Glob. J. Res. Anal. *3*, 275–276.

Ansorge, I., Steverding, D., Melville, S., Hartmann, C., and Clayton, C. (1999). Transcription of "inactive" expression sites in African trypanosomes leads to expression of multiple transferrin receptor RNAs in bloodstream forms. Mol. Biochem. Parasitol. *101*, 81–94.

Archer, S.K., Luu, V.D., De Queiroz, R.A., Brems, S., and Clayton, C. (2009). *Trypanosoma brucei* PUF9 regulates mRNAs for proteins involved in replicative processes over the cell cycle. PLoS Pathog. *5*, e1000565.

Aresta-Branco, F., Pimenta, S., and Figueiredo, L.M. (2015). A transcription-independent epigenetic mechanism is associated with antigenic switching in *Trypanosoma brucei*. Nucleic Acids Res. *44*, 3131–3146.

Bangs, J.D., Brouch, E.M., Ransom, D.M., and Roggy, J.L. (1996). A soluble secretory reporter system in *Trypanosoma brucei*. Studies on endoplasmic reticulum targeting. J. Biol. Chem. *271*, 18387–18393.

Barnwell, E.M., van Deursen, F.J., Jeacock, L., Smith, K. a, Maizels, R.M., Acosta-Serrano, A., and Matthews, K. (2010). Developmental regulation and extracellular release of a *VSG* expression-site-associated gene product from *Trypanosoma brucei* bloodstream forms. J. Cell Sci. *123*, 3401–3411.

Barquilla, A., Saldivia, M., Diaz, R., Bart, J.-M., Vidal, I., Calvo, E., Hall, M.N., and Navarro, M. (2012). Third target of rapamycin complex negatively regulates development of quiescence in *Trypanosoma brucei*. Proc. Natl. Acad. Sci. *109*, 14399–14404.

Batram, C. (2009). Functional analysis of the variant surface glycoprotein 3' untranslated region in *Trypanosoma brucei*. Diploma Thesis.

Batram, C. (2013). Die Kontrolle der monoallelen Expression, antigenen Variation und Entwicklung in *Trypanosoma brucei*. Dissertation.

Batram, C., Jones, N.G., Janzen, C.J., Markert, S.M., and Engstler, M. (2014). Expression site attenuation mechanistically links antigenic variation and development in *Trypanosoma brucei*. Elife *3*, e02324.

Becker, M., Aitcheson, N., Byles, E., Wickstead, B., Louis, E., and Rudenko, G. (2004). Isolation of the repertoire of *VSG* expression site containing telomeres of *Trypanosoma brucei* 427 using transformation-associated recombination in yeast. Genome Res. *14*, 2319–2329.

Benmerzouga, I., Concepción-acevedo, J., Kim, H., Anthula, V., Cross, G.A.M., Klingbeil, M.M., and Li,

B. (2014). *Trypanosoma brucei* Orc1 is essential for nuclear DNA replication and affects both *VSG* silencing and switching. Mol. Microbiol. *87*, 196–210.

Berberof, M., Vanhamme, L., Tebabi, P., Pays, A., Jefferies, D., Welburn, S., and Pays, E. (1995). The 3'-terminal region of the mRNAs for VSG and procyclin can confer stage specificity to gene expression in *Trypanosoma brucei*. EMBO J. *14*, 2925–2934.

Bernards, A., Lex, H.T., Van der Ploeg, A., Frasch, C.C., Borst, P., Boothroyd, J.C., Coleman, S., and Cross, G.A.M. (1981). Activation of trypanosome surface glycoprotein genes involves a duplication-transposition leading to an altered 3′ end. Cell *27*, 497–505.

Bernards, A., Lange, T.D., Huisman, M.J., and Borst, P. (1984). Two modes of activation of a single surface antigen gene of *Trypanosoma brucei*. Cell *36*, 163–170.

Berriman, M., Ghedin, E., Hertz-Fowler, C., Blandin, G., Renauld, H., Bartholomeu, D.C., Lennard, N.J., Caler, E., Hamlin, N.E., Haas, B., et al. (2005). The genome of the African trypanosome *Trypanosoma brucei*. Science *309*, 416–422.

Bitter, W., Gerrits, H., Kieft, R., and Borst, P. (1998). The role of transferrin-receptor variation in the host range of *Trypanosoma brucei*. Nature *391*, 499–502.

Blasco, M.A. (2007). The epigenetic regulation of mammalian telomeres. Nat Rev Genet *8*, 299–309.

Blum, M.L., Down, J.A., Gurnett, A.M., Carrington, M., Turner, M.J., and Wiley, D.C. (1993). A structural motif in the variant surface glycoproteins of *Trypanosoma brucei*. Nature *362*, 603–609.

Borst, P., and Ulbert, S. (2001). Control of VSG gene expression sites. Mol. Biochem. Parasitol. *114*, 17–27.

Brandenburg, J., Schimanski, B., Nogoceke, E., Nguyen, T.N., Padovan, J.C., Chait, B.T., Cross, G.A.M., and Günzl, A. (2007). Multifunctional class I transcription in *Trypanosoma brucei* depends on a novel protein complex. EMBO J *26*, 4856–4866.

Breidbach, T., Ngazoa, E., and Steverding, D. (2002). *Trypanosoma brucei*: *in vitro* slender-to-stumpy differentiation of culture-adapted, monomorphic bloodstream forms. Exp. Parasitol. *101*, 223–230.

Brems, S., Guilbride, D.L., Gundlesdodjir-Planck, D., Busold, C., Luu, V.D., Schanne, M., Hoheisel, J., and Clayton, C. (2005). The transcriptomes of *Trypanosoma brucei* Lister 427 and TREU927 bloodstream and procyclic trypomastigotes. Mol. Biochem. Parasitol. *139*, 163–172.

Broadhead, R., Dawe, H.R., Farr, H., Griffiths, S., Hart, S.R., Portman, N., Shaw, M.K., Ginger, M.L., Gaskell, S.J., McKean, P.G., et al. (2006). Flagellar motility is required for the viability of the bloodstream trypanosome. Nature *440*, 224–227.

Brown, R.C., Evans, D.A., and Vickerman, K. (1973). Changes in oxidative metabolism and ultrastructure accompanying differentiation of the mitochondrion in *Trypanosoma brucei*. Int. J. Parasitol. *3*, 691–704.

Bruce, D. (1895). Preliminary report on the tsetse fly disease or nagana in Zululand Durban. Bennett and Davis *Durban*, 18 pp.

Bruce, D., Harvey, D., Hamerton, A.E., Davey, J.B., and Bruce, L. (1912). The morphology of the trypanosome causing disease in nan in Nyasaland. Proc. R. Soc. London. Ser. B *85*, 423–433.

Brun, R. (1981). Stimulating effect of citrate and *cis*-aconitate on the transformation of *Trypanosoma brucei* bloodstream forms to procyclic forms *in vitro*. Zeitschrift Für Parasitenkd. *66*, 17–24.

Brun, R., Blum, J., Chappuis, F., and Burri, C. (2010). Human African trypanosomiasis. Lancet *375*, 148–159.

Capewell, P., Cren-Travaillé, C., Marchesi, F., Johnston, P., Clucas, C., Benson, R.A., Gorman, T.A., Calvo-Alvarez, E., Crouzols, A., Jouvion, G., et al. (2016). The skin is a significant but overlooked anatomical reservoir for vector-borne African trypanosomes. Elife e17716.

Cestari, I., and Stuart, K. (2015). Inositol phosphate pathway controls transcription of telomeric expression sites in trypanosomes. Proc. Natl. Acad. Sci. *112*, E2803–E2812.

Chanie, M., Adula, D., and Bogale, B. (2013). Socio-economic assessment of the impacts of trypanosomiasis on cattle in Girja district , southern Oromia region , southern Ethiopia. Acta Parasitol. Glob. *4*, 80–85.

Chung, C.T., Niemela, S.L., and Miller, R.H. (1989). One-step preparation of competent *Escherichia*

coli: transformation and storage of bacterial cells in the same solution. Proc. Natl. Acad. Sci. *86*, 2172–2175.

Clayton, C. (2013). The regulation of trypanosome gene expression by RNA-Binding proteins. PLoS Pathog. *9*, e1003680.

Conway, C., McCulloch, R., Ginger, M.L., Robinson, N.P., Browitt, A., and David Barry, J. (2002). Ku is important for telomere maintenance, but not for differential expression of telomeric *VSG* genes, in African trypanosomes. J. Biol. Chem. *277*, 21269–21277.

Cross, G.A. (1975). Identification, purification and properities of clone-specific glycoprotein antigenes constituting the surface coat of *Trypanosoma brucei*. Parasitology *71*, 393–417.

Cross, G.A.M., Kim, H.S., and Wickstead, B. (2014). Capturing the variant surface glycoprotein repertoire (the VSGnome) of *Trypanosoma brucei* Lister 427. Mol. Biochem. Parasitol. *195*, 59–73.

de Lange, T. (2005). Shelterin: The protein complex that shapes and safeguards human telomeres. Genes Dev. *19*, 2100–2110.

de Lange, T., Kooter, J.M., Michels, P.A.M., and Borst, P. (1983). Telomere conversion in trypanosomes. Nucleic Acids Res. *11*, 8149–8165.

Dean, S., Marchetti, R., Kirk, K., and Matthews, K.R. (2009). A surface transporter family conveys the trypanosome differentiation signal. Nature *459*, 213–217.

Deitsch, K.W., Lukehart, S.A., and Stringer, J.R. (2009). Common strategies for antigenic variation by bacterial, fungal and protozoan pathogens. Nat. Rev. Microbiol. *7*, 493–503.

Dejung, M., Subota, I., Bucerius, F., Dindar, G., Freiwald, A., Engstler, M., Boshart, M., Butter, F., and Janzen, C.J. (2016). Quantitative proteomics uncovers novel factors involved in developmental differentiation of Trypanosoma brucei. PLoS Pathog. *12*, e1005439.

Delauw, M.F., Pays, E., Steinert, M., Aerts, D., Van Meirvenne, N., and Le Ray, D. (1985). Inactivation and reactivation of a variant-specific antigen gene in cyclically transmitted *Trypanosoma brucei*. EMBO J. *4*, 989–993.

Denninger, V., and Rudenko, G. (2014). FACT plays a major role in histone dynamics affecting *VSG* expression site control in *Trypanosoma brucei*. Mol. Microbiol. *94*, 945–962.

Denninger, V., Fullbrook, A., Bessat, M., Ersfeld, K., and Rudenko, G. (2010). The FACT subunit TbSpt16 is involved in cell cycle specific control of *VSG* expression sites in *Trypanosoma brucei*. Mol. Microbiol. *78*, 459–474.

Devlin, R., Marques, C.A., Paape, D., Prorocic, M., and Zurita-leal, A.C. (2016). Mapping replication dynamics in *Trypanosoma brucei* reveals a link with telomere transcription and antigenic variation. Elife *5*, e12765.

Dindar, G., Anger, A.M., Mehlhorn, C., Hake, S.B., and Janzen, C.J. (2014). Structure-guided mutational analysis reveals the functional requirements for product specificity of DOT1 enzymes. Nat. Commun. *5*, 5313.

Droll, D., Minia, I., Fadda, A., Singh, A., Stewart, M., Queiroz, R., and Clayton, C. (2013). Post-transcriptional regulation of the trypanosome heat shock response by a zinc finger protein. PLoS Pathog. *9*, e1003286.

DuBois, K.N., Alsford, S., Holden, J.M., Buisson, J., Swiderski, M., Bart, J.M., Ratushny, A. V., Wan, Y., Bastin, P., Barry, J.D., et al. (2012). NUP-1 is a large coiled-coil nucleoskeletal protein in trypanosomes with lamin-like functions. PLoS Biol. *10*, e1001287.

Duraisingh, M.T., and Horn, D. (2016). Epigenetic regulation of virulence gene expression in parasitic protozoa. Cell Host Microbe *19*, 629–640.

Dutton, J.E. (1902). Preliminary note upon a trypanosome occurring in the blood of man. Thompson Yates Lab. Rep *4*, 455–468.

Dwinger, R.H., Rudin, W., Moloo, S.K., and Murray, M. (1988). Development of *Trypanosoma congolense*, *T. vivax* and *T. brucei* in the skin reaction induced in goats by infected *Glossina morsitans centralis*: a light and electron microscopical study. Res Vet Sci *44*, 154–163.

Engstler, M., and Boshart, M. (2004). Cold shock and regulation of surface protein trafficking convey

sensitization to inducers of stage differentiation in *Trypanosoma brucei*. Genes Dev. *18*, 2798–2811.

Engstler, M., Thilo, L., Weise, F., Grünfelder, C.G., Schwarz, H., Boshart, M., and Overath, P. (2004). Kinetics of endocytosis and recycling of the GPI-anchored variant surface glycoprotein in *Trypanosoma brucei*. J. Cell Sci. *117*, 1105–1115.

Engstler, M., Pfohl, T., Herminghaus, S., Boshart, M., Wiegertjes, G., Heddergott, N., and Overath, P. (2007). Hydrodynamic flow-mediated protein sorting on the cell surface of trypanosomes. Cell *131*, 505–515.

Fadda, A., Ryten, M., Droll, D., Rojas, F., Färber, V., Haanstra, J.R., Merce, C., Bakker, B.M., Matthews, K., and Clayton, C. (2014). Transcriptome-wide analysis of trypanosome mRNA decay reveals complex degradation kinetics and suggests a role for co-transcriptional degradation in determining mRNA levels. Mol. Microbiol. *94*, 307–326.

Fenn, K., and Matthews, K.R. (2007). The cell biology of *Trypanosoma brucei* differentiation. Curr. Opin. Microbiol. *10*, 539–546.

Ferguson, M.A., Homans, S.W., Dwek, R.A., and Rademacher, T.W. (1988). Glycosyl-phosphatidylinositol moiety that anchors *Trypanosoma brucei* variant surface glycoprotein to the membrane. Science *239*, 753–759.

Fey, K. (2011). Funktionsanalyse der C-terminalen Domäne des variablen Oberflächenglykoproteins von *Trypanosoma brucei* am Beispiel von MITat1.6. Diploma Thesis.

Figueiredo, L.M., and Cross, G. a M. (2010). Nucleosomes are depleted at the *VSG* expression site transcribed by RNA polymerase I in African trypanosomes. Eukaryot. Cell *9*, 148–154.

Figueiredo, L.M., Janzen, C.J., and Cross, G.A.M. (2008). A histone methyltransferase modulates antigenic variation in African trypanosomes. PLoS Biol. *6*, 1539–1548.

Figueiredo, L.M., Cross, G. a M., and Janzen, C.J. (2009). Epigenetic regulation in African trypanosomes: a new kid on the block. Nat. Rev. Microbiol. *7*, 504–513.

Fritz, M., Vanselow, J., Sauer, N., Lamer, S., Goos, C., Siegel, T.N., Subota, I., Schlosser, A., Carrington, M., and Kramer, S. (2015). Novel insights into RNP granules by employing the trypanosome's microtubule skeleton as a molecular sieve. Nucleic Acids Res. *43*, 8013–8032.

Futse, J.E., Brayton, K. a, Dark, M.J., Knowles, D.P., and Palmer, G.H. (2008). Superinfection as a driver of genomic diversification in antigenically variant pathogens. Proc. Natl. Acad. Sci. *105*, 2123–2127.

Gassen, A., Brechtefeld, D., Schandry, N., Arteaga-Salas, J.M., Israel, L., Imhof, A., and Janzen, C.J. (2012). DOT1A-dependent H3K76 methylation is required for replication regulation in *Trypanosoma brucei*. Nucleic Acids Res. *40*, 10302–10311.

Gerrits, H., Mußmann, R., Bitter, W., Kieft, R., and Borst, P. (2002). The physiological significance of transferrin receptor variations in *Trypanosoma brucei*. Mol. Biochem. Parasitol. *119*, 237–247.

Glover, L., and Horn, D. (2006). Repression of polymerase I-mediated gene expression at *Trypanosoma brucei* telomeres. EMBO Rep. *7*, 93–99.

Glover, L., Hutchinson, S., Alsford, S., McCulloch, R., Field, M.C., and Horn, D. (2013). Antigenic variation in African trypanosomes: the importance of chromosomal and nuclear context in *VSG* expression control. Cell. Microbiol. *15*, 1984–1993.

Glover, L., Hutchinson, S., Alsford, S., and Horn, D. (2016). VEX1 controls the allelic exclusion required for antigenic variation in trypanosomes. Proc. Natl. Acad. Sci. *113*, 7225–7230.

Goodwin, L.G. (1970). The pathology of African trypanosomiasis. Trans. R. Soc. Trop. Med. Hyg. *64*, 797–817.

Gottschling, D.E., Aparicio, O.M., Billington, B.L., and Zakian, V.A. (1990). Position effect at *S. cerevisiae* telomeres: Reversible repression of Pol II transcription. Cell *63*, 751–762.

Gräb, A. (2015). Charakterisierung von Tb427.08.510: Ein potenzieller Regulator der Expressionsstellen von *Trypanosoma brucei*. Bachelor Thesis.

Grießmann, M. (2014). Charakterisierung potentieller Regulatoren der Expressionsstelle des variablen Oberflächenproteins in *T. brucei*. Bachelor Thesis.

Grünfelder, C.G., Engstler, M., Weise, F., Schwarz, H., Stierhof, Y.-D., Morgan, G.W., Field, M.C., and Overath, P. (2003). Endocytosis of a glycosylphosphatidylinositol-anchored protein via clathrin-coated vesicles, sorting by default in endosomes, and exocytosis via RAB11-positive carriers. Mol. Biol. Cell *14*, 2029–2040.

Guizetti, J., and Scherf, A. (2013). Silence, activate, poise and switch! Mechanisms of antigenic variation in *Plasmodium falciparum*. Cell. Microbiol. *15*, 718–726.

Günzel, M. (2010). Charakterisierung des Transportweges von GPI-verankerten Proteinen in *T. brucei*. Dissertation.

Günzl, A., Kirkham, J.K., Nguyen, T.N., Badjatia, N., and Park, S.H. (2015). Mono-allelic VSG expression by RNA polymerase I in *Trypanosoma brucei*: Expression site control from both ends? Gene *556*, 68–73.

Hartel, A.J.W., Glogger, M., Guigas, G., Jones, N.G., Fenz, S.F., Weiss, M., and Engstler, M. (2015). The molecular size of the extra-membrane domain influences the diffusion of the GPI-anchored VSG on the trypanosome plasma membrane. Sci. Rep. *5*, 10394.

Hemphill, A., Lawson, D., and Seebeck, T. (1991). The cytoskeletal architecture of *Trypanosoma brucei*. J. Parasitol. *77*, 603–612.

Henning, J. (2012). Analyse der Funktion von N-Glykanen in variablen Oberflächenglykoproteinen von *Trypanosoma brucei* am Beispiel von MITat1.5. Bachelor Thesis.

Hertz-Fowler, C., Figueiredo, L.M., Quail, M. a, Becker, M., Jackson, A., Bason, N., Brooks, K., Churcher, C., Fahkro, S., Goodhead, I., et al. (2008). Telomeric expression sites are highly conserved in *Trypanosoma brucei*. PLoS One *3*, e3527.

Hirumi, H., and Hirumi, K. (1989). Continuous cultivation of *Trypanosoma brucei* blood stream forms in a medium containing a low concentration of serum protein without feeder cell layers. J. Parasitol. *75*, 985–989.

Hoeijmakers, J.H., Frasch, A.C., Bernards, A., Borst, P., and Cross, G.A. (1980). Novel expression-linked copies of the genes for variant surface antigens in trypanosomes. Nature *284*, 78–80.

Horn, D., and Cross, G.A.M. (1997). Position-dependent and promoter-specific regulation of gene expression in *Trypanosoma brucei*. EMBO J. *16*, 7422–7431.

Horn, D., and McCulloch, R. (2010). Molecular mechanisms underlying the control of antigenic variation in African trypanosomes. Curr. Opin. Microbiol. *13*, 700–705.

Hovel-Miner, G., Mugnier, M.R., Goldwater, B., Cross, G.A.M., and Papavasiliou, F.N. (2016). A conserved DNA repeat promotes selection of a diverse repertoire of *Trypanosoma brucei* surface antigens from the genomic archive. PLoS Genet. *12*, e1005994.

Hughes, K., Wand, M., Foulston, L., Young, R., Harley, K., Terry, S., Ersfeld, K., and Rudenko, G. (2007). A novel ISWI is involved in *VSG* expression site downregulation in African trypanosomes. EMBO J. *26*, 2400–2410.

Jackson, D.G., Owen, M.J., and Voorheis, H.P. (1985). A new method for the rapid purification of both the membrane-bound and released forms of the variant surface glycoprotein from *Trypanosoma brucei*. Biochem. J. *230*, 195–202.

Janzen, C.J., Lander, F., Dreesen, O., and Cross, G.A.M. (2004). Telomere length regulation and transcriptional silencing in KU80-deficient *Trypanosoma brucei*. Nucleic Acids Res. *32*, 6575–6584.

Janzen, C.J., Hake, S.B., Lowell, J.E., and Cross, G.A.M. (2006). Selective di- or trimethylation of histone H3 lysine 76 by two DOT1 homologs is important for cell cycle regulation in *Trypanosoma brucei*. Mol. Cell *23*, 497–507.

Jehi, S.E., Wu, F., and Li, B. (2014a). *Trypanosoma brucei* TIF2 suppresses VSG switching by maintaining subtelomere integrity. Cell Res *24*, 870–885.

Jehi, S.E., Li, X., Sandhu, R., Ye, F., Benmerzouga, I., Zhang, M., Zhao, Y., and Li, B. (2014b). Suppression of subtelomeric VSG switching by *Trypanosoma brucei* TRF requires its TTAGGG repeat-binding activity. Nucleic Acids Res. *42*, 12899–12911.

Jehi, S.E., Nanavaty, V., and Li, B. (2016). *Trypanosoma brucei* TIF2 and TRF suppress VSG switching using overlapping and independent mechanisms. PLoS One *11*, e0156746.

Kassem, A., Pays, E., and Vanhamme, L. (2014). Transcription is initiated on silent variant surface glycoprotein expression sites despite monoallelic expression in *Trypanosoma brucei*. Proc. Natl. Acad. Sci. *111*, 8943–8948.

Kennedy, P.G.E. (2013). Clinical features, diagnosis, and treatment of human African trypanosomiasis (sleeping sickness). Lancet Neurol. *12*, 186–194.

Kim, H.S., and Cross, G.A.M. (2010). TOPO3a influences antigenic variation by monitoring expression-site-associated VSG switching in *Trypanosoma brucei*. PLoS Pathog. *6*, e1000992.

Kim, H.S., and Cross, G.A.M. (2011). Identification of *Trypanosoma brucei* RMI1/BLAP75 homologue and its roles in antigenic variation. PLoS One *6*, e25313.

Kleine, F.K. (1909). Weitere wissenschaftliche Beobachtungen über die Entwicklung von Trypanosomen in Glossinen. Dtsch. Medizinische Wochenschrift *35*, 924–925.

Kohl, L., Sherwin, T., and Gull, K. (1999). Assembly of the paraflagellar rod and the flagellum attachment zone complex during the *Trypanosoma brucei* cell cycle. J. Eukaryot. Microbiol. *46*, 105–109.

Kooter, J.M., and Borst, P. (1984). Alpha-amanitin-insensitive transcription of variant surface glycoprotein genes provides further evidence for discontinuous transcription in trypanosomes. Nucleic Acids Res. *12*, 9457–9472.

Lacomble, S., Vaughan, S., Gadelha, C., Morphew, M.K., Shaw, M.K., McIntosh, J.R., and Gull, K. (2010). Basal body movements orchestrate membrane organelle division and cell morphogenesis in *Trypanosoma brucei*. J. Cell Sci. *123*, 2884–2891.

Landeira, D., and Navarro, M. (2007). Nuclear repositioning of the *VSG* promoter during developmental silencing in *Trypanosoma brucei*. J. Cell Biol. *176*, 133–139.

Landeira, D., Bart, J.-M., Van Tyne, D., and Navarro, M. (2009). Cohesin regulates *VSG* monoallelic expression in trypanosomes. J. Cell Biol. *186*, 243–254.

Laxman, S., Riechers, A., Sadilek, M., Schwede, F., and Beavo, J. a (2006). Hydrolysis products of cAMP analogs cause transformation of *Trypanosoma brucei* from slender to stumpy-like forms. Proc. Natl. Acad. Sci. *103*, 19194–19199.

Levis, R., Hazelrigg, T., and Rubin, G.M. (1985). Effects of genomic position on the expression of transduced copies of the white gene of *Drosophila*. Science *229*, 558–561.

Li, B., Espinal, A., and Cross, G.A.M. (2005). Trypanosome telomeres are protected by a homologue of mammalian TRF2. Mol. Cell. Biol. *25*, 5011–5021.

Liang, X.H., Haritan, A., Uliel, S., and Michaeli, S. (2003). *Trans* and *cis* splicing in trypanosomatids: Mechanism, factors, and regulation. Eukaryot. Cell *2*, 830–840.

Lira, C.B.B., Giardini, M.A., Neto, J.L.S., Conte, F.F., and Cano, M.I.N. (2007). Telomere biology of trypanosomatids: beginning to answer some questions. Trends Parasitol. *23*, 357–362.

Liu, A.Y.C., Van der Ploeg, L.H.T., Rijsewijk, F.A.M., Borst, P., and Chambon, P. (1983). The transposition unit of variant surface glycoprotein gene 118 of *Trypanosoma brucei*. J. Mol. Biol. *167*, 57–75.

Liu, H.-S., Jan, M.-S., Chou, C.-K., Chen, P.-H., and Ke, N.-J. (1999). Is green fluorescent protein toxic to the living cells? Biochem. Biophys. Res. Commun. *260*, 712–717.

Livingstone, D. (1857). Missionary Travels and Researches in South Africa. John Murray Londo *548*.

Losos, G.J., and Ikede, B.O. (1972). Review of pathology of diseases in domestic and laboratory animals caused by *Trypanosoma congolense*, *T. vivax*, *T. brucei*, *T. rhodesiense* and *T. gambiense*. Vet. Pathol. *9*, 1–71.

MacGregor, P., and Matthews, K.R. (2012). Identification of the regulatory elements controlling the transmission stage-specific gene expression of PAD1 in *Trypanosoma brucei*. Nucleic Acids Res. *40*, 7705–7717.

MacGregor, P., Savill, N.J., Hall, D., and Matthews, K.R. (2011). Transmission stages dominate trypanosome within-host dynamics during chronic infections. Cell Host Microbe *9*, 310–318.

MacGregor, P., Szöőr, B., Savill, N.J., and Matthews, K.R. (2012). Trypanosomal immune evasion, chronicity and transmission: an elegant balancing act. Nat. Rev. Microbiol. *10*, 431–438.

Mancini, P.E., and Patton, C.L. (1981). Cyclic 3′,5′-adenosine monophosphate levels during the developmental cycle of *Trypanosoma brucei brucei* in the rat. Mol. Biochem. Parasitol. *3*, 19–31.

Mani, J., Güttinger, A., Schimanski, B., Heller, M., Acosta-Serrano, A., Pescher, P., Späth, G., and Roditi, I. (2011). Alba-domain proteins of *Trypanosoma brucei* are cytoplasmic RNA-Binding proteins that interact with the translation machinery. PLoS One *6*, e22463.

Manna, P.T., Boehm, C., Leung, K.F., Natesan, S.K., and Field, M.C. (2014). Life and times: synthesis, trafficking, and evolution of VSG. Trends Parasitol. *30*, 251–258.

Marcello, L., and Barry, J.D. (2007). Analysis of the *VSG* gene silent archive in *Trypanosoma brucei* reveals that mosaic gene expression is prominent in antigenic variation and is favored by archive substructure. Genome Res. *17*, 1344–1352.

Marzluff, W.F., Wagner, E.J., and Duronio, R.J. (2008). Metabolism and regulation of canonical histone mRNAs: life without a poly(A) tail. Nat. Rev. Genet. *9*, 843–854.

Matthews, K.R., and Gull, K. (1994). Evidence for an interplay between cell cycle progression and the initiation of differentiation between life cycle forms of African trypanosomes. J. Cell Biol. *125*, 1147–1156.

Matthews, K.R., Sherwin, T., and Gull, K. (1995). Mitochondrial genome repositioning during the differentiation of the African trypanosome between life cycle forms is microtubule mediated. J. Cell Sci. *108*, 2231–2239.

McCulloch, R., Vassella, E., Burton, P., Boshart, M., and Barry, J.D. (2004). Transformation of monomorphic and pleomorphic *Trypanosoma brucei*. Methods Mol. Biol. *262*, 53–86.

McCulloch, R., Morrison, L.J., and Hall, J.P.J. (2015). DNA recombination strategies during antigenic variation in the African trypanosome. Microbiol Spectr. *3*, MDNA3–MDNA0016 – 2014.

McLintock, L.M., Turner, C.M., and Vickerman, K. (1993). Comparison of the effects of immune killing mechanisms on *Trypanosoma brucei* parasites of slender and stumpy morphology. Parasite Immunol. *15*, 475–480.

Michels, P. a. M., Van der Ploeg, L.H.T., Liu, A.Y.C., and Borst, P. (1984). The inactivation and reactivation of an expression-linked gene copy for a variant surface glycoprotein in *Trypanosoma brucei*. EMBO J. *3*, 1345–1351.

Michels, P.A.M., Bringaud, F., Herman, M., and Hannaert, V. (2006). Metabolic functions of glycosomes in trypanosomatids. Biochim Biophys Acta *1763*, 1463–1477.

Monahan, K., and Lomvardas, S. (2015). Monoallelic expression of olfactory receptors. Annu Rev Cell Dev Biol. *31*, 721–740.

Mony, B.M., and Matthews, K.R. (2015). Assembling the components of the quorum sensing pathway in African trypanosomes. Mol. Microbiol. *96*, 220–232.

Mony, B.M., Macgregor, P., Ivens, A., Rojas, F., Cowton, A., Young, J., Horn, D., and Matthews, K. (2013). Genome-wide dissection of the quorum sensing signalling pathway in *Trypanosoma brucei*. Nature *505*, 681–685.

Morrison, L.J., Majiwa, P., Read, A.F., and Barry, J.D. (2005). Probabilistic order in antigenic variation of *Trypanosoma brucei*. Int. J. Parasitol. *35*, 961–972.

Mugnier, M.R., Cross, G.A.M., and Papavasiliou, N.F. (2015). The *in vivo* dynamics of antigenic variation in *Trypanosoma brucei*. Science *2*, 1470–1473.

Muñoz-Jordán, J.L., Davies, K.P., and Cross, G.A. (1996). Stable expression of mosaic coats of variant surface glycoproteins in *Trypanosoma brucei*. Science *272*, 1795–1797.

Narayanan, M.S., and Rudenko, G. (2013). TDP1 is an HMG chromatin protein facilitating RNA polymerase i transcription in African trypanosomes. Nucleic Acids Res. *41*, 2981–2992.

Narayanan, M.S., Kushwaha, M., Ersfeld, K., Fullbrook, A., Stanne, T.M., and Rudenko, G. (2011). NLP is a novel transcription regulator involved in *VSG* expression site control in *Trypanosoma brucei*. Nucleic Acids Res. *39*, 2018–2031.

Navarro, M., and Cross, G. a (1996). DNA rearrangements associated with multiple consecutive directed antigenic switches in *Trypanosoma brucei*. Mol. Cell. Biol. *16*, 3615–3625.

Navarro, M., and Gull, K. (2001). A pol I transcriptional body associated with VSG mono-allelic

expression in *Trypanosoma brucei*. Nature *414*, 759–763.

Navarro, M., Cross, G.A.M., and Wirtz, E. (1999). *Trypanosoma brucei* variant surface glycoprotein regulation involves coupled activation / inactivation and chromatin remodeling of expression sites. EMBO J. *18*, 2265–2272.

Nguyen, T.N., Müller, L.S.M., Park, S.H., Siegel, T.N., and Günzl, A. (2013). Promoter occupancy of the basal class I transcription factor A differs strongly between active and silent *VSG* expression sites in *Trypanosoma brucei*. Nucleic Acids Res. *1*, 3164–3176.

Oberholzer, M., Marti, G., Baresic, M., Kunz, S., Hemphill, A., and Seebeck, T. (2007). The *Trypanosoma brucei* cAMP phosphodiesterases TbrPDEB1 and TbrPDEB2: flagellar enzymes that are essential for parasite virulence. FASEB J. *21*, 720–731.

Oberle, M., Balmer, O., Brun, R., and Roditi, I. (2010). Bottlenecks and the maintenance of minor genotypes during the life cycle of *Trypanosoma brucei*. PLoS Pathog. *6*, e1001023.

Ogbadoyi, E., Ersfeld, K., Robinson, D., Sherwin, T., and Gull, K. (2000). Architecture of the *Trypanosoma brucei* nucleus during interphase and mitosis. Chromosoma *108*, 501–513.

Overath, P., and Engstler, M. (2004). Endocytosis, membrane recycling and sorting of GPI-anchored proteins: *Trypanosoma brucei* as a model system. Mol. Microbiol. *53*, 735–744.

Overath, P., Czichos, J., Stock, U., and Nonnengaesser, C. (1983). Repression of glycoprotein synthesis and release of surface coat during transformation of *Trypanosoma brucei*. EMBO J. *2*, 1721–1728.

Overath, P., Czichos, J., and Haas, C. (1986). The effect of citrate/*cis*-aconitate on oxidative metabolism during transformation of *Trypanosoma brucei*. Eur. J. Biochem. *160*, 175–182.

Pays, E. (2005). Regulation of antigen gene expression in *Trypanosoma brucei*. Trends Parasitol. *21*, 517–520.

Pays, E. (2006). The variant surface glycoprotein as a tool for adaptation in African trypanosomes. Microbes Infect. *8*, 930–937.

Pays, E., Van Assel, S., Laurent, M., Darville, M., Vervoort, T., Van Meirvenne, N., and Steinert, M. (1983). Gene conversion as a mechanism for antigenic variation in Trypanosomes. Cell *34*, 371–381.

Pays, E., Staerz, U., Kanagawa, O., and Bevan, M. (1985). Telomeric reciprocal recombination as a possible mechanism for antigenic variation. Nature *316*, 562–564.

Pays, E., Lips, S., Nolan, D., Vanhamme, L., and Pérez-Morga, D. (2001). The *VSG* expression sites of *Trypanosoma brucei*: multipurpose tools for the adaptation of the parasite to mammalian hosts. Mol. Biochem. Parasitol. *114*, 1–16.

Pays, E., Vanhamme, L., and Pérez-Morga, D. (2004). Antigenic variation in *Trypanosoma brucei*: facts, challenges and mysteries. Curr. Opin. Microbiol. *7*, 369–374.

Pedram, M., and Donelson, J.E. (1999). The anatomy and transcription of a monocistronic expression site for a metacyclic variant surface glycoprotein gene in *Trypanosoma brucei*. J. Biol. Chem. *274*, 16876–16883.

Pena, A.C., Pimentel, M.R., Manso, H., Vaz-Drago, R., Pinto-Neves, D., Aresta-Branco, F., Rijo-Ferreira, F., Guegan, F., Pedro Coelho, L., Carmo-Fonseca, M., et al. (2014). *Trypanosoma brucei* histone H1 inhibits RNA polymerase I transcription and is important for parasite fitness *in vivo*. Mol. Microbiol. *93*, 645–663.

Pérez-Morga, D., Vanhollebeke, B., Paturiaux-Hanocq, F., Nolan, D., Lins, L., Homblé, F., Vanhamme, L., Tebabi, P., Pays, A., Poelvoorde, P., et al. (2005). Apolipoprotein L-I promotes trypanosome lysis by forming pores in lysosomal membranes. Science *309*, 469–472.

Pernis, B., Chiappino, G., Kelus, A.S., and Gell, P.G. (1965). Cellular localization of immunoglobulins with different allotypic specificities in rabbit lymphoid tissues. J. Exp. Med. *122*, 853–876.

Pfister, D.D., Burkard, G., Morand, S., Renggli, C.K., Roditi, I., and Vassella, E. (2006). A mitogen-activated protein kinase controls differentiation of bloodstream forms of *Trypanosoma brucei*. Eukaryot. Cell *5*, 1126–1135.

Povelones, M.L., Gluenz, E., Dembek, M., Gull, K., and Rudenko, G. (2012). Histone H1 plays a role in

heterochromatin formation and VSG expression site silencing in *Trypanosoma brucei*. PLoS Pathog. *8*, e1003010.

Ralston, K.S., Lerner, A.G., Diener, D.R., and Hill, K.L. (2006). Flagellar motility contributes to cytokinesis in *Trypanosoma brucei* and is modulated by an evolutionarily conserved dynein regulatory system. Eukaryot. Cell *5*, 696–711.

Reuner, B., Vassella, E., Yutzy, B., and Boshart, M. (1997). Cell density triggers slender to stumpy differentiation of *Trypanosoma brucei* bloodstream forms in culture. Mol. Biochem. Parasitol. *90*, 269–280.

Rico, E., Rojas, F., Mony, B.M., Szoor, B., MacGregor, P., and Matthews, K.R. (2013). Bloodstream form pre-adaptation to the tsetse fly in *Trypanosoma brucei*. Front. Cell. Infect. Microbiol. *3*, 78.

Robertson, M. (1912). Notes on the polymorphism of *Trypanosoma gambiense* in the blood and its relation to the exogenous cycle in *Glossina palpalis*. Proc. R. Soc. London. Ser. B *85*, 527–539.

Robinson, D.R., Sherwin, T., Ploubidou, A., Byard, E.H., and Gull, K. (1995). Microtubule polarity and dynamics in the control of organelle positioning, segregation, and cytokinesis in the trypanosome cell cycle. J. Cell Biol. *128*, 1163–1172.

Robinson, N.P., Burman, N., Melville, S.E., and Barry, J.D. (1999). Predominance of duplicative *VSG* gene conversion in antigenic variation in African trypanosomes. Mol. Cell. Biol. *19*, 5839–5846.

Roditi, I., Schwarz, H., Pearson, T.W., Beecroft, R.P., Liu, M.K., Richardson, J.P., Bühring, H.J., Pleiss, J., Bülow, R., and Williams, R.O. (1989). Procyclin gene expression and loss of the variant surface glycoprotein during differentiation of *Trypanosoma brucei*. J. Cell Biol. *108*, 737–746.

Roldan, A., Comini, M.A., Crispo, M., and Krauth-Siegel, R.L. (2011). Lipoamide dehydrogenase is essential for both bloodstream and procyclic *Trypanosoma brucei*. Mol. Microbiol. *81*, 623–639.

Rotureau, B., Subota, I., and Bastin, P. (2011). Molecular bases of cytoskeleton plasticity during the *Trypanosoma brucei* parasite cycle. Cell. Microbiol. *13*, 705–716.

Rotureau, B., Subota, I., Buisson, J., and Bastin, P. (2012). A new asymmetric division contributes to the continuous production of infective trypanosomes in the tsetse fly. Development *1850*, 1842–1850.

Rudenko, G., Bishop, D., Gottesdiener, K., and Van der Ploeg, L.H. (1989). Alpha-amanitin resistant transcription of protein coding genes in insect and bloodstream form *Trypanosoma brucei*. EMBO J. *8*, 4259–4263.

Ruepp, S., Furger, A., Kurath, U., Renggli, C.K., Hemphill, A., Brun, R., and Roditi, I. (1997). Survival of *Trypanosoma brucei* in the tsetse fly is enhanced by the expression of specific forms of procyclin. J. Cell Biol. *137*, 1369–1379.

Salmon, D., Vanwalleghem, G., Morias, Y., Denoeud, J., Krumbholz, C., Lhomme, F., Bachmaier, S., Kador, M., Gossmann, J., Dias, F.B.S., et al. (2012). Adenylate cyclases of *Trypanosoma brucei* inhibit the innate immune response of the host. Science *337*, 463–466.

Savill, N.J., and Seed, J.R. (2004). Mathematical and statistical analysis of the *Trypanosoma brucei* slender to stumpy transition. Parasitology *128*, 53–67.

Schell, D., Evers, R., Preis, D., Ziegelbauer, K., Kiefer, H., Lottspeich, F., Cornelissen, A.W., and Overath, P. (1991). A transferrin-binding protein of *Trypanosoma brucei* is encoded by one of the genes in the variant surface glycoprotein gene expression site. EMBO J. *10*, 1061–1066.

Schulz, E.G., and Heard, E. (2013). Role and control of X chromosome dosage in mammalian development. Curr. Opin. Genet. Dev. *23*, 109–115.

Schulz, D., Mugnier, M.R., Paulsen, E.-M., Kim, H.-S., Chung, C.W., Tough, D.F., Rioja, I., Prinjha, R.K., Papavasiliou, F.N., and Debler, E.W. (2015). Bromodomain proteins contribute to maintenance of bloodstream form stage identity in the african trypanosome. PLoS Biol. *13*, e1002316.

Schwede, A., Jones, N., Engstler, M., and Carrington, M. (2011). The VSG C-terminal domain is inaccessible to antibodies on live trypanosomes. Mol. Biochem. Parasitol. *175*, 201–204.

Seed, J.R., and Sechelski, J.B. (1989). Mechanism of long slender (LS) to short stumpy (SS) transformation in the African trypanosomes. J. Protozool. *36*, 572–577.

Seed, J.R., and Wenck, M.A. (2003). Role of the long slender to short stumpy transition in the life cycle

of the african trypanosomes. Kinetoplastid Biol. Dis. *2*, 3.

Shapiro, S.Z., Naessens, J., Liesegang, B., Moloo, S.K., and Magondu, J. (1984). Analysis by flow cytometry of DNA synthesis during the life cycle of African trypanosomes. Acta Trop. *41*, 313–323.

Sharma, R., Peacock, L., Gluenz, E., Gull, K., Gibson, W., and Carrington, M. (2008). Asymmetric cell division as a route to reduction in cell length and change in cell morphology in trypanosomes. Protist *159*, 137–151.

Sharma, R., Gluenz, E., Peacock, L., Gibson, W., Gull, K., and Carrington, M. (2009). The heart of darkness: growth and form of *Trypanosoma brucei* in the tsetse fly. Trends Parasitol. *25*, 517–524.

Sheader, K., Vaughan, S., Minchin, J., Hughes, K., Gull, K., and Rudenko, G. (2005). Variant surface glycoprotein RNA interference triggers a precytokinesis cell cycle arrest in African trypanosomes. Proc. Natl. Acad. Sci. *102*, 8716–8721.

Sherwin, T., and Gull, K. (1989). The cell division cycle of *Trypanosoma brucei brucei*: timing of event markers and cytoskeletal modulations. Philos. Trans. R. Soc. London. Ser. B Biol. Sci. *323*, 573–588.

Smith, J.D., Chitnis, C.E., Craig, A.G., Roberts, D.J., Hudson-Taylor, D.E., Peterson, D.S., Pinches, R., Newbold, C.I., and Miller, L.H. (1995). Switches in expression of *plasmodium falciparum* var genes correlate with changes in antigenic and cytoadherent phenotypes of infected erythrocytes. Cell *82*, 101–110.

Smith, T.K., Vasileva, N., Gluenz, E., Terry, S., Portman, N., Kramer, S., Carrington, M., Michaeli, S., Gull, K., and Rudenko, G. (2009). Blocking variant surface glycoprotein synthesis in *Trypanosoma brucei* triggers a general arrest in translation initiation. PLoS One *4*, e7532.

Stanne, T.M., and Rudenko, G. (2010). Active *VSG* expression sites in *Trypanosoma brucei* are depleted of nucleosomes. Eukaryot. Cell *9*, 136–147.

Stanne, T., Narayanan, M.S., Ridewood, S., Ling, A., Kushwaha, M., Wiesler, S., Wickstead, B., Wood, J., and Rudenko, G. (2015). Identification of the ISWI chromatin remodeling complex of the early branching eukaryote *Trypanosoma brucei*. J Biol Chem. *290*, 26954–26967.

Stanne, T.M., Kushwaha, M., Wand, M., Taylor, J.E., and Rudenko, G. (2011). TbISWI regulates multiple polymerase I (Pol I)-transcribed loci and is present at Pol II transcription boundaries in *Trypanosoma brucei*. Eukaryot. Cell *10*, 964–976.

Steger, D.J., Haswell, E.S., Miller, A.L., Wente, S.R., and O'Shea, E.K. (2003). Regulation of chromatin remodeling by inositol polyphosphates. Science *299*, 114–116.

Su, X.Z., Heatwole, V.M., Wertheimer, S.P., Guinet, F., Herrfeldt, J. a, Peterson, D.S., Ravetch, J. a, and Wellems, T.E. (1995). The large diverse gene family var encodes proteins involved in cytoadherence and antigenic variation of *Plasmodium falciparum*-infected erythrocytes. Cell *82*, 89–100.

Taylor, A.E., and Godfrey, D.G. (1968). A new organelle of bloodstream salivarian trypanosomes. J. Protozool *16*, 466–470.

Taylor, J.E., and Rudenko, G. (2006). Switching trypanosome coats: what's in the wardrobe? Trends Genet. *22*, 614–620.

Thon, G., Baltz, T., and Eisen, H. (1989). Antigenic diversity by the recombination of pseudogenes. Genes Dev. *3*, 1247–1254.

Thon, G., Baltz, T., Giroud, C., and Eisen, H. (1990). Trypanosome variable surface glycoproteins: composite genes and order of expression. Genes Dev. *9*, 1374–1383.

Tiengwe, C., Muratore, K.A., and Bangs, J.D. (2016). Surface proteins, ERAD, and antigenic variation in *Trypanosoma brucei*. Cell. Microbiol. *18*, 1673–1688.

Trindade, S., Rijo-Ferreira, F., Carvalho, T., Pinto-Neves, D., Guegan, F., Aresta-Branco, F., Bento, F., Young, S.A., Pinto, A., Van Den Abbeele, J., et al. (2016). *Trypanosoma brucei* parasites occupy and functionally adapt to the adipose tissue in mice. Cell Host Microbe *19*, 837–848.

Tsai, B.P., Wang, X., Huang, L., and Waterman, M.L. (2011). Quantitative profiling of in *vivo*-assembled RNA-protein complexes using a novel integrated proteomic approach. Mol. Cell. Proteomics *10*, M110.007385.

Turner, C.M., and Barry, J.D. (1989). High frequency of antigenic variation in *Trypanosoma brucei rhodesiense* infections. Parasitology *99*, 67–75.

Turner, C.M.R., Hunter, C.A., Barry, J.D., and Vickerman, K. (1986). Similarity in variable antigen type composition of *Trypanosoma brucei rhodesiense* populations in different sites within the mouse host. Trans. R. Soc. Trop. Med. Hyg. *80*, 824–830.

Turner, C.M.R., Barry, J.D., Maudlin, I., and Vickerman, K. (1988). An estimate of the size of the metacyclic variable antigen repertoire of *Trypanosoma brucei rhodesiense*. Parasitology *97*, 269–276.

Tyler, K.M., Matthews, K.R., and Gull, K. (1997). The bloodstream differentiation-division of *Trypanosoma brucei* studied using mitochondrial markers. Proc. R. Soc. London. Ser. B *264*, 1481–1490.

Tyler, K.M., Higgs, P.G., Matthews, K.R., and Gull, K. (2001). Limitation of *Trypanosoma brucei* parasitaemia results from density-dependent parasite differentiation and parasite killing by the host immune response. Proc. Biol. Sci. *268*, 2235–2243.

Uhl, B. (2009). Development of a quantitative real-time PCR protocol for expression studies in *Trypanosoma brucei*. Diploma Thesis.

Uzureau, P., Uzureau, S., Lecordier, L., Fontaine, F., Tebabi, P., Homble, F., Grelard, A., Zhendre, V., Nolan, D.P., Lins, L., et al. (2013). Mechanism of *Trypanosoma brucei gambiense* resistance to human serum. Nature *501*, 430–434.

Van Den Abbeele, J., Claes, Y., van Bockstaele, D., Le Ray, D., and Coosemans, M. (1999). *Trypanosoma brucei spp.* development in the tsetse fly: characterization of the post-mesocyclic stages in the foregut and proboscis. Parasitology *118*, 469–478.

Van Hellemond, J.J., Bakker, B.M., and Tielens, A.G.M. (2005). Energy metabolism and its compartmentation in *Trypanosoma brucei*. Adv. Microb. Physiol. *50*, 199–226.

Van Luenen, H.G.A.M., Kieft, R., Mußmann, R., Engstler, M., Ter Riet, B., and Borst, P. (2005). Trypanosomes change their transferrin receptor expression to allow effective uptake of host transferrin. Mol. Microbiol. *58*, 151–165.

Vanhamme, L., Poelvoorde, P., Pays, A., Tebabi, P., Van Xong, H., and Pays, E. (2000). Differential RNA elongation controls the variant surface glycoprotein gene expression sites of *Trypanosoma brucei*. Mol. Microbiol. *36*, 328–340.

Vanhamme, L., Paturiaux-Hanocq, F., Poelvoorde, P., Nolan, D.P., Lins, L., Abbeele, J.V.D., Pays, A., Tebabi, P., Xong, H.V., Jacquet, A., et al. (2003). Apolipoprotein L-1 is the trypanosome lytic factor of human serum. Nature *422*, 83–87.

Vanhollebeke, B., De Muylder, G., Nielsen, M.J., Pays, A., Tebabi, P., Dieu, M., Raes, M., Moestrup, S.K., and Pays, E. (2008). A haptoglobin-hemoglobin receptor conveys innate immunity to *Trypanosoma brucei* in humans. Science *320*, 677–681.

Vanhollebeke, B., Uzureau, P., Monteyne, D., Pérez-Morga, D., and Pays, E. (2010). Cellular and molecular remodeling of the endocytic pathway during differentiation of *Trypanosoma brucei* bloodstream forms. Eukaryot. Cell *9*, 1272–1282.

Vassella, E., and Boshart, M. (1996). High molecular mass agarose matrix supports growth of bloodstream forms of pleomorphic *Trypanosoma brucei* strains in axenic culture. Mol. Biochem. Parasitol. *82*, 91–105.

Vassella, E., Reuner, B., Yutzy, B., and Boshart, M. (1997). Differentiation of African trypanosomes is controlled by a density sensing mechanism which signals cell cycle arrest via the cAMP pathway. J. Cell Sci. *110*, 2661–2671.

Vassella, E., Krämer, R., Turner, C.M.R., Wankell, M., Modes, C., Van Den Bogaard, M., and Boshart, M. (2001). Deletion of a novel protein kinase with PX and FYVE-related domains increases the rate of differentiation of *Trypanosoma brucei*. Mol. Microbiol. *41*, 33–46.

Vickerman, K. (1965). Polymorphism and mitochondrial activity in sleeping sickness trypanosomes. Nature *208*, 762–766.

Vickerman, K., and Preston, T.M. (1976). Comparative cell biology of the kinetoplastid flagellates. In Biology of the Kinetoplastida, W.H.R. Lumsden, and D.A. Evans, eds. (London/New York/San

Francisco: Academic Press), pp. 35–130.

Wang, Q.P., Kawahara, T., and Horn, D. (2010). Histone deacetylases play distinct roles in telomeric *VSG* expression site silencing in African trypanosomes. Mol. Microbiol. *77*, 1237–1245.

Wheeler, R.J. (2010). The trypanolytic factor-mechanism, impacts and applications. Trends Parasitol. *26*, 457–464.

Wickstead, B. (2004). The small chromosomes of *Trypanosoma brucei* involved in antigenic variation are constructed around repetitive palindromes. Genome Res. *14*, 1014–1024.

Wickstead, B., Ersfeld, K., and Gull, K. (2002). Targeting of a tetracycline-inducible expression system to the transcriptionally silent minichromosomes of *Trypanosoma brucei*. Mol. Biochem. Parasitol. *125*, 211–216.

Wirtz, E., Leal, S., Ochatt, C., and Cross, G.A. (1999). A tightly regulated inducible expression system for conditional gene knock-outs and dominant-negative genetics in *Trypanosoma brucei*. Mol. Biochem. Parasitol. *99*, 89–101.

Woodward, R., and Gull, K. (1990). Timing of nuclear and kinetoplast DNA replication and early morphological events in the cell cycle of *Trypanosoma brucei*. J. Cell Sci. *95*, 49–57.

World Health Organization (2016). Trypanosomiasis, human African (sleeping sickness).

Xong, H.V., Vanhamme, L., Chamekh, M., Chimfwembe, C.E., Van Den Abbeele, J., Pays, A., Van Melrvenne, N., Hamers, R., De Baetselier, P., and Pays, E. (1998). A *VSG* expression site-associated gene confers resistance to human serum in *Trypanosoma rhodesiense*. Cell *95*, 839–846.

Yang, X., Figueiredo, L.M., Espinal, A., Okubo, E., and Li, B. (2009). RAP1 is essential for silencing telomeric *variant surface glycoprotein* genes in *Trypanosoma brucei*. Cell *137*, 99–109.

Yildirim, S., Castano, E., Sobol, M., Philimonenko, V. V, Dzijak, R., Venit, T., and Hozák, P. (2013). Involvement of phosphatidylinositol 4,5-bisphosphate in RNA polymerase I transcription. J. Cell Sci. *126*, 2730–2739.

Ziegelbauer, K., Quinten, M., Schwarz, H., Pearson, T.W., and Overath, P. (1990). Synchronous differentiation of *Trypanosoma brucei* from bloodstream to procyclic forms *in vitro*. Eur. J. Biochem. *192*, 373–378.

7 Appendix

7.1 Supporting information

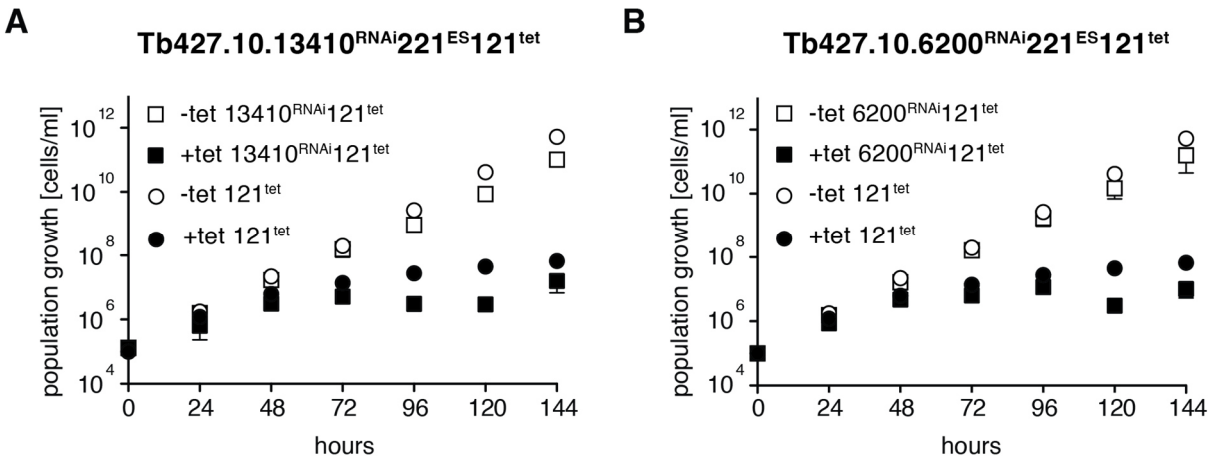

Figure 46: Knock-down of *Tb427.10.13410* or *Tb427.10.6200* does not alter the VSG 121 overexpression growth phenotype in monomorphic cells. (A) Tb427.10.13410 or **(B)** Tb427.10.6200 was down-regulated via RNAi simultaneously to the overexpression of VSG 121 in monomorphic trypanosomes (squares). Growth curves of tetracycline-induced (black) and non-induced (white) parasites are shown. Means (± SD) of three clones are shown. The parental $221^{ES}121^{tet}$ cell line (circles) served as a growth control (+tet black circle, -tet white circles). The cell lines were generated as part of the bachelor thesis of Matthias Grießmann.

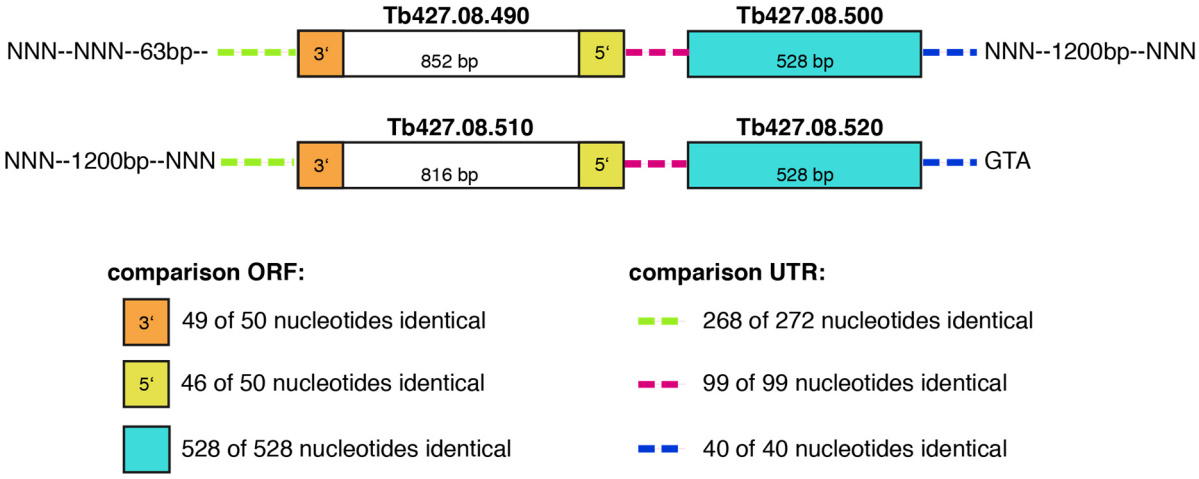

Figure 47: The gene array of *Tb427.08.490-08.520* in *Trypanosoma brucei*. The schematic representation illustrates the similar regions of the gene array. Boxes indicate the ORF and the dashed lines the intergenic regions (UTRs). Boxes or lines in the same color represent identical sequences and the number of identical nucleotides is given in the lower part of the model. The Gene ID is presented above the corresponding box and the numbers within the boxes state the annotated length of the ORF.

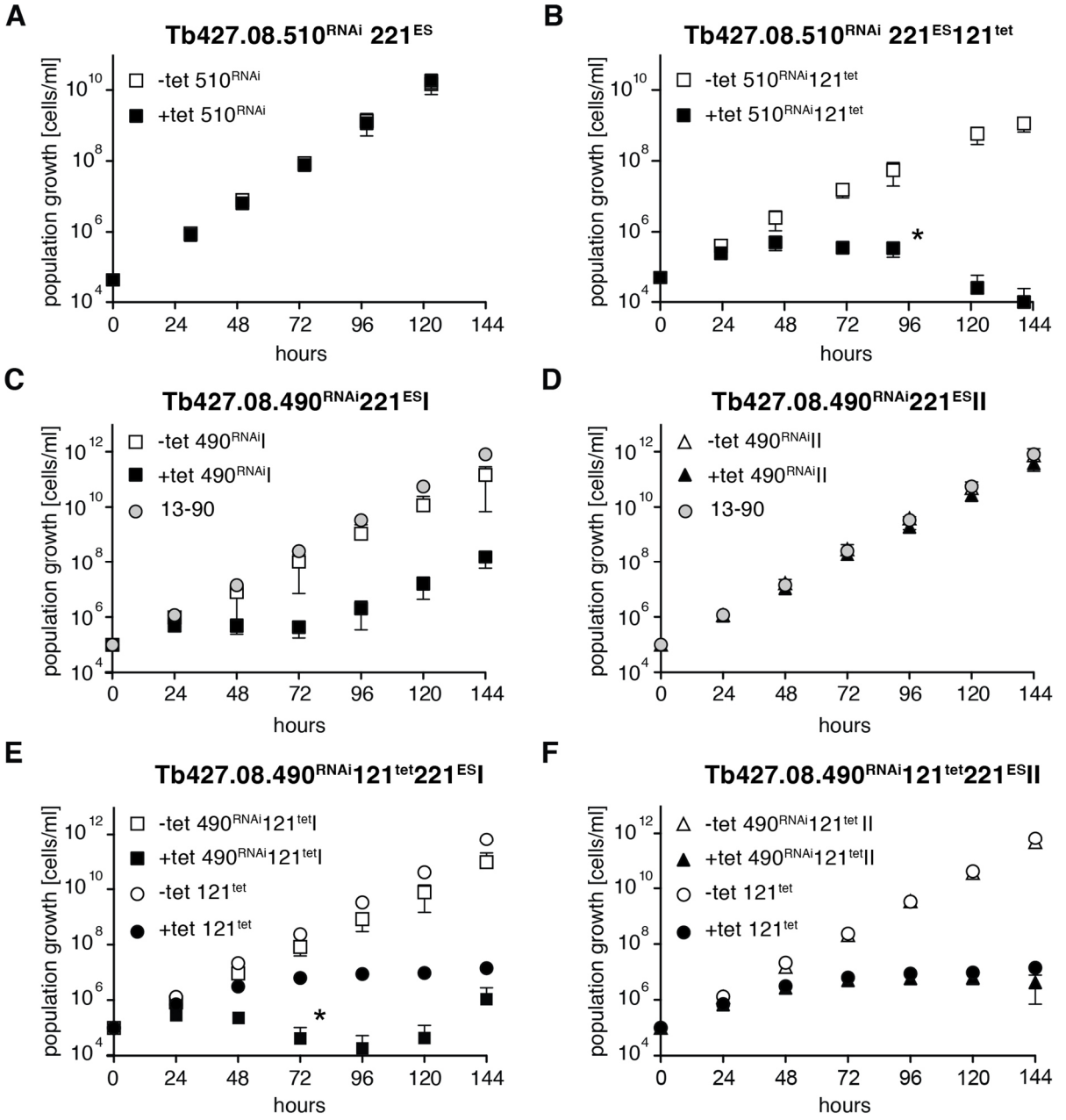

Figure 48: Knock-down of *Tb427.08.510* or *Tb427.08.490* alters the VSG 121 overexpression growth phenotype in monomorphic cells. Tb427.08.510 was down-regulated via RNAi **(A)** in BSF 13-90 parasites (Tb427.08.510^{RNAi}221ES) or **(B)** simultaneously to the overexpression of VSG 121 in monomorphic trypanosomes (Tb427.08.510^{RNAi}221ES121^{tet}). Growth curves of tetracycline-induced (black squares) and non-induced (white squares) parasites. Means (± SD) of **(A)** four clones and **(B)** two clones are shown. Christopher Batram generated the cell lines and conducted the growth analyses. At the time point indicated by the asterisk in B the clones started to die. Tb427.08.490 was down-regulated via RNAi **(C, D)** in BSF 13-90 parasites (Tb427.08.490^{RNAi}221ES) or **(E, F)** simultaneously to the overexpression of VSG 121 in monomorphic trypanosomes (Tb427.08.490^{RNAi} 221ES121^{tet}). Growth curves of tetracycline-induced (black) and non-induced (white) parasites are shown. **(C, E)** Clones displaying an altered growth compared to the parental cell line were termed 'I' (squares) and the means (± SD) of three clones are shown for each cell line. At the time point indicated by the asterisk in E two clones had died, only one resumed growth. **(D, F)** Clones displaying the same growth phenotype as the parental cell line were termed 'II' (triangles) and the means (± SD) of two clones are shown for each cell line. **(C, D)** The parental BSF 13-90 (grey circle) or **(E, F)** the parental 221ES121^{tet} cell line (circles) served as a growth control (+tet black circle, -tet white circles).

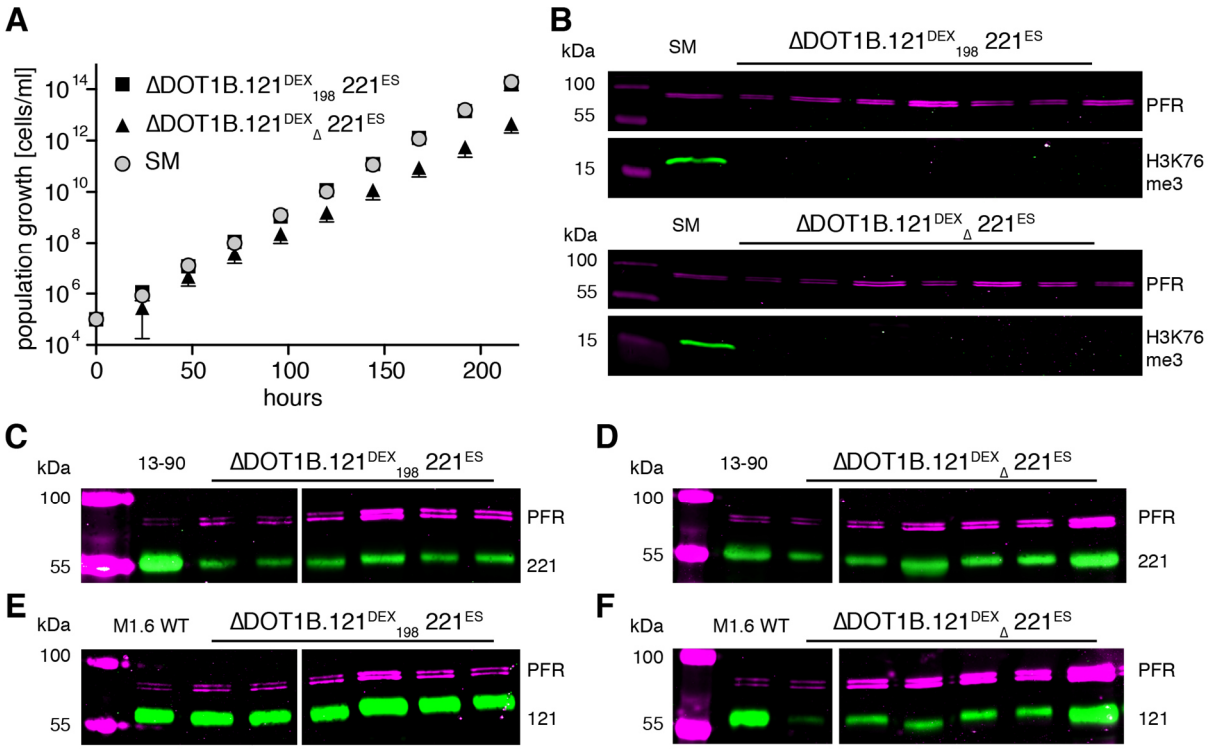

Figure 49: VSG double expressors in a DOT1B knock-out background. Transfection of the ΔDOT1B. 221ES cell line with pKD4 VSG 121 198 or pKD4 VSG 121 Δ(45-51) generated the cell lines ΔDOT1B.121$^{DEX}{}_{198}$221ES and ΔDOT1B.121$^{DEX}{}_{\Delta}$221ES, respectively. **(A)** Growth curves of the ΔDOT1B.121$^{DEX}{}_{198}$221ES (black squares) and the ΔDOT1B.121$^{DEX}{}_{\Delta}$221ES cell line (black triangle). Means (± SD) of five clones are shown for each cell line. The parental SM cell line (circles) served as a growth control. **(B)** Western blot analyses of the trimethylation levels of histone H3 (H3K76me3) in seven clones of the ΔDOT1B.121$^{DEX}{}_{198}$221ES and the ΔDOT1B.121$^{DEX}{}_{\Delta}$221ES cell line. The blots were stained with a H3K76me3 antibody (green) and detection of PFR proteins (magenta) served as a loading control. Protein samples of SM cells served as a positive control. **(C-F)** Western blot analyses of the VSG 221 and the VSG 121 expression levels in six clones of the ΔDOT1B.121$^{DEX}{}_{198}$221ES and the ΔDOT1B.121$^{DEX}{}_{\Delta}$221ES cell line. The blots were stained **(C, D)** with a VSG 221 antibody (magenta) or **(E, F)** with a VSG 121 antibody (green). Detection of PFR proteins (magenta) served as a loading control. Protein samples of MITat1.6 wild type cells natively expressing VSG 121 and the parental 13-90 cells natively expressing VSG 221 served as positive controls.

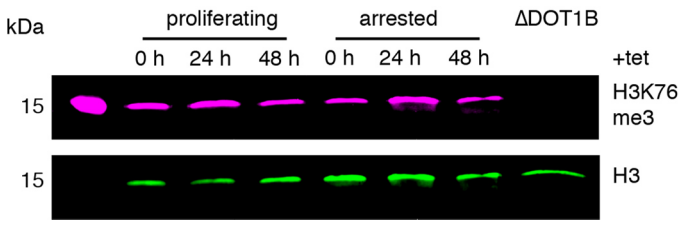

Figure 50: Proliferating pleomorphic VSG 121 overexpressors are no natural DOT1B knock-out cells. Western blot analyses of the trimethylation levels of histone H3 (H3K76me3) in a proliferating and a growth-arrested clone of the GFP:PAD1$_{UTR}$A1.1^{ES}121^{tet} cell line. The analyses were done with non-induced (0 h) parasites and cells overexpressing VSG 121 for 24 or 48 hours. The blots were stained with a H3K76me3 antibody (magenta) and detection of H3 proteins (green) served as a loading control. A protein sample of ΔDOT1B cells served as a negative control.

Table 15: Up-regulated transcripts upon VSG 121 overexpression in monomorphic and pleomorphic cells. The table shows the transcripts that were more than twofold up-regulated within 24 hours of VSG 121 overexpression in monomorphic and pleomorphic trypanosomes. Transcripts with FPKM (fragments per kilobase of transcript per million mapped reads) values below one in the non induced sample were excluded, except for the three in grey highlighted genes which are part of the *Tb427.08.490-08.520* gene array. Presented are the Gene IDs for the corresponding transcripts (TriTrypDB), the FPKM values for the respective transcript in the non-induced cells and the fold regulation within 24 hours of VSG 121 overexpression. Also short descriptions of the proteins are given and they are ranked according to their up-regulation in the pleomorphic VSG overexpressors.

	pleomorphic		**monomorphic**		**Description**
	FPKM 0 h	**24 h/0 h**	**FPKM 0h**	**24 h/0 h**	
Tb427.06.510	150.02	7.44	49.90	3.36	GPEET2 procyclin
Tb427.08.500	0.72	6.61	18.64	2.44	hypothetical protein
Tb427.10.10260	93.15	6.56	81.35	2.23	EP1 procyclin
Tb427.06.480	1.44	6.44	24.25	4.10	unspecified product
Tb427.10.10250	24.19	6.35	56.37	2.47	EP2 procyclin
Tb427.08.510	0.59	5.79	4.12	6.74	hypothetical protein
Tb427.06.520	50.18	5.10	55.62	2.08	EP3-2 procyclin
Tb427.05.4020	48.89	4.06	2.32	3.00	hypothetical protein
Tb427.08.6170	33.76	3.33	1.74	2.30	transketolase, putative
Tb427.08.490	1.45	3.24	80.62	2.60	hypothetical protein
Tb427.10.2360	12.91	2.79	65.51	2.19	hypothetical protein
Tb427.05.2260	16.48	2.73	32.38	2.63	hypothetical protein
Tb427.03.1500	28.02	2.55	89.96	2.18	VSG-related, putative
Tb427.10.2350	47.16	2.48	8.64	2.28	pyruvate dehydrogenase complex, putative
Tb427.04.3940	28.93	2.42	6.56	2.17	calpain-like cysteine peptidase, putative
Tb427.10.6200	22.88	2.39	1.24	2.03	hypothetical protein
Tb427.07.3520	91.35	2.29	88.70	2.33	hypothetical protein
Tb427.07.6110	14.99	2.21	2.19	2.43	hypothetical protein
Tb427.03.4650	21.37	2.19	7.31	2.03	C-8 sterol isomerase, putative
Tb427.04.3920	32.62	2.16	5.16	2.14	hypothetical protein
Tb427.10.11220	65.77	2.07	24.60	2.06	procyclic form surface glycoprotein
Tb427.05.2160	19.54	2.05	19.02	2.44	hypothetical protein
Tb427.07.420	1.12	2.02	9.18	2.02	hypothetical protein
Tb427.08.520	0.00	1.39	17.07	2.65	hypothetical protein

7.2 List of abbreviations

118	VSG 118
121	VSG 121
198	complete *VSG 121* 3' UTR
Δ	nucleotides 45-51 of the *VSG 121* 3' UTR were deleted
µg	microgram
µl	microlitre
µM	micromolar
A1.1	VSG AnTat1.1
AnTat	Antwerp Insitut Trypanozoon Antigen Typ
BLAS	blasticidin
BLE	phleomycin
bp	base pairs
BSA	bovine serum albumin
BSF	bloodstream form
cAMP	cyclic adenosine monophosphate
cDNA	complementary DNA
CDS	coding DNA sequence
DAPI	4',6-diamidino-2-phenylindole
ddH_2O	double-distilled water
DEX	double expressor
DIC	differential interference contrast
DMSO	dimethyl sulfoxide
DNA	desoxyribonucleic acid
EP1	PCF specific surface GPI-anchored glycoprotein
ER	endoplasmic reticulum
ES	bloodstream form expression site
ESAG	expression site associated gene
ESB	expression site body
FCS	fetal calf serum
FISH	fluorescence *in situ* hybridization
g	acceleration due to gravity
g	gram
GFP	green fluorescent protein
GPI	glycosylphosphatidylinositol
h	hour
HMI-9	culture medium for bloodstream form trypanosomes
HYG	hygromycin
IgG	immunoglobulin G
K	kinetoplast
kDA	kilodalton
l	liter
LipDH	lipoamide dehydrogenase
LS	leader sequence for ER import
M	molarity
mg	milligram
min	minute
MITat	Molteno Institute Trypanozoon antigen type
ml	milliliter
mM	millimolar
mRNA	messenger RNA
mVSG	metacyclic VSG

N	nucleus
NEO	neomycin (G-418)
ng	nanogram
nm	nanometer
ORF	open reading frame
PAD	proteins associated with differentiation
PBS	phosphate buffered saline
PCF	procyclic form
pCPT-cAMP	8-(4-chlorophenylthio)-cAMP
PCR	polymerase chain reaction
pdt	population doubling time
pFA	paraformaldehyde
PFR	paraflagellar rod
Pol	RNA polymerase
pro	promotor-proximal
PURO	puromycin
RFU	relative fluorescence unit
RNA	ribonucleic acid
RNAi	RNA interference
rpm	rounds per minute
RS	ribosomal spacer
RT	room temperature
SD	standard deviation
SDS	sodium dodecyl sulfate
sec	second
SIF	stumpy induction factor
sl	slender BSF
st	stumpy BSF
TDB	trypanosome dilution buffer
tel	telomere-proximal
tet	tetracycline
TLF	trypanolytic factor
TPE	telomere positioning effect
tub	tubulin
UTR	untranslated region
vPBS	PBS containing 45.9 mM sucrose und 10 mM glucose
VSG	variant surface glycoprotein
v/v	volume per volume
WT	wild type
w/v	weight per volume
YFP	yellow fluorescent protein

7.3 List of figures and tables

Figures

Tables

7.4 Publication list

Teile dieser Arbeit sind in folgender Publikation enthalten:

Henriette Zimmermann, Ines Subota, Christopher Batram, Susanne Kramer, Christian J. Janzen, Nicola G. Jones, Markus Engstler.

"A Quorum Sensing-independent Path to Stumpy Development in *Trypanosoma brucei*"

(Manuskript eingereicht bei PLoS Pathogens)

7.5 Eidesstattliche Erklärung

Erklärungen nach §4 Abs. 3 Satz 3, 5, 8 der Promotionsordnung der Fakultät für Biologie

Affidavit

I hereby declare that my thesis entitled: „ **Antigenic variation and stumpy development in *Trypanosoma brucei***" is the result of my own work.

I did not receive any help or support from commercial consultants. All sources and / or materials applied are listed and specified in the thesis.

Furthermore I verify that the thesis has not been submitted as part of another examination process neither in identical nor in similar form.

Eidesstattliche Erklärung

Hiermit erkläre ich an Eides statt, die Dissertation: „**Antigenic variation and stumpy development in *Trypanosoma brucei***", eigenständig, d. h. insbesondere selbständig und ohne Hilfe eines kommerziellen Promotionsberaters, angefertigt und keine anderen, als die von mir angegebenen Quellen und Hilfsmittel verwendet zu haben.

Ich erkläre außerdem, dass die Dissertation weder in gleicher noch in ähnlicher Form bereits in einem anderen Prüfungsverfahren vorgelegen hat.

Würzburg, den

Henriette Zimmermann

7.6 Danksagung

An dieser Stelle möchte ich mich bedanken

bei Markus für die Möglichkeit, mich auf die faszinierende Reise in die Welt der antigenen Variation und der Differenzierung in Trypanosomen zu begeben – danke, dass du mich bei jeder neuen Herausforderungen gefördert und unterstützt hast;

bei Prof. Dr. Klaus Brehm für die bereitwillige Übernahme des Zweitgutachtens;

bei Ines und Christopher für ihre stete Hilfe, ihre Inspiration und ihren Zuspruch, aber ganz besonders für unsere Freundschaft;

bei Susanne K. und Janne für viele wertvolle Diskussionen und aufmunternden Worte;

bei Nicola, Tim und Brooke für ihre Ratschläge und ihr Engagement;

bei den guten Seelen in unserem Lehrstuhl, die das Labor am Laufen halten und den Weg ebnen für die Arbeit von allen: Uli, Reinhild, Kathrin, Lidia, Elina, Patrick, Elisabeth, Silke, Beate, Barbara und Alex;

bei Sarah, Barti, Erick, Anne, Katharina, Helena und ganz besonders bei Ja(s)min für viele denkwürdige und unbezahlbare Augenblicke;

bei der gesamten Zoologie für eine wunderbare Zeit;

bei meinen Freunden für Ihren Beistand und die Ablenkungen;

bei Katja, Jana und Franzi für den Rückhalt, den sie mir geboten haben, und dafür, dass sie ein Teil meines Lebens sind;

bei meiner Familie, Schwiegerfamilie und Familie Winkler für Ihre Anteilnahme und Ermutigungen;

bei Marcus Koch, der immer an meiner Seite war und mich mit seiner Liebe mehr stützt, als er es je wahr haben könnte – danke, dass du an mich glaubst, mich bestärkst und mich verstehst;

sowie bei meiner Mutter, die mir Alles ermöglicht hat – durch ihre Liebe, ihre Unterstützung und ihren Glauben an mich habe ich die Kraft, alles zu erreichen.